

**Steerable needles in prostate brachytherapy  
From sketch to MDR-compliant batch**

de Vries, M.

**DOI**

[10.4233/uuid:93dee070-5e4b-42b1-97e4-c598bcf27084](https://doi.org/10.4233/uuid:93dee070-5e4b-42b1-97e4-c598bcf27084)

**Publication date**

2023

**Document Version**

Final published version

**Citation (APA)**

de Vries, M. (2023). *Steerable needles in prostate brachytherapy: From sketch to MDR-compliant batch*. [Dissertation (TU Delft), Delft University of Technology]. <https://doi.org/10.4233/uuid:93dee070-5e4b-42b1-97e4-c598bcf27084>

**Important note**

To cite this publication, please use the final published version (if applicable).  
Please check the document version above.

**Copyright**

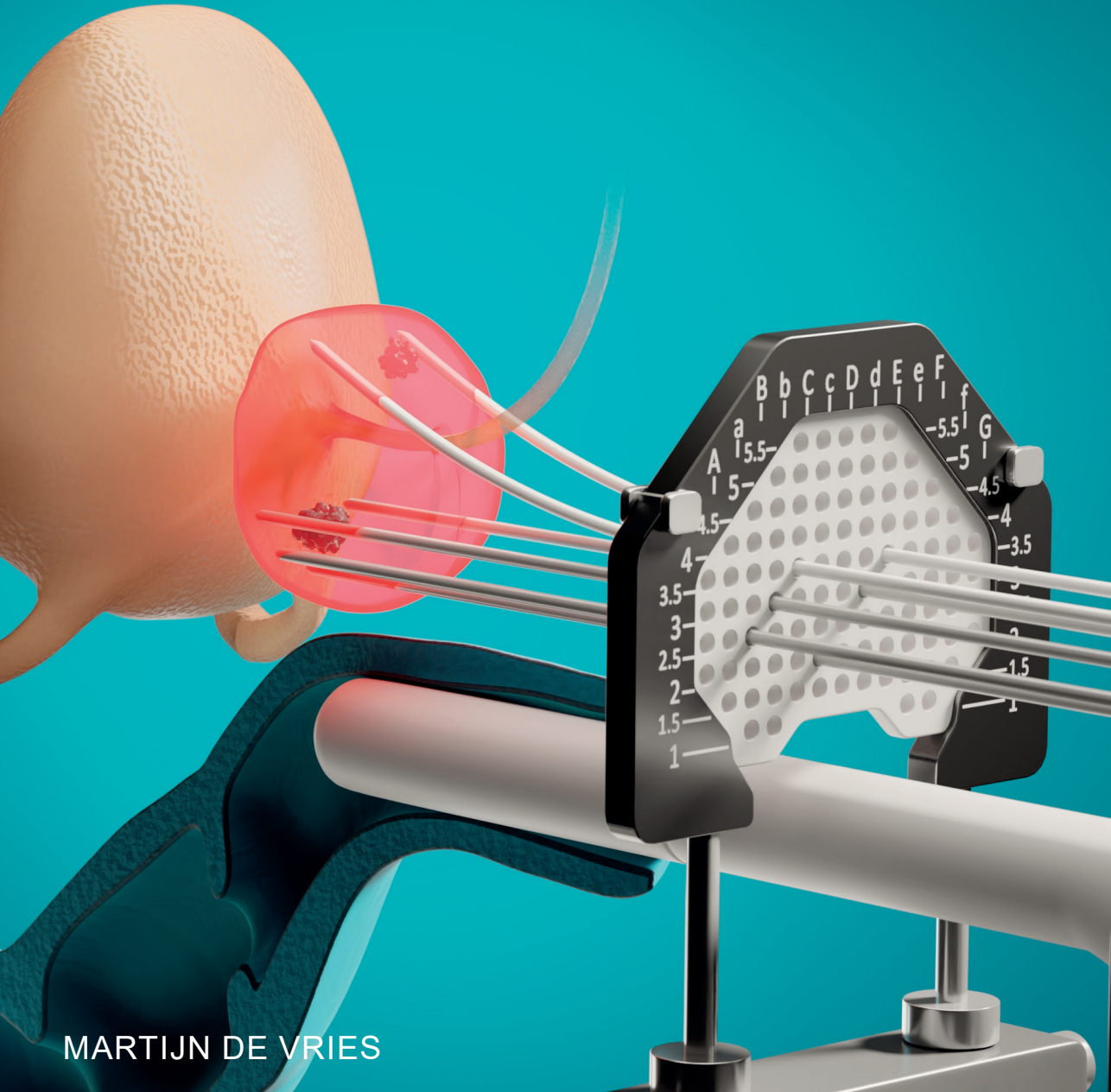
Other than for strictly personal use, it is not permitted to download, forward or distribute the text or part of it, without the consent of the author(s) and/or copyright holder(s), unless the work is under an open content license such as Creative Commons.

**Takedown policy**

Please contact us and provide details if you believe this document breaches copyrights.  
We will remove access to the work immediately and investigate your claim.

# STEERABLE NEEDLES IN PROSTATE BRACHYTHERAPY

From sketch to MDR-compliant batch





# **Steerable needles in prostate brachytherapy**

From sketch to MDR-compliant batch

**Martijn de Vries**



Title: Steerable needles in prostate brachytherapy  
Author: M. de Vries (martijndevries\_92@hotmail.com)

Printed by: ProefschriftMaken

Cover design: T. van den Elsen

ISBN 978-94-6469-646-2

2023 © M. de Vries

This research was supported by the European regional development fund under EU Interreg 2 Seas, grant: 2S04-022 and the Dutch Research Council (NWO) [nr. 15499].

All rights reserved. No part of this dissertation may be reproduced by any means or transmitted in any form without the written permission of the author or, when appropriate, of the publisher of the publications.

An electronic version of this dissertation is available at <https://repository.tudelft.nl/>

# Steerable needles in prostate brachytherapy

From sketch to MDR-compliant batch

## Dissertation

for the purpose of obtaining the degree of doctor

at Delft University of Technology

by the authority of the Rector Magnificus Prof.dr.ir. T.H.J.J. van der Hagen

chair of the Board for Doctorates

to be defended publicly on

Friday 1, December 2023 at 12.30 o'clock

by

**Martijn DE VRIES**

Master of Science in Biomedical Engineering,

Delft University of Technology, the Netherlands

born in Rotterdam, the Netherlands

This dissertation has been approved by the promotor.

**Composition of the doctoral committee:**

Rector Magnificus,	chairperson
Prof. dr. J.J. van den Dobbelsteen	Delft University of Technology, promotor
Prof. dr. J. Dankelman	Delft University of Technology, promotor

**Independent members:**

Prof. dr. ir. P. Breedveld	Delft University of Technology
Prof. dr. B.H.W. Hendriks	Delft University of Technology
Prof. dr. ir. J.J.W. Lagendijk	University Medical Center Utrecht
Prof. dr. R. Merzouki	University of Lille, France
Dr. ir. I.K.K. Kolkman-Deurloo	University Medical Center Rotterdam
Dr. D. Dodou	Delft University of Technology, reserve member

# CONTENTS

<b>SUMMARY   SAMENVATTING</b>	<b>1</b>
<b>1 INTRODUCTION</b>	<b>5</b>
1.1 Background	
1.2 Brachytherapy	
1.3 Prostate brachytherapy	
1.4 Hazards in prostate brachytherapy	
1.5 Steerable needles as a solution?	
1.6 Aims of this thesis	
1.7 Thesis outline	
<b>2 THERAPEUTIC PROSTATE CANCER INTERVENTIONS: QUANTIFICATION OF PUBIC ARCH INTERFERENCE AND NEEDLE POSITIONING ERRORS</b>	<b>13</b>
2.1 Introduction	
2.1.1 Background	
2.1.2 Hazards in needle positioning	
2.2 Literature search method	
2.2.1 Scientific literature search	
2.2.2 Eligibility criteria	
2.2.3 Literature search results	
2.3 Results	
2.3.1 Quantification of hazards	
2.3.2 Clinical guidelines	
2.4 Discussion	
2.4.1 Main findings	
2.4.2 Limitations	
2.4.3 Solution strategies	
2.4.4 Recommendations	
2.5 Conclusion	
<b>3 OVERCOMING PUBIC ARCH INTERFERENCE IN PROSTATE BRACHY THERAPY USING STEERABLE NEEDLES</b>	<b>39</b>
3.1 Purpose	
3.2 Materials and methods	
3.2.1 Patients	
3.2.2 Segmentation	
3.2.3 Anatomical rotation	
3.2.4 Overcoming pubic arch interference	
3.3 Results	
3.3.1 Pubic arch interference	
3.3.2 Needle steering	
3.4 Discussion	
3.5 Conclusion	

<b>4</b>	<b>AXIALLY RIGID STEERABLE NEEDLE WITH COMPLIANT ACTIVE TIP CONTROL</b>	<b>49</b>
	4.1 Introduction	
	4.2 Needle design	
	4.3 Computational simulation	
	4.3.1 Finite element model	
	4.3.2 Finite element analysis	
	4.4 Experimental evaluation	
	4.4.1 Experiment 1 – Fixed-bent needle steering	
	4.4.2 Experiment 2 – Clinical use case: active needle tip steering in prostate tissue	
	4.4.3 Experiment 3 – Active needle tip steering in ex-vivo tissue	
	4.5 Discussion	
	4.6 Conclusion	
<b>5</b>	<b>DOSIMETRIC BENEFITS AND PRECLINICAL PERFORMANCE OF STEERABLE NEEDLES IN HIGH-DOSE-RATE PROSTATE BRACHY THERAPY</b>	<b>69</b>
	5.1 Introduction	
	5.2 Materials and Methods	
	5.2.1 Study set-up	
	5.2.2 Treatment planning study	
	5.2.3 Implantation study	
	5.3 Results	
	5.4 Discussion	
	5.5 Conclusion	
<b>6</b>	<b>TOWARDS THE FIRST IN HUMAN TRIAL</b>	<b>83</b>
	6.1 Introduction	
	6.2 Investigational Medical Device Dossier (IMDD)	
	6.3 Clinical research protocol	
	6.4 Conclusion	
<b>7</b>	<b>MR-GUIDED HDR PROSTATE BRACHY THERAPY WITH TELEOPERATED STEERABLE NEEDLES</b>	<b>101</b>
	7.1 Introduction	
	7.2 Materials and Methods	
	7.2.1 System components	
	7.2.2 Control and communication	
	7.2.3 Experimental set-up	
	7.2.4 Prostate phantom	
	7.2.5 Experimental protocol	
	7.2.6 Data acquisition and analysis	
	7.3 Results	
	7.4 Discussion	
	7.5 Conclusions	

<b>8</b>	<b>STEERING MECHANISMS FOR PROSTATE AND BRAIN BRACHYTHERAPY</b>	<b>115</b>
	8.1 Introduction	
	8.2 Pull-push mechanism	
	8.2.1 Design	
	8.2.2 Summary of evaluation	
	8.3 Pre-bent tip	
	8.3.1 Design	
	8.3.2 Summary of evaluation	
	8.4 Discussion	
<b>9</b>	<b>FINAL DISCUSSION</b>	<b>127</b>
	9.1 Synopsis	
	9.2 Main findings	
	9.3 Active steerable needle as the solution!	
	9.4 Finding balance	
	9.5 Limitations	
	9.6 From innovation towards implementation	
	9.7 Future perspectives and other applications	
	9.8 Conclusion	
	<b>DANKWOORD</b>	<b>135</b>
	<b>SCIENTIFIC OUTPUT</b>	<b>137</b>
	<b>CURRICULUM VITAE</b>	<b>139</b>



# SUMMARY

Brachytherapy (BT) is a safe and effective technique to treat prostate cancer that has not spread outside the prostate gland (localised prostate cancer). Nonetheless, in current clinical practice hazards can arise in positioning the BT needles in the prostate for the purpose of irradiation. Intermediate structures can block access to the prostate and needle-tissue interactions can result in unexpected deflection of the needle inserted. These situations are undesirable because they lead to insufficient radiation of the prostate, potentially reducing treatment outcomes or resulting in patients being excluded from this treatment. Various techniques have been proposed in the literature to mitigate these hazards, of which actively steerable needles are considered very promising. However, manufacturing and cleaning such designs is often complex, while the low rigidity of the needles limits control and increases the risk of buckling when penetrating stiffer tissues such as the prostate. These factors have made implementation in BT protocols challenging.

A unique steering technique is proposed in this thesis that aims to provide improved flexibility in needle positioning while preserving high needle rigidity. This design solution will enable adaptive tip steering to control the unexpected deflections in tissue and create controlled curved needle trajectories to circumvent intermediate structures. Our investigation focuses on determining if our solution can facilitate the use of high-dose-rate (HDR) BT for a wider range of patients. Furthermore, we explore two other steering techniques for BT of prostate and brain cancers.

The hazards in literature were studied to define the requirements for the proposed steering solution, focusing on: (1) limitations in accessing the prostate gland due to interference from the pelvic bone, commonly referred to as pubic arch interference (PAI), and (2) errors in needle positioning. The level of PAI has been quantified to determine the magnitude of steering required and clinical guidelines gave us insight into the limits of the maximum allowable needle positioning error. In addition, datasets of patients with a large prostate volume have been analysed because this group of patients is traditionally expected to be at higher risk of PAI. These patients are frequently rejected in advance from undergoing BT. Contrary to the probability reported in literature, we found no clear relation between prostate volume and PAI. Our analysis showed that the level of PAI varied between patients ranging from no restriction to a significant level of access limitation. This variation implies that the current approach may exclude patients who could potentially be eligible, resulting in false positive outcomes. The findings of this study encouraged the more intraoperative approach with increased flexibility in needle positioning provided by our steering solution.

Prototypes of the needle design have been developed and tested in phantoms and *ex-vivo* tissue. Results showed that the steerable needle has similar targeting accuracy as the conventional rigid HDR BT needle, while adding the ability to insert the needle along a curved trajectory. A preclinical validation test was performed in the clinical setting by experienced physicians in the field of BT with the steerable needles and a developed prostate phantom. The planning of curved trajectories to circumvent the pubic arch was easily accomplished, and the implantation of steerable needles yielded successful results. There was an excellent consistency observed between the pre-, and post-implant treatment plans. This experiment provided compelling evidence that steerable needles can effectively achieve a highly conformal dose distribution in the prostate.

We completed all the necessary steps to conduct the first in human trial using this non CE-marked medical device. We compiled the Investigational Medical Device Dossier (IMDD) in accordance with the Medical Device Regulation 2017/745 (MDR) to ensure the safe application of the steerable needle in human patients.



This thesis presents a unique steerable needle that is ready for clinical investigation, with experiments and geometric and dosimetric analyses demonstrating the added value of this instrument in BT approaches. The design solution provides the physician improved control and flexibility in needle positioning to ensure a more intraoperative and patient-specific approach. Consequently, this breakthrough enables HDR BT as a treatment option for prostate cancer patients that are currently considered non-eligible because of a large prostate and/or PAI. Simple adjustments to the design parameters allow the steering principle to be used for other medical applications that may benefit from steerability.

# SAMENVATTING

Brachytherapie (BT) is een veilige en effectieve techniek om niet-uitgezaaide prostaatkanker te behandelen (lokale prostaatkanker). In de huidige klinische praktijk komen echter toch geregeld problemen voor bij het plaatsen van de BT-naalden in de prostaat ten behoeve van de daaropvolgende bestraling. Tussengelegen structuren kunnen de toegang tot de prostaat blokkeren, terwijl naald-weefsel interacties een onverwachte afbuiging van de naald kunnen veroorzaken. Deze situaties zijn ongewenst, aangezien ze kunnen leiden tot onvoldoende bestraling van de prostaat. Dit kan resulteren in een minder effectieve behandeling of kan zelfs leiden tot de exclusie van patiënten. In de literatuur zijn er verschillende technieken gepresenteerd om deze gevaren te mitigeren. Een actief stuurbare naald wordt hierbij als veelbelovend concept beschouwd. Het vervaardigen en reinigen van dergelijke ontwerpen is echter vaak complex, terwijl de lage rigiditeit van de naalden de controle kan beperken en het risico op knikken vergroot tijdens het penetreren van stijvere weefsels zoals de prostaat. Deze factoren zorgden er tot op heden voor dat implementatie in BT-protocollen een uitdaging was.

In dit proefschrift wordt een unieke stuurtechniek voorgesteld waarmee flexibiliteit bij het positioneren van BT-naalden verbeterd zou kunnen worden, terwijl naaldrigiditeit behouden blijft. Met behulp van actieve sturing aan de tip van de naald kunnen onverwachte afbuigingen in het weefsel beheerst worden en kunnen er gecontroleerde kromme naaldtrajecten worden gecreëerd om tussengelegen structuren te omzeilen. In dit onderzoek evalueren wij of deze oplossing ervoor kan zorgen dat een grotere groep prostaatkankerpatiënten behandeld zou kunnen worden door middel van high-dose-rate (HDR) BT. Daarnaast onderzoeken wij twee andere sturingstechnieken voor BT in de prostaat en hersenen.

Om de criteria voor naaldsturing bij prostaat BT te definiëren, zijn de potentiële gevaren met betrekking tot de plaatsing van naalden onderzocht, met speciale aandacht voor (1) beperkingen bij het bereiken van de prostaatklier doordat het schaambeentje in de weg ligt, gewoonlijk aangeduid als pubic arch interferentie (PAI), en (2) fouten bij het positioneren van de naald. De mate van PAI is gekwantificeerd om de benodigde sturing van de naald te bepalen, terwijl momenteel gehanteerde klinische richtlijnen inzicht gaven in de maximaal toegestane fout bij het positioneren van een naald. Daarnaast zijn er datasets van patiënten met een groot prostaatvolume geanalyseerd, omdat normaliter verwacht wordt dat deze groep patiënten een grotere kans op PAI heeft. Daarom komt het vaak voor dat deze patiënten op voorhand al niet in aanmerking komen voor BT. In tegenstelling tot de relatie die in de literatuur is gerapporteerd, vonden wij geen duidelijk verband tussen prostaatvolume en PAI. Onze analyse toonde aan dat het niveau van PAI tussen patiënten varieert van geen PAI tot een significante hoeveelheid PAI. Deze variatie impliceert dat de huidige benadering mogelijk patiënten uitsluit die potentieel in aanmerking zouden kunnen komen voor een behandeling met BT. De bevindingen van dit onderzoek pleiten daarom voor een meer intra-operatieve benadering met een grotere flexibiliteit bij het positioneren van de naalden, hetgeen door onze stuurtechniek kan worden geboden.

Prototypes van het naaldontwerp zijn ontwikkeld en vervolgens getest in fantomen en *ex-vivo* weefsel. De resultaten toonden aan dat de stuurbare naald een vergelijkbare plaatsingsnauwkeurigheid heeft als de conventionele rigide HDR BT-naald, terwijl de stuurbare naald ook langs een gebogen traject ingebracht kan worden. Tevens is een preklinische validatietest van de stuurbare naalden uitgevoerd in de conventionele BT-setting met een ontwikkeld prostaatfantom door ervaren klinici op het gebied van BT. Het plannen van de gebogen trajecten om het schaambeentje te omzeilen was eenvoudig te realiseren en de stuurbare naalden werden succesvol ingebracht. Het resultaat was een uitstekende consistentie tussen de behandelplannen voorafgaand aan en na afloop van de naaldimplantaties. Dit experiment leverde overtuigend bewijs dat stuurbare naalden een zeer conforme dosisverdeling in de prostaat kunnen bereiken.

In dit onderzoek zijn alle noodzakelijke stappen voltooid om in de toekomst klinische testen uit te voeren met dit medische instrument, waarbij CE-certificering nog niet aanwezig is. Wij hebben het Investigational Medical Device Dossier (IMDD) samengesteld in overeenstemming met de Medical Device Regulation 2017/745 (MDR) om de veilige toepassing van deze stuurbare naald bij menselijke patiënten te waarborgen.

Dit proefschrift presenteert een unieke stuurbare naald die gereed is voor klinisch onderzoek. De experimenten, geometrische analyse en de dosimetrische analyse tonen de meerwaarde van dit instrument aan voor HDR prostaat BT. Deze ontwerpoplossing biedt de clinicus een verbeterde controle en flexibiliteit bij het plaatsen van de naald en garandeert een meer intra-operatieve en patiënt-specifieke aanpak. Hierdoor kan deze doorbraak ervoor zorgen dat HDR BT een mogelijke behandeloptie wordt voor prostaatankerpatiënten die momenteel niet in aanmerking komen vanwege een te grote prostaat en/of PAI. Door middel van eenvoudige aanpassingen aan de ontwerpparameters kan dit sturingsprincipe ook voor andere medische toepassingen worden gebruikt die mogelijk baat hebben bij de stuurbaarheid van een instrument.

# 1

Introduction

## 1.1 BACKGROUND

Worldwide, cancer is a serious health problem with an estimated amount of 19.3 million new cases presented every year and 10.0 million deaths in 2020 [1]. This destructive disease, characterised by uncontrolled cell differentiation, is rated second in leading causes of death in the United States [2]. Current possible cancer treatments include surgery, medicines and radiation therapy to kill or stunt the growth of malignant tumour cells. One type of radiation therapy can be applied internally, known as brachytherapy (BT). This modality has gained wide acceptance as a treatment option for organ-confined tumours. The success of BT has increased with the emerging imaging modalities, technological advances and individual treatment planning possibilities.

## 1.2 BRACHYTHERAPY

BT is a minimally invasive procedure that is well-suited for treating various tumour sites in the body, including the breast, cervix and prostate. The term "*brachy*" is derived from the Greek word for "*short*", referring to the fact that radioactive sources are positioned inside or in the vicinity of the area that requires treatment. The sources are delivered through needles and left *in situ* for a specified amount of time to deliver the required doses of radiation, depending on the cancer type, the specific BT technique and the treatment plan. In interstitial BT, the needles are inserted through the skin and into soft tissue, guided towards the target volume using imaging techniques such as ultrasound (US), magnetic resonance imaging (MRI), or computed tomography (CT). Because each source contribution has a heterogeneous dose distribution, the dose around the needles is much higher compared to the reference dose. The cumulative dose, derived from the individual doses per needle, creates a distribution within the target volume which is prescribed to isodoses. Consequently, careful choice of the needle positions is crucial to optimally irradiate the target volume while minimising exposure to surrounding healthy tissues and organs-at-risk (OARs). Figure 1.1 shows the specificity of BT in terms of dose distribution in the prostate in comparison with external beam radiation therapy (EBRT).

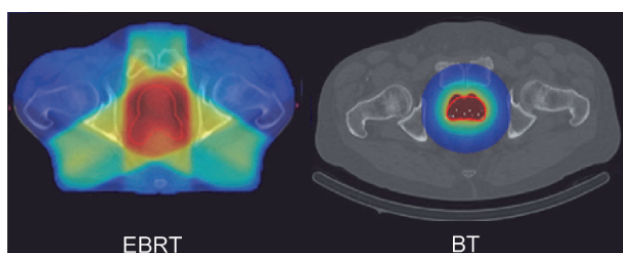


**Figure 1.1 – Example of dose distribution for a prostate treatment plan with external beam radiation therapy (EBRT) and brachytherapy (BT).** The plan is calculated on the same patient. The red surface represents the high-dose regions, the yellow surface the intermediate-high-dose regions, the dark blue surface the low-dose regions, and the azure blue surface the intermediate-dose regions (adapted from [4]).

## 1.3 PROSTATE BRACHYTHERAPY

Prostate cancer is the second most diagnosed cancer in men with an estimated 375,300 deaths worldwide in 2020 and is considered the first cause of death in 48 out of 185 countries [3]. Generally, prostate cancer is detected in an early and localised stage, with no spread outside the prostate gland, and curative treatments such as radical prostatectomy (RP), EBRT or BT can be performed. The choice of treatment depends on several factors, such as comorbidities, type and stage of the cancer, patient's anatomy and preference.

A comparative analysis of prostate cancer treatments showed that BT, as monotherapy or as boost in combination with EBRT, is very successful and appears superior to RP or EBRT alone as indicated in Figure 1.2 [4]. Considering these findings, this safe and effective treatment should be made available as treatment option for as many prostate cancer patients as possible [5].

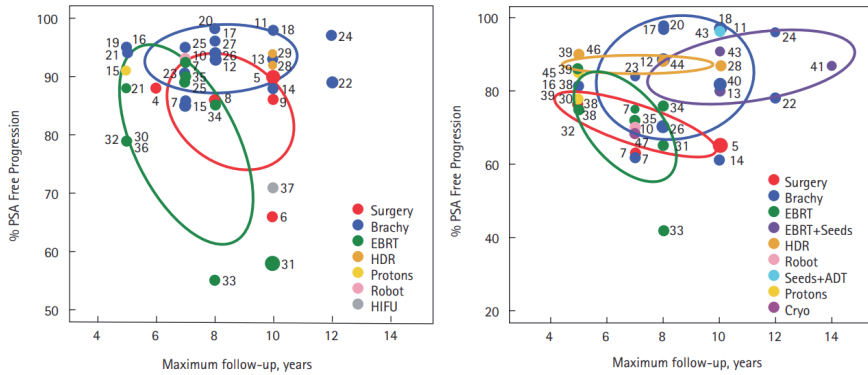


**Figure 1.2 - Percentage prostate-specific antigen (PSA)-free progression at maximum follow-up for patients with (left) low-risk and (right) intermediate-risk prostate cancer treated with a range of therapeutic options.** Brachy = brachytherapy; HDR = high-dose-rate; ADT = androgen deprivation therapy; Cryo = cryotherapy; HIFU = high intensity focused ultrasound (retrieved from [4]).

BT employs various techniques for irradiating the prostate using needles and transrectal ultrasound (TRUS) for guidance. These techniques include low-dose-rate (LDR), high-dose-rate (HDR), and pulsed-dose-rate (PDR), of which LDR and HDR BT are performed most frequently. LDR BT involves permanent placement of radioactive seeds, such as iodine-125 or palladium-103, directly into the target volume. The seeds are implanted using hollow needles with either loose or stranded seeds, in which multiple seeds and spacers are interlinked. The implanted seeds deliver a low dose of radiation over a period of several weeks or months. HDR BT is characterised by the use of a high dose of radiation, such as iridium-192, for several minutes. The conventional HDR BT needles comprise of an inner and outer needle. After the insertion of the HDR BT needles, the inner needles are retracted while the outer needles are left *in situ*. This creates multiple channels intended for remote afterloading with a source dwell. On-line optimisation of the dose distribution is possible by optimisation of the time the source spends at each dwell positions. Figure 1.3 shows a typical set-up for conventional prostate BT. To ensure an optimal distribution of needles within the target volume, a transperineal template with evenly spaced holes, positioned 5 mm apart, is utilised. This template enables the needles to be inserted in a straight and parallel manner.

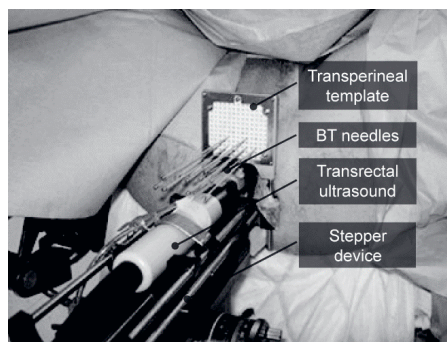


**Figure 1.3 - Conventional prostate BT set-up.** The set-up includes BT needles and the stepper device including the transrectal ultrasound probe and the transperineal template (adapted from [6]).

## 1.4 HAZARDS IN PROSTATE BRACHYTHERAPY

BT improves the lives of many prostate cancer patients (Figure 1.2). Still, insufficient spatial distribution of the needles (i.e., total needle geometry) inside the target volume can occur, caused by factors such as inaccessibility of the prostate and needle targeting errors. These factors can influence the efficiency and efficacy of the procedure; non-conformity to the treatment plan may result in underdosage of the tumour or overdosage of the OARs. According to the research of Zelefsky et al. it was estimated that 15 to 20% of patients obtained a suboptimal dose coverage due to underdosing the target volume or overdosing the rectum or urethra [7].

The conventional BT needle lacks adequate adaptability to effectively address these hazards once it has been inserted into the tissue. HDR BT needles are rigid and bound to linear trajectories, while LDR BT needles are also rigid but feature a bevelled tip. The asymmetric forces on the tip can offer some degree of control during the insertion, but steering is challenging as it depends on the resistance of the tissue it interacts with. In practice, achieving the intended needle geometry in BT procedures may require multiple attempts at needle insertion or improvising with *ad hoc* solutions. These actions are often considered suboptimal as they may cause additional tissue damage, require adaptations to the clinical set-up or workflow and do not necessarily achieve the intended needle geometry.

If an insufficient total needle geometry is expected prior to the procedure because of inaccessibility of the target volume, the patient is generally considered non-eligible for BT. The patient is recommended a course of androgen deprivation therapy (ADT) to downsize the prostate gland, although this approach is associated with negative side effects. Alternatively, another treatment, such as EBRT, may be considered.

## 1.5 STEERABLE NEEDLES AS A SOLUTION?

To minimise both access restriction to the target volume and needle targeting errors, it is necessary to enhance flexibility in needle positioning. This thesis proposes various solution strategies to mitigate these hazards. The approach that we explore is the use of active steerable needles, as previous research has demonstrated their potential to significantly improve BT outcomes by ensuring adherence to the treatment plan and enhancing accessibility of the prostate [8,9]. Such steerable needles can modify needle-tissue interactions during the insertion to control the needle trajectory and accurately reach the target site. In addition, these needles can be used to circumvent anatomical structures and sensitive tissues to obtain an adequate total needle geometry.

Various active steering techniques have been proposed in literature, such as cable-driven instruments or actuated needle tips (Figure 1.4) [9–17]. Only three active steerable instruments have been commercialised which are all cable-driven and induce pivoting of the needle tip by cable pulling [12,15,17]. These designs have low axial and flexural rigidity, which can hinder precise control and increases the risk of buckling when penetrating stiffer tissues and membranes [18]. Furthermore, the fabrication process for most steerable instruments is complex, while subsequent cleaning, sterilisation and implementation into the BT set-up can pose additional challenges. Therefore, the development and utilisation of steerable needles require careful consideration of their mechanical properties, manufacturing complexity, and the practical implementation within the BT workflow.

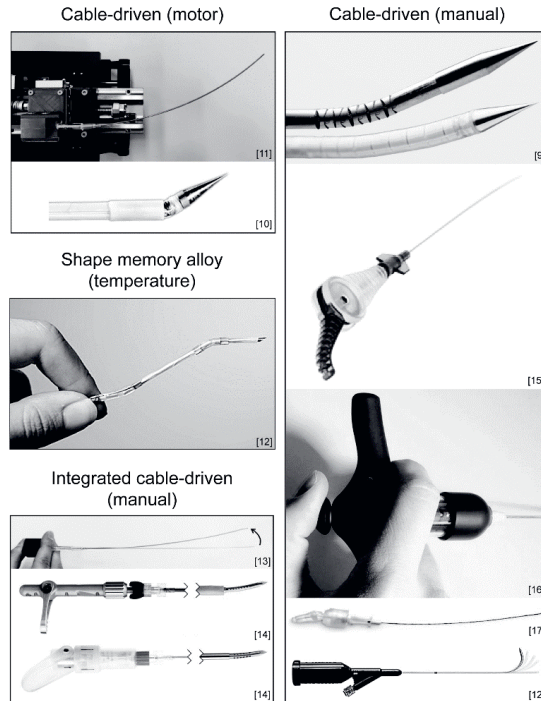


**Figure 1.4 – State-of-the-art of active steerable needles.** The steerable needles are divided on the basis of the steering control principle. The method to control the steering is indicated between parentheses (retrieved from [9–17]).

## 1.6 AIMS OF THIS THESIS

The associated aims of this thesis are to:

- 1) demonstrate a unique steerable needle design for HDR prostate BT (*technical innovation*),

A steering control principle is presented and is explored in the context of the clinical application of HDR prostate BT. The purpose of the design is to introduce flexibility in needle positioning, while maintaining high axial and flexural rigidity. The balance between flexibility and rigidity should ensure controllability during the insertion, while minimising the risk for buckling. No major changes to the current clinical workflow and set-up shall be introduced.

The prostate, being a deeply situated organ with high tissue stiffness, poses challenges during needle insertion. Tissue resistance, calcifications, and tissue deformation can cause undesired deflection of the needle, resulting in deviations from the planned trajectory and treatment plan. To address these issues, the steerable needle should enable active control of the needle tip in multiple planes, allowing for precise adjustment to mitigate these perturbations and ensure accurate targeting. Furthermore, the steerable needle should facilitate curved trajectories with varying radii to navigate around intermediate structures such as the pubic arch.



By incorporating this novel steering control principle, the goal is to enhance intraoperative needle maneuverability and improve targeting accuracy in HDR prostate BT without disrupting the established clinical workflow and set-up.

- 2) evaluate if the developed steerable needle can enable HDR prostate BT for a patient population, which is currently considered non-eligible (*clinical application*).

In current clinical practice with rigid BT needles, the pubic arch can block the access to the prostate gland hampering an adequate dose distribution. This obstruction, known as pubic arch interference (PAI), poses a challenge in delivering effective treatment and has led to the exclusion of patients from BT protocols.

The introduction of a steerable needle which allows for curved trajectories holds the potential to address this issue by providing access to the previously inaccessible prostate volume affected by PAI. This innovation could open up the possibility of offering BT as a treatment option for patients with larger prostates and/or PAI.

This thesis introduces a novel steering technique and explores the clinical application of the steerable needle in the context of HDR prostate BT. The outcomes of this research hold potential benefits for both medical specialists and engineers. The insights gained through this dissertation can contribute to the knowledge and expertise of professionals and the outcomes will be in direct interest for treatment of prostate cancer patients.

### 1.7 THESIS OUTLINE

The outline of this thesis is presented in Figure 1.5. Throughout Chapter 2 to 5 the design phases for the development and validation of our design solution are covered. In Chapter 2, we explore and quantify the hazards related to needle positioning in prostate BT. We evaluate the clinical guidelines which are used in current practice and we present solutions strategies to mitigate the hazards. This will provide an understanding of the clinical need and relevant design requirements. In Chapter 3, we evaluate if the clinical guidelines related to prostate volume and prostate accessibility are sufficient, and we elaborate on the steerable needle as a solution strategy. Datasets of patients with a large prostate are analysed to geometrically determine the required amount of needle steering for the proposed instrument. We virtually apply the steering technique to 27 patients using their diagnostic magnetic resonance (MR) scans. Chapter 4 shows the steering principle of the proposed steerable needle: the bendable lever. A manufactured prototype is presented and tests are performed in phantoms and *ex-vivo* tissue to verify, among other things, the steerability and targeting accuracy of the instrument. Validation of the steerable needle in the clinical setting is described in Chapter 5. Treatment planning and implantation studies are performed by experienced physicians in the field of BT, with the steerable needle and a developed prostate phantom. Chapter 6 describes the route towards the first in human trial with the steerable needle (Chapter 4). We show an example how to comply with the Medical Device Regulations 2017/745 if a medical device is intended for clinical investigation.

Chapter 7 and 8 have a more explorative nature. We investigate the feasibility of robotic control of the developed steerable needle (Chapter 4) using MRI for guidance in Chapter 7. In Chapter 8, we elaborate on the use of two other steering mechanisms for different medical applications: the pull-push mechanism for low-dose-rate (LDR) prostate BT and the pre-bent needle tip for micro-brachytherapy (micro-BT) of the brain. Chapters 2 to 5 and Chapter 7 are independent articles, which have been published in or submitted to scientific journals. The content of individual chapters can therefore be partly overlapping. Chapter 6 is a monograph which is not intended for publication. Chapter 8 includes two summaries of which the article related to micro-BT is published [19].

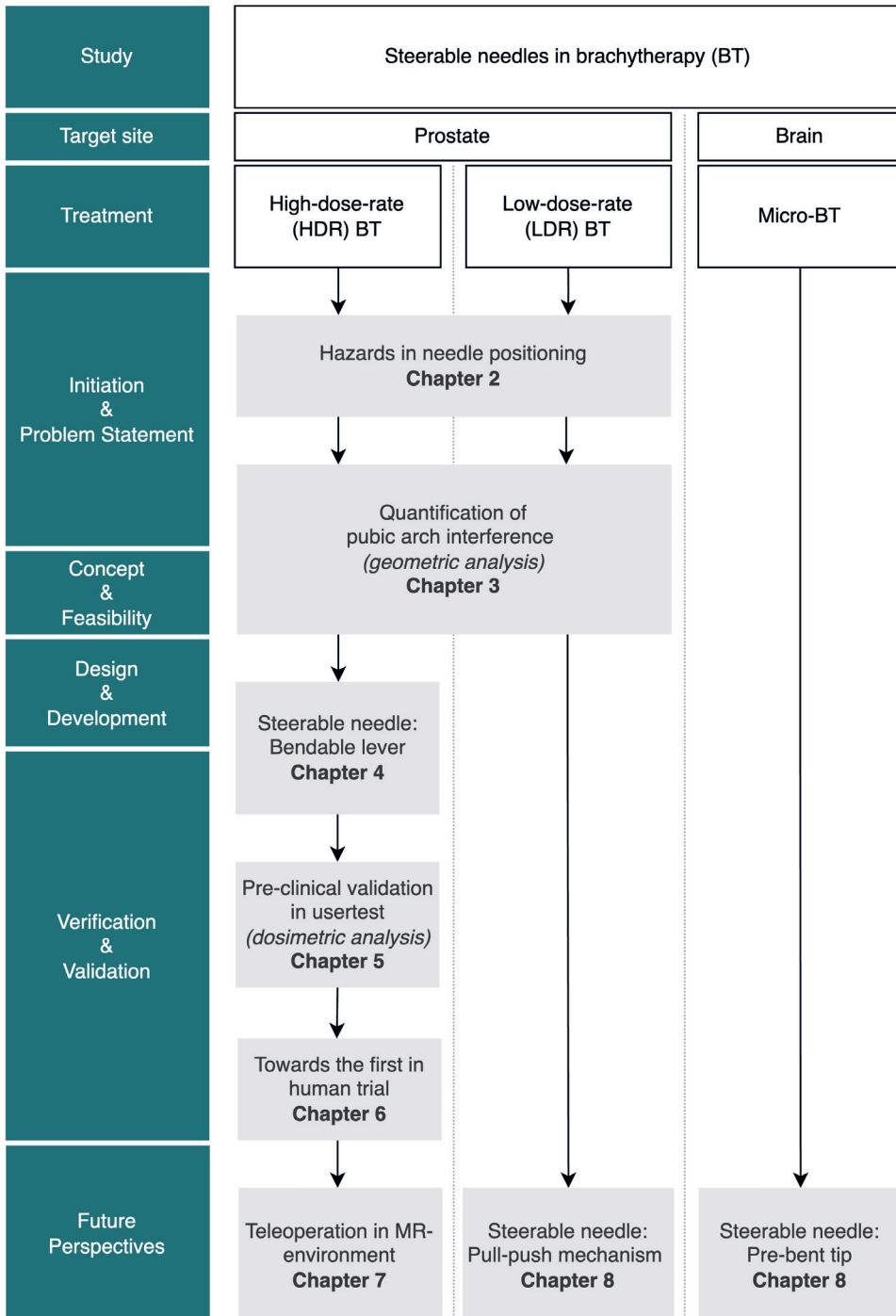


**Figure 1.5 – Outline of this thesis.** The green boxes include the design phases for a medical device and additional information. The white and grey boxes state the subjects and the chapters of this thesis, respectively.

## REFERENCES

- [1] Sung H, Ferlay J, Siegel RL, Laversanne M, Soerjomataram I, Jemal A, et al. Global Cancer Statistics 2020: GLOBOCAN Estimates of Incidence and Mortality Worldwide for 36 Cancers in 185 Countries. *CA Cancer J Clin* 2021;71:209–49. <https://doi.org/10.3322/caac.21660>.
- [2] Siegel RL, Miller KD, Wagle NS, Jemal A. Cancer statistics, 2023. *CA Cancer J Clin* 2023;73:17–48. <https://doi.org/10.3322/caac.21763>.
- [3] Gandaglia G, Leni R, Bray F, Fleshner N, Freedland SJ, Kibel A, et al. Epidemiology and Prevention of Prostate Cancer. *Eur Urol Oncol* 2021;4:877–92. <https://doi.org/10.1016/j.euo.2021.09.006>.
- [4] Grimm P, Billiet I, Bostwick D, Dicker AP, Frank S, Immerzeel J, et al. Comparative analysis of prostate-specific antigen free survival outcomes for patients with low, intermediate and high risk prostate cancer treatment by radical therapy. Results from the Prostate Cancer Results Study Group. *BJU Int* 2012;109:22–9. <https://doi.org/10.1111/j.1464-410X.2011.10827.x>.
- [5] Demanes DJ, Rodriguez RR, Altieri GA. High dose rate prostate brachytherapy: the California Endocurietherapy (CET) Method. *Radiother Oncol* 2000;57:289–96.
- [6] Al-Saihi O, Mitra A, Payne H. Challenge of dose escalation in locally advanced unfavourable prostate cancer using HDR brachytherapy. *Prostate Cancer Prostatic Dis* 2006;9:370–3. <https://doi.org/10.1038/sj.pcan.4500893>.
- [7] Zelefsky MJ, Cohen GN, Taggar AS, Kollmeier M, McBride S, Mageras G, et al. Real-time intraoperative evaluation of implant quality and dose correction during prostate brachytherapy consistently improves target coverage using a novel image fusion and optimization program. *Pr Radiat Oncol* 2017;7:319–24. <https://doi.org/10.1016/j.ppro.2017.01.009>.
- [8] Khadem M, Rossa C, Usmani N, Sloboda RS, Tavakoli M. Geometric control of 3D needle steering in soft-tissue. *Automatica* 2019;101:36–43. <https://doi.org/10.1016/j.automatica.2018.11.018>.
- [9] De Jong TL, van de Berg NJ, Tas L, Moelker A, Dankelman J, van den Dobbelsteen JJ. Needle placement errors: Do we need steerable needles in interventional radiology? *Med Devices Evid Res* 2018;11:259–65. <https://doi.org/10.2147/MDER.S160444>.
- [10] Van de Berg NJ, van Gerwen DJ, Dankelman J, van den Dobbelsteen JJ. Design Choices in Needle Steering - A Review. *IEEE/ASME Trans Mechatronics* 2015;20:2172–83. <https://doi.org/10.1109/TMECH.2014.2365999>.
- [11] Yamada A, Naka S, Nitta N, Morikawa S, Tani T. A Loop-Shaped Flexible Mechanism for Robotic Needle Steering. *IEEE Robot Autom Lett* 2018;3:648–55. <https://doi.org/10.1109/LRA.2017.2779273>.
- [12] Scali M, Pusch TP, Breedveld P, Dodou D. Needle-like instruments for steering through solid organs: A review of the scientific and patent literature. *Proc Inst Mech Eng Part H J Eng Med* 2017;231:250–65. <https://doi.org/10.1177/0954411916672149>.
- [13] Duong CT, Le CD, Nguyen DN. Effect of Surface Roughness on Friction of CoCrMo-on-UHMWPE Bearing in Total Hip Arthroplasty Under Lubrication of Bovine Serum Albumin. vol. 69. 2020. [https://doi.org/10.1007/978-981-13-5859-3\\_45](https://doi.org/10.1007/978-981-13-5859-3_45).
- [14] Van de Berg NJ, Meeuwse FC, Doukas M, Kronreif G, Moelker A, van den Dobbelsteen JJ. Steerable needles for radio-frequency ablation in cirrhotic livers. *Sci Rep* 2021;11. <https://doi.org/10.1038/s41598-020-77869-3>.
- [15] AprioMed, Steerable FNA biopsy needle 21G. <https://apriomed.com/products/morrison-steerable-needle/> (accessed 13 July 2023).
- [16] Van de Berg NJ, Dankelman J, van den Dobbelsteen JJ. Endpoint Accuracy in Manual Control of a Steerable Needle. *J Vasc Interv Radiol* 2017;28:276–283.e2. <https://doi.org/10.1016/j.jvir.2016.07.018>.
- [17] Kratchman LB, Rahman MM, Saunders JR, Swaney PJ, Webster III RJ. Toward robotic needle steering in lung biopsy: a tendon-actuated approach. *Med Imaging 2011 Vis Image-Guided Procecd Model* 2011;7964:796411. <https://doi.org/10.1117/12.878792>.
- [18] Crossley D. Sharp turning steerable needle - Patent WO 2018/067808 AI. Patent 2018.
- [19] De Vries M, Klaassen NJM, Morsink NC, van Nimwegen SA, Nijssen JFW, van den Dobbelsteen JJ. Dedicated holmium microsphere administration device for MRI-guided interstitial brain microbrachytherapy. *Med Eng Phys* 2021;96:13–21. <https://doi.org/10.1016/j.medengphy.2021.07.009>.

# 2

## Therapeutic prostate cancer interventions: quantification of pubic arch interference and needle positioning errors

Martijn de Vries\*, Jette Bloemberg\*, Luigi A.M.J.G. van Riel, Theo M. de Reijke, Aimée Sakes, Paul Breedveld, John J. van den Dobbelsteen

*Under review (2023)*

\* Authors contributed equally to the realisation of the paper

### **ABSTRACT**

Needle positioning in line with the pre-planned needle positions is crucial in prostate cancer interventions and becomes more critical with the advance of more targeted therapies. This study focuses on the quantification of and current guidelines on the hazards related to needle positioning in prostate cancer treatment, in particular (1) access restrictions to the prostate gland by the pubic arch, so-called pubic arch interference (PAI) and (2) needle positioning errors. Next, we propose solution strategies to mitigate these hazards. The literature search in the Embase, Medline ALL, Web of Science Core Collection, and Cochrane Central Register of Controlled Trials databases resulted in 50 included articles. PAI was reported in a significant proportion of patients with various prostate volumes. The level of reported PAI varied between 0 and 22.3 mm, depending on the patient's position and the measuring method. Needle positioning errors were subdivided into misplacement and displacement. Low-dose-rate brachytherapy induced the largest reported misplacement errors (up to 10 mm), especially in the cranio-caudal direction and the largest displacement errors were reported for high-dose-rate brachytherapy in the cranio-caudal direction (up to 47 mm), generally increasing over time. Current clinical guidelines related to prostate volume, needle positioning accuracy, and maximum allowable PAI are ambiguous and compliance in the clinical setting differs between institutions. Solutions, such as steerable needles, assist in the mitigation of the hazards and potentially allow the physician to proceed with the procedure.

## 2.1 INTRODUCTION

### 2.1.1 Background

Prostate cancer is the second most-diagnosed cancer in men and the fifth leading cause of cancer-related deaths worldwide in 2020 [1]. When detected in an early and localised stage, treatments such as radical prostatectomy, external beam radiation therapy or brachytherapy can be performed. Brachytherapy modalities include low-dose-rate brachytherapy (LDR BT), high-dose-rate brachytherapy (HDR BT), and pulsed-dose-rate brachytherapy (PDR BT), in which radioactive sources or catheters are placed in the prostate for irradiation. These techniques are often employed as whole-gland monotherapy and provide high rates of oncological control. This is at risk of negative side effects for the patient, such as irritative micturition, urinary incontinence, erectile dysfunction, and rectal toxicity, thereby lowering the quality of life (QOL) [2, 3].

Over the past decade, a trend toward focal (boost) therapies has been observed that can potentially minimise negative side effects [2, 3]. This method is a shift from whole-gland treatment to targeting the tumour, while sparing the surrounding healthy tissue, thereby preserving genitourinary and gastrointestinal function [4]. Brachytherapy can be applied as a focal (boost) therapy in which the tumour is irradiated with high dosages, whilst the remainder of the prostate gland is treated with a lower dose. Focal treatment modalities include e.g., brachytherapy, focal laser ablation (FLA), irreversible electroporation, cryotherapy, high-intensity focussed ultrasound, and photodynamic therapy. These are percutaneous procedures in which needles are guided through the perineal skin to reach the target volume for treatment. However, potential perturbations while passing intermediate structures may cause hazardous situations. This study provides an overview of the quantification of these hazards and the associated current guidelines, and solution strategies to mitigate these hazards.

### 2.1.2 Hazards in needle positioning

Two hazards, widely reported in literature, can hamper adequate needle positioning. First, the pubic arch can restrict access to the ventrolateral part of the prostate. This affects the total needle geometry (i.e., the spatial composition of all inserted needles) in the target volume [5] as depicted in Figure 2.1, assuming currently available, rigid needles are inserted parallel to each other in the horizontal direction. This phenomenon is known as pubic arch interference (PAI). Accessibility of all regions inside the target volume is a requirement in focal (boost) therapies and brachytherapy as whole-gland monotherapy to obtain homogeneity of the total needle geometry and to ensure an effective treatment [6]. The level of PAI indicates to what extent a homogeneous needle distribution can be achieved.

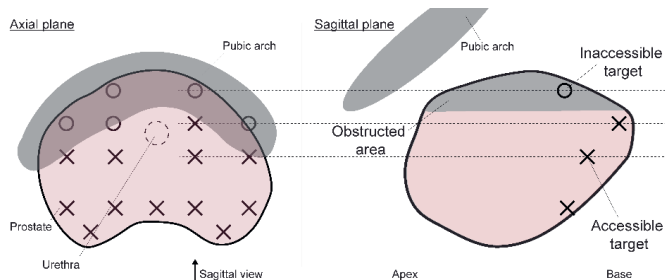


**Figure 2.1 - Schematic of total needle geometry in patients with pubic arch interference (PAI).** The planned total needle geometry, indicated in the axial plane, is based on the needle geometry of Mate et al. [7]. The pubic arch obstructs parts of the prostate resulting in a non-conformal total needle geometry, indicated by the light grey area in the sagittal plane, making accessible targets (X) inaccessible (O) using the transperineal approach with parallel horizontal trajectories (i.e., perpendicular to the transperineal template) using straight needle insertion.

Secondly, needle positioning errors can arise from misplacement (i.e., the needle is positioned in a location different from the planned location due to unwanted needle deflections [8]) or needle displacement (i.e., the needle is shifted to a different location after positioning). Erroneous individual needle positioning induces treatment of unintended areas (Figure 2.2), which might lead to under-treatment of tumour tissue or overtreatment of healthy tissue (e.g., urethra, bladder, rectum, and neurovascular bundle), leading to similar side effects as documented for whole-gland treatment modalities, such as irritative micturition, urinary incontinence, erectile dysfunction, and rectal toxicity, thereby lowering the QoL [2, 3].

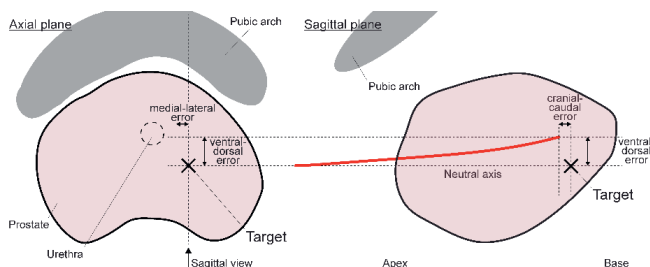


**Figure 2.2 - Schematic of individual needle positioning errors in the prostate.** The directions of the positioning error of the needle (red line) are shown in the axial and sagittal planes. The needle deviated from the neutral axis and did not reach the target (X).

In this study, the term ‘hazard’ is used to refer to potential sources of harm related to transperineal needle positioning. These hazards are (1) access restrictions to the prostate gland, i.e., PAI and (2) needle positioning errors. Insight into the quantification of these hazards and solution strategies to mitigate them can provide information about the impact of different hazards and may give clues about how to minimise these hazards. To our knowledge, a systematic overview of the scientific literature on the quantification of the hazards related to transperineal needle positioning in prostate cancer treatments and their corresponding guidelines is not yet available. Here we intend to fill this gap by providing a systematic overview of the quantification of these hazards. Furthermore, we propose solution strategies to mitigate these hazards. First, the scientific literature search method is described in Section 2. In Section 3, the hazards are quantified, the associated guidelines are described and clinical aspects are reported. Section 4 discusses solution strategies to mitigate the hazards, and Section 5 presents the conclusions of this study.

## 2.2 LITERATURE SEARCH METHOD

### 2.2.1 Scientific literature search

The literature search was executed using the Embase, Medline ALL, Web of Science Core Collection, and Cochrane Central Register of Controlled Trials databases and included journal articles and conference abstracts in the English language. We used tailored search terms for each database using thesaurus terms (MeSH). The search keywords of the queries were organised into three categories: (a) therapy (e.g., brachytherapy, ablation therapy, laser ablation), (b) target (e.g., prostate, prostate tumour), and (c) needles and challenges or hazards (e.g., needle, catheter, probe, pubic) (Figure 2.3). The publication year for the conference abstracts was limited to 2019 – 2022.

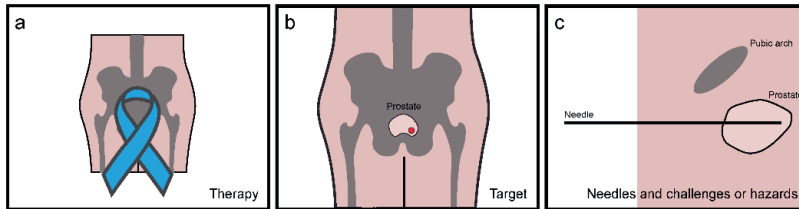


**Figure 2.3 - Visual representation of the search query.** Figures limit the search to (a) therapy (b) target site, and (c) needles and challenges or hazards.

### 2.2.2 Eligibility criteria

Throughout this review, the needle is defined as the device used to puncture tissues and position the energy or radiation source in the target volume. Only interventions were included with which prostate cancer can be treated locally via the transperineal pathway without resecting the prostate, excluding articles on diagnostics, treatment of benign tumours, (partial) resection of the prostate, and prostate volume determination. Needles that are used for the administration of systemic therapy, such as immunotherapy and chemotherapy, were excluded. Regarding the study conditions, only clinical studies were accepted, whereas preclinical, phantom, animal, and simulation studies were excluded. Furthermore, only studies focused on the quantitative assessment of needle positioning were accepted, excluding studies solely focused on needle design, planning, patient selection, physician learning curve, automated needle detection, functional or biological outcomes, hospitalisation time, and costs. Hazards unrelated to needle positioning were excluded, such as prostate movement due to bladder filling, brachytherapy seed migration, and inter-observer variability.

### 2.2.3 Literature search results

The search yielded 3309 articles (last update December 2022). Based on the eligibility criteria, the titles, abstracts, and full texts were checked subsequently. After full-text inspection, 50 articles were identified by M.V. and J.B., fulfilling all eligibility criteria (Figure 2.4).

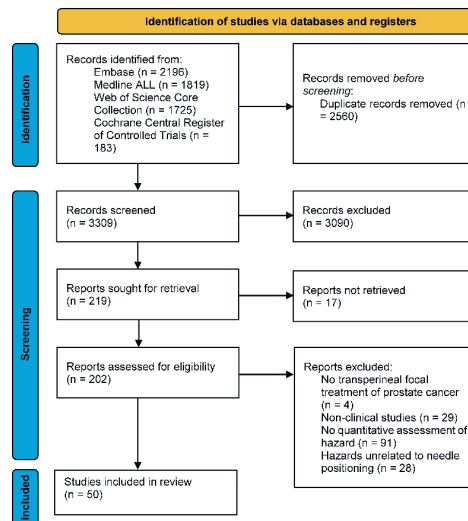


**Figure 2.4 - PRISMA flow diagram of the literature selection method.**



## 2.3 RESULTS

### 2.3.1 Quantification of hazards

#### *Pubic arch interference (PAI)*

PAI has been assessed in fifteen included studies, as shown in table 2.1. Eleven studies described the level of prostate obstruction by the pubic arch and fifteen studies reported the incidence of PAI for various prostate volumes. Sejpal et al. [9] researched the largest patient population, with 243 patients, and reported that 47 patients (19.3%) showed PAI during needle insertion.

PAI quantification is generally performed on transrectal ultrasound (TRUS)-computed tomography (CT) fusion imaging or magnetic resonance imaging (MRI) scans, with the patient in supine position, while needle implantation is performed under transrectal ultrasound (TRUS) guidance with the patient in dorsal lithotomy position. The patient's position significantly influenced the level of observed PAI, ranging from 0 mm, if total clearance between the pubic arch and the prostate was observed, to 22.3 mm [13]. Tinchet et al. [5] studied the level of PAI for seven patients after CT scans in both lithotomy and supine position. The authors reported that the patient's posture change from supine position to lithotomy position decreased the level of PAI by 5 mm [5]. Next to posture change, the used imaging modality also induced discrepancies. Martin et al. [10] assessed PAI on TRUS, CT, and MRI scans. They found a linear correlation between PAI on the CT and MRI scans with the patient in supine position, while 75% of patients had larger values for PAI on CT compared to MRI. They reported PAI on CT and MRI of  $2.9 \pm 0.6$  mm and  $2.0 \pm 0.6$  mm (average  $\pm$  standard error), respectively. PAI on the TRUS scans with the patient in lithotomy position was  $0.6 \pm 0.5$  mm, which was significantly different from both CT and MRI ( $p < 0.06$ ). Strang et al. [11] reported that nine patients appeared to have PAI on CT, while only four of these nine patients had PAI on TRUS. The change in patients' posture from supine to lithotomy position and imaging modality reduced obstruction by the pubic arch by 11.8 mm on average. In contrast, Wallner et al. [12] showed a decrease of only 0.4 mm.

**Table 2.1 – Overview of studies that evaluated pubic arch interference (PAI).** For each study, the following information is reported: the level of PAI [mm], percentage of patients with PAI [%], imaging modality and patient position used for the assessment of prostate volume, prostate volume [cc], treatment, and reference. Clearance between the pubic arch and the prostate is reported as 0 mm PAI.  $\bar{x}$  = median,  $\bar{x}$  = average  $\pm$  standard deviation, and (..) = range.

Level of PAI [mm]	Number of patients	Number of patients with PAI (%)	Imaging modality	Patient position	Prostate volume [cc]	Treatment	Authors (citation)	Year
$\bar{x} = 9.5 \pm 6.9$ (0 – 22.3)	27	85.2	MRI	Supine	$\bar{x} = 92.3 \pm 38.0$ (48.0 – 178.9)	HDR BT	De Vries et al. [13]	2022
(0 – 15.1)	40	25	MRI	Supine	$\bar{x} = 63.8 \pm 18.4$	LDR BT	Zheng et al. [14]	2019
$\bar{x} = 2.0 \pm 0.6$ (0 – 12.5)	41	80.5	MRI	Supine				
$\bar{x} = 2.9 \pm 0.6$ (0 – 12.5)	41	82.9	CT	Supine		LDR BT	Martin et al. [10]	2017
$\bar{x} = 0.6 \pm 0.5$ (0 – 4)	41	46.3	TRUS (5 mm)	Lithotomy	$\bar{x} = 32.6 \pm 2.3$			
(0 – > 5)	21	14.3	TRUS (5 mm)	Lithotomy	$\bar{x} = 28.5$ $\bar{x} = 28.1$ (17.6 – 42.2)	LDR BT	Fukada et al. [15]	2012
(0 – > 5)	21	28.6	CT (3 mm)	Lithotomy				

(0 – > 5)	21	23.8	CT + TRUS fusion	Lithotomy	$\bar{x} = 29.5$ $\bar{x} = 28.8$ (19.0 – 39.9)			
(0 – 10)	5	100	TRUS (5 mm)	Lithotomy	< 50 cc	LDR BT	Ryu et al. [16]	2012
n/a	145	5.5	TRUS (7.5 MHz)	Lithotomy	$\bar{x} = 40.0$ (33.8 – 86.0)	LDR BT	Gibbons et al. [17]	2009
$\bar{x} = 6$ (0 – 10)	243	19.3	CT (5 mm)	Supine		LDR BT	Sejpal et al. [9]	2009
	243		TRUS (5 mm)	Lithotomy	$\bar{x} = 44.7 \pm 11.1^*$			
n/a	40	40	CT (5 mm)	n/a	$\bar{x} = 56 \pm 17$	LDR/HDR BT	Nickers et al. [18]	2006
n/a	50	6	TRUS (7.5 MHz, 5 mm)	Lithotomy	$\bar{x} = 32$ (17 – 52)	LDR BT	Henderson et al. [19]	2003
$\bar{x} = 12.2 \pm 3.4$ (8 – 20)	9	100	CT	Supine	$\bar{x} = 30.9 \pm 9.8$	LDR BT	Strang et al. [11]	2001
$\bar{x} = 0.4 \pm 3.6$ (0 – 7)	14	28.6	TRUS (7 MHz, 5 mm)	Lithotomy	$\bar{x} = 39.0 \pm 18.1$			
$\bar{x} = 12.7$ (10 – 21)	7	100	CT (5 mm)	Supine	$\bar{x} = 34.6 \pm 11.4$ (17 – 48)	BT	Tincher et al. [5]	2000
$\bar{x} = 7.8$ (6 – 12)	7	100	CT (5 mm)	Lithotomy				
(0 – 13)*	21	71.4*	CT (5 mm)	Supine		LDR BT	Wang et al. [20]	2000
	33	n/a	TRUS (6 MHz, 5 mm)	Lithotomy	$\bar{x} = 57^*$ (50 – 95)*			
$\bar{x} = 0$ (0 – 20)	97	46.4*	CT (5 mm)	Supine		LDR BT	Bellon et al. [21]	1999
	97		TRUS (6 MHz)	Lithotomy	$\bar{x} = 36$ (15 – 131)			
$\bar{x} = 2.2 \pm 3.5^*$ (0 – 10)	16	62.5	CT (5 mm)	Supine		LDR BT	Wallner et al. [12]	1999
$\bar{x} = 1.8 \pm 4.1^*$ (0 – 10)	16	50	TRUS (6 MHz)	Lithotomy	$\bar{x} = 36$ (22 – 55)			
n/a	54	5.6	TRUS (4 or 5 MHz)	Lithotomy	$\leq 60$ cc	HDR BT	Borghede et al. [22]	1997

BT = brachytherapy, CT = computed tomography, HDR BT = high-dose-rate brachytherapy, LDR BT = low-dose-rate brachytherapy, MRI = magnetic resonance imaging, n/a = not available, TRUS = transrectal ultrasound. \*If not specified in the manuscript, a best approximation was made based on the information in the graphs.

### Needle positioning error

Thirty-five included studies documented quantitative needle positioning errors. Tables 2.2 and 2.3 show the reported misplacement and displacement errors, respectively. Most studies (80%, 28/35) documented the error for an HDR BT treatment, 11% (4/35) for an LDR BT treatment, 6% (2/35) for a PDR BT treatment, and 3% (1/35) for an FLA treatment. The included studies reported needle misplacement and displacement assessed on anatomical images of the patient, but used different procedures and methodologies, such as (1) whether or not to change patient posture to allow for a specific imaging method and (2) varying imaging modalities, time intervals, and reference markers.

The patient's position regularly changed between the preoperative, intraoperative, and postoperative procedure [23-27], potentially influencing needle misplacement and displacement. Both Carrara et al. [28] and Cepek et al. [29] reported a single position (i.e., lithotomy position) for the entire duration of the procedure to minimise movement of the prostate and the tumour. Cepek et al. [29] documented misplacement errors after a needle insertion depth of 84 to 171 mm with symmetrical bevel-tip needles during FLA procedures. The authors reported errors in the cranio-caudal, ventral-dorsal, and medial-lateral directions of 1.1 mm, 1.8 mm, and 0 mm, respectively. They discussed that the error was caused mainly by needle deflection due to the initial skin puncture and the heterogeneity of tissue [29]. Carrara et al. [28] documented mean needle displacement of 0.8 and 0.0 mm in the ventral-dorsal and medial-lateral directions, respectively. In contrast, in the study by Buus et al. [30], patients were placed in supine position for the preoperative MRI scan, in lithotomy position during implantation phase, and again in supine position for the second MRI scan to measure the error. The authors reported mean cranio-caudal needle displacements of 2.2 and 5.0 mm between the first and second HDR BT fraction and after the second HDR BT fraction, respectively. Another patient position transition was described by Mullokandov et al. [31]. In their study, the patients were taken out of the lithotomy position and placed in a frog-leg position (i.e., flexing the hips and abducting the legs) after implantation. The authors reported mean cranio-caudal needle displacements of 2 and 10 mm between the first and second HDR BT fraction and after the second HDR BT fraction, respectively.

Quantification of the error was performed using different imaging modalities, time intervals, and reference markers such as metal markers, bone anatomy, or other implanted needles [32, 33]. Solely Smith et al. [34] measured the error along the entire needle length, while in other studies the end position of the distal tip was evaluated. Most studies used CT to measure the error (54%, 19/35), while some studies used X-ray (29%, 10/35), TRUS (20%, 7/35), MRI (11%, 4/35) or a combination of multiple imaging modalities (14%, 5/35). The time between the reference image and imaging after implantation ranged from nine minutes to four weeks.

**Table 2.2 – Overview of studies that evaluated needle misplacement in transperineal prostate interventions.** For each study, the following information is reported: needle misplacement divided into cranio-caudal, ventral-dorsal, and medial-lateral directions, imaging modality used for the assessment of misplacement, treatment, patient position pre-, intra-, and postoperatively, time between implantation and error measurement, and reference.  $\bar{x}$  = median,  $\bar{x} \pm$  average  $\pm$  standard deviation, and (..) = range.

Needle misplacement $\pm$ SD (range) [mm] (measurement method)			Number of patients	Imaging modality	Treatment	Needle tip	Patient posture change (pre-, intra-, postoperative)	Time [h]	Authors (citation)	Year
Cranio- caudal	Ventral- dorsal	Medial- lateral								
$\bar{x} = 3.8 \pm 3.2$ (FM)	n/a	$\bar{x} = 1.6 \pm 2.1$ (FM)	2	X-ray	HDR BT	Conical	No change	0.25	Smith et al. [34]	2018
$\bar{x} = 3.8 \pm 0.2$ (AM)	$\bar{x} = 1.5 \pm 0.1$ (AM)	$\bar{x} = 1.3 \pm 0.1$ (AM)	15	TRUS (6 MHz)	LDR BT	Bevel	No change	n/a	Jamaluddin et al. [35]	2017
$\bar{x} = 1.1$ (AM)	$\bar{x} = 1.8$ (AM)	$\bar{x} = 0^a$ (AM)	10	MRI (1.5T)	FLA, robotic implantation	Sym- metrical bevel	No change	0.15	Cepek et al. [29]	2015
n/a	> 2 (MF)	> 4 (MF)	5	TRUS (6.5 MHz), X- ray	LDR BT, robotic implantation	Trocar	n/a	1	Fichtinger et al. [36]	2008
n/a	$\bar{x} = 1.8 \pm 0.6^b$ (AM)	$\bar{x} = 1.8 \pm 0.6^b$ (AM)	30	TRUS (1 mm)	HDR BT	n/a	n/a	n/a	Szlag et al. [37]	2008

n/a	$\bar{x} = 3$ (0 – 10) <sup>b</sup> (AM)	$\bar{x} = 3$ (0 – 10) <sup>b</sup> (AM)	10	MRI (0.5T)	LDR BT	Bevel	No change	0.08 – 0.17	Cormack et al. [38]	2000
$\bar{x} = 4.5$ (IOF)	$\bar{x} = 2.2$ (IOF)	$\bar{x} = 2.0$ (IOF)	10	X-ray	LDR BT	n/a	n/a – lithotomy – supine	72	Tascher- eau et al. [39]	2000

MF = marker frames attached to needle guide, AM = anatomical marker (e.g., bone, urethra, ventral rectal wall, urethra, prostate base), FM = fiducial marker (e.g., gold maker), IOF = isocentric orthogonal films, CT = computed tomography, FLA = focal laser ablation, HDR BT = high-dose-rate brachytherapy, LDR BT = low-dose-rate brachytherapy, MRI = magnetic resonance imaging, n/a = not available or not applicable, TRUS = transrectal ultrasound, US = ultrasound. <sup>a</sup>No statistically significant difference, no significant displacement, <sup>b</sup>Ventral-dorsal and medial-lateral errors were measured together as a single error, <sup>c</sup>Cranio-caudal, ventral-dorsal, and medial-lateral errors were measured together as a single error, <sup>d</sup>Cranio-caudal and medial-lateral errors were measured together as a single error, <sup>e</sup>Total error between all fractions was documented.

**Table 2.3 – Overview of studies that evaluated needle displacement transperineal prostate interventions.** For each study, the following information is reported: needle displacement in cranio-caudal direction before the first fraction, between the first and second fraction, and after the second fraction, needle displacement in ventral-dorsal and medial-lateral direction before the first fraction unless otherwise indicated, imaging modality, treatment, patient position pre-, intra-, and postoperatively, time between implantation and error measurement, reference.  $\bar{x}$  = median,  $\bar{x}$  = average or mean, SD = standard deviation, and (..) = range.

Needle displacement ± SD (range) [mm] (measurement method)											
Cranio-caudal			Ventral-dorsal	Medial-lateral	Number of patients	Imaging modality	Treatment (number of fractions)	Patient posture change	Time [h]	Authors (citation)	Year
<1 fraction	1-2 fraction	> 2 fractions	<1 fraction	<1 fraction							
$\bar{x} = 0.9 \pm 0.4$ (FM)	n/a	n/a	n/a	n/a	20	TRUS	HDR BT (1)	n/a	n/a	David et al. [40]	2019
n/a	n/a	n/a	$\bar{x} = 1.0$ (-1.7 – 1.8) (AM)	$\bar{x} = 0.9$ (-0.9 – 1.5) (AM)	10	TRUS	HDR BT (1)	n/a	0.18	Wu et al. [41]	2019
n/a	$\bar{x} = 2.2 \pm 1.8$ (IM)	$\bar{x} = 5.0 \pm 3.0$ <sup>f</sup> (IM)	n/a	n/a	24	MRI (1.5T)	HDR BT (2)	Supine – lithotomy – supine	1 – 3	Buus et al. [30]	2018
n/a	$\bar{x} = 0.9$ (0 – 5.5) (during fraction) (AM)	n/a	$\bar{x} = 0.5$ (0 – 2.1) (during fraction) (AM)	0.6 (0 – 2.9) (during fraction) (AM)	17	MRI (1.5T)	HDR BT, self-anchoring catheter (1)	No change	n/a	Maenhout et al. [42]	2018
n/a	n/a	n/a	$\bar{x} = 0.8 \pm 0.9$ (AM)	$\bar{x} = 0.0 \pm 1.8$ (AM)	7	TRUS (1 mm)	HDR BT (2)	No change	1 – 2	Carrara et al. [28]	2017
n/a	(0-18) <sup>g</sup> (FM)	n/a	n/a	n/a	162	X-ray	HDR BT (4)	n/a	0 – 36	Aluwini et al. [43]	2016
n/a	$\bar{x} = 8.7 \pm 3.3$ (2.7 ± 1.1 – 14.7 ± 1.7) (FM)	n/a	n/a	n/a	20	CT (2 mm)	HDR BT (4)	n/a – lithotomy – supine	0 – 24	Reynés-Llompарт et al. [27]	2016
n/a	$\bar{x} = 0.97 \pm 0.76$ <sup>c</sup> (FM)	n/a	$\bar{x} = 0.97 \pm 0.76$ <sup>c</sup> (1 – 2 fraction) (FM)	$\bar{x} = 0.97 \pm 0.76$ <sup>c</sup> (1 – 2 fraction) (FM)	33	CT (1 mm)	HDR BT (2)	n/a	6	Peddada et al. [44]	2015
n/a	$\bar{x} = -0.22 \pm 0.2$ <sup>g</sup> (FM)	n/a	$\bar{x} = -0.02 \pm 0.06$ <sup>g</sup> (>1 fraction) (FM)	$\bar{x} = 0.01 \pm 0.04$ <sup>g</sup> (>1 fraction) (FM)	23	CT (2 mm)	PDR BT, self-anchoring catheter (24)	n/a	2.2 – 48	Dinkla et al. [45]	2014

$\bar{x} = 6 \pm 4$ (FM)	$\bar{x} = 12 \pm 6$ (FM)	$\bar{x} = 12 \pm 6$ (FM)	n/a	n/a	30	CT (1.25 mm)	HDR BT (5)	n/a	6 – 54	Kawa- kami et al. [46]	2014
n/a	$\bar{x} = 5.8 \pm 1.9$ (-13 – 12) (FM, AM)	n/a	n/a	n/a	13	CT (2 mm)	HDR BT (3,4)	n/a – lithotomy – supine	0 – 48	Huang et al. [23]	2013
n/a	$\bar{x} = 3.5$ (-14 – 13) (AM method)	n/a	n/a	n/a	26	CT (1.25 mm)	HDR BT (1,2)	n/a – lithotomy – supine	36 – 672	Koval- chuk et al. [26]	2012
n/a	$\bar{x} = 4.3 \pm 2.7$ (0.3 – 10) (FM)	$\bar{x} = 5.9 \pm 3.6$ (-2.3 – 12.9) (FM)	n/a	n/a	30	CT (3 mm)	HDR BT (7)	n/a	21 – 69	Takenaka et al. [47]	2012
n/a	$\bar{x} = 5.1$ (1.9 – 10.1) (FM)	n/a	n/a	n/a	15	CT (3 mm)	HDR BT (2)	n/a	24	Foster et al. [48]	2011
n/a	$\bar{x} = 12.6$ (0.6 – 24.6) (FM)	n/a	n/a	n/a	22	CT, X-ray	HDR BT (2)	n/a	24	Fox et al. [49]	2011
$\bar{x} = 11.1 \pm 7.6$ (FM)	n/a	n/a	n/a	n/a	20	CT (3 mm, 1.5-mm interval), X-ray	HDR BT (1)	n/a – lithotomy – supine	2 – 3	Holly et al. [25]	2011
0 – 0.5 (AM)	0 – 0.4 (AM)	n/a	0 – 1.3 <sup>b</sup> , 0 – 1.0 <sup>b</sup> (1-2 fraction) (AM)	0 – 1.3 <sup>b</sup> , 0 – 1.0 <sup>b</sup> (1-2 fraction) (AM)	25	TRUS	HDR BT (1)	n/a	0.83 – 1.2	Milickov et al. [50]	2011
$\bar{x} = 7.5$ (-2.9 – 23.9) (FM)	n/a	n/a	n/a	n/a	25	CT (3 mm), X-ray	HDR BT (2)	n/a – lithotomy – supine	1.4 – 6.1	Whitaker et al. [24]	2011
$\bar{x} = 4.5 \pm 1.7$ (FM)	$\bar{x} = 5.6 \pm 3.6$ (FM)	$\bar{x} = 6.4 \pm 4.2$ (FM)	n/a	n/a	91	CT (3 mm), X-ray	HDR BT (3)	n/a	0 – 48	Tiong et al. [51]	2010
n/a	$\bar{x} = 7$ (-14 – 24) (FM)	n/a	n/a	n/a	64	CT (3 mm)	HDR BT (4,7,9)	n/a	72 – 120	Yoshida et al. [52]	2010
n/a	$\bar{x} = 7.9$ (0 – 21) (AM)	$\bar{x} = 3.8$ (0 – 25.5) (AM)	n/a	n/a	20	CT (3 mm)	HDR BT (3)	n/a	21 – 28	Simnor et al. [53]	2009
n/a	$\bar{x} = 2.7$ (-6.0 – 13.5) (AM)	n/a	n/a	n/a	10	CT (3 mm)	HDR BT (2)	n/a	24	Kim et al. [54]	2007
	$\bar{x} = 5.4$ (-3.75 – 18.0) (FM)										
	$\bar{x} = 1.0$ (0-6) (day 2), $\bar{x} = 1.2$ (0-6) (day 3) (FM)		n/a	n/a	43	CT (2 mm)	PDR BT, self- anchoring catheter (46)	n/a	24 – 48	Pieters et al. [55]	2006

n/a	$\bar{x} = 2$ (0 – 4) (FM, AM)	$\bar{x} = 10$ (5 – 23) (FM, AM)	n/a	n/a	50	CT (2 & 5 mm)	HDR BT (4)	n/a – lithotomy – frog-leg	3 – 28	Mullokandov et al. [31]	2004
n/a	$\bar{x} = 11.5$ (0 – 47) (IM)	n/a	n/a	n/a	20	CT (5 mm)	HDR BT (2)	n/a	18 – 24	Hoskin et al. [56]	2003
n/a	$\bar{x} = 16 \pm 6$ , $\bar{x} = 18$ (AM) $\bar{x} = 15 \pm 4$ , $\bar{x} = 12$ (FM)	n/a	n/a	n/a	47	X-ray	HDR BT (4)	n/a	2 – 48	Pellizzon et al. [33]	2003
n/a	$\bar{x} = 20$ (FM, AM)	$\bar{x} = 4$ (FM, AM)	n/a	n/a	10	TRUS (7.5 MHz, 5 mm), X-ray	HDR BT (4)	No change	6 – 36	Martinez et al. [57]	2001
n/a	$\bar{x} = 6.8$ (0 – 31.4) (FM)	$\bar{x} = 3.9$ (0 – 10.4) (FM)	n/a	n/a	96	X-ray	HDR BT (4)	n/a	5 – 40	Damore et al. [32]	2000
	$\bar{x} = 8.3$ (0 – 25.6) (AM)	$\bar{x} = 4.2$ (0 – 9.1) (AM)									

AM = anatomical marker (e.g., bone, urethra, ventral rectal wall, urethra, prostate base), FM = fiducial marker (e.g., gold marker), IM = ink markers on the patient's skin or measurement of the needle outside the patient's body, CT = computed tomography, HDR BT = high-dose-rate brachytherapy, MRI = magnetic resonance imaging, n/a = not available or not applicable, PDR BT = pulsed-dose-rate brachytherapy, TRUS = transrectal ultrasound. <sup>a</sup>No statistic significant difference, no significant displacement, <sup>b</sup>Ventral-dorsal and medial-lateral errors were measured together as a single error, <sup>c</sup>Cranio-caudal, ventral-dorsal, and medial-lateral errors were measured together as a single error, <sup>d</sup>Cranio-caudal and medial-lateral errors were measured together as a single error, <sup>e</sup>Total error between all fractions was documented, <sup>f</sup>Total error between 1<sup>st</sup> and 3<sup>rd</sup> fractions were documented.

Displacement errors were only reported for HDR BT and PDR BT. Most studies documented displacement in the cranio-caudal direction (i.e., 86%, 30/35), of which the largest average error of 20 mm was documented by Martinez et al. [57], who used 1.9-mm diameter flexible plastic needles with metal stylets during HDR BT. The authors stated that despite the needles being attached to the template, which was sutured to the perineal skin, the needles displaced up to 31 mm in the caudal direction [57]. They stated that the elasticity of perineal tissues was most likely the cause of needle displacement [57].

Pieters et al. [55] developed unique PDR BT catheters with an umbrella anchoring mechanism at the tip to fixate the catheter inside the prostate gland. The authors stated that self-anchoring catheters showed an absolute mean displacement of 1 mm [55] compared to mean displacements of 11 to 13 mm in HDR BT of conventional needles [25, 49, 56]. The self-anchoring catheters were also used for HDR BT by Maenhout et al. [42], who reported an average three-dimensional (3D) error of 1.3 mm.

### 2.3.2 Clinical guidelines

Figure 2.5 provides a proposed decision-making process integrated into the current clinical workflow so that physicians can decide on the continuation of the procedure. This process includes published clinical guidelines retrieved from the included studies related to prostate volume, PAI, and needle positioning error. Exceeding a limit may result in patient exclusion or requires a solution to make the patient eligible again. In case of experiencing PAI during HDR or PDR BT treatment, one solution is to optimize the radiation dose by considering the actual positions of the implanted BT catheters. The radiation dose is determined by the dwell positions, i.e., the locations along the catheter where the radioactive sources reside, and the corresponding dwell times, i.e., the amount of time the radioactive sources reside at their dwell positions. By increasing the dwell times of the ventral catheters, it becomes feasible to sufficiently irradiate the entire prostate also in case of PAI occurrence. However, a drawback is the potential creation of high-dose areas, which could impact nearby healthy organs at risk (OARs).

#### *Prostate volume*

Prostate volume is traditionally used as an indicator for the occurrence of PAI and is calculated on preoperative scans using the elliptical approximation: Prostate volume (cc) =  $\pi / 6$  (height x width x length) of the prostate [17]. The American Brachytherapy Society (ABS) guidelines state that brachytherapy for a prostate volume of > 60 cc is technically more challenging as PAI is more prevalent in enlarged prostates. Thus, the ABS reported a prostate volume of > 60 cc as a relative contraindication for prostate brachytherapy [58]. In contrast, the revised Groupe Européen de Curiethérapie and the European Society for Radiotherapy & Oncology (GEC-ESTRO) Advisory Committee for Radiation Oncology Practice (ACROP) prostate brachytherapy guidelines, published in 2022, state that a prostate gland of > 50 – 60 cc is no longer a contraindication for prostate brachytherapy as larger prostates can be successfully implanted if there is minimal PAI [59]. In some institutions, borderline cases with a prostate volume of 55 to 60 cc are generally better examined in accordance with the GEC-ESTRO ACROP guidelines. The prostate and the OARs are segmented on MRI or CT and digitally rotated to estimate the level of PAI in lithotomy position as described by de Vries et al. [13]. However, no guidelines are reported for adequate rotation related to posture change from supine to lithotomy position.

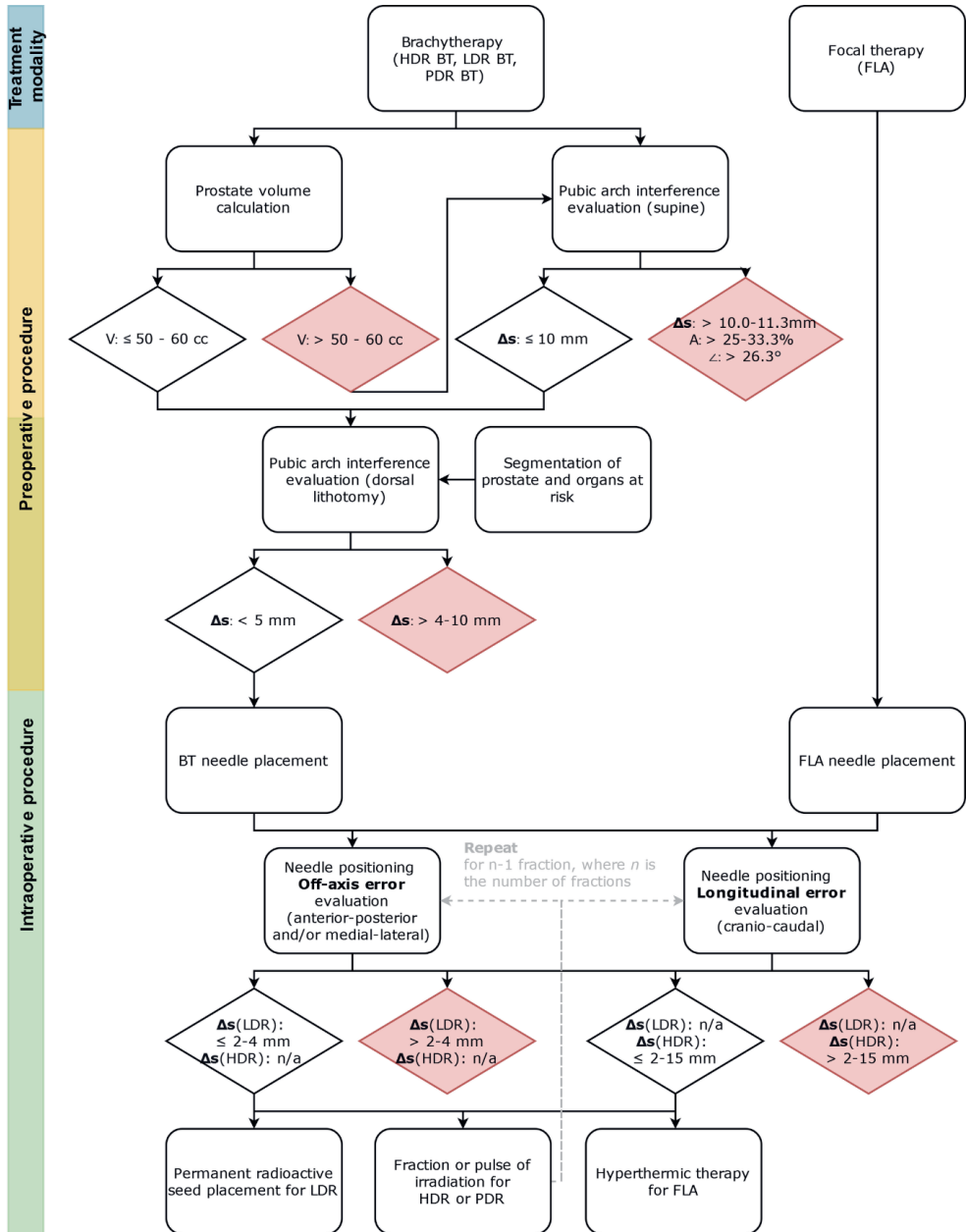


**Figure 2.5 - Decision-tree for conformity to treatment plan including clinical guidelines.** Rounded rectangle shapes indicate procedural steps. Diamond shapes indicate the limits. Exceeding a limit (red diamond shape) requires a solution (see Figure 2.7). Note that the preoperative procedure (indicated in yellow) and the intraoperative procedure (indicated in green) partially overlap as the approaches differ between institutions. V = prostate volume, Δs = orthogonal distance from the inner surface of the pubic arch to the ventral border of the prostate in mm, A = obstructed area by the pubic arch compared to total prostate cross-section in %, ∠ = angle between the pubic symphysis and ventral border of the prostate.



### Pubic arch interference

Prior to needle implantation, the level of PAI is measured on an MRI or CT scan with the patient in supine position to estimate the risk of obstruction during needle implantation with the patient in lithotomy position. Figure 2.6 indicates various methods to quantify PAI.

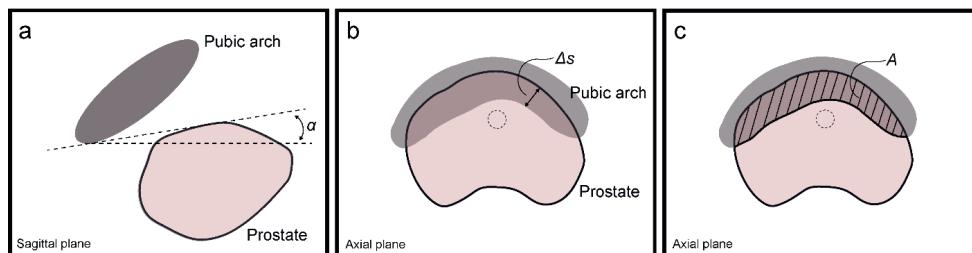


**Figure 2.6 - Measuring methods of pubic arch interference (PAI).** (a) Angle ( $\alpha$ ) between pubic symphysis and ventral border of prostate, (b) Orthogonal distance ( $\Delta s$ ) from inner surface of pubic arch to ventral border of the prostate and (c) Prostate area obstructed ( $A$ ) by the pubic arch compared to total prostate cross-section.

Firstly, the angle of PAI can be calculated in the sagittal plane by drawing two lines on the scan; one horizontal line through the pubic symphysis and one line connecting the most ventral point of the prostate with the most dorsal point of the pubic arch at the pubic symphysis (Figure 2.6a). Angle  $\alpha$  between the pubic symphysis and ventral border of the prostate is the angle that can be related to a boundary value above which PAI is likely to occur. Zheng et al. [14] retrospectively analysed MRI scans of 40 prostate cancer patients and suggested a boundary value of  $\alpha = 26.3^\circ$  to predict the occurrence of PAI in lithotomy position. They reported that the angle  $\alpha$  of PAI was statistically correlated with the occurrence of PAI ( $p < 0.01$ ).

Secondly, besides the angle of PAI, the distance of the obstruction between pubic arch and prostate can be assessed (Figure 2.6b). Multiple studies reported a threshold of 10.0 mm obstruction in supine position, assessed by overlaying the narrowest part of the pubic arch over the largest contour of the prostate in the axial plane and measured from the point of the prostate, which was at the greatest perpendicular distance from the caudal edge of the pubic arch [9, 21]. Zheng et al. [14] suggested the boundary value of 11.3 mm as a reliable predictor of intraoperative PAI. They calculated PAI by using two parallel lines in sagittal plane through the pubic symphysis and reported a statistical correlation between distance and PAI ( $p < 0.01$ ). When the distance exceeded 11.3 mm PAI was reported to be excessive.

Lastly, Bellon et al. [21] and Henderson et al. [19] considered 25% and 33% obstruction of the prostate diameter in the axial plane as an indication of excessive PAI (Figure 2.6c), respectively. These approximations were not based on a rigorous study. Some studies assessed PAI based on TRUS visualisations with the patient in lithotomy position. This position is associated with less PAI and larger accessibility of the prostate due to pelvic rotation than supine position [5]. Strang et al. [11] excluded patients with  $> 4$  mm PAI, while Fukada et al. [15] expected excessive PAI if  $> 5$  mm obstruction was shown, and Ryu et al. [16] excluded patients with  $> 10$  mm PAI.

### Needle positioning error

Needle misplacement errors are affected by the needle-tissue interaction forces [60], needle design [61], and the implantation procedure [62]. On the other hand, needle displacement errors depend on the duration of treatment and perturbations between the needle positioning and treatment phase [49]. In HDR BT and PDR BT, the patient receives multiple treatment fractions, whereas in LDR BT and FLA,

the patient receives a single dose. Multiple treatment fractions increase the time between needle positioning and treatment, which is associated with an increase in positioning error.

Several studies described correction of the needle position after the detection of misplacement or displacement. Aluwini et al. [43] reported that 43.8% of the HDR BT patients required at least one correction of the needle position of more than 3 mm, mostly in the cranial direction. Whitaker et al. [24] showed that 67% of the needles had a displacement in the cranio-caudal direction of at least 5 mm that required correction, and Tiong et al. [51] stated that up to three needles had to be corrected in cranio-caudal direction per fraction in HDR BT to lower the percentage of fractions from 82.3% to 12.2% in which displacements over 3 mm occurred. Buus et al. [30] reported that needle displacements of 3 and 5 mm introduced a decrease of 5 and 10% in target coverage for HDR BT, respectively. The authors proposed a 3D-positioning error threshold of 3 mm, calculated between HDR BT fractions, from the needle tip position relative to the corresponding transperineal template opening. For a single-fraction treatment with a dose of  $\geq 15$  Gy, they stated that displacement should be less than 2 mm due to the absence of the averaging dose effect of multiple fractions. Kolkman-Deurloo et al. [63] and Tiong et al. [51] analysed the effect of needle displacements in HDR BT on X-ray scans along the longitudinal axis in simulation studies and recommended corrections of needles with an error exceeding 3 mm. It should be noted that the location of the needles in the transperineal template dictated the impact of the error on the OARs, as the needles in the dorsal rows were close to the rectum and the needles in the ventral rows were close to the urethra. Kolkman-Deurloo et al. [63] discussed that needles in the second and third dorsal rows of the transperineal template generally have larger impact on the dose coverage than needles in the ventral rows of the template because of the higher dwell weights (i.e., the relative contribution of a needle to the total administered dose in brachytherapy). Ventral rows of the template are less critical due to the lower dwell weights provided such that the dose to the urethra is not too high. Poder et al. [64] reported that 3D-source positioning errors in HDR BT plans could be up to 2 to 5 mm while avoiding significant ( $> 10\%$ ) changes in the dose volume histogram of the prostate. Similarly, Mason et al. [65] investigated needle positioning errors and reported a threshold of approximately 2 – 3 mm based on a minimum value required for error detection and avoiding unnecessary countermeasures assessed by a physician. Nevertheless, the effect of the needle error still depended on the location of the needle in the target volume, the direction of the positioning error, and the weights of the dwells. Poder et al. [64] found that displacement of heavily weighted catheters, mainly around the urethra, resulted in undertreatment of the central region. Regarding the direction of the error, they stated that errors of 3 mm in the cranial-caudal direction (i.e., longitudinal errors) were more sensitive than the off-axis errors, lateral errors were more sensitive than medial errors and cranial errors had more impact on the dose plan compared to caudal errors. For off-axis errors, Fichtinger et al. [36] reported a limit of 2 mm, whereas Borghede et al. [22] reported a limit of 3–4 mm, both for LDR BT procedures. For longitudinal errors, limits were reported for HDR BT procedures, ranging from 2 mm [30] to 15 mm [47], whilst most studies reported a limit of 3 mm [23, 43, 51] or 5 mm [24, 32, 33, 53]. This shows that reported limits for needle positioning errors depend amongst others on the location of the needle and the direction of the needle positioning error.

## 2.4 DISCUSSION

### 2.4.1 Main findings

This work provided an overview of the quantification of hazards related to needle positioning in transperineal treatment procedures of localised prostate cancer. We distinguished between the total needle geometry required in the target volume and the individual needle positioning. Firstly, access restrictions to the prostate gland by the pubic arch affects the total needle geometry as the ventrolateral part of the prostate cannot be reached considering the conventional linear trajectories. Obstructions of the prostate up to 22.3 mm were reported for various prostate volumes.

Secondly, individual needle positioning non-conformal to the treatment plan can potentially affect the treatment efficacy. Needle positioning errors were subdivided into mis- and displacement. Needle misplacement was reported for LDR BT, HDR BT, and FLA procedures, in which for LDR BT largest errors were reported, especially in the cranio-caudal direction. Needle displacement was only reported for HDR BT and PDR BT as these techniques involve fractionated doses, while LDR BT and FLA are single-dose treatments. Displacements were reported in all directions. The largest displacement was measured in the cranio-caudal direction, and generally increased over time.

Reported clinical guidelines indicate limits regarding prostate volume, PAI, and needle positioning error that, when exceeded, demand for patient exclusion from the procedure or solutions to minimise the impact on the treatment. However, these guidelines are general, ambiguous and compliance in the clinical setting differs between institutions.

### 2.4.2 Limitations

The evaluation of the needle position and the level of PAI depend on (1) patient posture change, (2) imaging modality and specifications, (3) moment of assessment, (4) implemented assessment method, and (5) the assessor.

Firstly, patient posture change from supine to lithotomy position introduces discrepancies, and the use of multiple imaging modalities can introduce imaging co-registration inaccuracies [21]. Buus et al. [30] reported that their average MRI-US co-registration error was 0.52 mm with a maximum of 0.95 mm. They stated that organ motion induced by patient posture change affected the outcomes. This is substantiated by Yamoah et al. [66], who revealed that preoperative planning for LDR BT resulted in poorer biochemical control and higher urinary toxicity compared to interventions with intraoperative planning using solely TRUS in lithotomy position.

Secondly, the imaging modality and specifications contribute to uncertainties in the quantitative measurements. CT slice thickness introduces an uncertainty of the needle position because of partial volume artefacts. Kovalchuk et al. [26] considered uncertainty in needle tip determination of 0.63 mm as this was half the slice thickness of their CT slices. Kim et al. [67] reported that an increased CT slice thickness increased the obtained dose error after simulations with random shifting of HDR BT catheters. The mean dose error was 0.7% for 2-mm slices, 1.1% for 3-mm slices, and 1.7% for 5-mm slices. Regarding MRI, Ballester et al. [68] described that the voxel size can change delineation due to blurring [68]. Concerning TRUS, Fedorov et al. [69] described that TRUS images have poor contrast at the apex and base of the prostate and can affect the image due to the TRUS probe compressing the prostate gland. Furthermore, ultrasound has a resolution of 200 microns, resulting in the lack of tumour visualisation because of limited sensitivity [70].

Thirdly, time can be a confounding factor as the observed error depends on the moment of evaluation. Kim et al. [54] described that maximum catheter displacement occurred in the 12 hours after the first fraction for HDR BT, while Taschereau et al. [8] reported misplacement of the needles 72 hours after positioning, which makes these measurements potentially to a greater extent subjected to the influence of oedema and organ motion.

Fourthly, the assessment method influences the analysis. For example, PAI quantification can be performed by three different methods, and needle positioning errors can be assessed using bone anatomy, metal markers, or other implanted needles as reference markers. Kim et al. [54] reported an average discrepancy of 2.7 mm in needle displacement between measurements using the ischial bone or two gold markers as reference markers.

Lastly, inter-observer variability plays a role in the assessment. Kim et al. [54] reported a difference in displacement error detection of  $1.0 \pm 0.9$  mm with a maximum difference of 5.0 mm between two observers. Therefore, the error threshold should be large enough to be detected, considering all the above-stated inaccuracies, and low enough to avoid a significant impact on the treatment plan.

2.4.3 Solution strategies

To operate below the upper limit of the guidelines for needle positioning, countermeasures can be implemented to enable continuation in line with the treatment plan (Figure 2.7). Minimising PAI can be achieved in several ways, subdivided into four pillars: (1) neo-adjuvant hormonal therapy, (2) positioning strategy, (3) needle design, and (4) needle guidance. Improving needle positioning accuracy can be related to (1) positioning strategy and (2) needle design.

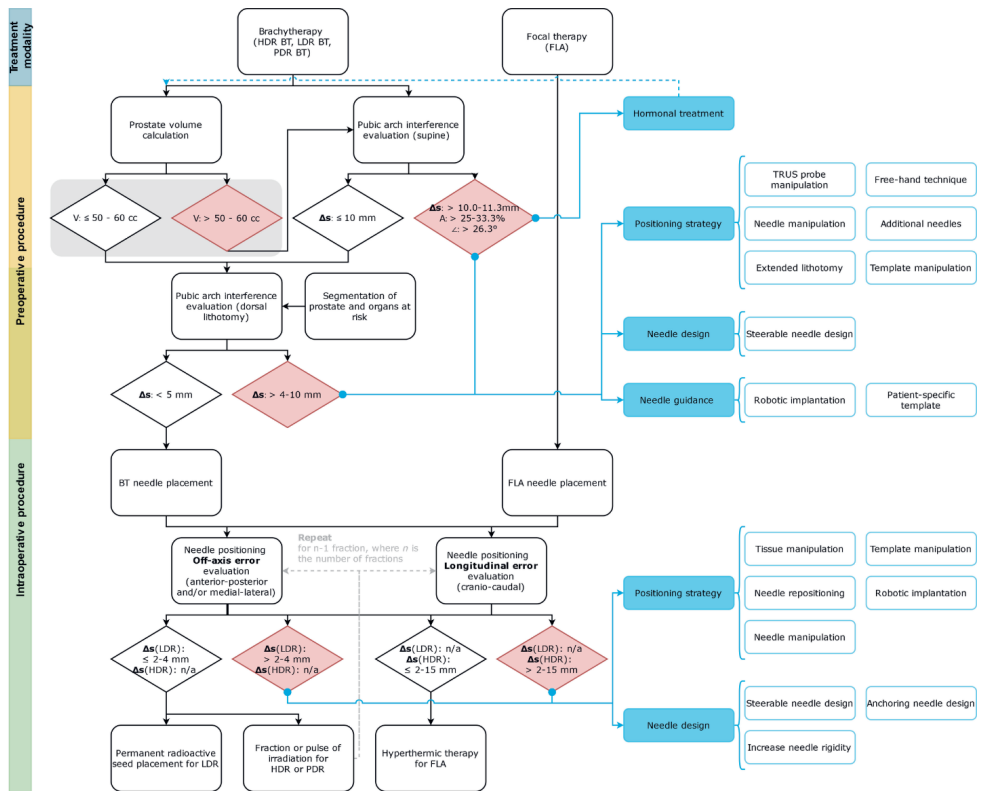


**Figure 2.7 - Overview of solutions to hazards in needle positioning in transperineal prostate interventions.** Rounded rectangle shapes indicate procedural steps. Diamond shapes indicate limits. Exceeding the limit (red diamond shapes) requires a solution. Blue rectangle shapes indicate solutions for the procedural steps that the blue line with the dot grasps, the blue-outlined rectangle shapes indicate examples of the solutions. V = prostate volume,  $\Delta s$  = orthogonal distance from the inner surface of the pubic arch to the ventral border of the prostate in mm, A = obstructed area by the pubic arch compared to total prostate cross-section in %,  $\angle$  = angle between the pubic symphysis and the ventral border of the prostate. The grey block overlaid on the limits for prostate volume indicates that the guideline for prostate volume is superfluous according to new brachytherapy guidelines.

Clinical institutions often use hormonal therapy, such as androgen deprivation therapy (ADT), to downsize the prostate gland and reduce the risk of PAI. For example, Kucway et al. [71] showed a volume reduction of the prostate of 33% after 3 - 4 months of ADT. Traditionally, this therapy is performed prior to the brachytherapy treatment in patients with prostate volumes of 50 - 60 cc or with observed excessive PAI [9, 19, 71]. Sejpal et al. [9] reported that 27% of the patients received ADT due to an enlarged prostate or PAI > 10 mm. On the other hand, this therapy can induce severe side effects for the patient, such as erectile dysfunction, hot flushes, increased cardiovascular morbidity, and consequently a lower QOL [72-75]. The ABS, therefore, concluded that ADT is only recommended in patients with observed PAI, as no benefit was shown from adding ADT to prostate brachytherapy for low-risk and favourable intermediate-risk patients without PAI [76].

Despite preoperative PAI assessment and the use of ADT in many patients, PAI can still occur during needle implantation. Figure 2.8 shows techniques to obtain a conformal total needle geometry if PAI occurs [11]. Regarding positioning strategies, the patient's lithotomy position can be extended, the TRUS probe, the transperineal template or the needle can be manipulated [77], and the needles can be positioned using a free-hand technique without the use of a transperineal template or guide [17, 78]. However, the free-hand technique is reported to be difficult and requires experience from the physician, as buckling of the needle can occur due to the absence of the transperineal template for guidance [17].

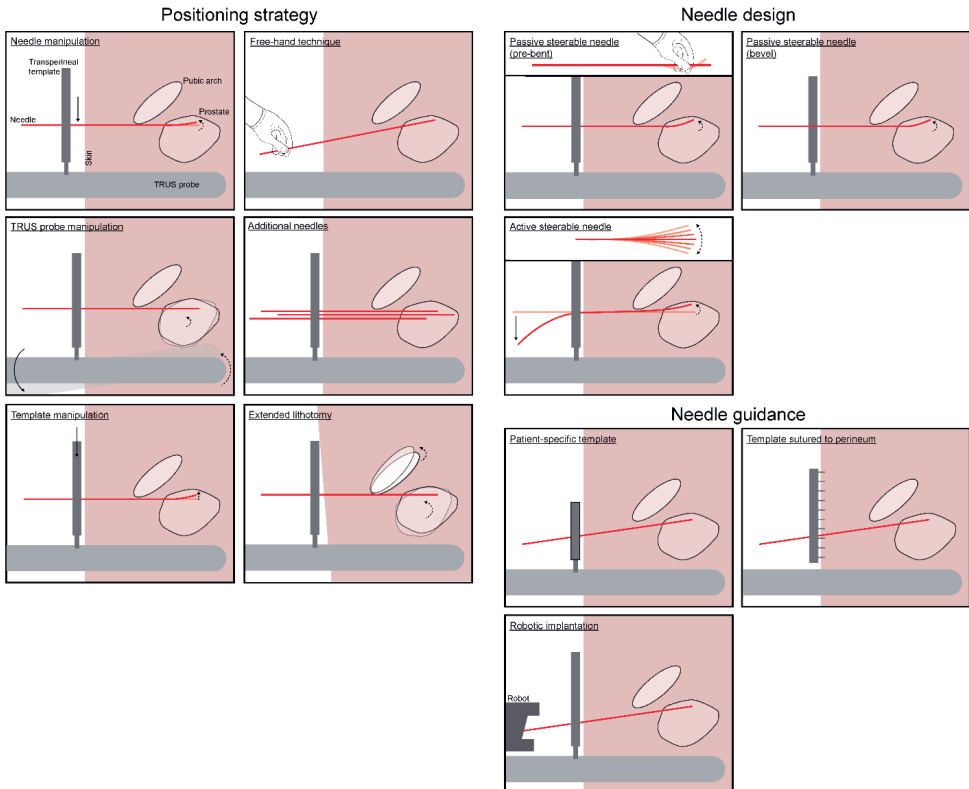


**Figure 2.8 - Overview of solutions to improve total needle geometry in prostate with pubic arch interference (PAI).** The positioning strategy can be altered by needle manipulation, a free-hand positioning technique, transrectal ultrasound (TRUS) probe manipulation, using additional needles, template manipulation, or positioning the patient in the extended lithotomy position. The needle design can be changed by developing a passive steerable needle (e.g., with a pre-bent or a bevel-shaped tip) or an active steerable needle. The needle guidance can be adapted by using a patient-specific template, a template sutured to the patient's perineum instead of attached to the TRUS probe, or robotic implantation of the needle.

Concerning needle guidance strategies, the needles can be obliquely positioned using a robotic device for angulated approaches, a template sutured to the patient's perineum instead of attached to the TRUS probe, or a patient-specific template [30]. For needle design-related solutions, a needle with an asymmetric tip can be steered using the asymmetric needle-tissue force distribution on the needle tip [61], while occasionally the distal tip of a needle is bent in an adequate angle by the physician to circumvent the pubic arch. On the other hand, asymmetric needle tip steering depends on needle-tissue interaction forces making needle control challenging, and a substantial on-site modification in the design of the medical device potentially increases the risk on a needle positioning error. Such designs are referred to as passive steerable needles [79]. De Vries et al. [80] proposed using steerable needles with tip control, known as active steerable needles, to overcome PAI and optimise the dose distribution. Podder et al. [81] described that steerable needles could create curvatures conform the prostate geometry while reducing the total number of needles required, thereby minimising oedema and potentially improving treatment outcomes.

Needle positioning accuracy can be improved by changing the needle design or altering the positioning strategy, as indicated in Figure 2.9. Off-axis errors can be minimised by means of steerable needles that counteract perturbations or robotic devices that minimise insertion or friction forces, thus theoretically reducing needle deflection. Bloemberg et al. [82] described a wasp-inspired, self-propelling, steerable needle that could incorporate an optical fibre for FLA. To reduce longitudinal needle displacement errors, the prostate can be stabilised, the needle can be anchored in the transperineal template sutured to the perineal skin, or the needle design can be adjusted to accomplish needle anchoring once they are inside the prostate [55]. Taschereau et al. [8] used two additional stabilisation needles but observed no significant influence on needle displacement. Self-anchoring catheters were described by Pieters et al. [55] and Maenhout et al. [42], with which external fixation in the transperineal template became unnecessary and needle displacement was minimised.

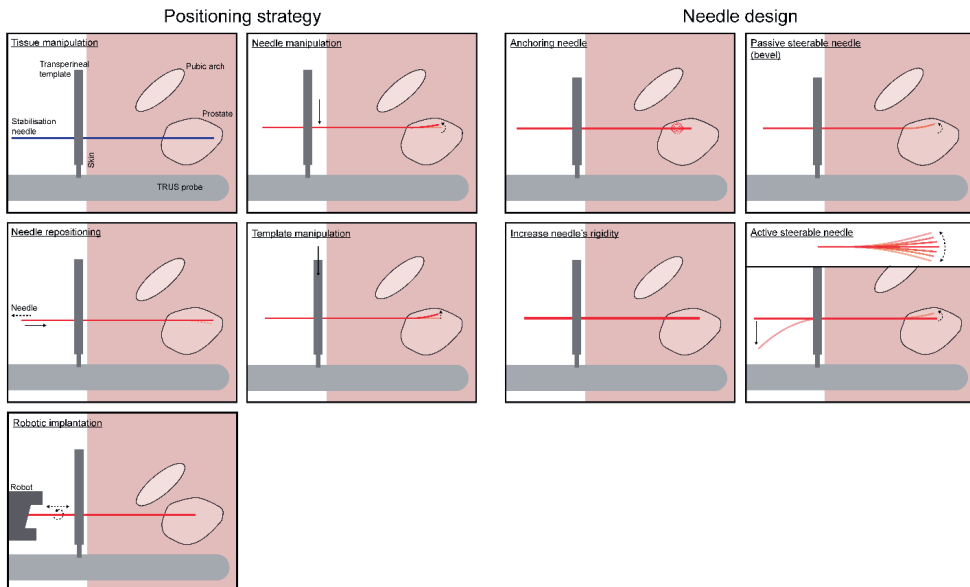


**Figure 2.9 - Overview of solutions to improve transperineal needle positioning into the prostate.** Needle positioning accuracy can be improved by altering the positioning strategy or changing the needle design. The positioning strategy can be altered by tissue manipulation, needle manipulation, needle repositioning, template manipulation, or robotic implantation. The needle design can be changed by developing an anchoring needle, a passive steerable needle (e.g., with a bevel-shaped tip), or an active steerable needle.

An overarching solution for needle misplacement and displacement errors is repositioning the needles by advancing or retracting them or completely re-implanting them; however, this induces additional tissue trauma [83-85]. In current clinical practice, imaging is often performed after a treatment fraction to evaluate the longitudinal error of the needles, after which displaced needles are advanced again. Keyes et al. [84] described seven patients in which the needles for LDR BT were re-implanted to ensure coverage of the underdosed areas of the prostate. All patients had excellent dosimetry after the re-implantation procedure [84]. Hughes et al. [85] stated that re-implantation increased the prostate dose metrics D90 (i.e., the minimum dose received by 90% of target volume) and V100 (the percentage of the target volume that received at least 100% of the prescription dose [86]) from 49 Gy to 201 Gy and from 46% to 98%, respectively. Noteworthy is the absence of studies related to needle positioning in ablative therapies compared to brachytherapy, which could be explained by the fact that these relatively new ablative therapies are often still in the clinical trial phase [87]. In contrast, brachytherapy has been performed since the early twentieth century [88, 89].

### 2.4.4 Recommendations

Future research should be conducted to better relate hazards of needle positioning in transperineal treatment procedures of localised prostate cancer and clinical outcomes. With this, congruent and adequate guidelines related to PAI and needle positioning error can be implemented. We expect a trend toward novel devices with which challenges in needle positioning can be mitigated, including (1) robotically controlled needles that can be obliquely inserted to improve the accessibility of the target volume and (2) active steerable needles that allow for positioning along curved trajectories to optimise total needle geometry with high positioning accuracy. These solutions should be combined with high-resolution imaging methods like MRI for precise target volume identification and needle guidance. In the scientific literature, steerable needles and brachytherapy robots compatible with MRI are already upcoming; however, these are not common in clinical practice yet [90, 91].

## 2.5 CONCLUSION

This systematic review of the scientific literature examines the hazards and guidelines associated with needle positioning during transperineal prostate procedures. Current clinical guidelines regarding prostate volume, needle positioning accuracy and maximum allowable PAI are ambiguous, thus a case-specific approach is recommended to avoid a suboptimal procedure or patient exclusion. Steerable needles can offer intraoperative flexibility in needle placement and allow for correction of perturbations while overcoming PAI to ensure an optimised treatment.

## REFERENCES

- [1] Sung H, Ferlay J, Siegel RL, Laversanne M, Soerjomataram I, Jemal A, et al. Global cancer statistics 2020: GLOBOCAN estimates of incidence and mortality worldwide for 36 cancers in 185 countries. *CA: a cancer journal for clinicians*. 2021;71(3):209-49. <https://doi.org/10.3322/caac.21660>.
- [2] Jain A, Deguet A, Iordachita I, Chintalapani G, Vikal S, Blevins J, et al. Intra-operative 3D guidance and edema detection in prostate brachytherapy using a non-isocentric C-arm. *Med Image Anal*. 2012;16:731-43. <https://doi.org/10.1016/j.media.2010.07.011>.
- [3] Frank SJ, Pisters LL, Davis J, Lee AK, Bassett R, Kuban DA. An assessment of quality of life following radical prostatectomy, high dose external beam radiation therapy and brachytherapy iodine implantation as monotherapies for localized prostate cancer. *The Journal of urology*. 2007;177(6):2151-6. <https://doi.org/10.1016/j.juro.2007.01.134>.
- [4] De La Rosette J, Ahmed H, Barentsz J, Johansen TB, Brausi M, Emberton M, et al. Focal therapy in prostate cancer-report from a consensus panel. *J Endourol*. 2010;24:775-80. <https://doi.org/10.1089/end.2009.0596>.
- [5] Tincher SA, Kim RY, Ezekiel MP, Zinsli T, Fiveash JB, Raben DA, et al. Effects of pelvic rotation and needle angle on pubic arch interference during transperineal prostate implants. *Int J Radiat Oncol Biol Phys*. 2000;47:361-3. [https://doi.org/10.1016/s0360-3016\(00\)00434-x](https://doi.org/10.1016/s0360-3016(00)00434-x).
- [6] Jamema SV, Sajju S, Shetty UM, Pallad S, Deshpande D, Shrivastava S. Dosimetric comparison of inverse optimization with geometric optimization in combination with graphical optimization for HDR prostate implants. *Journal of Medical Physics/Association of Medical Physicists of India*. 2006;31(2):89. <https://doi.org/10.4103/0971-6203.26694>.
- [7] Mate TP, Gottesman JE, Hatton J, Gribble M, Van Hollebeke L. High dose-rate afterloading 192Iridium prostate brachytherapy: Feasibility report. *Int J Radiat Oncol Biol Phys*. 1998;41:525-33. [https://doi.org/10.1016/s0360-3016\(98\)00097-2](https://doi.org/10.1016/s0360-3016(98)00097-2).
- [8] Taschereau R, Poulitot J, Roy J, Tremblay D. Seed misplacement and stabilizing needles in transperineal permanent prostate implants. *Radiother Oncol*. 2000;55:59-63. [https://doi.org/10.1016/s0167-8140\(00\)00162-6](https://doi.org/10.1016/s0167-8140(00)00162-6).
- [9] Sejal SV, Sathiaseelan V, Helenowski IB, Kozlowski JM, Carter MF, Nadler RB, et al. Intra-operative pubic arch interference during prostate seed brachytherapy in patients with CT-based pubic arch interference of  $\leq 1$  cm. *Radiother Oncol*. 2009;91:249-54. <https://doi.org/10.1016/j.radonc.2009.02.006>.
- [10] Martin GV, Pugh TJ, Mahmood U, Kudchadker RJ, Wang J, Bruno TL, et al. Permanent prostate brachytherapy postimplant magnetic resonance imaging dosimetry using positive contrast magnetic resonance imaging markers. *Brachytherapy*. 2017;16:761-9. <https://doi.org/10.1016/j.brachy.2017.04.004>.
- [11] Strang JG, Rubens DJ, Brasacchio RA, Yu Y, Messing EM. Real-time US versus CT determination of pubic arch interference for brachytherapy. *Radiology*. 2001;219:387-93. <https://doi.org/10.1148/radiology.219.2.r01ma37387>.
- [12] Wallner K, Ellis W, Russell K, Cavanagh W, Blasko J. Use of TRUS to predict pubic arch interference of prostate brachytherapy. *Int J Radiat Oncol Biol Phys*. 1999;43:583-5. [https://doi.org/10.1016/s0360-3016\(98\)00459-3](https://doi.org/10.1016/s0360-3016(98)00459-3).
- [13] De Vries M, Wilby S, Palmer AL, Polak W, O'Hea I, Hodgson D, et al. Overcoming pubic arch interference in prostate brachytherapy using steerable needles. *Journal of Contemporary Brachytherapy*. 2022;14(5):495-500. <https://doi.org/10.5114/jcb.2022.121562>.
- [14] Zheng Y, Wu J, Chen S, Liu Y, Zhang G. Predicting pubic arch interference in permanent prostate brachytherapy based on the specific parameters derived from nuclear magnetic resonance imaging. *J Contemp Brachytherapy*. 2018;10:405-10. <https://doi.org/10.5114/jcb.2018.79247>.
- [15] Fukada J, Shigematsu N, Nakashima J, Ohashi T, Kawaguchi O, Oya M. Predicting pubic arch interference in prostate brachytherapy on transrectal ultrasonography-computed tomography fusion images. *J Radiat Res*. 2012;53:753-9. <https://doi.org/10.1093/jrr/rrs020>.



- [16] Ryu B, Bax J, Edirisinge C, Lewis C, Chen J, D'Souza D, et al. Prostate brachytherapy with oblique needles to treat large glands and overcome pubic arch interference. *Int J Radiat Oncol Biol Phys.* 2012;83:1463-72. <https://doi.org/10.1016/j.ijrobp.2011.10.012>.
- [17] Gibbons EP, Smith RP, Beriwal S, Krishna K, Benoit RM. Overcoming pubic arch interference with free-hand needle placement in men undergoing prostate brachytherapy. *Brachytherapy.* 2009;8:74-8. <https://doi.org/10.1016/j.brachy.2008.04.007>.
- [18] Nickers P, Thissen B, Jansen N, Deneufbourg JM. 192Ir or 125I prostate brachytherapy as a boost to external beam radiotherapy in locally advanced prostatic cancer: A dosimetric point of view. *Radiother Oncol.* 2006;78:47-52. <https://doi.org/10.1016/j.radonc.2005.09.002>.
- [19] Henderson A, Laing RW, Langley SEM. Identification of pubic arch interference in prostate brachytherapy: Simplifying the transrectal ultrasound technique. *Brachytherapy.* 2003;2:240-5. <https://doi.org/10.1016/j.brachy.2003.11.001>.
- [20] Wang H, Wallner K, Sutlief S, Blasko J, Russell K, Ellis W. Transperineal brachytherapy in patients with large prostate glands. *Int J Cancer.* 2000;90:199-205. [https://doi.org/10.1002/1097-0215\(20000820\)90:4<199::Aid-ijc3>3.0.Co;2-c](https://doi.org/10.1002/1097-0215(20000820)90:4<199::Aid-ijc3>3.0.Co;2-c).
- [21] Bellon J, Wallner K, Ellis W, Russell K, Cavanagh W, Blasko J. Use of pelvic CT scanning to evaluate pubic arch interference of transperineal prostate brachytherapy. *Int J Radiat Oncol Biol Phys.* 1999;43:579-81. [https://doi.org/10.1016/s0360-3016\(98\)00466-0](https://doi.org/10.1016/s0360-3016(98)00466-0).
- [22] Borghede G, Hedelin H, Holmäng S, Johansson KA, Sernbo G, Mercke C. Irradiation of localized prostatic carcinoma with a combination of high dose rate iridium-192 brachytherapy and external beam radiotherapy with three target definitions and dose levels inside the prostate gland. *RADIOTHER ONCOL.* 1997;44:245-50. [https://doi.org/10.1016/s0167-8140\(97\)00122-9](https://doi.org/10.1016/s0167-8140(97)00122-9).
- [23] Huang Y, Miller B, Doemer A, Babij D, Kumar S, Frontera R, et al. Online correction of catheter movement using CT in high-dose-rate prostate brachytherapy. *Brachytherapy.* 2013;12:260-6. <https://doi.org/10.1016/j.brachy.2012.08.008>.
- [24] Whitaker M, Hruby G, Lovett A, Patanjali N. Prostate HDR brachytherapy catheter displacement between planning and treatment delivery. *Radiother Oncol.* 2011;101:490-4. <https://doi.org/10.1016/j.radonc.2011.08.004>.
- [25] Holly R, Morton GC, Sankrecha R, Law N, Cisecki T, Loblaw DA, et al. Use of cone-beam imaging to correct for catheter displacement in high dose-rate prostate brachytherapy. *Brachytherapy.* 2011;10:299-305. <https://doi.org/10.1016/j.brachy.2010.11.007>.
- [26] Kovalchuk N, Furutani KM, MacDonald OK, Pisansky TM. Dosimetric effect of interfractional needle displacement in prostate high-dose-rate brachytherapy. *Brachytherapy.* 2012;11:111-8. <https://doi.org/10.1016/j.brachy.2011.05.006>.
- [27] Reynés-Llompert G, Pino F, Modolell I, Gullón C, Pera J, Gutierrez C, et al. Impact of prostate catheter displacement in inverse planning-simulated annealing and geometric optimization. *Brachytherapy.* 2016;15:112-7. <https://doi.org/10.1016/j.brachy.2015.10.003>.
- [28] Carrara M, Tenconi C, Mazzeo D, Romanyukha A, Borroni M, Pignoli E, et al. Study of the correlation between rectal wall in vivo dosimetry performed with MOSkins and implant modification during TRUS-guided HDR prostate brachytherapy. *Radiation Measurements.* 2017;106:385-90. <https://doi.org/10.1016/j.radmeas.2017.03.016>.
- [29] Cepek J, Lindner U, Ghai S, Louis AS, Davidson SRH, Gertner M, et al. Mechatronic system for in-bore MRI-guided insertion of needles to the prostate: An in vivo needle guidance accuracy study. *J Magn Reson Imaging.* 2015;42:48-55. <https://doi.org/10.1002/jmri.24742>.
- [30] Buus S, Lizondo M, Hokland S, Rylander S, Pedersen EM, Tanderup K, et al. Needle migration and dosimetric impact in high-dose-rate brachytherapy for prostate cancer evaluated by repeated MRI. *Brachytherapy.* 2018;17:50-8. <https://doi.org/10.1016/j.brachy.2017.08.005>.
- [31] Mullokandov E, Gejerman G. Analysis of serial CT scans to assess template and catheter movement in prostate HDR brachytherapy. *Int J Radiat Oncol Biol Phys.* 2004;58:1063-71. <https://doi.org/10.1016/j.ijrobp.2003.08.020>.

- [32] Damore SJ, Syed AMN, Puthawala AA, Sharma A. Needle displacement during HDR brachytherapy in the treatment of prostate cancer. *Int J Radiat Oncol Biol Phys.* 2000;46:1205-11. [https://doi.org/10.1016/s0360-3016\(99\)00477-0](https://doi.org/10.1016/s0360-3016(99)00477-0).
- [33] Pellizzon ACA, Salvajoli JV, Novaes PERS, Maia MAC, Ferigno R, Fogaroli RC. Needle displacement during high-dose-rate afterloading brachytherapy boost and conventional external beam radiation therapy for initial and local advanced prostate cancer. *Urol Int.* 2003;70:200-4. <https://doi.org/10.1159/000068775>.
- [34] Smith RL, Hanlon M, Panettieri V, Millar JL, Matheson B, Haworth A, et al. An integrated system for clinical treatment verification of HDR prostate brachytherapy combining source tracking with pretreatment imaging. *Brachytherapy.* 2018;17:111-21. <https://doi.org/10.1016/j.brachy.2017.08.004>.
- [35] Jamaluddin MF, Ghosh S, Waine MP, Sloboda RS, Tavakoli M, Amanie J, et al. Quantifying 125I placement accuracy in prostate brachytherapy using postimplant transrectal ultrasound images. *Brachytherapy.* 2017;16:306-12. <https://doi.org/10.1016/j.brachy.2016.11.015>.
- [36] Fichtinger G, Fiene JP, Kennedy CW, Kronreif G, Iordachita I, Song DY, et al. Robotic assistance for ultrasound-guided prostate brachytherapy. *Med Image Anal.* 2008;12:535-45. <https://doi.org/10.1016/j.media.2008.06.002>.
- [37] Szlag M, Śłosarek K, Rembielak A, Białas B, Fijałkowski M, Bystrzycka J. Real-time brachytherapy for prostate cancer - Implant analysis. *Rep Pract Oncol Radiother.* 2008;13:9-14. [https://doi.org/10.1016/s1507-1367\(10\)60076-4](https://doi.org/10.1016/s1507-1367(10)60076-4).
- [38] Cormack RA, Tempany CM, D'Amico AV. Optimizing target coverage by dosimetric feedback during prostate brachytherapy. *Int J Radiat Oncol Biol Phys.* 2000;48:1245-9. [https://doi.org/10.1016/s0360-3016\(00\)00742-2](https://doi.org/10.1016/s0360-3016(00)00742-2).
- [39] Taschereau R, Pouliot J, Roy J, Tremblay D. Seed misplacement and stabilizing needles in transperineal permanent prostate implants. *Radiotherapy and Oncology.* 2000;55(1):59-63. [https://doi.org/10.1016/S0167-8140\(00\)00162-6](https://doi.org/10.1016/S0167-8140(00)00162-6).
- [40] David A, Brennan V, Cohen G, Damato A. Is there a clinically meaningful change in anatomy during planning of US HDR prostate brachytherapy? *Radiother Oncol.* 2019;133:S586. [https://doi.org/10.1016/s0167-8140\(19\)31472-0](https://doi.org/10.1016/s0167-8140(19)31472-0).
- [41] Wu CHD, Thind K, Husain S, Watt E. Prostate and catheter motion in prostate hdr brachytherapy: from operating room to shielded delivery vault. *Radiother Oncol.* 2019;139:S29. [https://doi.org/10.1016/s0167-8140\(19\)33352-3](https://doi.org/10.1016/s0167-8140(19)33352-3).
- [42] Maenhout M, van der Voort van Zyp JRN, Borot de Battisti M, Peters M, van Vulpen M, van den Bosch M, et al. The effect of catheter displacement and anatomical variations on the dose distribution in MRI-guided focal HDR brachytherapy for prostate cancer. *Brachytherapy.* 2018;17:24-30. <https://doi.org/10.1016/j.brachy.2017.04.239>.
- [43] Aluwini S, Busser WMH, Baartman LEA, Bhawanie A, Alemayehu WG, Boormans JL, et al. Fractionated high-dose-rate brachytherapy as monotherapy in prostate cancer: Does implant displacement and its correction influence acute and late toxicity? *Brachytherapy.* 2016;15:707-13. <https://doi.org/10.1016/j.brachy.2016.05.008>.
- [44] Peddada AV, Blasi OC, White GA, Monroe AT, Jennings SB, Gibbs GL. Prevention of needle displacement in multifraction high-dose-rate prostate brachytherapy: A prospective volumetric analysis and technical considerations. *Pract Radiat Oncol.* 2015;5:228-37. <https://doi.org/10.1016/j.prr.2014.11.004>.
- [45] Dinkla AM, Pieters BR, Koedooder K, Wieringen N, Laarse R, Bel A. Prostate volume and implant configuration during 48 hours of temporary prostate brachytherapy: Limited effect of oedema. *Radiat Oncol.* 2014;9. <https://doi.org/10.1186/s13014-014-0272-9>.
- [46] Kawakami S, Ishiyama H, Terazaki T, Soda I, Satoh T, Kitano M, et al. Catheter displacement prior to the delivery of high-dose-rate brachytherapy in the treatment of prostate cancer patients. *J Contemp Brachytherapy.* 2014;6:161-6. <https://doi.org/10.5114/jcb.2014.43619>.
- [47] Takenaka T, Yoshida K, Ueda M, Yamazaki H, Miyake S, Tanaka E, et al. Assessment of daily needle applicator displacement during high-dose-rate interstitial brachytherapy for prostate cancer using daily CT examinations. *J Rad Res.* 2012;53:469-74. <https://doi.org/10.1269/jrr.11168>.

- [48] Foster W, Cunha JAM, Hsu IC, Weinberg V, Krishnamurthy D, Pouliot J. Dosimetric impact of interfraction catheter movement in high-dose rate prostate brachytherapy. *Int J Radiat Oncol Biol Phys.* 2011;80:85-90. <https://doi.org/10.1016/j.ijrobp.2010.01.016>.
- [49] Fox CD, Kron T, Leahy M, Duchesne G, Williams S, Tai KH, et al. Interfraction patient motion and implant displacement in prostate high dose rate brachytherapy. *Med Phys.* 2011;38:5838-43. <https://doi.org/10.1118/1.3641865>.
- [50] Milickovic N, Mavroidis P, Tselis N, Nikolova I, Katsilieri Z, Kefala V, et al. 4D analysis of influence of patient movement and anatomy alteration on the quality of 3D U/S-based prostate HDR brachytherapy treatment delivery. *Med Phys.* 2011;38:4982-93. <https://doi.org/10.1118/1.3618735>.
- [51] Tiong A, Bydder S, Ebert M, Caswell N, Waterhouse D, Spry N, et al. A Small Tolerance for Catheter Displacement in High-Dose Rate Prostate Brachytherapy is Necessary and Feasible. *Int J Radiat Oncol Biol Phys.* 2010;76:1066-72. <https://doi.org/10.1016/j.ijrobp.2009.03.052>.
- [52] Yoshida K, Yamazaki H, Nose T, Shiomi H, Yoshida M, Mikami M, et al. Needle applicator displacement during high-dose-rate interstitial brachytherapy for prostate cancer. *Brachytherapy.* 2010;9:36-41. <https://doi.org/10.1016/j.brachy.2009.04.006>.
- [53] Simnor T, Li S, Lowe G, Ostler P, Bryant L, Chapman C, et al. Justification for inter-fraction correction of catheter movement in fractionated high dose-rate brachytherapy treatment of prostate cancer. *Radiother Oncol.* 2009;93:253-8. <https://doi.org/10.1016/j.radonc.2009.09.015>.
- [54] Kim Y, Hsu IC, Pouliot J. Measurement of craniocaudal catheter displacement between fractions in computed tomography-based high dose rate brachytherapy of prostate cancer. *J Appl Clin Med Phys.* 2007;8:2415. <https://doi.org/10.1120/jacmp.v8i4.2415>.
- [55] Pieters BR, van der Grient JNB, Blank LECM, Koedooder K, Hulshof MCCM, de Reijke TM. Minimal displacement of novel self-anchoring catheters suitable for temporary prostate implants. *Radiother Oncol.* 2006;80:69-72. <https://doi.org/10.1016/j.radonc.2006.06.014>.
- [56] Hoskin PJ, Bownes PJ, Ostler P, Walker K, Bryant L. High dose rate afterloading brachytherapy for prostate cancer: Catheter and gland movement between fractions. *Radiother Oncol.* 2003;68:285-8. [https://doi.org/10.1016/s0167-8140\(03\)00203-2](https://doi.org/10.1016/s0167-8140(03)00203-2).
- [57] Martinez AA, Pataki I, Edmundson G, Sebastian E, Brabbins D, Gustafson G. Phase II prospective study of the use of conformal high-dose-rate brachytherapy as monotherapy for the treatment of favorable stage prostate cancer: A feasibility report. *Int J Radiat Oncol Biol Phys.* 2001;49:61-9. [https://doi.org/10.1016/s0360-3016\(00\)01463-2](https://doi.org/10.1016/s0360-3016(00)01463-2).
- [58] Davis BJ, Horwitz EM, Lee WR, Crook JM, Stock RG, Merrick GS, et al. American Brachytherapy Society consensus guidelines for transrectal ultrasound-guided permanent prostate brachytherapy. *Brachytherapy.* 2012;11:6-19. <https://doi.org/10.1016/j.brachy.2011.07.005>.
- [59] Henry A, Pieters BR, Siebert FA, Hoskin P. GEC-ESTRO ACROP prostate brachytherapy guidelines. *Radiotherapy and Oncology.* 2022;167:244-51. <https://doi.org/10.1016/j.radonc.2021.12.047>.
- [60] Van Gerwen DJ, Dankelman J, van den Dobbelsteen JJ. Needle–tissue interaction forces—A survey of experimental data. *Medical engineering & physics.* 2012;34(6):665-80. <https://doi.org/10.1016/j.medengphy.2012.04.007>.
- [61] Misra S, Reed KB, Douglas AS, Ramesh K, Okamura AM. Needle-tissue interaction forces for bevel-tip steerable needles. 2008 2nd IEEE RAS & EMBS International Conference on Biomedical Robotics and Biomechanics; 2008: IEEE. <https://doi.org/10.1109/BIOROB.2008.4762872>.
- [62] Wan G, Wei Z, Gardi L, Downey DB, Fenster A. Brachytherapy needle deflection evaluation and correction. *Med Phys.* 2005;32:902-9. <https://doi.org/10.1118/1.1871372>.
- [63] Kolkman-Deurloo IKK, Roos MA, Aluwini S. HDR monotherapy for prostate cancer: A simulation study to determine the effect of catheter displacement on target coverage and normal tissue irradiation. *Radiother Oncol.* 2011;98:192-7. <https://doi.org/10.1016/j.radonc.2010.12.009>.
- [64] Poder J, Carrara M, Howie A, Cutajar D, Bucci J, Rosenfeld A. Derivation of in vivo source tracking error thresholds for TRUS-based HDR prostate brachytherapy through simulation of source positioning errors. *Brachytherapy.* 2019;18:711-9. <https://doi.org/10.1016/j.brachy.2019.05.001>.

- [65] Mason J, Henry A, Bownes P. Error detection thresholds for routine real time in vivo dosimetry in HDR prostate brachytherapy. *Radiother Oncol.* 2020;149:38-43. <https://doi.org/10.1016/j.radonc.2020.04.058>.
- [66] Yamoah K, Eldredge-Hindy HB, Zaorsky NG, Palmer JD, Doyle LA, Sendeci JA, et al. Large prostate gland size is not a contraindication to low-dose-rate brachytherapy for prostate adenocarcinoma. *Brachytherapy.* 2014;13:456-64. <https://doi.org/10.1016/j.brachy.2014.04.003>.
- [67] Kim Y, Hsu IC, Lessard E, Vujic J, Pouliot J. Dosimetric impact of prostate volume change between CT-based HDR brachytherapy fractions. *Int J Radiat Oncol Biol Phys.* 2004;59:1208-16. <https://doi.org/10.1016/j.ijrobp.2004.02.053>.
- [68] Ballester MAG, Zisserman AP, Brady M. Estimation of the partial volume effect in MRI. *Medical Image Analysis.* 2002;6(4):389-405. [https://doi.org/10.1016/S1361-8415\(02\)00061-0](https://doi.org/10.1016/S1361-8415(02)00061-0).
- [69] Fedorov A, Khalil S, Sánchez CA, Lasso A, Fels S, Tuncali K, et al. Open-source image registration for MRI-TRUS fusion-guided prostate interventions. *International journal of computer assisted radiology and surgery.* 2015;10(6):925-34. <https://doi.org/10.1007/s11548-015-1180-7>.
- [70] Klotz CL. Can high resolution micro-ultrasound replace MRI in the diagnosis of prostate cancer? *European urology focus.* 2020;6(2):419-23. <https://doi.org/10.1016/j.euf.2019.11.006>.
- [71] Kucway R, Vicini F, Huang R, Stromberg J, Gonzalez J, Martinez A. Prostate volume reduction with androgen deprivation therapy before interstitial brachytherapy. *J Urol.* 2002;167:2443-7. [https://doi.org/10.1016/s0022-5347\(05\)65001-x](https://doi.org/10.1016/s0022-5347(05)65001-x).
- [72] Press RH, Morgan TM, Cutrell PK, Zhang C, Chen Z, Rahnema S, et al. Patient-reported health-related quality of life outcomes after HDR brachytherapy between small (<60 cc) and large (≥60 cc) prostate glands. *Brachytherapy.* 2019;18:13-21. <https://doi.org/10.1016/j.brachy.2018.08.009>.
- [73] Kopp RP, Marshall LM, Wang PY, Bauer DC, Barrett-Connor E, Parsons JK, et al. The burden of urinary incontinence and urinary bother among elderly prostate cancer survivors. *European Urology.* 2013;64(4):672-9. <https://doi.org/10.1016/j.eururo.2013.03.041>.
- [74] Saigal CS, Gore JL, Krupski TL, Hanley J, Schonlau M, Litwin MS. Androgen deprivation therapy increases cardiovascular morbidity in men with prostate cancer. *Cancer: Interdisciplinary International Journal of the American Cancer Society.* 2007;110(7):1493-500. <https://doi.org/10.1002/ncr.22933>.
- [75] Basaria S, Lieb J, Tang AM, DeWeese T, Carducci M, Eisenberger M, et al. Long-term effects of androgen deprivation therapy in prostate cancer patients. *Clinical endocrinology.* 2002;56(6):779-86. <https://doi.org/10.1046/j.1365-2265.2002.01551.x>.
- [76] Keyes M, Merrick G, Frank SJ, Grimm P, Zelefsky MJ. Use of Androgen Deprivation Therapy with Prostate Brachytherapy, A Systematic Literature Review. *Brachytherapy.* 2017;16(2):245. <https://doi.org/10.1016/j.brachy.2016.11.017>.
- [77] Stone NN, Stock RG. Prostate brachytherapy in patients with prostate volumes ≥ 50 cm<sup>3</sup>: Dosimetric analysis of implant quality. *Int J Radiat Oncol Biol Phys.* 2000;46:1199-204. [https://doi.org/10.1016/s0360-3016\(99\)00516-7](https://doi.org/10.1016/s0360-3016(99)00516-7).
- [78] Roy JN, Wallner KE, Chiu-Tsao ST, Anderson LL, Ling CC. CT-based optimized planning for transperineal prostate implant with customized template. *INT J RADIAT ONCOL BIOL PHYS.* 1991;21:483-9. [https://doi.org/10.1016/0360-3016\(91\)90800-J](https://doi.org/10.1016/0360-3016(91)90800-J).
- [79] Van de Berg NJ, Dankelman J, van den Dobbelaars JJ. Design of an actively controlled steerable needle with tendon actuation and FBG-based shape sensing. *Medical Engineering & Physics.* 2015;37(6):617-22. <https://doi.org/10.1016/j.medengphy.2015.03.016>.
- [80] De Vries M, Sikorski J, Misra S, van den Dobbelaars J. Axially rigid steerable needle with compliant active tip control. *PLoS one.* 2021;16(12):e0261089. <https://doi.org/10.1371/journal.pone.0261089>.
- [81] Podder TK, Dicker AP, Hutapea P, Darvish K, Yu Y. A novel curvilinear approach for prostate seed implantation. *Med Phys.* 2012;39:1887-92. <https://doi.org/10.1118/1.3694110>.
- [82] Bloembergen J, Trauzettel F, Coolen B, Dodou D, Breedveld P. Design and evaluation of an MRI-ready, self-propelled needle for prostate interventions. *PLoS one.* 2022;17(9):e0274063. <https://doi.org/10.1371/journal.pone.0274063>.

- [83] Marcu LG, Lawson JM. Technical and dosimetric aspects of iodine-125 seed reimplantation in suboptimal prostate implants. *Br J Radiol.* 2013;86. <https://doi.org/10.1259/bjr.20130058>.
- [84] Keyes M, Pickles T, Agranovich A, Kwan W, Morris WJ. 125I reimplantation in patients with poor initial dosimetry after prostate brachytherapy. *Int J Radiat Oncol Biol Phys.* 2004;60:40-50. <https://doi.org/10.1016/j.ijrobp.2004.02.011>.
- [85] Hughes L, Waterman FM, Dicker AP. Salvage of suboptimal prostate seed implantation: Reimplantation of underdosed region of prostate base. *Brachytherapy.* 2005;4:163-70 . <https://doi.org/10.1016/j.brachy.2005.03.002>.
- [86] Morris WJ, Spadinger I, Keyes M, Hamm J, McKenzie M, Pickles T. Whole prostate D90 and V100: A dose-response analysis of 2000 consecutive 125I monotherapy patients. *Brachytherapy.* 2014;13:32-41. <https://doi.org/10.1016/j.brachy.2013.08.006>.
- [87] Natarajan S, Raman S, Priester AM, Garritano J, Margolis DJA, Lieu P, et al. Focal Laser Ablation of Prostate Cancer: Phase I Clinical Trial. *J Urol.* 2016;196:68-75. <https://doi.org/10.1016/j.juro.2015.12.083>.
- [88] Skowronek J. Current status of brachytherapy in cancer treatment—short overview. *Journal of contemporary brachytherapy.* 2017;9(6):581-9. <https://doi.org/10.5114/jcb.2017.72607>.
- [89] Devlin PM, Holloway CL, Stewart AJ. *Brachytherapy: applications and techniques*: Springer Publishing Company; 2015.
- [90] Fischer GS, Iordachita I, Csoma C, Tokuda J, DiMaio SP, Tempny CM, et al. MRI-compatible pneumatic robot for transperineal prostate needle placement. *Ieee-Asme Transactions on Mechatronics.* 2008;13:295-305. <https://doi.org/10.1109/TMECH.2008.924044>.
- [91] Siepel FJ, Maris B, Welleweerd MK, Groenhuis V, Fiorini P, Stramigioli S. Needle and biopsy robots: A review. *Current Robotics Reports.* 2021;2(1):73-84. <https://doi.org/10.1007/s43154-020-00042-1>.

# 3

## Overcoming pubic arch interference in prostate brachytherapy using steerable needles

Martijn de Vries, Sarah L. Wilby, Antony L. Palmer, Wojciech Polak, Inna O'Hea, Dominic Hodgson, John J. van den Dobbelssteen

*Published in Journal of Contemporary Brachytherapy (2022)*

## ABSTRACT

A proportion of patients are not directly eligible for prostate brachytherapy (BT) due to pubic arch interference (PAI). Constraints in positioning sources behind the pubic arch due to linear, horizontal needle paths may hamper effective irradiation of the target volume. This work evaluates the effect of prostate volume ( $V_p$ ) and patient posture change on the amount of PAI and demonstrates that steerable needles may broaden the inclusion criteria for patients with enlarged prostates and observed PAI. Twenty-seven patients ( $V_p > 60$  cc) were included in this study. Access obstruction to the prostate was assessed, using diagnostic Magnetic Resonance Imaging (MRI) scans, after six upward rotations of the pelvis and the prostate in 5 degree steps to indicate the effect of patient posture change from supine to lithotomy position. For the patients with PAI, we evaluated if the steerable needle could access the obstructed volume of the prostate. The data show no clear relation between  $V_p$  and PAI. Of 23 of the 27 patients in which PAI was observed, 14 showed obstruction of the prostate of  $\geq 10$  mm in the supine position (mean PAI  $\pm$  standard deviation:  $15.2 \pm 3.8$  mm). Anatomical rotation reduced PAI by 4.8 mm after every 10 degrees of upward rotation, still resulting in obstructions of  $8.1 \pm 2.4$  mm in 10 of the 14 cases after 15 degrees rotation. The steerable needle enabled access to all the required coordinates of the prostate. The ability to steer along curved paths enables prostate BT for patients with enlarged prostates and PAI and reduces the change of needing to abandon treatment.

### 3.1 PURPOSE

The American National Cancer Institute SEER program reports that 12.5% of men will be diagnosed with prostate cancer during their lifetime, with this being responsible for 10.7% of all male cancer mortality in 2022 [1]. Prostate brachytherapy (BT) is a cancer treatment which delivers a radiation dose to the target volume while sparing surrounding organs at risk [2]. Unfortunately, a proportion of men are not directly considered eligible for BT as access to the anterolateral part of the prostate can be obstructed by the pubic arch in the conventional treatment approaches utilising parallel running, straight implant needles. This is referred to as pubic arch interference (PAI). Limitations in positioning low-dose-rate (LDR) sources or high-dose-rate (HDR) source dwells, behind the pubic arch may prevent effective irradiation as an adequate implant geometry in the target volume cannot be obtained.

The American Brachytherapy Society (ABS) guidelines state that a prostate volume ( $V_p$ ) of  $> 60$  cc is technically more challenging as PAI is more prevalent with enlarged prostates, and such a prostate volume is a relative contraindication for BT [3]. Earlier studies reported that 9% to 38% of patients had a  $V_p \geq 60$  cc [4–7]. However, the relation between  $V_p$  and the occurrence of PAI is not strong and large prostates have been successfully implanted with good results for both dosimetry and biochemical control without excessive toxicity [2,5,7]. Therefore, the Groupe Européen de Curiothérapie and the European Society for Radiotherapy & Oncology (GEC-ESTRO) Advisory Committee for Radiation Oncology Practice (ACROP) have recently adapted their guidelines related to gland size which now state that a prostate volume of  $> 50 - 60$  cc is no longer a contraindication for BT if there is minimal PAI [2]. A threshold of 10 mm overlap by the pubic arch is used to indicate minimal PAI on the magnetic resonance imaging (MRI) or computed tomography (CT) scan, with the patient in supine position, for minimising the incidence of PAI during the procedure, with the patient in lithotomy position [4,8]. For PAI in the lithotomy position a threshold of 5 mm is reported [8,9].

The change in body position causes an anatomical rotation of the pelvis and prostate, estimated at 15 degrees by Strang et al. [10], with associated improved accessibility of the prostate [11]. However, the relation between change in position corresponding obstruction is patient specific, and earlier studies showed that a significant proportion of patients with enlarged prostates had excessive PAI of  $\geq 10$  mm. Zheng et al. [12] reported that 10 of 40 patients with a mean  $V_p$  of 64 cc had PAI up to 15.1 mm on MRI scans, while Bellon et al. [4] showed that 3 of 9 patients with a  $V_p > 60$  cc had 10 to 20 mm PAI on CT scans, and Wang et al. observed PAI up to 13 mm on CT scans in 71% of the 21 patients with a prostate volume  $> 50$  cc [6]. In addition to the prevalence of PAI in enlarged prostates, smaller prostate glands can be difficult to access if the pubic arch is narrow, observed in 5% to 25% of patients with a  $V_p < 60$  cc [8,13,14].

In practice, attempts to correct minimal PAI can be made by implanting sources in a different position to that planned, or manipulating the ultrasound probe [9,15], while excessive PAI demands more drastic solutions. The patient can be placed in extended lithotomy position [4,11,15] but this increases the risk for rectal needle penetration [16] and can result in movement of the prostate because of probe angulation or inflation [17,18]. Besides, not all patients are able to be manipulated into the required body positions [16]. Free-hand oblique needle implantations without the use of a transperineal template are difficult and require experience [19,20]. These solutions demand adjustments to the clinical set-up and workflow and can result in an inadequate dose coverage [18]. Another solution to overcome PAI is downsizing the prostate with the use of hormonal therapy, such as androgen deprivation therapy (ADT) [8,15]. ADT decreases the prostate volume by 25 to 40 % in 3 months, but is associated with significant costs, prolonged treatment time, and morbidity [21,22]. Occasionally, excessive PAI is encountered at the time of implantation. The planned implant geometry and the dosimetry requirements cannot be met and another subsequent curative treatment is required, such as external beam radiotherapy [9]. This introduces additional costs for the healthcare system and a considerable anxiety for the patient.



Steerable needles that enable circumventing of interference from the pubic arch may facilitate proper distribution of the source positions without a change in clinical set-up and thereby potentially ensure adequate irradiation of the target volume [23]. Such needles allow for increased flexibility in needle placement and may extend the treatment options for patients with enlarged and obstructed prostates. To investigate the potential benefits of steerable needles the present work evaluates PAI in 27 patients. Through simulation of the rotations of the pelvis and the prostate, we show the extent to which steerable needles can be used in patients with enlarged prostates and observed PAI.

### 3.2 MATERIALS AND METHODS

#### 3.2.1 Patients

The datasets of 27 anonymised patients were included. All patients had undergone a diagnostic MRI scan (MAGNETOM Aera 1.5T, Siemens Healthineers, Erlangen, Germany) in the supine position. The patient eligibility criteria for this study included clinical stage T1–T3b cancer, a Gleason score of  $\geq 3+3$ , any serum PSA and an original  $V_p$  of  $\geq 60$  cc based on the formula:  $V_p = \pi/6 \times (\text{height} \times \text{width} \times \text{length})$ . This choice excluded small prostates as the literature reports that the potential of PAI is lower in a smaller  $V_p$  [4].

#### 3.2.2 Segmentation

The prostate, pubic arch, urethra and rectum were segmented manually by an experienced medical physics technician approved for procedure by a doctor (see Figure 3.1, Top). The urethra was not always entirely visible

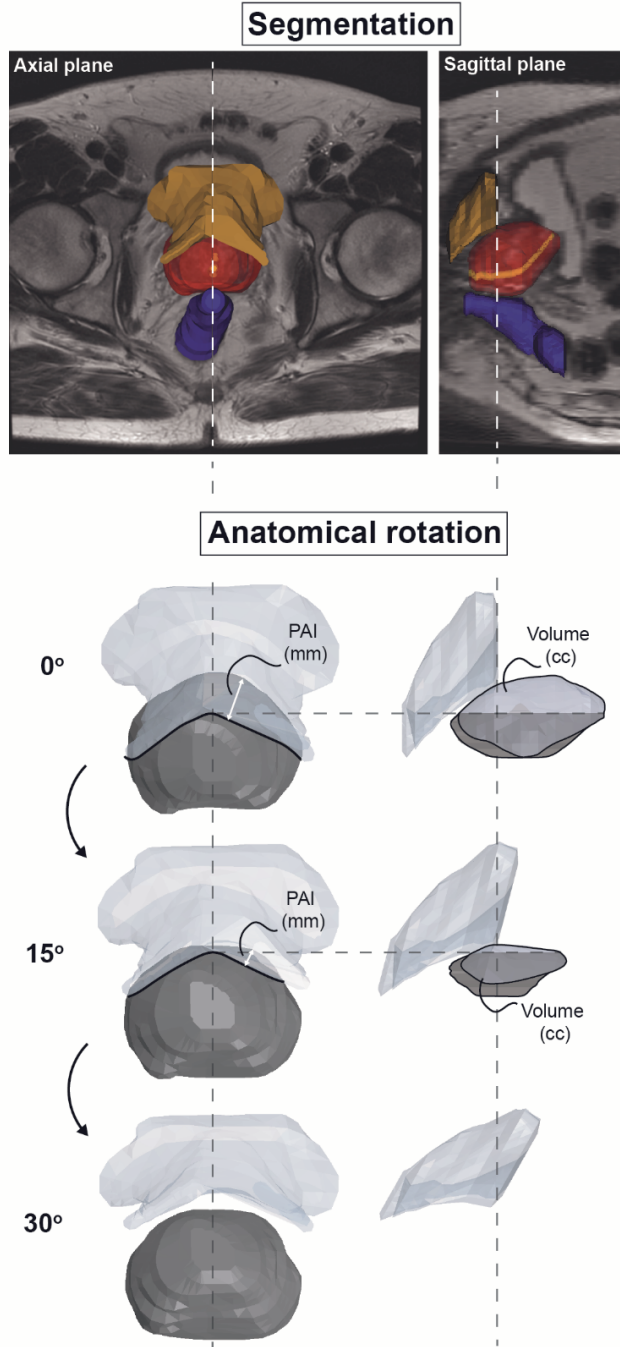


Figure 3.1 – Pipeline for the evaluation of the prostate datasets. Top: Segmentation of prostate, urethra, pubic arch, and rectum for all datasets. Bottom: Anatomical rotation of the prostate and the pubic arch over six angles: 0°, 5°, 10°, 15°, 20°, 25°.

on MRI, therefore a best estimate was made based on any visible parts and clinical experience. The pubic arch was contoured as a single structure. Where the pubic arch separates, a slither was added to the contour to connect the left and right sides.

### 3.2.3 Anatomical rotation

All MRI datasets were loaded into 3D Slicer (<http://www.slicer.org/>) and SolidWorks (Dassault Systèmes SOLIDWORKS Corp.) for image processing. The pubic arch was outlined in the axial reference plane of the prostate and the accessible part of the prostate was subtracted from the whole gland to evaluate the obstructed volume and the maximum interference in supine position.

The relationship between PAI and  $V_p$  was evaluated. To compare supine and lithotomy positions, PAI was quantified after six upward rotations of the anatomy in 5 degree steps, ranging from 0 to 30 degrees (see Figure 3.1, Bottom). PAI of  $\geq 10$  mm and  $\geq 5$  mm were considered excessive in supine and lithotomy position, respectively.

### 3.2.4 Overcoming pubic arch interference

In the sagittal plane distances were measured from the perineum to the plane where maximum PAI was found, indicating the required needle insertion depth. If the MRI scan length was not sufficient to detect the perineum, a best approximation was made based on the anatomy of patients with sufficient scan length. The maximum amount of PAI defined the upper limit for needle steering which is compared to the results reported by de Vries et al. [23]. In their study, experiments were performed in which a novel steerable needle was inserted in tissue simulants and *ex-vivo* bovine tissue. The authors reported lateral steering up to 20 mm over an insertion depth of 100 mm, and similar targeting accuracy for both the steerable needles and the conventional rigid HDR BT needles, while adding the ability to steer along curved paths. Figure 3.2 illustrates the set-up for needle steering in a patient with PAI.

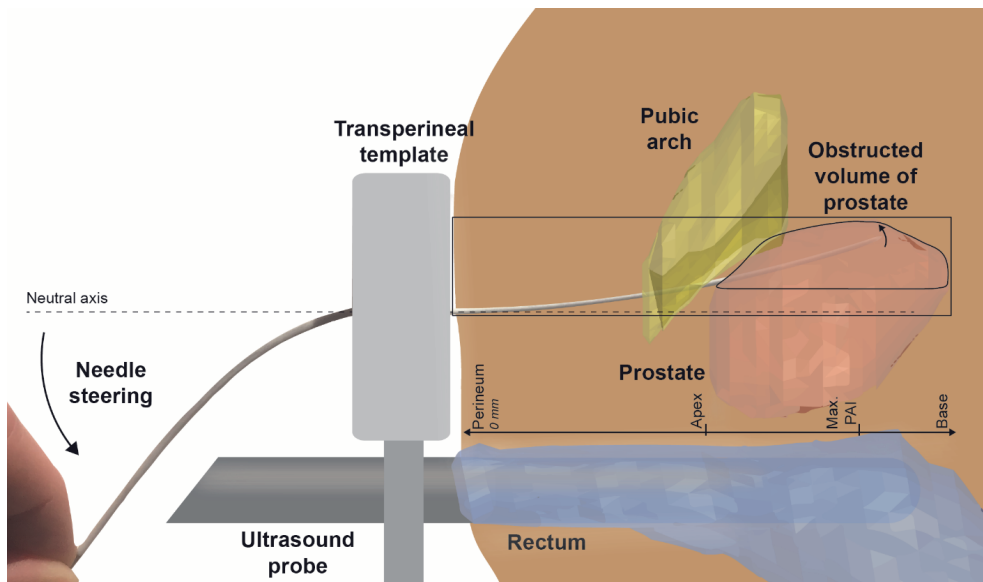


**Figure 3.2 – Prostate BT set-up with a steerable needle.** The steerable needle is steered upwards to access the obstructed volume of the prostate, inaccessible with linear insertion paths.

The steerable needle illustrated comprises of a toolled inner needle, having an integrated pull-push mechanism, and a flexible outer catheter. Bending the proximal end of the needle allows for adjustments of the outer catheter pathway and withdrawal of the inner needle creates a work channel for HDR BT.

### 3.3 RESULTS

#### 3.3.1 Pubic arch interference

Figure 3.3 indicates no clear relationship between  $V_p$  and PAI. Figure 3.4 shows the quantification of PAI related to anatomical rotation. In 23 of the 27 patients, the anterolateral part of the prostate is obstructed, and of these 14 are considered to have excessive PAI in supine position with PAI (mean  $\pm$  standard deviation) of  $15.2 \pm 3.8$  mm.

Four patients had no observed PAI. Change in posture from supine to lithotomy position caused an anatomical rotation of the pelvis which reduced PAI by 4.8 mm after 10 degrees of rotation and halved PAI with every 15 degrees of rotation. Nevertheless, a 15 degrees rotation is still associated with excessive PAI of more than 5 mm in 10 of the 14 cases. These 10 cases had a PAI of  $8.1 \pm 2.4$  mm. The obstructed volume of the prostate decreased non-linearly with anatomical rotation.

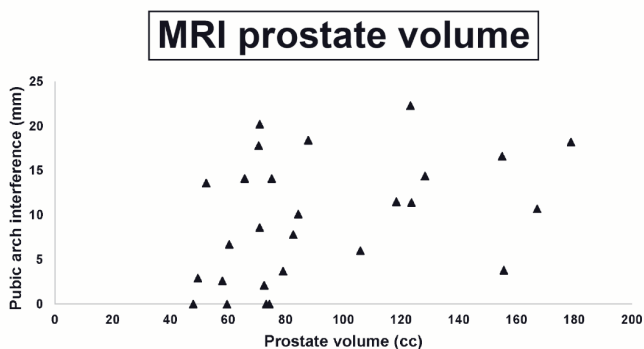
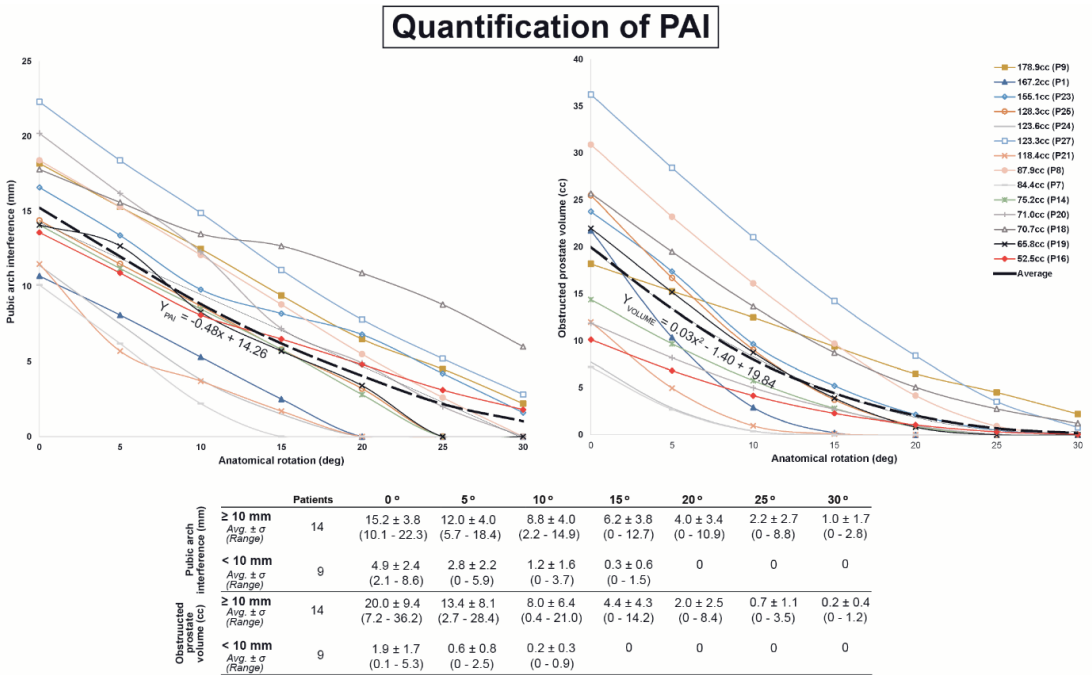


Figure 3.3 – Pubic arch interference versus MRI prostate volume for all datasets.



**Figure 3.4 – Quantification of PAI and the obstructed prostate volume related to anatomical rotation.** Only the patients with PAI ≥ 10 mm in the supine position (0° anatomical rotation) based on the original MRI scan are shown in the graphs. The dashed lines indicate the average of the datasets, which include the corresponding equation. The table describes the pubic arch interference and the obstructed prostate volume for all patients with PAI (< 10 mm and ≥ 10 mm).

### 3.3.2 Needle steering

For the patients considered in this study, lateral steering up to 22.3 mm was required over a distance of 73.7 mm in the supine position, and 12.7 mm over a distance of 91 mm after 15 degrees rotation. Figure 3.5 shows that the steerable needle allows for reaching of all the required coordinates after 0 to 15 degrees of anatomical rotation.

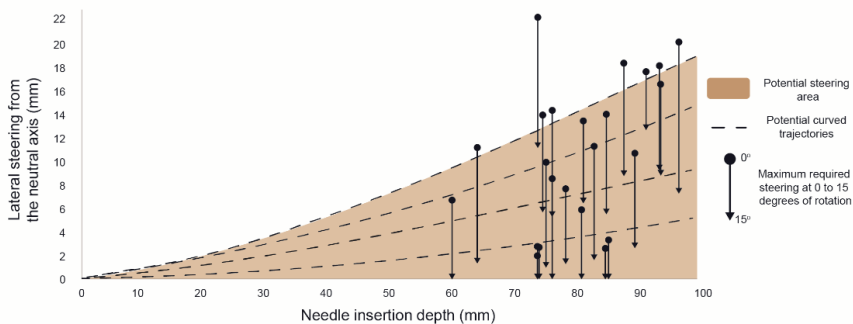


**Figure 3.5 – Steerable needle paths to circumvent PAI.** The amount of interference after 0 and 15 degrees of anatomical rotation is compared to the needle paths from (20). The brown area indicates the potential steering area of the steerable needle inside the body of the patient as illustrated in Figure 3.2. The dotted black lines show potential curved needle paths. Steering is applied directly after piercing the perineum, referred to as 0 mm needle insertion depth.

### 3.4 DISCUSSION

This work evaluates PAI in patients with large prostates and demonstrates the effect of anatomical rotation and the potential value of steerable needles to overcome PAI in a simulation study. Our results indicate no clear relation between  $V_p$  and PAI, while excessive PAI in the supine position was observed in half of the patients. The change in posture from supine to lithotomy position resulted in improved accessibility of the prostate, but obstructions of more than 5 mm still occurred after 15 degrees of anatomical rotation, which is estimated in literature to relate the supine and lithotomy position [10]. A steerable needle, as presented by de Vries et al. [23], may be able to overcome PAI in these cases allowing for the inclusion of patients with enlarged prostates and excessive PAI in prostate BT protocols.

In some clinical institutions, patients with a prostate of > 50 - 60 cc are currently considered ineligible for BT. However, large prostates have been successfully implanted with good results [2], while  $V_p$  calculations can be inaccurate which is substantiated by the discrepancy we found between the calculated  $V_p$  and the  $V_p$  based on the segmented prostate; 4 of the 27 datasets appeared to have a prostate gland < 60 cc. To avoid exclusion of patients to the BT procedure based on  $V_p$ , the GEC-ESTRO ACROP guidelines proposed the evaluation of PAI in enlarged prostates. However, no standard definitions were established for the degree of PAI. Even in small prostate glands difficulties can arise in combination with a narrow pubic arch [4]. One study noted that 19% of 243 patients with a mean  $V_p$  of 44.7 cc were likely to obtain an insufficient dose due to PAI [8], Peschel et al. reported that 25% of patients required a modified implant [13], and 5.5% of 145 patients in the study of Gibbons et al. having a mean  $V_p$  of 46.0 cc needed  $\geq 1$  implant needle inserted under an oblique angle without the aid of the needle template as the pubic arch was obstructing the prostate [14].

The change from supine to lithotomy position can facilitate access to the anterolateral part of the prostate. This posture change is estimated at 15 degrees by Strang et al. based on trigonometry [10] and associated with a decrease in PAI of 4.9 mm reported by Tincher et al. [11]. In our analysis every 10 degrees of rotation causes a reduction in PAI of 4.8 mm. The discrepancy in these findings indicates the variability between patients in either the amount of PAI or in the degree of obtained anatomical rotation from supine to lithotomy position. Either way, it is difficult to preoperatively predict the amount of PAI occurring during the subsequent procedure. As a general guide  $\geq 10$  mm PAI in supine position and  $\geq 5$  mm PAI in lithotomy position is considered excessive PAI [4,8,9]. According to the threshold in supine position, 52% of patients in this work would be considered not directly suitable for prostate BT. When 15 degrees anatomical rotation between the supine and lithotomy position is considered, 37% of patients showed excessive PAI. One solution to make these patients eligible for prostate BT is downsizing the prostate with hormonal therapy, such as ADT. Nonetheless, this therapy takes months and can result in significant side effects for the patient. Press et al. concluded that hormonal therapy induced worsening of several scores, including quality of life, incontinence and sexual function, with a tendency to lower vitality [7], whilst Lee et al. stated that ADT may lead to increased acute urinary morbidity [21]. Other approaches can overcome minimal PAI, such as manipulating rigid implant needles and the ultrasound probe, while extending the lithotomy position can overcome more excessive PAI. Although, patient repositioning requires adaptations to the set-up and can have limitations [16–18].

It should be noted that, in this simulated study, the prostate and the pubic bone rotate equally without the influence of biomechanics, thus this work indicates the range to which PAI can occur after posture change from supine to lithotomy position. The maximum PAI and the corresponding insertion depth are taken as a requirement for the end position for the steerable needle which is compared to the reported curved trajectories. In this experiment the steering was applied directly after piercing the perineum, while the physician may prefer passing beneath the pubic bone first to diminish the chance of collisions. This will, in fact, reduce the potential lateral steering. In addition, the steerable needle is developed for source positioning in HDR BT. The steering principle can be used for LDR BT but requires a redesign to allow for seed implantation. We expect that this will not affect the functionality. The ability to follow

the curved trajectories should be evaluated in a clinical setting as steering was only performed in tissue simulants and *ex-vivo* bovine tissue. In the clinical setting, challenges may arise such as the limited workspace for applying steering and real time imaging of non-straight implant needles in 3D.

The novel steerable needle as presented in the study of de Vries et al. [23] can overcome PAI making members of the patient group with enlarged prostates and excessive PAI directly suitable for prostate BT without the need for prior hormonal therapy. This spares patients the side effects, and the healthcare system the costs, related to hormonal therapy. Additionally, PAI can be evaluated intraoperatively and *ad hoc* steering can be used to generate a homogeneous implant geometry in patients with PAI. Further research should be performed to investigate the dose plans with the use of steerable needles, and the corresponding workflow, in a clinical setting.

### 3.5 CONCLUSION

The proposed *ad hoc* steering approach allows for more intraoperative flexibility in needle placement independently from the amount of anatomical rotation and obstruction of the prostate by the pubic arch. This reduces the change of needing to abandon treatment and suggests that preoperative hormonal therapy to downsize the prostate may not be necessary. This solution will limit exclusion criteria and allows patients with enlarged prostates and PAI to consider BT as treatment option.

### REFERENCES

- [1] Siegel RL, Miller KD, Fuchs HE, Jemal A. Cancer statistics, 2022. *CA Cancer J Clin* 2022;72:7–33. <https://doi.org/https://doi.org/10.3322/caac.21708>.
- [2] Henry A, Pieters BR, André Siebert F, Hoskin P. GEC-ESTRO ACROP prostate brachytherapy guidelines. *Radiother Oncol* 2022;167:244–51. <https://doi.org/10.1016/j.radonc.2021.12.047>.
- [3] Davis BJ, Horwitz EM, Lee WR, Crook JM, Stock RG, Merrick GS, et al. American Brachytherapy Society consensus guidelines for transrectal ultrasound-guided permanent prostate brachytherapy. *Brachytherapy* 2012;11:6–19. <https://doi.org/10.1016/j.brachy.2011.07.005>.
- [4] Bellon J, Wallner K, Ellis W, Russell K, Cavanagh W, Blasko J. Use of pelvic CT scanning to evaluate pubic arch interference of transperineal prostate brachytherapy. *Int J Radiat Oncol Biol Phys* 1999;43:579–81. [https://doi.org/10.1016/S0360-3016\(98\)00466-0](https://doi.org/10.1016/S0360-3016(98)00466-0).
- [5] Vigneault E, Mbodji K, Beaudet MÉ, Després P, Lavallée MC, Martin AG, et al. Does prostate volume has an impact on biochemical failure in patients with localized prostate cancer treated with HDR boost? *Radiother Oncol* 2016;121:304–9. <https://doi.org/10.1016/j.radonc.2016.09.013>.
- [6] Wang H, Wallner K, Sutlief S, Blasko J, Russell K, Ellis W. Transperineal brachytherapy in patients with large prostate glands. *Int J Cancer* 2000;90:199–205. [https://doi.org/10.1002/1097-0215\(20000820\)90:4<199::Aid-ijc3>3.0.Co;2-c](https://doi.org/10.1002/1097-0215(20000820)90:4<199::Aid-ijc3>3.0.Co;2-c).
- [7] Press RH, Morgan TM, Cutrell PK, Zhang C, Chen Z, Rahnema S, et al. Patient-reported health-related quality of life outcomes after HDR brachytherapy between small (<60 cc) and large (≥60 cc) prostate glands. *Brachytherapy* 2019;18:13–21. <https://doi.org/10.1016/j.brachy.2018.08.009>.
- [8] Sejjal S, Sathiseelan V, Helenowski I, Kozlowski J, Carter M, Nadler R, et al. Intra-operative pubic arch interference during prostate seed brachytherapy in patients with CT-based pubic arch interference of ≤1 cm. *Radiother Oncol* 2009;91:249–54. <https://doi.org/10.1016/j.radonc.2009.02.006>.
- [9] Fukada J, Shigematsu N, Nakashima J, Ohashi T, Kawaguchi O, Oya M. Predicting pubic arch interference in prostate brachytherapy on transrectal ultrasonography-computed tomography fusion images. *J Radiat Res* 2012;53:753–9. <https://doi.org/10.1093/jrr/rrs020>.
- [10] Strang JG, Rubens DJ, Brasacchio RA, Yu Y, Messing EM. Real-time US versus CT determination of pubic arch interference for brachytherapy. *Radiology* 2001;219:387–93. <https://doi.org/10.1148/radiology.219.2.r01ma37387>.

- [11] Tincher SA, Kim RY, Ezekiel MP, Zinsli T, Fiveash JB, Raben DA, et al. Effects of pelvic rotation and needle angle on pubic arch interference during transperineal prostate implants. *Int J Radiat Oncol Biol Phys* 2000;47:361–3. [https://doi.org/10.1016/s0360-3016\(00\)00434-x](https://doi.org/10.1016/s0360-3016(00)00434-x).
- [12] Zheng Y, Wu J, Chen S, Liu Y, Zhang G. Predicting pubic arch interference in permanent prostate brachytherapy based on the specific parameters derived from nuclear magnetic resonance imaging. *J Contemp Brachytherapy* 2018;10:405–10. <https://doi.org/10.5114/jcb.2018.79247>.
- [13] Peschel RE, King CR, Roberts K. Pubic arch interference in permanent prostate implant patients. *J Brachytherapy Int* 1998;14:241–8.
- [14] Gibbons EP, Smith RP, Beriwal S, Krishna K, Benoit RM. Overcoming pubic arch interference with free-hand needle placement in men undergoing prostate brachytherapy. *Brachytherapy* 2009;8:74–8. <https://doi.org/10.1016/j.brachy.2008.04.007>.
- [15] Henderson A, Laing RW, Langley SEM. Identification of pubic arch interference in prostate brachytherapy: Simplifying the transrectal ultrasound technique. *Brachytherapy* 2003;2:240–5. <https://doi.org/10.1016/j.brachy.2003.11.001>.
- [16] Song DY, Burdette EC, Fiene J, Armour E, Kronreif G, Deguet A, et al. Robotic needle guide for prostate brachytherapy: Clinical testing of feasibility and performance. *Brachytherapy* 2011;10:57–63. <https://doi.org/10.1016/j.brachy.2010.01.003>.
- [17] Ishiyama H, Satoh T, Kitano M, Kotani S, Uemae M, Baba S, et al. Interactive-plan technique conquers the disadvantages of volume-reducing hormone therapy in 125I permanent implantation for localized prostate cancer. *Int J Clin Oncol* 2009;14:53–5. <https://doi.org/10.1007/s10147-008-0799-6>.
- [18] Stone NN, Roy J, Hong S, Lo YC, Stock RG. Prostate gland motion and deformation caused by needle placement during brachytherapy. *Brachytherapy* 2002;1:154–60. [https://doi.org/10.1016/S1538-4721\(02\)00058-2](https://doi.org/10.1016/S1538-4721(02)00058-2).
- [19] Siau T, Cunha A, Berenson D, Atamturk A, Hsu IC, Goldberg K, et al. NPIP: A skew line needle configuration optimization system for HDR brachytherapy. *Med Phys* 2012;39:4339–46. <https://doi.org/10.1118/1.4728226> LB - 22830767.
- [20] Ryu B, Bax J, Edirisinge C, Lewis C, Chen J, D'Souza D, et al. Prostate brachytherapy with oblique needles to treat large glands and overcome pubic arch interference. *Int J Radiat Oncol Biol Phys* 2012;83:1463–72. <https://doi.org/10.1016/j.ijrobp.2011.10.012>.
- [21] Lee WR. The role of androgen deprivation therapy combined with prostate brachytherapy. *Urology* 2002;60:39–44. [https://doi.org/10.1016/S0090-4295\(02\)01568-6](https://doi.org/10.1016/S0090-4295(02)01568-6).
- [22] Quan AL, Ciezki JP, Reddy CA, Angermeier K, Ulchaker J, Mahadevan A, et al. Improved biochemical relapse-free survival for patients with large/wide glands treated with prostate seed implantation for localized adenocarcinoma of prostate. *Urology* 2006;68:1237–41. <https://doi.org/10.1016/j.urology.2006.08.1095>.
- [23] De Vries M, Sikorski J, Misra S, van den Dobbelsteen JJ. Axially rigid steerable needle with compliant active tip control. *PLoS One* 2021;16:e0261089. <https://doi.org/10.1371/journal.pone.0261089>.

# 4

## Axially rigid steerable needle with compliant active tip control

Martijn de Vries, Jakub Sikorski, Sarthak Misra, John. J. van den Dobbelssteen

*Published in PLOS ONE (2021)*



## ABSTRACT

Steerable instruments allow for precise access to deeply-seated targets while sparing sensitive tissues and avoiding anatomical structures. In this study we present a novel omnidirectional steerable instrument for prostate high-dose-rate (HDR) brachytherapy (BT). The instrument utilises a needle with internal compliant mechanism, which enables distal tip steering through proximal instrument bending while retaining high axial and flexural rigidity. Finite element analysis evaluated the design and the prototype was validated in experiments involving tissue simulants and *ex-vivo* bovine tissue. Ultrasound (US) images were used to provide visualisation and shape-reconstruction of the instrument during the insertions. In the experiments lateral tip steering up to 20 mm was found. Manually controlled active needle tip steering in inhomogeneous tissue simulants and *ex-vivo* tissue resulted in mean targeting errors of 1.4 mm and 2 mm in 3D position, respectively. The experiments show that steering response of the instrument is history-independent. The results indicate that the endpoint accuracy of the steerable instrument is similar to that of the conventional rigid HDR BT needle while adding the ability to steer along curved paths. Due to the design of the steerable needle sufficient axial and flexural rigidity is preserved to enable puncturing and path control within various heterogeneous tissues. The developed instrument has the potential to overcome problems currently unavoidable with conventional instruments, such as pubic arch interference in HDR BT, without major changes to the clinical workflow.

## 4.1 INTRODUCTION

Percutaneous needles are commonly used in minimally invasive diagnostics and therapeutic procedures. The trajectory and endpoint of the inserted needle influence the effectiveness of the procedure [1,2]. Misplacement may cause misdiagnosis, additional tissue damage and less effective therapy outcomes [3–6]. One medical procedure that requires optimisation is prostate brachytherapy (BT) [7,8]. This technique employs ionising radiation via  $\leq 25$  rigid implant needles under ultrasound (US) guidance to kill or stunt the growth of malignant tumour cells [9,10]. Conventional high-dose-rate (HDR) BT needles are rigid and restricted to linear insertion paths so that deep-seated targets close to sensitive tissues or organs are challenging to reach. Physicians are challenged in needle placement by catheter displacement and deformation, tissue movement and deformation, needle deflection and imaging limitations [7,11–18]. These transformations are a result of respiratory motion, movement of the patient, tissue anisotropy and inhomogeneity, anatomical structure interference, intermediate calcifications, edema and tissue compression and stretching [5,13,19–26]. To counteract these issues physicians are often limited to suboptimal correcting actions such as needle base or tissue manipulations [24,27]. Reinsertion of the needle is in fact much required [5]. This induces additional tissue damage, postprocedural tissue swelling and increases patient discomfort and procedure time [5,27–30]. Therefore, needle targeting demands improvement [11]. Another problem that arises with HDR BT needles is accessibility in large prostates. The Groupe Européen de Curiethérapie and the European Society for Radiotherapy & Oncology (GEC-ESTRO) and American Brachytherapy Society (ABS) guidelines state that a prostate of respectively  $> 50$  cubic centimetres (cc) and  $> 60$  cc is technically more challenging [31]. They report this limit as a relative contraindication for prostate BT because of blockage of the anterolateral area of the prostate [24,32–34]. This phenomenon, known as pubic arch interference (PAI), hampers a homogeneous irradiation of the whole gland and excludes a large patient group.

Steerable needles could play a part in correcting for needle bending, sparing sensitive tissues and avoiding anatomical structures, such as the pubic arch in prostate BT [30]. Multiple passive and active steering techniques have been proposed in academic literature and evaluated in experimental set-ups, such as pre-curved needles, cable-driven instruments or actuated needle tips [7,21,35–45]. On the contrary, only a few active steerable instruments have been commercialised: the Pakter Curved Needle Set (Cook Medical Inc., Bloomington, IN, USA), the Morrison Steerable Needle (AprioMed AB, Uppsala, Sweden), the Osseoflex SN Steerable Needle (Merit Medical Systems, South Jordan, UT, USA) and the Seeker Steerable Biopsy Needle (PneumRx, Mountain View, CA, USA) [27]. The last three instruments are cable driven and induce pivoting of the needle tip by cable pulling [4]. However, such designs have reduced axial and flexural rigidity and lack accurate control for penetrating stiffer tissue and membranes without buckling, thereby limiting the clinical applicability [46].

This work describes an omnidirectional steerable instrument that can be manually controlled where axial and flexural rigidity are preserved for increased controllability during needle insertions. The instrument is based on a single-piece compliant structure that enables distal tip steering through proximal instrument bending and is compatible with the existing approach for prostate HDR BT. We present the design of the steerable needle in section 2 which is evaluated with computational simulations in section 3. Steering performance of the prototype is assessed in US-guided experiments with tissue simulants and *ex-vivo* bovine tissue in section 4. This section demonstrates the ability to accurately steer the needle along curved paths and add value to HDR BT.

## 4.2 NEEDLE DESIGN

The instrument comprises a commercially available flexible outer catheter of polyoxymethylene (POM) (ProGuide sharp 6F needle, Elekta Instrument AB, Stockholm, Sweden) with a conical distal tip and a steerable patented steel inner needle (PWS140A, Eileen's Emporium, Gloucester, United Kingdom) (Figure 4.1). The inner needle is a single-piece long slender rod, containing four parallel running segments, with a length of 205 mm and diameter of 1.40 mm.

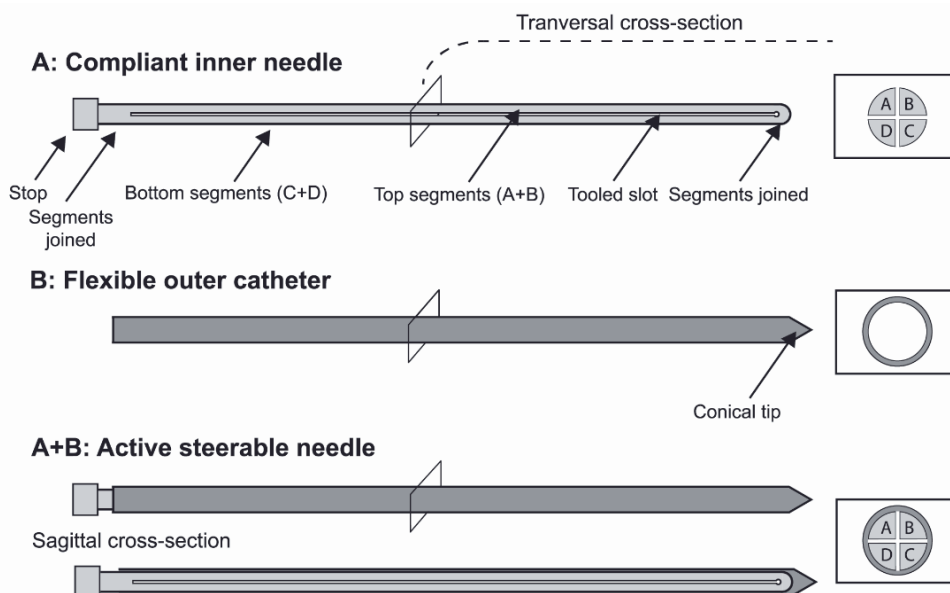


**Figure 4.1 - Schematic of the steerable needle assembly.** (A) Inner needle. (B) Outer catheter. The assembly of (A) and (B) forms the active steerable needle (A+B). The boxes show the transversal cross-section of each part.

The inner needle contains a compliant mechanism as it transmits input forces at the proximal end to articulate the distal tip. A lateral input force induces instrument deflection which causes axial pushing and pulling of the segments. This topological synthesis is achieved by an electrical discharge machined slot of 0.12 mm over a length of 185 mm in both the sagittal and coronal plane, effectively splitting the rod in four equal quarters while leaving both ends of the needle joined. Simultaneous translation of the four segments in different ratios results in omnidirectional tip steering. The flexible catheter follows the deflections of the inner needle, which can be withdrawn from the instrument leaving behind a work channel with a lumen of 1.45 mm. Figure 4.2 and 4.3 show the schematic and actual use of the needle during steering, respectively.

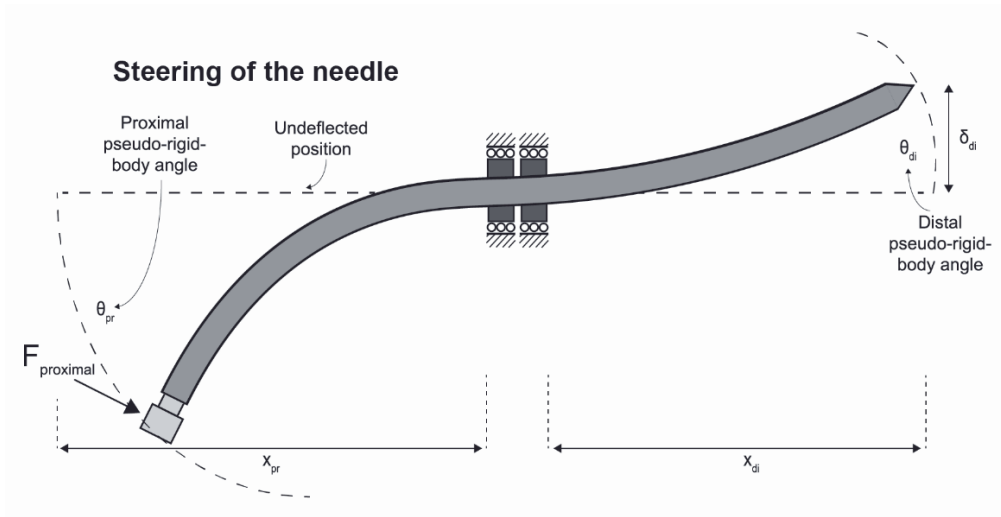


**Figure 4.2 - Schematic of needle steering.** An applied force on the proximal end of the needle ( $F_{\text{proximal}}$ ) results in deflection of the distal end of the needle ( $\delta_{\text{di}}$ ). The roller supports in the middle function as flexure bearings for needle deflection.

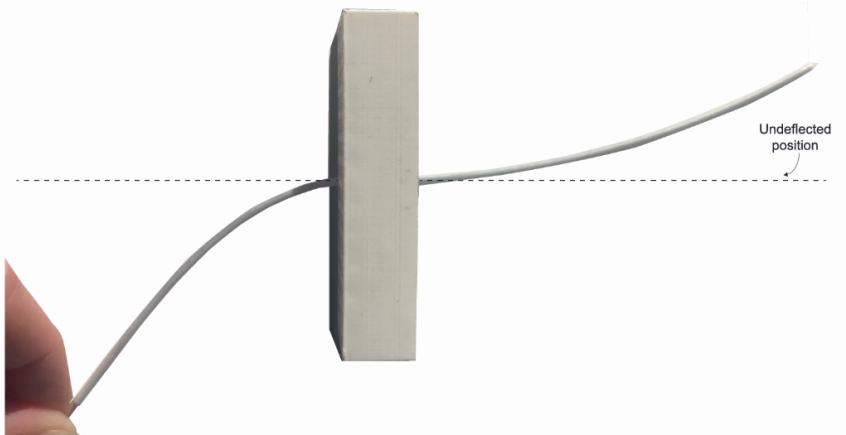


**Figure 4.3 - Needle steering with the manufactured prototype.** An applied force on the proximal end of the needle results in deflection of the distal end of the needle. The needle guide in the middle functions as flexure bearings for needle deflection.

The segments of the inner needle can be translated in axial direction inside the outer catheter while moving in the direction normal to its plane is restricted by the roller support. The roller support and design of the inner needle result in a flexure bearing and a compliant mechanism for the kinematic requirement of distal tip steering. The translation of segments with respect to each other is referred to as relative translation. The output deflection occurs in opposite direction to the input force, as the four segments move relative to each other during bending. This is indicated by the pseudo-rigid body (PRB) model in Figure 4.4.

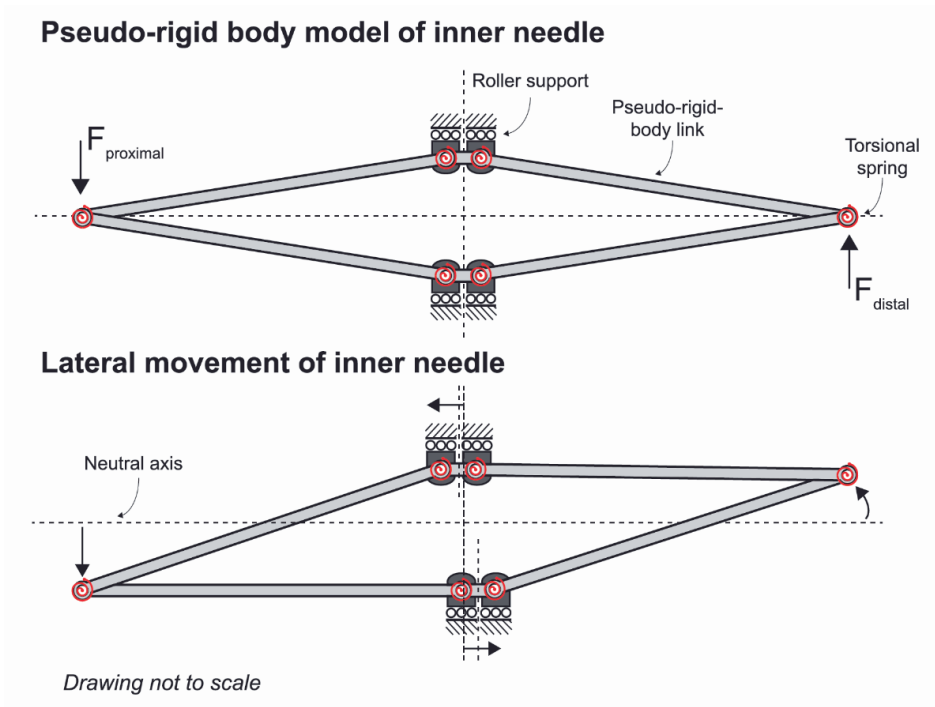


**Figure 4.4 - Pseudo-rigid body model of the inner needle.** The inner needle is modelled with six pseudo-rigid-body links and six torsional springs. The horizontal segments and roller supports indicate the needle guiding. Downward movement of the proximal end results in axial pushing of the bottom segment and axial pulling of the upper segment resulting in upward movement of the distal tip.

An increase in the rotational degrees-of-freedom (DOFs) from 0 for the conventional rigid inner needle to 2 for the novel steerable needle is accomplished by its design. This is at the expense of a decrease of 11.8 % in principal moment of inertia for the cross-section illustrated in Figure 1.A compared to a rigid inner needle. This results in a theoretical flexural rigidity ( $E * I$ ) of  $34.85 * 10^{-3} (N * m^2)$  for the steerable inner needle, where  $E = 205 \text{ GPa}$  (CES EduPack 2019, Granta Design Limited, Cambridge, United Kingdom) and  $I = 0.17 \text{ mm}^4$ . The axial rigidity ( $E * A$ ) of the inner needle reflects the ability to resist axial loads. A decrease in area from 1.54 to 1.22  $\text{mm}^2$  results in a theoretical reduction of 20.8% in axial rigidity.

## 4.3 COMPUTATIONAL SIMULATION

### 4.3.1 Finite element model

A static finite element analysis in ABAQUS/CAE 2017 (Simulia, Johnston, RI, USA) evaluates the configuration of the inner needle, assesses theoretical maximum stress and deflection, and relates input bending and output steering outside of a medium. Table 4.1 shows the properties of the inner needle and outer catheter used in the finite element model. Figure 4.2 shows the critical dimensions used in the analysis.

<b>Outer catheter</b>	Length	200 mm
	Outer diameter	2.0 mm
	Inner diameter	1.5 mm
	Young's modulus	1 GPa
	Simplification	Two open ends
<b>Inner needle</b>	Length	208 mm
	Outer diameter	1.4 mm
	Young's modulus	205 GPa
	Simplification	1 slot over 185 mm No starting hole for wire-EDM No proximal stop
	<b>Needle guide</b>	Length
	Simplification	Modelled as roller boundary condition

**Table 4.1 - Properties of the finite element model.**

The outer catheter is modelled as a homogenous shell with two open ends and linear quadratic S4R nodes. The inner needle contains one slot over 185 mm, splitting the needle into two halves. The inner needle contains linear hexahedral shaped elements (C3D8R nodes) on which 3D stress analysis is performed. The needle guide is modelled as a roller boundary condition constraining shift and rotation of the outer catheter. Input bending around the Z-axis is allowed over the whole proximal needle length up to the needle guide. Distal tip angle ( $\theta_{di}$ ) and deflection ( $\delta_{di}$ ) are measured for multiple PRB angles ( $\theta_{pr}$ : 10°, 30°, 50°, 70°, 90°) and multiple proximal needle lengths ( $X_{pr}$ : 20 mm, 50 mm, 80 mm, 110 mm). Relative translation between the upper and lower segment is measured on predefined nodes in the centre of the roller support.

### 4.3.2 Finite element analysis

Geometric chances occur in the model during bending. Figure 4.5 shows the computational model of the inner needle in straight and bent condition. Simultaneous pushing and pulling the upper and lower segment result in a relative translation causing needle steering. Outward shift of the segments from the neutral line is restricted by the catheter, however inward shift is probable. Maximum stresses during downward bending are found at the top surface on the proximal end of the upper segment.

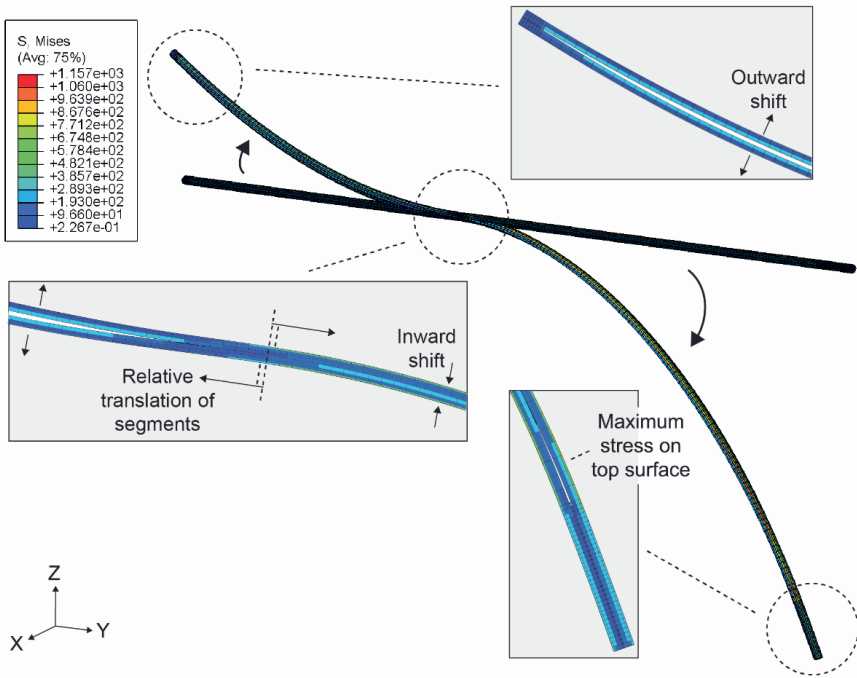


**Figure 4.5 – The finite element model of the active steerable needle in normal and bent condition.** The boxes show the configuration of the inner needle during bending. The arrows indicate the direction of the shift of the segments. Stress and bending apply for the computational model with  $X_{pr} = 120$  mm and  $\theta_{pr} = 70^\circ$ .

Figure 4.6 gives an overview of the proximal PRB input angle and the corresponding relative translation of the segments. A shorter proximal needle length increases distal tip angle and deflection while affecting maximum stress. Maximum stress (1855 MPa), maximum distal tip deflection (37.8 mm) and maximum distal angle (41.6°) are found for the sharpest angle (90°). This indicates that the steerable needle stays below the elastic limit (~ 2700 - 3300 MPa) of the patented steel material (CES EduPack 2019, Granta Design Limited, Cambridge, United Kingdom). This information shows us the feasibility of the steerable instrument.

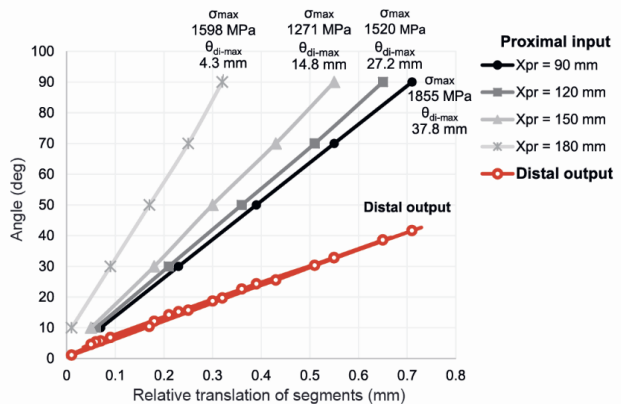


**Figure 4.6 – The relationship between proximal input angle and relative translation between segments for different proximal needle lengths.** The red line indicates the distal output. Markers on the distal output line relate to the vertically aligned markers on the input lines. Maximum stress and deflection is described for all proximal inputs.

## 4.4 EXPERIMENTAL EVALUATION

A prototype is manufactured in order to translate the use of the steerable instrument into practice. Three validation experiments determine steering characteristics in soft tissue simulants and *ex-vivo* bovine tissue using US imaging.

### 4.4.1 Experiment 1 – Fixed-bent needle steering

The influence of the initial insertion depth on needle steering and the endpoint precision are assessed inside a homogeneous medium for set curvatures.

#### 4.4.1.1 Materials and Method

##### *Set-up and procedure*

A porcine gelatin tissue simulant (Gelatin, Dr. Oetker, Bielefeld, Germany) of 10 wt.% at room temperature ( $\sim 20$  °C) and a mould with predefined curvatures to ensure reproducibility of the bending are used. The tissue simulant is confined within in a transparent Poly (methyl methacrylate) (PMMA) container (200 x 112 x 112 mm). The front plate of the container (thickness: 12 mm) contains holes ( $\varnothing$  2.1 mm) functioning as a needle guide. Rectangular compartments in the front face of the tissue simulant are filled with air. These compartments are located above every insertion hole and function as reference for coordinate  $\langle 0,0,0 \rangle$  on the US images. The mould is attached to a linear slide which allows for controlled translation. The slide can be lifted in X-direction using blocks and the container can be moved in Y-direction for a new puncture. The needle is inserted in the tissue simulant for 20 mm in a straight orientation to overcome puncture and cutting forces. After every insertion, US imaging with the Robotic Ultrasound System (RobUST) [47] is used with a sweep over two lengths of the tissue simulant. Dependence of steering performance on insertion depth is evaluated for two, initially straight, insertion paths ( $d_{\text{straight}} = 0$  mm and  $d_{\text{straight}} = 40$  mm). Two different proximal bending angles (slight angle:  $22.5^\circ$  and sharp angle:  $45^\circ$ ) are applied to determine steering capability over a length of 100 mm.

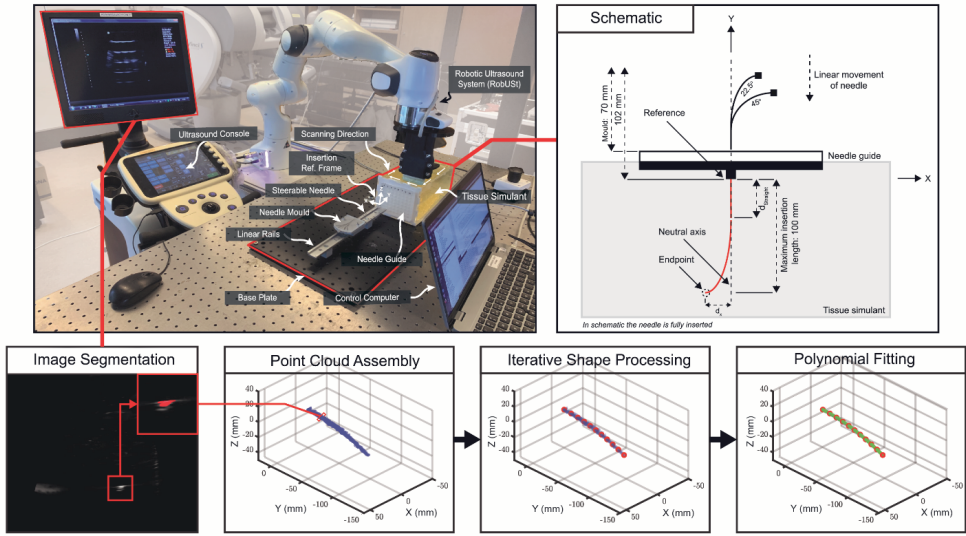
##### *Image processing and analysis*

Figure 4.7 shows a schematic of the experimental set-up and the process of 3D needle shape reconstruction using RobUST, which comprises of a Sonix Touch L14-5/38 (BK Medical, Peabody, MA, USA) transducer mounted on a Panda (Franka Emika GmbH, Munich, Germany) robotic arm. RobUST is used to scan a predefined volume of the tissue simulant. During the scan, 2D US images are recorded at 20 Hz, along with the corresponding information about the transducer pose expressed in the RobUST reference frame. The set of US images is segmented using constant intensity thresholding to create a point cloud containing the silhouette of the instrument. Each silhouette is processed by a shape reconstruction algorithm that extracts a continuous shape of the needle described by a 3<sup>rd</sup> order polynomial with coefficients  $(A_i, B_i, C_i, D_i \in \mathbb{R}^3)$  and length  $(l_i \in \mathbb{R}^+)$  [48]. The location  $(p_i(s) \in \mathbb{R}^3)$  of a point lying on the shape at the distance  $(s \in [0; l_i])$  can be calculated from polynomial coefficients as:

$$p_i(s) = A_i + sB_i + s^2C_i + s^3D_i = [I_3 \ I_3s \ I_3s^2 \ I_3s^3] \begin{bmatrix} A_i \\ B_i \\ C_i \\ D_i \end{bmatrix}, \quad (1)$$

where  $I_3$  is the 3x3 identity matrix.





**Figure 4.7 - Set-up and pipeline for shape reconstruction of the fixed-bent needle steering experiment.** The Robotic Ultrasound System (RobUST) is used for shape reconstruction of the steerable instrument. For each insertion, RobUST performs a volumetric scan of the tissue simulant, recording US images along with corresponding transducer pose data, expressed in the global reference frame at the base of the robotic manipulator. The silhouette of the instrument is segmented from each frame. All segmented data are assembled in a point cloud. The point cloud is processed using an iterative shape reconstruction algorithm, described in detail in Suligoj et al. [47]. The iterative shape algorithm first generates a series of points along the instrument (red dots). These points are used to fit a third order polynomial (green) describing the continuous shape of the instrument.

The last point on the reconstructed 3D needle shape in the XY-plane determines the achieved lateral needle steering. The uncontrolled needle deflection at the distal end is assessed in XZ-plane. The trials of the same condition are averaged and standard deviation ( $\pm \sigma$ ) is reported.

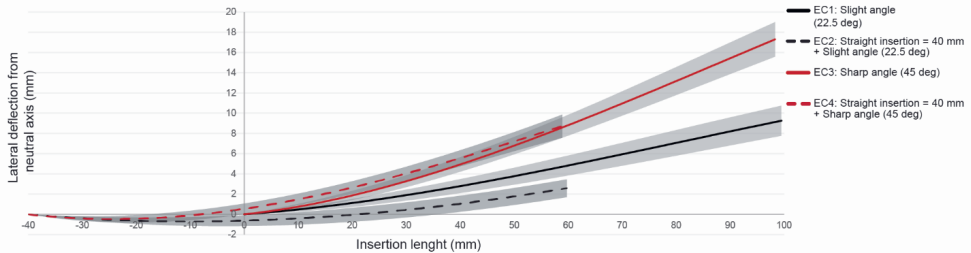
4.4.1.2 Results

Table 4.2 gives an overview of steering for all experimental conditions (EC's). The results show that an increased bending input at the proximal end enlarges the angle for lateral tip steering in the tissue simulant what is expected from section 3. Maximum fixed-bent needle steering of 20.2 mm laterally over a distance of 97.7 mm is found. In Z-direction an unwanted error occurred in all trials which increased with insertion depth.

**Table 4.2 - Steering capability of the steerable needle in the fixed-bent needle steering experiment.** The mean error  $\pm$  standard deviation ( $\pm \sigma$ ) in X,- Y,- and Z-direction for two different proximal bending angles and two initial straight insertion depths in a homogeneous tissue simulant.

		Proximal bending angle	
		22.5°	45°
N = 33		EC1	EC3
0 mm	<i>n</i>	8	9
	Mean Y (length)	0.5 $\pm$ 0.2	1.7 $\pm$ 1.7
	error X (steering)	9.3 $\pm$ 1.5	17.3 $\pm$ 1.7
$\pm \sigma$	Z (error)	-3.9 $\pm$ 0.9	-3.8 $\pm$ 4.3
	<i>d</i> <sub>straight</sub>	EC2	EC4
40 mm	<i>n</i>	8	8
	Mean Y (length)	0.2 $\pm$ 0.2	1.2 $\pm$ 0.7
	error X (steering)	2.6 $\pm$ 0.9	8.7 $\pm$ 1.1
$\pm \sigma$	Z (error)	-2.7 $\pm$ 1.3	-4.9 $\pm$ 1.5

Figure 4.8 shows smooth curvatures for all conditions. Superimposing the needle trajectories of EC2 over EC1 and EC4 over EC3 indicate that steering response of the needle does not depend on the initial insertion depth. A mean distal tip error of 2.2 mm and 0.1 mm were respectively obtained. Noteworthy is that uncontrolled absolute deflections of 1.2 mm and 2.0 mm from the neutral axis were already observed after 40 mm for EC2 and EC4.



**Figure 4.8 - Lateral deflection of the steerable needle over insertion length in the fixed-bent needle steering experiment.** The mean error  $\pm \sigma$  in lateral direction for two different proximal bending angles and two initial straight insertion depths. The curves characterised by steering after 40 mm are superimposed on the curves of steering from  $\langle 0,0,0 \rangle$  to determine what the influence of the initial depth is on needle steering.

#### 4.4.2 Experiment 2 – Clinical use case: Active needle tip steering in prostate tissue simulant

In prostate BT, rigid needles are inserted over approximately 90 mm into the prostate gland for internal irradiation using transrectal US for real-time visualisation [49]. In this experiment, manual active steering and real-time needle guidance via 2D US imaging evaluates endpoint accuracy in inhomogeneous tissue simulants. The accuracy is assessed over a maximum lateral distance of 15 mm. Straight needle insertions with the steerable inner needle and a commercially available rigid HDR BT inner needle (ProGuide Obturator, Elekta Instrument AB, Stockholm, Sweden) are performed to place the use of steering in context.

##### 4.4.2.1 Materials and Method

###### *Set-up*

2D US imaging (Phillips HD7 XE) is used for both needle guidance and definition of the target site located at the distal surface of the tissue simulant illustrated in Figure 4.9. The target is a horizontal PETG wedge mounted on a slide. Images are taken after every puncture with a Dino-Lite Digital PC-Microscope (AM73915MZTL 5 Megapixel, 10–140x) fixed in a vertical assembly. Both are aligned with the neutral axis.

###### *Tissue simulant design*

Two tissue-mimicking blocks (350 x 130 x 90 mm) of poly(vinyl alcohol) (PVA) are manufactured. One soft tissue simulant approaches the Young's modulus of muscular and adipose tissue ( $\sim 15$  kPa) [50]. One stiff tissue simulant mimics the Young's modulus of prostatic tissue ( $\sim 50$  kPa) [51]. As stiffness of the phantom can influence needle deflection, needle steering is performed in both tissue simulants [52]. PVA is a synthetic polymer that can mimic mechanical properties of human tissue by performing freeze-thaw cycles (FTC's) and is suitable for US visualisation [53–55].

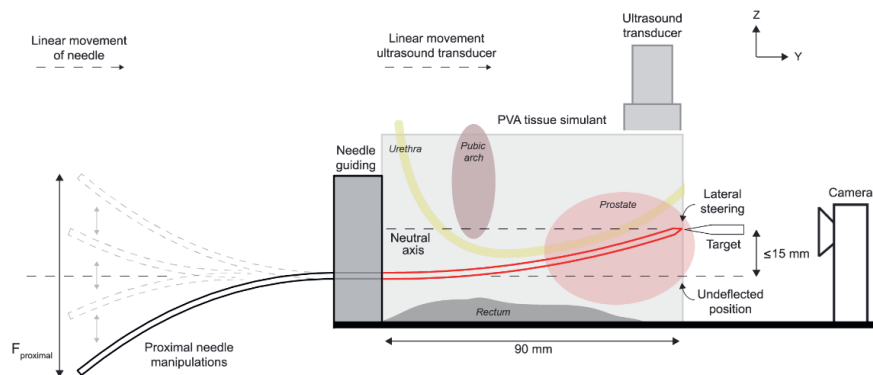


**Figure 4.9 - Set-up of active needle steering experiment in prostate tissue simulant.** Proximal needle manipulations in Z-direction allow for steering at the distal tip. Insertion of the needle in the prostate tissue simulant and movement of the US transducer is performed bimanually. The camera visualises the back surface of the tissue simulant in transversal plane. The prostate, pubic arch, urethra and rectum are illustrated in the figure in sagittal plane to demonstrate the clinical applicability of the steerable needle for prostate brachytherapy. The pubic arch and urethra are circumvented to reach occluded prostate tissue.

These FTC's create a polyvinyl alcohol cryogen (PVA-C) due to polymer cross-linking, used in earlier research as a simulant for prostate tissue [56]. Within this study, the soft and stiff tissue simulants are made with 10 wt.% PVA-C with 1 and 5 FTC's, respectively. The Young's modulus of the tissue simulant was evaluated by a compression test. The PVA powder (SELVOL™, Sekisui Specialty Chemicals America, Dallas, Texas) is dissolved in a 60:40 mixture of water and coolant (Talamex, Lankhorst Taselaar B.V., Heerenveen, The Netherlands) to prevent expansion of the volume.

### Procedure

Manual active steering towards a target is assessed. The experimenter bimanually controls the steerable needle and the US transducer for visualisation of the tip position and the target location in sagittal plane. When reaching the distal wall of the PVA block the target is removed and the needle is punctured out of the tissue simulant to define the end location of the needle tip and error in Z-direction with the Dino-Lite Digital PC-Microscope. Additionally, needle insertions without steering and with the ProGuide Obturator are performed. The endpoint accuracy of the needle is evaluated in fourteen experimental conditions, described in section 4.2.2. All experimental conditions are randomised for each tissue simulant of  $\sim 20^\circ$ . First, all insertions in the soft tissue simulant are performed followed by insertions in the stiff tissue simulant.

### Data and statistical analysis

The mean absolute errors  $\pm \sigma$  are evaluated for all experimental conditions and statistical analysis (IBM SPSS Statistics 25) is performed to investigate performance of the developed steerable needle. To verify the non-normal error distribution a Shapiro-Wilk's test, the normal Q-Q plots and a visual inspection of their histograms are performed. If normality is found, a one-way ANOVA is done and Tukey's HSD procedure evaluates the differences between conditions. Unequal sample sizes are analysed in a Games-Howell test. A  $p$ -value  $< .05$  is considered statistically significant.

## 4.4.2.2 Results

Table 4.3 shows the mean absolute errors  $\pm \sigma$  of all experimental conditions for both the adipose tissue simulant and the prostatic tissue simulant. Active steering (EC1 - EC5) results in a mean endpoint error of 1.44 mm.

N = 200		<u>Active steering</u>				<u>No steering</u>	<u>ProGuide Obturator</u>	
		<i>lateral</i>		<i>lateral out-of-path</i>		<i>neutral axis</i>	<i>neutral axis</i>	<i>reference</i>
		EC1	EC2	EC3	EC4	EC5	EC6	EC7
		7.5 mm	15 mm	7.5 mm	15 mm			
<b>Adipose tissue simulant (soft)</b>	<i>n</i>	10	10	10	10	20	20	20
	Mean absolute error (mm)	1.52	2.45	1.19	1.59	1.45	2.42	2.01
	$\pm \sigma$	$\pm 0.93$	$\pm 1.70$	$\pm 0.80$	$\pm 1.12$	$\pm 0.83$	$\pm 0.82$	$\pm 0.87$
<b>Prostatic tissue simulant (stiff)</b>	<i>n</i>	10	10	10	10	20	20	20
	Mean absolute error (mm)	1.27	1.64	1.23	0.91	1.15	6.86	2.03
	$\pm \sigma$	$\pm 1.13$	$\pm 1.40$	$\pm 0.78$	$\pm 1.14$	$\pm 0.83$	$\pm 1.74$	$\pm 0.62$
<b>Total</b>		1.39	2.05	1.21	1.25	1.30	4.64	2.02
		$\pm 1.02$	$\pm 1.57$	$\pm 0.77$	$\pm 1.16$	$\pm 0.84$	$\pm 2.62$	$\pm 0.75$

**Table 4.3 - The endpoint errors of the steerable needle and the reference needle per tissue simulant.** The endpoint error is measured after every puncture showing the mean absolute error and standard deviation ( $\pm \sigma$ ) in millimetres per experimental condition. The rigid ProGuide Obturator is used as reference. In EC1, EC2 and EC5 active needle steering is allowed over the entire insertion length. In EC3 and EC4 the needle is first inserted without steering over 90 mm and then withdrawn for 50 mm. Subsequently, the needle is actively steered out of the created needle path towards the target. In EC6 the steerable needle is inserted over 90 mm without active steering. In EC7 the rigid ProGuide Obturator is inserted. The absence of US guidance for EC6 and EC7 allows for determination of the Euclidean distance between the endpoint of the needle tip and the neutral axis.

A Kruskal-Wallis test showed no statistically significant difference in obtained error for the experimental conditions related to active lateral needle steering (EC1 – EC4) in both soft tissue simulants. A one-way ANOVA analysis yielded statistically significant variation between the normally distributed EC5, EC6 and EC7 for both the low stiffness tissue simulant  $F(2,57) = 6.612, p = .003$  and the high stiffness tissue simulant  $F(2,57) = 138.500, p < .001$ . A post hoc Tukey test showed that the reference group with the conventional rigid ProGuide Obturator (EC7) did not differ significantly from the group with active steering on the neutral axis (EC5) in both tissue simulants. EC6 differed significantly from EC5 ( $p = .002$ ) in the soft tissue simulant and from both EC5 ( $p < .001$ ) and EC7 ( $p < .001$ ) in the stiff tissue simulant.

The Games-Howell post hoc test indicated no significant differences in endpoint accuracy in the adipose tissue simulant between the steerable needle and the ProGuide Obturator. In the prostatic tissue simulant the actively steered needle on the neutral axis ( $M = 1.15, \sigma = .83$ ) had a statistically significant smaller error than the conventional rigid HDR BT inner needle ( $M = 2.03, \sigma = .62, p = .009$ ). Noteworthy is that no steering with the steerable needle resulted in significant differences from EC3 ( $p = .014$ ) and EC5 ( $p = .012$ ) in the adipose tissue simulant and in statistically significant variation from all experimental conditions in the prostatic tissue simulant ( $p < .001$ ).

### 4.4.3 Experiment 3 – Active needle tip steering in ex-vivo tissue

Manual active needle tip steering towards targets is executed in *ex-vivo* bovine tissue with real-time US needle tracking. This experiment evaluates adaptive needle path control during insertions and final endpoint accuracy in a more challenging medium.

#### 4.4.3.1 Materials and Method

##### *Set-up and procedure*

The PMMA container and the RobUSt system are used in this set-up. The container holds inhomogeneous bovine tissue (Blade steak, Benali, Rotterdam, The Netherlands) embedded in 20 wt.% porcine gelatin (Gelatin, Dr. Oetker, Bielefeld, Germany). On each trial, the steerable needle is inserted through a layer of gelatin into the bovine tissue reaching the initial needle position. Omnidirectional needle steering is allowed from this position over 90 mm towards the target ( $\varnothing$  0.5 mm). Continuous back and forth US scanning in Y-direction over the top surface of the tissue is executed to determine location of the needle tip and target in transversal plane. A cursor is used to locate the target when the US transducer is in the same plane.

##### *Image processing and data analysis*

Needle tracking inside the *ex-vivo* tissue is performed using RobUSt in a fashion similar to section 4.1.1. Nevertheless, due to environmental clutter within the bovine tissue the silhouette segmentation of the needle and target is performed manually for each image without employing the polynomial reconstruction. The segmented shapes are used to identify the position of the tip of the instrument with respect to the target. Figure 4.10 shows the set-up of the experiment and the trajectory of the needle towards the target for one of the trials.

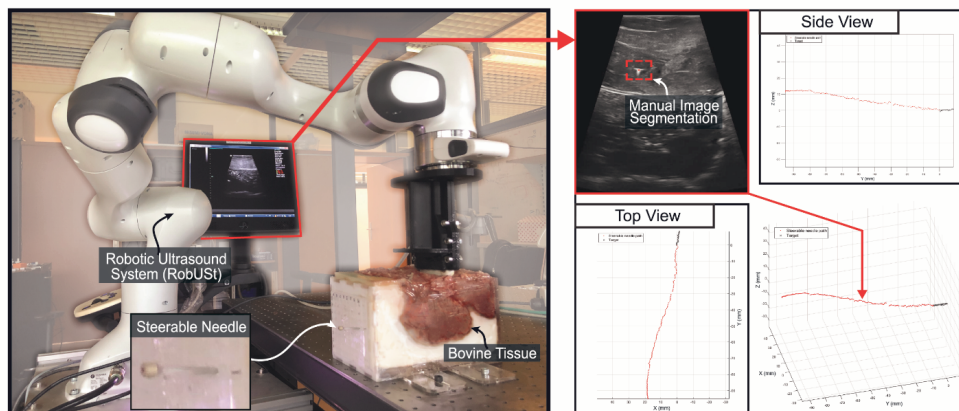


**Figure 4.10 - Set-up of active needle steering experiment in *ex-vivo* tissue.** The trajectory of the steerable needle (red) over a length of 90 mm towards a target (black) located laterally from the neutral axis. Control of the steerable needle was performed in 3D. Segmentation of the needle and target from the US images are used for analysis.

#### 4.4.3.2 Results

Needle steering in X,- and Z-direction towards the targets was required over distances ranging from 3.3 to 17.3 mm and 0.9 to 11.8 mm, respectively. Steering towards the target over a 90 mm insertion depth resulted in a 3D error of  $2.0 \pm 2.6$  mm and a 2D error in the plane of the target of  $0.9 \pm 2.0$  mm. The 2D error did not consider the error in Y-direction as insertion depth was a set value.

### 4.5 DISCUSSION

This work presents a novel omnidirectional steerable instrument for prostate HDR BT. The instrument comprises a commercially available outer catheter and a compliant steerable inner needle, which replaces the conventional rigid non-steerable inner needle currently used in HDR BT. Steering of the inner needle allows for adjustments of the catheter pathway and withdrawal of the inner needle creates a work channel for the medical procedure. Thus, the clinician can overcome pubic arch interference and correct for deflections to obtain a homogeneous dose distribution.

To the authors' best knowledge, this is the first steerable needle whereby active tip control is achieved by exploiting structural mechanics, without the use of external actuation means such as magnetic forces, optical heating, robotic actuation or a joystick at the proximal end. The internal compliant mechanism enables distal tip steering with two rotational DOFs through proximal needle bending. A reduction in flexural and axial rigidity of 11.8% and 20.8% is observed respectively compared to a rigid inner needle. However, the flexural rigidity of the proposed design is much higher than for the designs reported in literature [45,46]. Moreover, no buckling was observed in our prostate tissue mimicking and *ex-vivo* experiments, suggesting that the design has sufficient axial rigidity for placement of HDR BT catheters.

The computational model showed a linear relation between input angle and relative translation of the segments associated with distal tip deflection. Validation experiments demonstrated needle steering up to 20 mm and controllability of the prototype in tissue simulants and in *ex-vivo* tissue. The fixed-bent needle steering experiment showed that steering in tissue was history-independent. The clinical use case experiment related to prostate brachytherapy showed high endpoint accuracy of the steerable needle in a soft and stiff inhomogeneous tissue simulant. These errors were comparable to those of a rigid HDR BT needle. The results of the *ex-vivo* experiment indicated that path corrections were feasible in a more challenging medium and off axis targets can be accurately reached following curved needle paths.

The results from the finite element analysis demonstrate that the inner needle stays in the elastic region of the material and will return to its initial position after removal of the applied input. It should be noted that the computational model is a simplification of the developed needle. The input is modelled as a circular deflection around the X-axis, while in real practice a lateral force results in a more hyperbolic shape at the proximal needle end. This input, approached in Exp. 1, is more representative for the final clinical application as the circular curvature is hard to obtain and workspace outside the body can be limited. The friction coefficient was kept constant while the simulation indicates that segments are translating over each other. Therefore, friction can play a role in the relationship between proximal input and distal output. This aspect is not addressed in this study.

The fixed-bent needle steering experiment demonstrated steering regardless the initial straight insertion depth due to articulations at the distal tip. This is a distinct advantage over non-holonomic asymmetric tip needles because their steering solely depends on needle-tissue interaction and pushing the needle through tissue is required to generate needle deflection. Small differences in lateral steering were found for the slight angle in Exp. 1 as spontaneous deflections in the opposite direction occurred over the

initial straight insertion depth and insertion speed was not kept constant. In addition, uncontrolled deflection increased with insertion depth. This spontaneous deflection can be a consequence of the decreased flexural rigidity of the needle. Robotic control could counter this error but requires feedback control via imaging, electromagnetic tracking or shape sensing. We compensate for the error by steering manually. This affects medical device management, costs and clinical workflow to a lower extent than teleoperation.

Earlier studies reported needle placement errors up to 3 mm in a prostate and 8 mm in a prostate phantom for conical tip and bevel tip brachytherapy needles, respectively [5,20]. A 3 mm error together with the 5 mm perineal template grid could theoretically cause a catheter void of 11 mm in very extreme cases [57]. In practice, rigid brachytherapy needle withdrawal and reinsertion are often required [5]. The steerable needle does not have to be fully withdrawn for error compensation which potentially reduces tissue trauma. The steerable needle can be partially withdrawn and steering out of the initial path allows for targeting with high accuracy indicated by EC3 and EC4 in Exp. 2.

In the clinical use case experiment we found similar endpoint errors for the rigid ProGuide Obturator in 2D and the steerable inner needle in one direction regardless the degree of active steering. But, results indicated that active steering is essential as its absence decreased the endpoint accuracy. In *ex-vivo* tissue the steerable needle obtained a similar error in 3D and lower error in 2D as compared to the ProGuide Obturator in 2D in Exp. 2. In conclusion, the endpoint error of the developed steerable needle stays below the mean acceptable error of 2.7 mm for targeted lesions reported after a questionnaire under 125 interventional radiologists [11].

The bovine tissue of Exp. 3 contained high amounts of connective tissue which complicated smooth insertions. Besides, it was a challenge to control needle steering in two planes during insertion with visual feedback processing. Small needle retractions were therefore allowed in all trials. We found that the axial and flexural rigidity of the developed steerable needle enables puncturing and path control in inhomogeneous tissue simulants and in *ex-vivo* bovine tissue. Furthermore, the developed steerable needle is compatible with currently applied devices in HDR BT and may improve needle targeting without major changes to the clinical workflow.

## 4.6 CONCLUSION

A novel axially rigid steerable instrument for HDR BT was developed and validated in this work. Manual omnidirectional steering is possible with the aid of a compliant mechanism. Validation experiments show high targeting accuracy in tissue simulants and *ex-vivo* tissue while visualisation of the needle is possible with US. The developed steerable needle has the ability to steer along curved paths preserving its axial and flexural rigidity. The needle has the potential to add value to medical procedures currently performed with rigid needles and enlarge the patient group eligible for prostate HDR BT.



## REFERENCES

- [1] Welleweerd MK, Siepel FJ, Groenhuis V, Veltman J, Stramigioli S. Design of an end-effector for robot-assisted ultrasound-guided breast biopsies. *Int J Comput Assist Radiol Surg* 2020;15:681–90. <https://doi.org/10.1007/s11548-020-02122-1>.
- [2] Van de Berg NJ, Dankelman J, van den Dobbelsteen JJ. Endpoint Accuracy in Manual Control of a Steerable Needle. *J Vasc Interv Radiol* 2017;28:276–283.e2. <https://doi.org/10.1016/j.jvir.2016.07.018>.
- [3] Youk JH, Kim EK, Kim MJ, Kwak JY, Son EJ. Analysis of false-negative results after US-guided 14-gauge core needle breast biopsy. *Eur Radiol* 2010;20:782–9. <https://doi.org/10.1007/s00330-009-1632-y>.
- [4] Kratchman LB, Rahman MM, Saunders JR, Swaney PJ, Webster III RJ. Toward robotic needle steering in lung biopsy: a tendon-actuated approach. *Med Imaging 2011 Vis Image-Guided Proced Model* 2011;7964:796411. <https://doi.org/10.1117/12.878792>.
- [5] Sadjadi H, Hashtrudi-Zaad K, Fichtinger G. Needle deflection estimation: prostate brachytherapy phantom experiments. *Int J Comput Assist Radiol Surg* 2014;9:921–9. <https://doi.org/10.1007/s11548-014-0985-0>.
- [6] Cormack RA, Tempany CM, D'Amico A V. Optimizing target coverage by dosimetric feedback during prostate brachytherapy. *Int J Radiat Oncol Biol Phys* 2000;48:1245–9. [https://doi.org/10.1016/S0360-3016\(00\)00742-2](https://doi.org/10.1016/S0360-3016(00)00742-2).
- [7] Varnamkhasti ZK, Konh B. Design and Performance Study of a Novel Minimally Invasive Active Surgical Needle. *J Med Device* 2019;13:1–9. <https://doi.org/10.1115/1.4044526>.
- [8] Podder TK, Dicker AP, Hutapea P, Darvish K, Yu Y. A novel curvilinear approach for prostate seed implantation. *Med Phys* 2012;39:1887–92. <https://doi.org/10.1118/1.3694110>.
- [9] Fröhlich G, Ágoston P, Lövey J. The Effect of Needle Number on the Quality of High-dose-rate Prostate Brachytherapy Implants. *Pathol Oncol Res* 2010:593–9. <https://doi.org/10.1007/s12253-010-9252-z>.
- [10] Kolkman-Deurloo IKK, Deleye XGJ, Jansen PP, Koper PCM. Anatomy based inverse planning in HDR prostate brachytherapy. *Radiother Oncol* 2004;73:73–7. <https://doi.org/10.1016/j.radonc.2004.08.014>.
- [11] De Jong TL, van de Berg NJ, Tas L, Moelker A, Dankelman J, van den Dobbelsteen JJ. Needle placement errors: Do we need steerable needles in interventional radiology? *Med Devices Evid Res* 2018;11:259–65. <https://doi.org/10.2147/MDER.S160444>.
- [12] Foster W, Cunha JAM, Hsu IC, Weinberg V, Krishnamurthy D, Pouliot J. Dosimetric impact of interfraction catheter movement in high-dose rate prostate brachytherapy. *Int J Radiat Oncol Biol Phys* 2011;80:85–90. <https://doi.org/10.1016/j.ijrobp.2010.01.016>.
- [13] Yoshida K, Yamazaki H, Kotsuma T, Akiyama H, Takenaka T, Masui K, et al. Edema worsens target coverage in high-dose-rate interstitial brachytherapy of mobile tongue cancer: A report of two cases. *J Contemp Brachytherapy* 2017;9:66–70. <https://doi.org/10.5114/jcb.2017.65163>.
- [14] Yoshioka Y, Yoshida K, Yamazaki H, Nonomura N, Ogawa K. The emerging role of high-Dose-Rate (HDR) brachytherapy as monotherapy for prostate cancer. *J Radiat Res* 2013;54:781–8. <https://doi.org/10.1093/jrr/rrt027>.
- [15] De Battisti MB, Denis De Senneville B, Maenhout M, Hautvast G, Binnekamp D, Lagendijk JJW, et al. Adaptive planning strategy for high dose rate prostate brachytherapy - A simulation study on needle positioning errors. *Phys Med Biol* 2016;61:2177–95. <https://doi.org/10.1088/0031-9155/61/5/2177>.
- [16] Seppenwoolde Y, Kolkman-Deurloo IK, Sijkema D, de Langen M, Praag J, Jansen P, et al. HDR prostate monotherapy - Dosimetric effects of implant deformation due to posture change between TRUS- and CT-imaging. *Radiother Oncol* 2008;86:114–9. <https://doi.org/10.1016/j.radonc.2007.11.004>.
- [17] Stone NN, Roy J, Hong S, Lo YC, Stock RG. Prostate gland motion and deformation caused by needle placement during brachytherapy. *Brachytherapy* 2002;1:154–60. [https://doi.org/10.1016/S1538-4721\(02\)00058-2](https://doi.org/10.1016/S1538-4721(02)00058-2).
- [18] Abolhassani N, Patel R, Moallem M. Needle insertion into soft tissue: A survey. *Med Eng Phys* 2007;29:413–31. <https://doi.org/10.1016/j.medengphy.2006.07.003>.
- [19] Riviere CN, Thakral A, Iordachita II, Mitroi G, Stoianovici D. Predicting respiratory motion for active canceling during percutaneous needle insertion. *Annu Reports Res React Institute, Kyoto Univ* 2001;4:3477–80. <https://doi.org/10.1109/iembs.2001.1019580>.



- [20] Milickovic N, Mavroidis P, Tselis N, Nikolova I, Katsilieri Z, Kefala V, et al. 4D analysis of influence of patient movement and anatomy alteration on the quality of 3D U/S-based prostate HDR brachytherapy treatment delivery. *Med Phys* 2011;38:4982–93. <https://doi.org/10.1118/1.3618735>.
- [21] Webster RJ, Kim JS, Cowan NJ, Chirikjian GS, Okamura AM. Nonholonomic modeling of needle steering. *Int J Rob Res* 2006;25:509–25. <https://doi.org/10.1177/0278364906065388>.
- [22] Palacio-Torralba J, Good DW, McNeill SA, Reuben RL, Chen Y. Histology-based homogenization analysis of soft tissue: Application to prostate cancer. *J R Soc Interface* 2017;14. <https://doi.org/10.1098/rsif.2017.0088>.
- [23] Roesthuis RJ, Veen YRJ Van, Jahya A, Misra S. Mechanics of Needle-Tissue Interaction. *Int. Conf. Intell. Robot. Syst.*, 2011. <https://doi.org/https://doi.org/10.1109/IROS.2011.6094969>.
- [24] Tincher SA, Kim RY, Ezekiel MP, Zinsli T, Fiveash JB, Raben DA, et al. Effects of pelvic rotation and needle angle on pubic arch interference during transperineal prostate implants. *Int J Radiat Oncol Biol Phys* 2000;47:361–3. [https://doi.org/10.1016/S0360-3016\(00\)00434-X](https://doi.org/10.1016/S0360-3016(00)00434-X).
- [25] de Battisti MB, de Senneville BD, Maenhout M, Lagendijk JJW, van Vulpen M, Hautvast G, et al. Fiber Bragg gratings-based sensing for real-time needle tracking during MR-guided brachytherapy. *Med Phys* 2016;43:5288–97.
- [26] Alterovitz R, Pouliot J, Taschereau R, Joe Hsu IC, Goldberg K. Simulating needle insertion and radioactive seed implantation for prostate brachytherapy. *Stud Health Technol Inform* 2003;94:19–25. <https://doi.org/10.3233/978-1-60750-938-7-19>.
- [27] Scali M, Pusch TP, Breedveld P, Dodou D. Needle-like instruments for steering through solid organs: A review of the scientific and patent literature. *Proc Inst Mech Eng Part H J Eng Med* 2017;231:250–65. <https://doi.org/10.1177/0954411916672149>.
- [28] Eapen L, Kayser C, Deshaies Y, Perry G, E C, Morash C, et al. Correlating the degree of needle trauma during prostate brachytherapy and the development of acute urinary toxicity. *Int J Radiat Oncol Biol Phys* 2004;59:1392–4. <https://doi.org/10.1016/j.ijrobp.2004.01.041>.
- [29] Torabi M, Gupta R, Walsh CJ. Compact robotically steerable image-guided instrument for multi-adjacent-point (MAP) targeting. *IEEE Trans Robot* 2014;30:802–15. <https://doi.org/10.1109/TRO.2014.2304773>.
- [30] Khadem M, Rossa C, Usmani N, Sloboda RS, Tavakoli M. Geometric control of 3D needle steering in soft-tissue. *Automatica* 2019;101:36–43. <https://doi.org/10.1016/j.automatica.2018.11.018>.
- [31] Mallick S, Rath GK, Benson R. Practical radiation oncology. 2019. <https://doi.org/10.1007/978-981-15-0073-2>.
- [32] Bellon J, Wallner K, Ellis W, Russell K, Cavanagh W, Blasko J. Use of pelvic CT scanning to evaluate pubic arch interference of transperineal prostate brachytherapy. *Int J Radiat Oncol Biol Phys* 1999;43:579–81. [https://doi.org/10.1016/S0360-3016\(98\)00466-0](https://doi.org/10.1016/S0360-3016(98)00466-0).
- [33] Davis BJ, Horwitz EM, Lee WR, Crook JM, Stock RG, Merrick GS, et al. American Brachytherapy Society consensus guidelines for transrectal ultrasound-guided permanent prostate brachytherapy. *Brachytherapy* 2012;11:6–19. <https://doi.org/10.1016/j.brachy.2011.07.005>.
- [34] Harris AA, Martin B, Stang K, Hentz C, Farooq A, Baldea K, et al. Impact of Prostate Gland Size  $\geq 60$  cc on Physician and Patient-Reported Toxicity after High Dose Rate Prostate Brachytherapy. *Int J Radiat Oncol* 2018;102:e116. <https://doi.org/10.1016/j.ijrobp.2018.07.315>.
- [35] Chevie J. Flexible needle steering using ultrasound visual servoing. Signal and Image processing. Université Rennes 1, 2017. n.d.
- [36] Van de Berg NJ, van Gerwen DJ, Dankelman J, van den Dobbelsteen JJ. Design Choices in Needle Steering - A Review. *IEEE/ASME Trans Mechatronics* 2015;20:2172–83. <https://doi.org/10.1109/TMECH.2014.2365999>.
- [37] de Vries M, Klaassen NJM, Morsink NC, van Nimwegen SA, Nijsen JFW, van den Dobbelsteen JJ. Dedicated holmium microsphere administration device for MRI-guided interstitial brain microbrachytherapy. *Med Eng Phys* 2021;96:13–21. <https://doi.org/10.1016/j.medengphy.2021.07.009>.
- [38] Engh JA, Podnar G, Kondziolka D, Riviere CN. Toward effective needle steering in brain tissue. *Annu Int Conf IEEE Eng Med Biol - Proc* 2006:559–62. <https://doi.org/10.1109/IEMBS.2006.260167>.
- [39] Dupont PE, Lock J, Itkowitz B, Butler E. Design and control of concentric-tube robots. *IEEE Trans Robot* 2010;26:209–25. <https://doi.org/10.1109/TRO.2009.2035740>.

- [40] Ryu SC, Quek ZF, Koh JS, Renaud P, Black RJ, Moslehi B, et al. Design of an optically controlled MR-compatible active needle. *IEEE Trans Robot* 2015;31:1–11. <https://doi.org/10.1109/TRO.2014.2367351>.
- [41] Burgner J, Swaney PJ, Bruns TL, Clark MS, Rucker DC, Burdette EC, et al. An Autoclavable Steerable Cannula Manual Deployment Device: Design and Accuracy Analysis. *J Med Devices, Trans ASME* 2012;6:1–7. <https://doi.org/10.1115/1.4007944>.
- [42] Farooq MU, Xu B, Ko SY. A concentric tube-based 4-DOF puncturing needle with a novel miniaturized actuation system for vitrectomy. *Biomed Eng Online* 2019;18:1–16. <https://doi.org/10.1186/s12938-019-0666-x>.
- [43] Webster RJ, Okamura AM, Cowan NJ. Toward active cannulas: Miniature snake-like surgical robots. *IEEE Int Conf Intell Robot Syst* 2006:2857–63. <https://doi.org/10.1109/IROS.2006.282073>.
- [44] Webster RJ, Romano JM, Cowan NJ. Mechanics of precurved-tube continuum robots. *IEEE Trans Robot* 2009;25:67–78. <https://doi.org/10.1109/TRO.2008.2006868>.
- [45] Van de Berg NJ, Meeuwse FC, Doukas M, Kronreif G, Moelker A, van den Dobbelsteen JJ. Steerable needles for radio-frequency ablation in cirrhotic livers. *Sci Rep* 2021;11. <https://doi.org/10.1038/s41598-020-77869-3>.
- [46] Crossley D. Sharp turning steerable needle - Patent WO 2018/067808 A1. Patent 2018.
- [47] Suligoj F, Heunis CM, Sikorski J, Misra S. RobUST—An Autonomous Robotic Ultrasound System for Medical Imaging. *IEEE Access* 2021;9:67456–65. <https://doi.org/10.1109/access.2021.3077037>.
- [48] Sikorski J, Denasi A, Bucchi G, Scheggi S, Misra S. Vision-Based 3-D Control of Magnetically Actuated Catheter Using BigMag - An Array of Mobile Electromagnetic Coils. *IEEE/ASME Trans Mechatronics* 2019;24:505–16. <https://doi.org/10.1109/TMECH.2019.2893166>.
- [49] Podder T, Clark D, Sherman J, Fuller D, Messing E, Rubens D, et al. In vivo motion and force measurement of surgical needle intervention during prostate brachytherapy. *Med Phys* 2006;33:2915–22. <https://doi.org/10.1118/1.2218061>.
- [50] Farrer AI, Odéen H, Bever J De, Coats B, Parker DL, Payne A, et al. Characterization and evaluation of tissue-mimicking gelatin phantoms for use with MRgFUS. *J Ther Ultrasound* 2015:1–11. <https://doi.org/10.1186/s40349-015-0030-y>.
- [51] Rouvière O, Melodelima C, Dinh AH, Bratan F, Pagnoux G, Sanzalone T, et al. Stiffness of benign and malignant prostate tissue measured by shear-wave elastography: a preliminary study. *Eur Soc Radiol* 2017:1858–66. <https://doi.org/10.1007/s00330-016-4534-9>.
- [52] Veen YRJ Van, Jahya A, Misra S. Macroscopic and microscopic observations of needle insertion into gels. *J Eng Med* 2012;226:441–9. <https://doi.org/10.1177/0954411912443207>.
- [53] Hassan CM, Peppas NA. Structure and applications of poly(vinyl alcohol) hydrogels produced by conventional crosslinking or by freezing/thawing methods. *Adv Polym Sci* 2000;153:37–65. [https://doi.org/10.1007/3-540-46414-x\\_2](https://doi.org/10.1007/3-540-46414-x_2).
- [54] Jiang S, Liu S, Feng W. PVA hydrogel properties for biomedical application. *J Mech Behav Biomed Mater* 2011;4:1228–33. <https://doi.org/10.1016/j.jmbbm.2011.04.005>.
- [55] Zell K. Acoustical properties of selected tissue phantom materials for ultrasound imaging. *Phys Med Biol* 2007. <https://doi.org/10.1088/0031-9155/52/20/N02>.
- [56] Li P, Jiang S, Yu Y, Yang J, Yang Z. Biomaterial characteristics and application of silicone rubber and PVA hydrogels mimicked in organ groups for prostate brachytherapy. *J Mech Behav Biomed Mater* 2015;49:220–34. <https://doi.org/10.1016/j.jmbbm.2015.05.012>.
- [57] Straßmann G, Olbert P, Hegele A, Richter D, Fokas E, Timmesfeld N, et al. Advantage of robotic needle placement on a prostate model in HDR brachytherapy. *Strahlentherapie Und Onkol* 2011;187:367–72. <https://doi.org/10.1007/s00066-011-2185-y>.



# 5

## Dosimetric benefits and preclinical performance of steerable needles in high-dose-rate prostate brachytherapy

Martijn de Vries, Miranda E.M.C. Christianen, Lorne Luthart, Kim C. de Vries, Inger-Karine K.K. Kolkman-Deurloo, John J. van den Dobbelssteen

*Under review (2023)*

## ABSTRACT

Prostate cancer patients with an enlarged prostate and/or excessive pubic arch interference (PAI) are generally considered non-eligible for high-dose-rate (HDR) brachytherapy (BT). Steerable needles have been developed to make these patients eligible again. This study aims to validate the dosimetric impact and performance of steerable needles within the conventional clinical setting. HDR BT treatment plans were generated, needle implantations were performed in a prostate phantom, with prostate volume  $> 55 \text{ cm}^3$  and excessive PAI of 10 mm, and pre- and post-implant dosimetry were compared considering the dosimetric constraints: prostate  $V_{100} > 95\%$  (13.50 Gy), urethra  $D_{0.1\text{cm}^3} < 115\%$  (15.53 Gy) and rectum  $D_{1\text{cm}^3} < 75\%$  (10.13 Gy). The inclusion of steerable needles resulted in a notable enhancement of the dose distribution and prostate  $V_{100}$  compared to treatment plans exclusively employing rigid needles to address PAI. Furthermore, the steerable needle plan demonstrated better agreement between pre- and post-implant dosimetry (prostate  $V_{100}$ : 96.24% vs. 93.74%) compared to the rigid needle plans (79.13% vs. 72.86% and 87.70% vs. 81.76%), with no major changes in the clinical workflow and no changes in the clinical set-up. The steerable needle approach allows for more flexibility in needle positioning, ensuring a highly conformal dose distribution, and hence, HDR BT is a feasible treatment option again for prostate cancer patients with an enlarged prostate and/or excessive PAI.

## 5.1 INTRODUCTION

High-dose-rate (HDR) brachytherapy (BT) for prostate cancer patients enables optimisation of the dose distribution in the target volume. This is achieved through on-line adjustments of dwell times and dwell positions, resulting in excellent clinical outcomes [1]. However, certain challenges persist, including: 1) pubic arch interference (PAI), 2) too wide prostates, and 3) lesions ventral to the urethra. These situations may result in either underdosage of the target volume or excluding the patient and pursuing another therapy. Current clinical guidelines prescribe that a prostate volume ( $V_p$ ) of  $> 50\text{-}60\text{ cm}^3$  requires special attention due to the risk of PAI affecting the anterolateral portion of the prostate [2,3]. To reduce the risk of encountering PAI during needle insertion,  $V_p$  is calculated prior to the procedure on the MRI, CT or ultrasound scan. This calculation employs an elliptical approximation formula:  $V_p\text{ (cm}^3\text{)} = \pi / 6$  (height x width x length of the prostate) [4]. However, the volume calculation can be faulty, and an enlarged prostate is not necessarily a harbinger for PAI. This method potentially excludes eligible patients from this beneficial treatment option [5,6].

At our institution<sup>(b)</sup>, patients with a  $V_p$  ranging from 50 to 60  $\text{cm}^3$ , without any contraindications, may be admitted if no PAI is expected. To assess the risk of encountering PAI, a digital rotation of the segmented pelvis and prostate is performed using the preoperative 3D imaging set, simulating the lithotomy position of the patient [7]. However, this method lacks established guidelines, and discrepancies arise due to interpatient and interobserver variability. Occasionally, the implantation procedure must be aborted because of significant inaccessibility of the target volume. These patients require another curative treatment such as stereotactic body radiation therapy, e.g. using CyberKnife [8,9]. This introduces additional costs for the healthcare system and a considerable mental and physical burden on the patient.

A widely employed approach to minimise the risk of PAI and enhance access to the prostate is by downsizing the prostate through a course of androgen deprivation therapy (ADT). However, observational studies have indicated that this 3-12-month therapy is associated with a decrease in quality of life and the potential for increased morbidity and mortality [10]. Alternative solutions include adjustments to the clinical set-up, workflow or patient positioning, but these may not always be practical or desired [11].

To address these challenges, we propose the use of specially developed steerable needles, offering enhanced flexibility in needle positioning [12]. Using these steerable needles, curved trajectories can be created and PAI can be overcome to obtain a conformal dose distribution in the prostate. This can be achieved without requiring prior PAI risk assessments or any adaptations to the clinical set-up.

The aims of this work are twofold: firstly, to validate the dosimetric consequences of using steerable needles on a non-eligible HDR prostate BT case; and secondly, to assess the feasibility of using the steerable needles in the conventional HDR BT setting. The study entails a treatment planning investigation utilising the Oncentra Prostate Treatment Planning System (TPS) (Elekta Instrument AB, Stockholm, Sweden). An anthropomorphic prostate phantom is developed and employed for the planning study, followed by actual needle implantations to evaluate performance, dosimetric parameters, and clinical workflow. If conformal dosimetry is obtained by using steerable needles, exclusion of such patients from HDR BT could be unnecessary and preoperative ADT for prostate downsizing could be avoided in men with enlarged prostates and/or excessive PAI.

## 5.2 MATERIALS AND METHODS

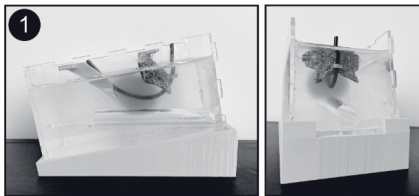
A dataset was selected from the anonymised MRI patient database with enlarged prostates ( $V_p > 55\text{ cm}^3$ ) [7]. This dataset served as the basis for the development of a prostate phantom, which

incorporated the average PAI of the patient database (10 mm). A comprehensive study encompassing treatment planning and evaluation of the implantation procedure was conducted. This study compared the conventional procedure employing rigid needles to the proposed approach that incorporated both rigid and steerable needles.

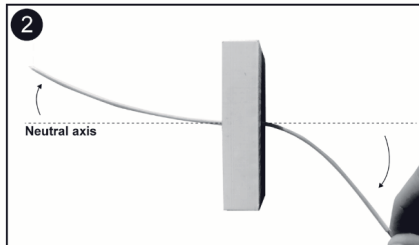
### 5.2.1 Study set-up

Treatment planning and needle implantations followed our current clinical HDR prostate BT protocol, utilising the developed phantom, novel steerable needles, real-time transrectal ultrasound (TRUS) visualisation, and the established clinical treatment planning and optimisation protocol (Figure 5.1). The steerable needle comprises of a 245 mm stainless spring steel (AISI 301) steerable inner obturator, placed inside a 240 mm flexible polyoxymethylene (POM) ProGuide sharp, conical shaped, 6F needle (Elekta Instrument AB, Stockholm, Sweden). The design of the steerable inner obturators is based on the steering principle described by de Vries et al. where proximal bending of the steerable needle allows distal tip steering over 360 degrees in the axial plane [12]. This design serves two purposes: 1) to circumvent intermediate anatomical and sensitive structures and 2) to counteract unwanted deflections during a controlled insertion by utilising the transperineal template as a pivot point.

#### Anthropomorphic prostate phantom



#### Steerable needle



#### Ultrasonography

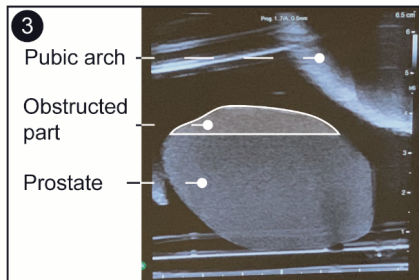


**Figure 5.1 – The clinical set-up.** 1) The anthropomorphic prostate phantom, placed on a 10 degrees wedge to mimic patient's lithotomy position with the rectum parallel to the implanting direction to ensure proper ultrasound visualisation, 2) The steerable

needle, steered from the neutral axis by bending the proximal end, 3) The prostate and the pubic arch, visualised by using transrectal ultrasound (TRUS) imaging in a sagittal plane. The obstructed part of the prostate is outlined. 4) The overall set-up. The steerable needle is inserted in the prostate phantom by the physician under TRUS guidance. The equipment included rigid needles, comprising of 240 mm ProGuide sharp 6F needles and the 245 mm ProGuide Obturators, Oncentra Prostate TPS, OncoSelect Stepper and Endo-Cavity Rotational Mover, Martinez prostate transperineal template (Elekta Instrument AB, Stockholm, Sweden) and the multiplane 9 MHz TRUS transducer (E14CL4b) connected to the bkSpecto Ultrasound Machine (BK Medical, Nærum, Denmark).

### 5.2.1.1 Prostate phantom

A novel prostate phantom was developed because the commercially available prostate phantoms only replicate anatomical structures and provide contrast for multi-modality imaging. For the present study, the phantom needed to possess realistic mechanical properties to mimic instrument insertions and incorporate a pubic arch obstruction, reflecting the average PAI observed in the patient database. PAI was measured in an axial plane in terms of the greatest perpendicular overlap distance from the caudal edge of the pubic arch to the ventral prostate border, as indicated by de Vries et al. [7]. Two phantoms were produced, aiming for similarity to each other and mimicking the patient's anatomy, including the prostate gland, pubic arch and the organs at risk (OARs) comprising of the rectum and the urethra. These phantoms were fabricated from polyvinyl alcohol (PVA) as this biomaterial exhibits similar microstructure and mechanical properties as that of human soft tissue [13]. Slight variations resulted in the first phantom used for the treatment planning study having a  $V_p$  of 57.2 cm<sup>3</sup>, while the second phantom, employed in the implantation study, had a  $V_p$  of 59.3 cm<sup>3</sup>. The prostate tissue simulant contained 7 wt.% PVA (Sigma-Aldrich, St. Louis, Missouri, United States) with a compressive modulus of elasticity of 54.6 ± 4.6 kPa after two freeze-thaw cycles (FTCs) in line with real prostate tissue (58.8 ± 8.2 kPa) and the prostate phantom developed by Shaaer et al. [14,15]. The prostate tissue simulant was embedded in a PVA solution with 6 wt.% with one FTC completed (29.4 ± 1.2 kPa). PVA was solved in 20% demineralised water (Orphi Farma B.V., Dordrecht, the Netherlands) and 80% dimethyl sulfoxide (DMSO 99.7+%, Laboratorium Discounter, IJmuiden, the Netherlands) to form a transparent suspension for the prostate and the surrounding tissue [16]. Needle-tissue interaction forces in the phantom were considered comparable to clinical use by the physicians (MC & KV). To visually distinguish the prostate gland, 0.05 ml of contrast fluid (Food color, Tasty me, Tilburg, the Netherlands) was added to the prostate tissue suspension, while 3 wt.% of silica particles (Silica gel 60 .015-.040mm, Merck KGaA, Darmstadt, Germany) was used for acoustic scattering on the ultrasound visualisation [17]. The pubic arch was 3D-printed with polylactic acid (PLA) plastic and coated with metal particles for ultrasonography.

### 5.2.2 Treatment planning study

Five pre-implant treatment plans were created for HDR BT monotherapy using the Flexitron afterloader (Elekta Instrument AB, Stockholm, Sweden) (Figure 5.2). These plans involved delineating the target volume, the pubic arch and the OARs using TRUS images. The implant geometry was designed based on the implantation pattern from Mate et al. to cover the entire prostate [18].

Plan A represented a treatment scenario for a patient without PAI, making this case eligible for HDR prostate BT. This plan served as the baseline plan including 17 rigid needles, aligning with the simulation study of Kolkman-Deurloo et al. [19]. Plans B, C, D and E simulated a case with PAI. Plans B and C exclusively employed rigid needles. In plan B, six rigid needles were removed from plan A as they were virtually located within the obstructed region of the prostate. Compared to plan B, plan C introduced six rigid needles to the accessible part of the prostate, specifically in the ventral area to optimise the treatment plan.



Plans D and E took a different approach by replacing those six rigid needles with six curved trajectories, reflecting the steerable needles to reach the ventral region of the prostate behind the pubic arch. This was performed at the discretion of the physicians to ensure coverage of the obstructed part of the prostate gland. Planning of the steerable needle trajectories was conducted in the TPS, with one pivot point per trajectory. Ventral steering up to 10 mm was applied after passing below the pubic arch to prevent needle-bone collisions and maintain the intended curved trajectories, in accordance with the principles described by de Vries et al. [12]. Plan E incorporated a higher degree of steering compared to plan D.

Dwell-time optimisation was performed using the inverse optimisation modality of the Oncentra Prostate software. For HDR BT monotherapy, the prescription dose for the target volume was set at  $2 \times 13.5$  Gy according to Morton et al. [20]. The dosimetric objectives specified in Table 5.1, including prostate  $V_{100}$ ,  $V_{150}$  and  $V_{200}$ ,  $D_{0.1\text{cm}^3}$  urethra,  $D_{1\text{cm}^3}$  rectum, and the prostate  $V_{200}/V_{100}$  ratio, were utilised to assess the quality of the treatment plans via dose-volume histogram (DVH) outcomes. The ratio of prostate  $V_{200}$  to  $V_{100}$  showed the degree of dose heterogeneity within the treatment plans.

### 5.2.3 Implantation study

Needle implantations were carried out in accordance with treatment plans B, C and E by an experienced HDR BT physician (MC) with entry-level experience in the use of the steerable needles after an on-site hands-on training of 20 minutes. The steerable needle approach with a higher degree of steering (plan E) was performed solely because it yielded better DVH outcomes compared to plan D and training had shown that 10 mm of lateral steering could easily be achieved. Two conventional rigid needles were inserted into the prostate on either side of the urethra (template coordinate C3 and E3) to stabilise the prostate gland in analogy with current practice with prostate stabilisation needles.

The implementation of plan E commenced with the physician choosing the needle type and determining the sequence for implantation. In current practice this implies first implanting ventrally located needles for visualisation purposes and then implanting more dorsally. For each steerable needle, the planned curved trajectory was displayed, and a selected steerable needle was positioned at the desired template coordinate. While observing the sagittal plane on the ultrasound, the steerable needle was advanced, allowing for steering and making slight retractions as necessary to stay on the intended trajectory and mitigate potential unwanted deflections caused by interactions between the needle and the tissue. Throughout this procedure, all six steerable needles were tracked by manipulating the TRUS transducer while the live-plan setting in Oncentra Prostate was enabled. Subsequently, rigid needles were inserted in pairs on either side of the urethra, and advanced to their designated end positions. This adhered to established practice, ensuring the completion of the implant geometry for plan E. Reconstruction of the implanted needles was performed in Oncentra Prostate TPS as in current practice. Next, six steerable needles were withdrawn from the phantom, leaving behind eleven rigid needles, thus replicating the implant geometry as specified in plan B. Finally, six rigid needles were added to the configuration of plan B to construct the implant geometry of plan C. The quality of the post-implant treatment plans was assessed based on DVH outcomes, and the time taken for each needle type during the implantation procedure was recorded.

## 5.3 RESULTS

The pre-implant treatment plans are shown in Figure 5.2. Ventral steering was applied over an insertion depth up to 58 mm after passing below the pubic arch.

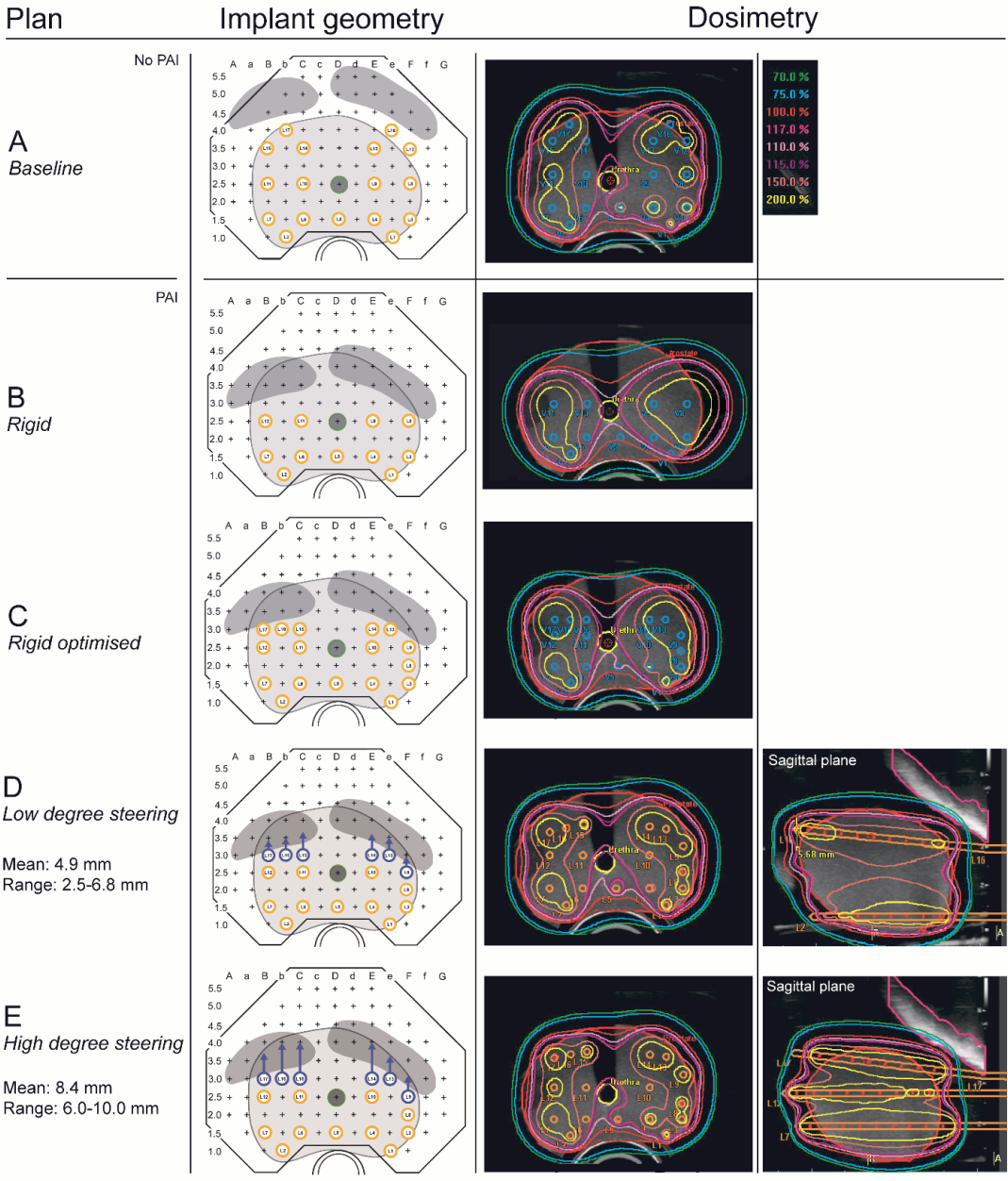


**Figure 5.2 – Treatment planning study.** Column 2 presents the implant geometry for each plan in the reference plane on the Martinez template projection. Column 3 shows the corresponding dosimetry. Column 4 displays the curved trajectories for plans D and E around the pubic arch in a sagittal plane and the legend of the isodose lines. Plan A is the baseline plan with no pubic arch interference (PAI). Plans B - E show obstruction of the prostate due to PAI. Steerable needles are indicated in blue, vectors show the degree and direction of steering, and rigid needles are indicated in orange in Column 2. The mean and range of distal tip steering with steerable needles are indicated in Column 1. Other colours in Column 2: light grey = prostate tissue, dark grey = pubic arch and green = urethra.

Table 5.1 shows an increase up to 17.1% in prostate  $V_{100}$ , which denotes the prostate volume receiving at least 100% of the prescribed dose, in the pre-implant treatment plans that incorporate steerable needles (D and E), as compared to the plans employing rigid needles (B and C). The dose to the urethra remained below the dose constraint of 115% in all pre-implant treatment plans. The DVH values in plan E closely resembled the outcomes observed in the baseline plan (A), where PAI was not a consideration. These findings signify an adequate dose coverage in the prostate while minimising potential harm to the OARs.

Parameter	Objective	Plan A	Plan B		Plan C		Plan D	Plan E		
		Baseline	Rigid		Rigid optimised		Low degree steering	High degree steering		
		Pre-implant treatment plan	Pre-implant treatment plan	Post-implant treatment plan	Pre-implant treatment plan	Post-implant treatment plan	Pre-implant treatment plan	Pre-implant treatment plan	Post-implant treatment plan	
Pubic arch interference		-	10 mm		10 mm		10 mm	10 mm		
# Rigid needles		17	11		17		11	11		
# Steerable needles		-	-		-		6	6		
DVH information	Prescribed dose	13.50 Gy								
Prostate	$V_{100}$	> 95 %	97.00 %	79.13 %	72.86 %	87.70 %	81.76 %	93.54 %	96.24 %	93.74 %
	$V_{150}$		37.48 %	37.62 %	36.06 %	40.72 %	36.69 %	37.95 %	38.88 %	37.85 %
	$V_{200}$		13.34 %	21.78 %	21.24 %	18.84 %	18.37 %	15.10 %	13.20 %	16.02 %
	$V_{200}/V_{100}$		0.14	0.28	0.29	0.21	0.22	0.16	0.14	0.17
Urethra	$D_{0.1\text{ cm}^3}$	< 115 % (15.53 Gy)	114.71 % (15.49 Gy)	114.90 % (15.51 Gy)	114.89 % (15.51 Gy)	114.71 % (15.49 Gy)	114.89 % (15.51 Gy)	114.61 % (15.47 Gy)	114.61 % (15.47 Gy)	114.89 % (15.51 Gy)
Rectum	$D_1\text{ cm}^3$	< 75 % (10.13 Gy)	79.87 % (10.78 Gy)	79.26 % (10.70 Gy)	79.37 % (10.72 Gy)	79.64 % (10.75 Gy)	68.92 % (9.30 Gy)	79.74 % (10.77 Gy)	79.73 % (10.76 Gy)	79.70 % (10.80 Gy)
Total implantation time										
Rigid needles						12 min 48 sec				6 min 56 sec
Steerable needles						-				10 min 24 sec

**Table 5.1 – Dose-volume histogram information of the pre- and post-implant treatment plans.** Comparison of dosimetry per treatment plan before implantation for all plans and after needle implantation for plans B, C and E. The dose-volume histogram (DVH) information indicates the dosimetric objectives and results. Per plan the amount of pubic arch interference and the type of needles used are reported. Implantation time is stated for plans C and E with 17 needles per type of needle used.

The physician successfully implanted all needles, closely adhering to the planned curved trajectories with the steerable needles. There were only minor issues with two of the steerable needles, which were positioned somewhat too medially, resulting in a slight increase in urethral dose. All steerable needles were clearly visible during TRUS imaging, and there was sufficient working space to bend the proximal end of the needles for precise distal tip steering. Figure 5.3 shows the implant geometry and post-implant dosimetry of the steerable needle plan E after needle reconstruction. The average implantation time of a steerable needle was 2.5 times longer compared to rigid needles, mainly due to the need for multiple evaluation moments during insertion. Besides, one steerable needle required reinsertion

because it deviated more than 3 mm from the planned trajectory within the first 60 mm of insertion, as detected through real-time TRUS imaging. No changes in clinical set-up and no major changes in clinical workflow were required for executing plan E.

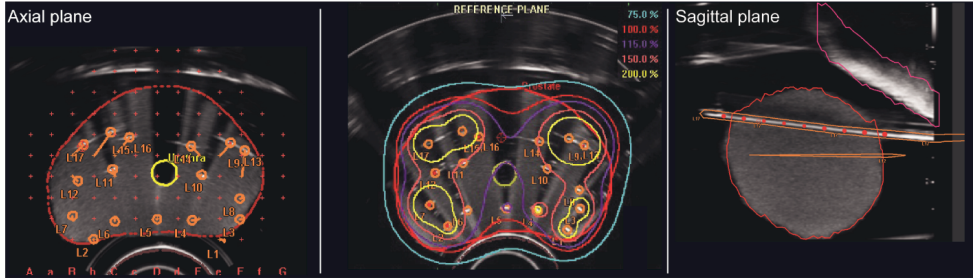


**Figure 5.3 – Implant geometry and post-implant dosimetry of the steerable needle approach (plan E).** Left image shows the implant geometry including 11 rigid needles and 6 steerable needles, central image displays the dosimetry and right image visualises the curved trajectory of one steerable needle which was inserted below the pubic arch and reached the obstructed part of the prostate behind the pubic arch conform the planned curved trajectory indicated in orange.

After implantation, the steerable needle approach (plan E) had a sufficient prostate  $V_{100}$  of 93.74% and a clinically appropriate dose distribution, indicated by the  $V_{200}/V_{100}$  ratio (Table 5.1). The doses to the OARs were similar to those in the pre-implant treatment plan. In comparison with all other plans, the steerable needle plan demonstrated the closest adherence to the pre-implant treatment plan. This was attributed to the steerable needles' ability to mitigate undesired deflections, which was not possible with rigid needles. A decrease in prostate  $V_{100}$  of only 2.5% was observed in plan E, while the rigid needle plans exhibited a more substantial decrease of ~6% when comparing post-implant to pre-implant treatment plans.

## 5.4 DISCUSSION

This work presents the dosimetric benefits of a steerable needle approach in HDR prostate BT. It assesses the feasibility of planning curved trajectories, implanting the steerable needles according to the treatment plan in the clinical setting, reconstructing the needles and creating a post-implant treatment plan. We simulated a case by a phantom study in which a patient, normally non-eligible for HDR BT due to an enlarged prostate gland and excessive PAI, could effectively undergo treatment using a combination of conventional rigid needles and developed steerable needles. Six steerable needles were introduced, maintaining the same total needle count as in the baseline plan, which did not consider PAI and solely employed rigid needles. The steerable needle approaches showed both improved spatial distribution of all needles and target coverage compared to the rigid needle plans while sparing the OARs. The dosimetry of the steerable needle plan with high degree of steering closely approached the DVH outcomes for the plan without PAI consideration. To the authors knowledge, this is the first study where steerable needles are used in HDR prostate BT to overcome PAI in an anthropomorphic phantom and in which pre- and post-implant dosimetry outcomes are reported.

Two prostate phantoms were developed due to limitations in shelf life, preventing the use of the same model for both treatment planning and implantation phases. A minor difference of  $2.1 \text{ cm}^3$  in  $V_p$  was observed between the phantoms, attributable to possible mold leakage and intraobserver variability. Nevertheless, discrepancies from 4 to 10% between both phases are common in current practice due to prostate deformations, edema and delineation variability [21,22]. Our phantoms exhibited similarities in volume and elasticity to the phantom developed by Shaaer et al. but are distinguished in two aspects. Firstly, we used heterogeneous PVA, which is a prostate-like material, instead of homogeneous gelatin. Secondly, we incorporated a pubic arch a feature not present in their phantom [15]. Similarly, Ryu et al.

developed a 60 cm<sup>3</sup> prostate phantom that included a pubic arch, but their model was made of homogeneous agar [23]. Noteworthy is the overdosing of the rectum in all plans. Row 1.0 of the Martinez template could not be placed properly for reaching the dorsal part of the target volume because of the small spacing between rectum and prostate in the phantom. Therefore, caution is advised when interpreting DVH data for the rectum, and future phantom models should consider increasing spacing to reduce rectal dose.

A decrease in target coverage was observed in all plans post-implant, possibly caused by the increase in  $V_p$  and unwanted needle deflections during the insertions. Nonetheless, the steerable needle approach demonstrated better adherence to the pre-implant treatment plan. This was attributed to the steerable needles' ability to be controlled during insertion, allowing for precisely following the planned trajectories, which was not possible with the rigid needles. Considering the limited amount of training, this finding implies a steep learning curve for using the steerable needles.

Next to unwanted deflections, inaccessibility of the prostate may only become apparent during the procedure. Various techniques can be applied in such cases, including TRUS transducer angulation, needle manipulations or extending patient's lithotomy position. However, these actions can compromise dose conformity and patient's comfort. As a result, alternative approaches have been explored, such as customised templates with angulated needle paths and non-parallel needle implantations [4,23–27]. Ryu et al. performed a study for low-dose-rate (LDR) BT, using oblique needles in a 60 cm<sup>3</sup> prostate phantom, aiming to overcome PAI [23]. Their results were promising, with a prostate  $V_{100}$  of 97%,  $V_{150}$  of 41.8% and  $V_{200}$  of 17.1%. However, 25 needles were required for obtaining this level of dose coverage while sparing the OARs. Gibbons *et al.* implanted up to seven LDR BT needles free-hand behind the pubic arch in eight patients with a mean  $V_p$  of 46 cm<sup>3</sup> [4]. Their results showed a prostate  $V_{100}$  of 96.3% and  $V_{150}$  of 81.6%, but they did not investigate dose to the urethra. While these previous studies have shown potential in addressing the challenge, our study stands out as it achieved similar outcomes to these approaches without necessitating significant changes in the clinical set-up [4,23–25]. Only some minor changes to the clinical workflow were required, which were very easy to implement. First, the Oncentra Prostate TPS did not allow for applying smooth curved trajectories in the pre-implant treatment plan setting, thus one pivot point per trajectory was incorporated to simulate a curvature. Secondly, implantation of the steerable needles was performed in the live-plan setting. This may challenge visualisation if steering in multiple directions is applied; tilt scanning with TRUS imaging produces 3D images for the live-plan while reconstruction in the TPS is performed in orthogonal planes. Thirdly, the steerable needles were inserted one by one, directly at the planned end position each time, which slightly increased implantation time compared to inserting rigid needles performed in pairs.

For future optimisation, steerable needles hold the potential to circumvent the urethra for treatment of ventrally located tumours, treat wider prostates than the transperineal template allows, address small prostates with a narrow pubic arch, avoid the penile bulb and neurovascular bundle, or enhance overall dosimetry outcomes. In case of a targeting error with a rigid needle, reported to be up to 3.8 mm [28], the steerable inner obturator can be employed to mitigate the unwanted deflection without additional tissue damage associated with a full reinsertion. Additionally, steerable needles can be implanted conforming the prostate's geometry. Earlier studies have shown that this approach required 30% to 80% fewer needles, and Podder et al. have discussed the potential reduction of edema and urinary incontinence [27,29].

## 5.5 CONCLUSION

The utilisation of steerable needles offers increased flexibility in needle positioning, necessitating only minor adjustments to the existing clinical workflow. The curved trajectories can be easily planned in the Oncentra Prostate TPS, and the implantation process can be executed with minimal impact on implantation time, while maintaining excellent agreement between pre- and post-implant treatment plans. This work clearly demonstrates that a highly conformal dose distribution can be achieved using steerable needles, and hence, HDR BT is a feasible treatment option again for prostate cancer patients with enlarged prostates and/or excessive PAI. Importantly, this may eliminate the necessity for preoperative ADT for prostate downsizing. The steerable needles are ready for implementation in clinical practice with no further developments or investments required.

## REFERENCES

- [1] Aluwini S, Busser WMH, Ghidey W, Boormans JL, Kirkels WJ, Jansen PP, et al. Toxicity and quality of life after high-dose-rate brachytherapy as monotherapy for low- and intermediate-risk prostate cancer. *Radiother Oncol* 2015;117:252–7. <https://doi.org/10.1016/j.radonc.2015.09.019>.
- [2] Henry A, Pieters BR, André Siebert F, Hoskin P. GEC-ESTRO ACROP prostate brachytherapy guidelines. *Radiother Oncol* 2022;167:244–51. <https://doi.org/10.1016/j.radonc.2021.12.047>.
- [3] Davis BJ, Horwitz EM, Lee WR, Crook JM, Stock RG, Merrick GS, et al. American Brachytherapy Society consensus guidelines for transrectal ultrasound-guided permanent prostate brachytherapy. *Brachytherapy* 2012;11:6–19. <https://doi.org/10.1016/j.brachy.2011.07.005>.
- [4] Gibbons EP, Smith RP, Beriwal S, Krishna K, Benoit RM. Overcoming pubic arch interference with free-hand needle placement in men undergoing prostate brachytherapy. *Brachytherapy* 2009;8:74–8. <https://doi.org/10.1016/j.brachy.2008.04.007>.
- [5] Bellon J, Wallner K, Ellis W, Russell K, Cavanagh W, Blasko J. Use of pelvic CT scanning to evaluate pubic arch interference of transperineal prostate brachytherapy. *Int J Radiat Oncol Biol Phys* 1999;43:579–81. [https://doi.org/10.1016/S0360-3016\(98\)00466-0](https://doi.org/10.1016/S0360-3016(98)00466-0).
- [6] Stone NN, Stock RG. Prostate brachytherapy in men with gland volume of 100cc or greater: Technique, cancer control, and morbidity. *Brachytherapy* 2013;12:217–21. <https://doi.org/10.1016/j.brachy.2012.10.002>.
- [7] De Vries M, Wilby SL, Palmer AL, Polak W, Hea IO, Hodgson D, et al. Overcoming pubic arch interference in prostate brachytherapy using steerable needles. *Contemp Brachytherapy* 2022;14. <https://doi.org/10.5114/jcb.2022.121562>.
- [8] Aluwini S, van Rooij P, Hoogeman M, Bangma C, Kirkels WJ, Incrocci L, et al. CyberKnife Stereotactic Radiotherapy as Monotherapy. *J Endourol* 2010;24:865–9. <https://doi.org/10.1089=end.2009.0438>.
- [9] Aluwini S, Van Rooij P, Hoogeman M, Kirkels W, Kolkman-Deurloo IK, Bangma C. Stereotactic body radiotherapy with a focal boost to the MRI-visible tumor as monotherapy for low- and intermediate-risk prostate cancer: Early results. *Radiat Oncol* 2013;8. <https://doi.org/10.1186/1748-717x-8-84>.
- [10] Keyes M, Merrick G, Frank S J, Grimm P ZMJ. Use of Androgen Deprivation Therapy with Prostate Brachytherapy, A Systematic Literature Review. *Brachytherapy* 2017;16:245–65. <https://doi.org/10.1016/j.brachy.2016.11.017>.
- [11] Sejjal S, Sathiseelan V, Helenowski I, Kozlowski J, Carter M, Nadler R, et al. Intra-operative pubic arch interference during prostate seed brachytherapy in patients with CT-based pubic arch interference of  $\leq 1$  cm. *Radiother Oncol* 2009;91:249–54. <https://doi.org/10.1016/j.radonc.2009.02.006>.
- [12] De Vries M, Sikorski J, Misra S, van den Dobbelsteen JJ. Axially rigid steerable needle with compliant active tip control. *PLoS One* 2021;16:e0261089. <https://doi.org/10.1371/journal.pone.0261089>.
- [13] Li P, Jiang S, Yu Y, Yang J, Yang Z. Biomaterial characteristics and application of silicone rubber and PVA hydrogels mimicked in organ groups for prostate brachytherapy. *J Mech Behav Biomed Mater* 2015;49:220–34. <https://doi.org/10.1016/j.jmbbm.2015.05.012> LB - 26042767.
- [14] Krouskop TA, Wheeler TM, Kallel F, Garra BS, Hall T. Elastic moduli of breast and prostate tissues under compression. *Ultrason Imaging* 1998;20:260–74. <https://doi.org/10.1177/016173469802000403>.
- [15] Shaaer A, Alrashidi S, Chung H, Loblaw A, Morton G, Paudel M, et al. Multipurpose ultrasound-based prostate phantom for use in interstitial brachytherapy. *Brachytherapy* 2021;20(6):1139–1145. <https://doi.org/10.1016/j.brachy.2021.07.003>.
- [16] Jiang S, Liu S, Feng W. PVA hydrogel properties for biomedical application. *J Mech Behav Biomed Mater* 2011;4:1228–33. <https://doi.org/10.1016/j.jmbbm.2011.04.005>.
- [17] Fromageau J, Brusseau E, Vray D, Gimenez G, Delacharte P. Characterization of PVA cryogel for intravascular ultrasound elasticity imaging. *IEEE Trans Ultrason Ferroelectr Freq Control* 2003;50:1318–24. <https://doi.org/10.1109/TUFFC.2003.1244748>.



- [18] Mate TP, Gottesman JE, Hatton J, Gribble M, Van Hollebeke L. High dose-rate afterloading <sup>192</sup>Iridium prostate brachytherapy: Feasibility report. *Int J Radiat Oncol Biol Phys* 1998;41:525–33. [https://doi.org/10.1016/s0360-3016\(98\)00097-2](https://doi.org/10.1016/s0360-3016(98)00097-2).
- [19] Kolkman-Deurloo I-KK, Roos MA, Aluwini S. HDR monotherapy for prostate cancer: A simulation study to determine the effect of catheter displacement on target coverage and normal tissue irradiation. *Radiother Oncol* 2011;98:192–7. <https://doi.org/10.1016/j.radonc.2010.12.009>.
- [20] Morton G, McGuffin M, Chung HT, Tseng CL, Helou J, Ravi A, et al. Prostate high dose-rate brachytherapy as monotherapy for low and intermediate risk prostate cancer: Efficacy results from a randomized phase II clinical trial of one fraction of 19 Gy or two fractions of 13.5 Gy. *Radiother Oncol* 2020;146:90–6. <https://doi.org/10.1016/j.radonc.2020.02.009>.
- [21] Kim Y, Hsu I-C, Lessard E, Vujic J, Pouliot J. Dosimetric impact of prostate volume change between CT-based HDR brachytherapy fractions. *Int J Radiat Oncol Biol Phys* 2004;59:1208–16. <https://doi.org/10.1016/j.ijrobp.2004.02.053>.
- [22] Yang X, Rossi PJ, Jani AB, Mao H, Zhou Z, Curran WJ, et al. Improved prostate delineation in prostate HDR brachytherapy with TRUS-CT deformable registration technology: A pilot study with MRI validation. *J Appl Clin Med Phys* 2017;18:202–10. <https://doi.org/10.1002/acm2.12040>.
- [23] Ryu B, Bax J, Edirisinge C, Lewis C, Chen J, D'Souza D, et al. Prostate brachytherapy with oblique needles to treat large glands and overcome pubic arch interference. *Int J Radiat Oncol Biol Phys* 2012;83:1463–72. <https://doi.org/10.1016/j.ijrobp.2011.10.012>.
- [24] Cunha JAM, Hsu I-C, Pouliot J. Dosimetric equivalence of nonstandard HDR brachytherapy catheter patterns. *Med Phys* 2009;36:233–9. <https://doi.org/10.1118/1.3041166>.
- [25] Van den Bosch MR, Lips IM, Lagerburg V, van Vulpen M, Lagendijk JJW, Moerland MA. Feasibility of adequate dose coverage in permanent prostate brachytherapy using divergent needle insertion methods. *Radiother Oncol* 2008;86:120–5. <https://doi.org/10.1016/j.radonc.2007.10.037>.
- [26] Wallner K, Chiu-Tsao ST, Roy J, Arterbery VE, Whitmore W, Jain S, et al. An improved method for computerized tomography-planned transperineal <sup>125</sup>Iodine prostate implants. *J Urol* 1991;146:90–5. [https://doi.org/10.1016/s0022-5347\(17\)37721-2](https://doi.org/10.1016/s0022-5347(17)37721-2).
- [27] Podder TK, Dicker AP, Hutapea P, Darvish K, Yu Y. A novel curvilinear approach for prostate seed implantation. *Med Phys* 2012;39:1887–92. <https://doi.org/10.1118/1.3694110>.
- [28] Szlag M, Ślosarek K, Rembielak A, Białas B, Fijałkowski M, Bystrzycka J. Real-time brachytherapy for prostate cancer - Implant analysis. *Reports Pract Oncol Radiother* 2008;13:9–14. [https://doi.org/10.1016/S1507-1367\(10\)60076-4](https://doi.org/10.1016/S1507-1367(10)60076-4).
- [29] Rabiei M, Ko SY, Podder TK, Lederer J, Konh B. HDR Brachytherapy Planning using Active Needles- Preliminary Investigation on Dose Planning. *Proc IEEE RAS EMBS Int Conf Biomed Robot Biomechanics* 2022;2022-August:1–20. <https://doi.org/10.1109/BioRob52689.2022.9925426>.





# 6

Towards the first in human trial

### 6.1 INTRODUCTION

The Medical Device Regulation 2017/745 (MDR) has recently implemented more stringent legislation for medical device manufacturers operating within the EU. The standard research file of the Centrale Commissie Mensgebonden Onderzoek (CCMO) has also been adapted for non-CE-marked medical devices, used in clinical investigations to comply with the requirements of Article 82 and Annex I of the MDR. Such devices are not intended for market introduction, and do not require a quality management system (QMS) and post-market clinical follow-up. The standard research file includes the Investigational Medical Device Dossier (IMDD), specifying all items that must be covered for an application to a Medical Research Ethics Committee (MREC) in the Netherlands. In all circumstances the quality, safety and performance of the medical device must be guaranteed before using it in or on subjects or patients. Therefore, the use of the IMDD is recommended for in-house, custom-made or investigational medical devices. We show an example for the steps that are required for the manufacturing of a medical device at an academic institution with no compliance to ISO 9001 or ISO 13485 which is intended for clinical investigation.

### 6.2 INVESTIGATIONAL MEDICAL DEVICE DOSSIER (IMDD)

In this chapter the focus is on the developed steerable needle for high-dose-rate (HDR) prostate brachytherapy (BT) described in Chapter 4, hereafter referred to as 'Steerable Obturator' or 'medical device'. The Steerable Obturator is an investigational medical device for the purpose of a clinical investigation (Medical Research Involving Human Subjects (WMO)) conform Article 82 of the MDR, in which the TU Delft is considered 'manufacturer' as the institution is acting as 'sponsor of the clinical investigation'.

We compiled the IMDD for this non-CE-marked device within the scope of the MDR and meet the requirements of the Regulation (EU) 2017/745 of the European Parliament and of the Council on medical devices, amending Directive 2001/83/EC, Regulation (EC) No 178/2002 and Regulation (EC) No 1223/2009 and repealing Council Directives 90/385/EEC and 93/42/EEC. The flowchart in Figure 6.1 shows the sequence of steps involved in the completion of the IMDD. It is important to highlight that the manufacturing facility lacked ISO certification, necessitating the implementation of multiple protocols. These protocols were compiled, based on the ISO 13485 standard and the Medical Device Regulation (MDR). Adherence to these protocols was imperative and the involvement of experts was crucial to ensure compliance throughout the manufacturing process.

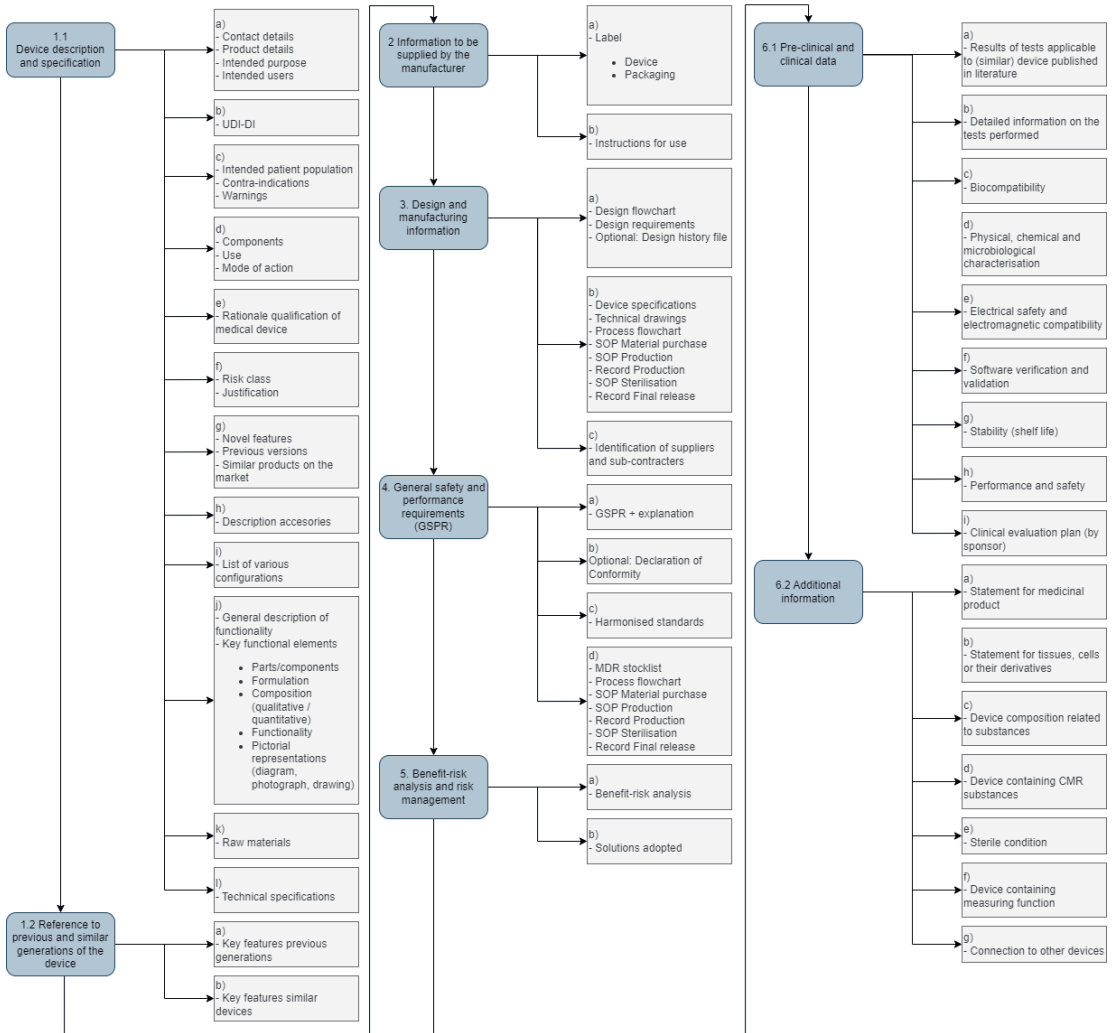


Figure 6.1 – Flowchart for all steps required to compile the IMDD to comply with the requirements of Article 82 and Annex I of the Medical Device Regulation 2017/745.

Some examples of the steps approached upon to compose the IMDD are provided below:

### *Chapter 1.1.e – Rationale qualification of medical device*

The Steerable Obturator is qualified as a medical device, because:

A medical device means any instrument, apparatus, appliance, software, implant, reagent, material or other article intended by the manufacturer to be used, alone or in combination, for human beings for one or more of the following specific medical purposes: diagnosis, prevention, monitoring, prediction, prognosis, treatment or alleviation of disease.

As per the underlined definition above the Steerable Obturator is considered a medical device “INSTRUMENT USED IN COMBINATION FOR TREATMENT OF DISEASE”

### *Chapter 1.1.f – Risk class of the device and justification*

The Steerable Obturator is intended to be used in combination with another device, but the classification rules apply separately to each of the devices in accordance with Annex VIII, Chapter II, 3.2 of Medical Device Regulation 2017/745. Therefore, risk class of the device is Class IIA.

The Steerable Obturator is not in direct contact with the patient. The Steerable Obturator is covered by the commercially available 240 mm ProGuide sharp 6F needle (Elekta Instrument AB, Sweden). The Steerable Obturator Assembly, comprising of the Steerable Obturator and ProGuide sharp 6F needle, is implanted in the body through the perineal skin for positioning of the ProGuide sharp 6F needle according to the treatment plan. After positioning, the Steerable Obturator is withdrawn while the ProGuide sharp 6F needle is left *in situ*. The Steerable Obturator Assembly is intended for transient use (<< 60 minutes) and is disposable.

# Steerable Obturator for high-dose-rate prostate brachytherapy

## 1. Preparing for use

Before the Steerable Obturator Assembly is ready for use, the following preparations have to be performed.



**1.1.** The Steerable Obturator is sterile and hold in a sterile medical device cassette.



**1.2.** Buy-in of sterile ProGuide® sharp 6F needle - 240 mm (Elekta, Sweden).

Catalogue (Applicator guide)  
part number:  
110580 - 110583



**1.3.** Buy-in of sterile Steel Implant Needle (1.9 mm stainless steel trocar needles 240 mm, Elekta, Sweden).

Catalogue (Applicator guide)  
part number:  
083066



**1.4.** Collect 2 pens:  
1 **BLUE** coloured pen, and  
1 **BLACK** coloured pen.

These pens are used to fill in the form regarding needle geometry and free-lengths used in current clinical practice.

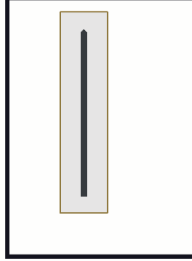
If 2 pens are not available, distinction between the ProGuide and Steerable Obturator can be made using text.

## 2. Getting ready for procedure

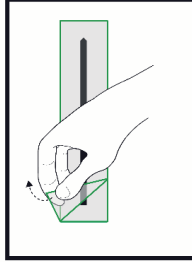
This section describes the actions which have to be performed before implantation

**Note: For maintenance of sterility, the actions have to be performed in the operating room and by at least 2 people:**

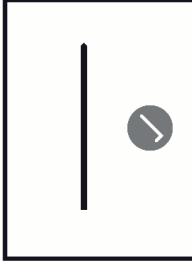
- Sterile personnel (**sterile**)
- Non sterile personnel



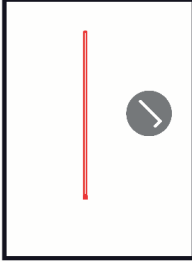
**2.1. Sterile** Collect package of **sterile** ProGuide® sharp 6F needle and place on a non-sterile flat surface. Check packaging for any damages and check labelling for legibility and shelf-life expiration date before use.



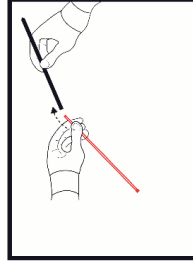
**2.2. Sterile** Open package of the ProGuide® sharp 6F needle.  
\*Do not touch **sterile parts!**



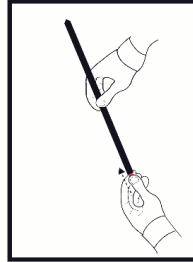
**2.3. Sterile** Collect ProGuide® sharp 6F needle with one hand.



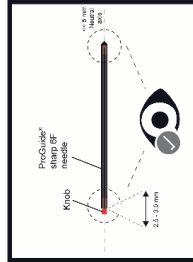
**2.4. Sterile** Collect Steerable Obturator with other hand from the sterile medical device cassette. Check for any damages and dents.



**2.5. Sterile** Place Steerable Obturator with the distal tip in ProGuide® sharp 6F needle for Steerable Obturator Assembly to allow for insertion of the ProGuide® sharp 6F needle.



**2.6. Sterile** Push Steerable Obturator into ProGuide® sharp 6F needle until blockage of distal end of ProGuide® sharp 6F needle.

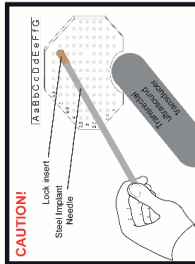


**2.7. Sterile** Check position of Steerable Obturator in the ProGuide® sharp 6F needle. When the Steerable Obturator is completely inserted into the ProGuide® sharp 6F needle, the distance between the knob and the end of the ProGuide® sharp 6F needle is about 2.5- 3.0 mm. Check straightness of Steerable Obturator Assembly (< 5 mm from neutral axis).

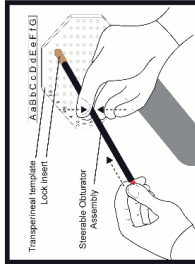
**The Steerable Obturator Assembly is now ready for use.**

## 3. Use during procedure according to treatment plan

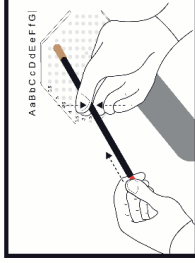
This section describes the actions which have to be performed during implantation



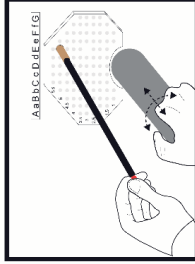
**3.1. Sterile - CAUTION!**  
Insert the Steel Implant Needle in the pre-defined template lock insert and pierce the perineum as in current clinical practice. After piercing, retract the Steel Implant Needle.



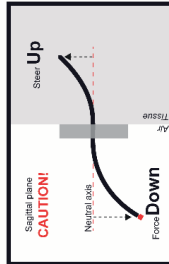
**3.2. Sterile** Take the proximal end of the Steerable Oburator Assembly in one hand and support the middle of the free length with the other hand. Insert the Steerable Oburator Assembly in the pre-defined template lock insert.



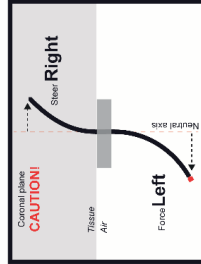
**3.3. Sterile** Manipulate transrectal ultrasound transducer to visualize the Steerable Oburator Assembly for guidance.



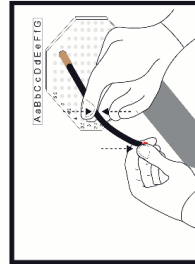
**3.4. Sterile** Manipulate transrectal ultrasound transducer to visualize the Steerable Oburator Assembly for guidance.



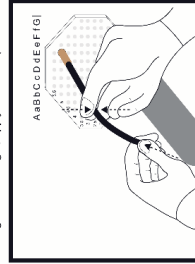
**3.5.a Sterile - CAUTION!**  
Maximum angle from neutral axis on proximal end: 45°  
Steering direction: Up, Apply force: Down (and vice versa)



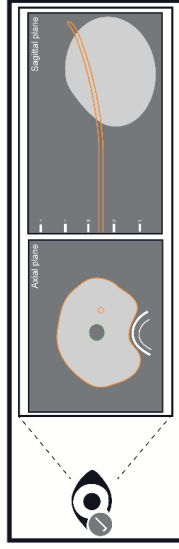
**3.5.b Sterile - CAUTION!**  
Maximum angle from neutral axis on proximal end: 45°  
Steering direction: Right, Apply force: Left (and vice versa)



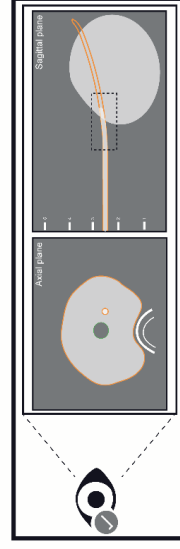
**3.7. Sterile** Bend the proximal end by one hand to steer the distal tip of the Steerable Oburator Assembly. Support the middle of the free length with the other hand.



**3.8. Sterile** Push the knob to insert the Steerable Oburator Assembly. Support the middle of the free length with the other hand. Guide the Steerable Oburator Assembly by using ultrasound. If necessary, release the hand for guiding from the

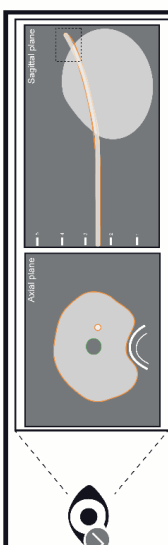


**3.6.** Follow the planned trajectory visualised in Oncentra Prostate treatment planning system by applying steering during insertion of Steerable Oburator Assembly.

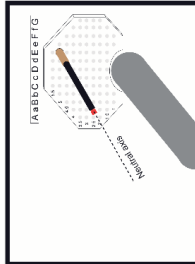


**3.9.** Check if Steerable Oburator Assembly follows planned trajectory  
**Sterile** if not, apply extra steering in the required direction (conform step 3.5).

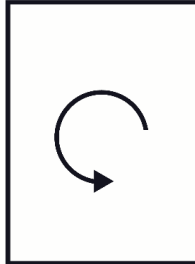




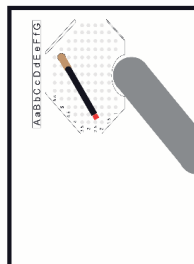
**3.10.** Check if Steerable Obturator Assembly reached the planned end-location.  
**Sterile:** If not, slightly retract the Steerable Obturator Assembly and apply extra steering in the required direction (conform step 3.).



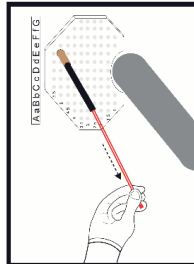
**3.11. Sterile** If end-location is reached, stop pushing the Steerable Obturator Assembly and stop applying steering so that Steerable Obturator Assembly returns to the neutral axis at the proximal end. Release the Steerable Obturator Assembly.



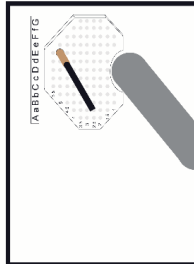
**3.12. Sterile** Repeat step 3.1 - 3.11 for the subsequent Steerable Obturator Assembly. If no Steerable Obturator Assembly is required, continue to step 3.13.



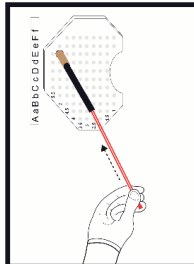
**3.13.** Indicate the coordinate of the ProGuide® sharp 6F needles (with a **BLUE** coloured pen or text) if containing a **Steerable Obturator**; on the form used in current clinical practice. Indicate the coordinate of the ProGuide® sharp 6F needles containing a **Rigid ProGuide® Obturator** (with a **BLACK** coloured pen or text) on the form used in current clinical practice.



**3.14. Sterile** Retract the Steerable Obturator(s) from the ProGuide® sharp 6F needle(s), leave the ProGuide® sharp 6F needle(s) in place as in current clinical practice and check for fluid on Steerable Obturator(s). If present, retract ProGuide® sharp 6F needle and insert new Steerable Obturator Assembly.



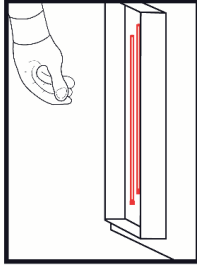
**3.15. Sterile** Lock the lock insert as in current practice to hold the the ProGuide® sharp 6F needle(s) in place.  
The ProGuide® sharp 6F needle(s) are ready for the 1st fraction in the HDR BT procedure.



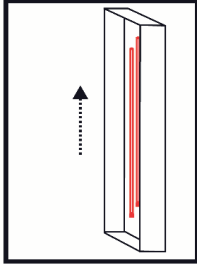
**3.16. Prior to 2nd fraction - CAUTION!** Insert the **Steerable Obturator(s)** in the ProGuide® sharp 6F needle(s) as indicated (with the **BLUE** color or by text), and the **rigid ProGuide® Obturator(s)** in the ProGuide® sharp 6F needle(s) as indicated (with the **BLACK** color or by text). Push the Steerable and Rigid Obturator Assemblies to the required end-positions as in current practice.

## 4. Disposal

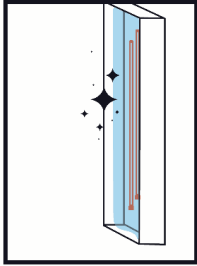
**Important: The Steerable Obturator is for single use only.**  
To process and dispose the Steerable Obturator after use, the next steps remain:



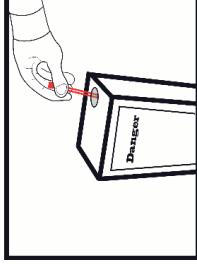
4.1. Collect the Steerable Obturator in a separate container



4.2. After collection of all Steerable Obturators: Transport the container to the Brachy Bunker or to L. Luthart.



4.3. Cleaning of Steerable Obturators as in current clinical practice with Sekumatic by L. Luthart, for visual inspection on damages and dents



4.4. Dispose the Steerable Obturator in a Medical Sharps Disposal Container.

## 5. Warning and precautions

### **Important notices:**


- 1) The Steerable Obturator should only be used by qualified physicians, trained in brachytherapy techniques. The physician is responsible for its proper clinical use. The Steerable Obturator should be handled by the physician as in current practice with the rigid ProGuide® Obturator for corresponding steps. The cautions, warnings and notes for these steps apply to the Steerable Obturator.
- 2) Read all instructions prior to use. Observe all cautions and warnings throughout these instructions. Failure to do so may result in complications.
- 3) The physician must have received the necessary training before usage of the Steerable Obturator.
- 4) Use the Steerable Obturator in combination with 240 mm ProGuide® sharp 6F needle.
- 5) It is recommended to start with the implantation of the Steerable Obturator Assemblies prior to the implantation of the rigid ProGuide® Obturator Assemblies for the purpose of visualisation with TRUS and the required workspace for bending of the Steerable Obturator Assemblies.
- 6) Implantation of the Steerable Obturator Assemblies is according to the pre-implant treatment plan.
- 7) Use Steel Implant Needle to pierce the perineum prior to implantation with Steerable Obturator Assembly.
- 8) Assist Steerable Obturator Assembly with your free hand at the middle of the free length.
- 9) Bending the proximal end in a certain direction in a certain plane results in steering of the distal tip in the opposite direction in the same plane.

### **CAUTION:**

- 1) Do not use the Steerable Obturator unless its sterile and undamaged. Remove a non-sterile or damaged Steerable Obturator from clinical use.
- 2) Do not use the Steerable Obturator if shelf-life is exceeded. Remove Steerable Obturator from clinical use.
- 3) Insert the Steerable Obturator as far as possible into the ProGuide® sharp 6F needle up to the needle tip to create the Steerable Obturator Assembly.
- 4) Do not use a ProGuide® needle with a length other than 240 mm, a diameter other than 6F and a tip other than sharp conical.
- 5) Do not use the Steerable Obturator Assembly unless its straightness is <= 5 mm from the neutral axis. Remove a non-straight Steerable Obturator from clinical use.
- 6) Maximum angle from neutral axis during bending at the proximal end may not exceed 45° from the neutral axis.
- 7) Do not use the ProGuide® sharp 6F needle if fluid is found on the Steerable Obturator after retraction from the ProGuide® sharp 6F needle. Retract ProGuide® sharp 6F needle and remove ProGuide® sharp 6F needle and Steerable Obturator from clinical use. Use a new Steerable Obturator Assembly.
- 8) Prior to the second fraction: Only use the correct Obturator (ProGuide or Steerable) as indicated on the form for pushing the ProGuide® sharp 6F needle, if required.
- 9) Steerable Obturator is MR-unsafe.









## 6. Steerable Obturator explanation of symbols on label of medical device

Steerable Obturator  
Steerable obturator for Brachytherapy  
Exclusively for clinical investigation










 TU Delft  
Stevinweg 1  
2628 CN Delft  
The Netherlands

**REF** P91372\_SO2022\_01

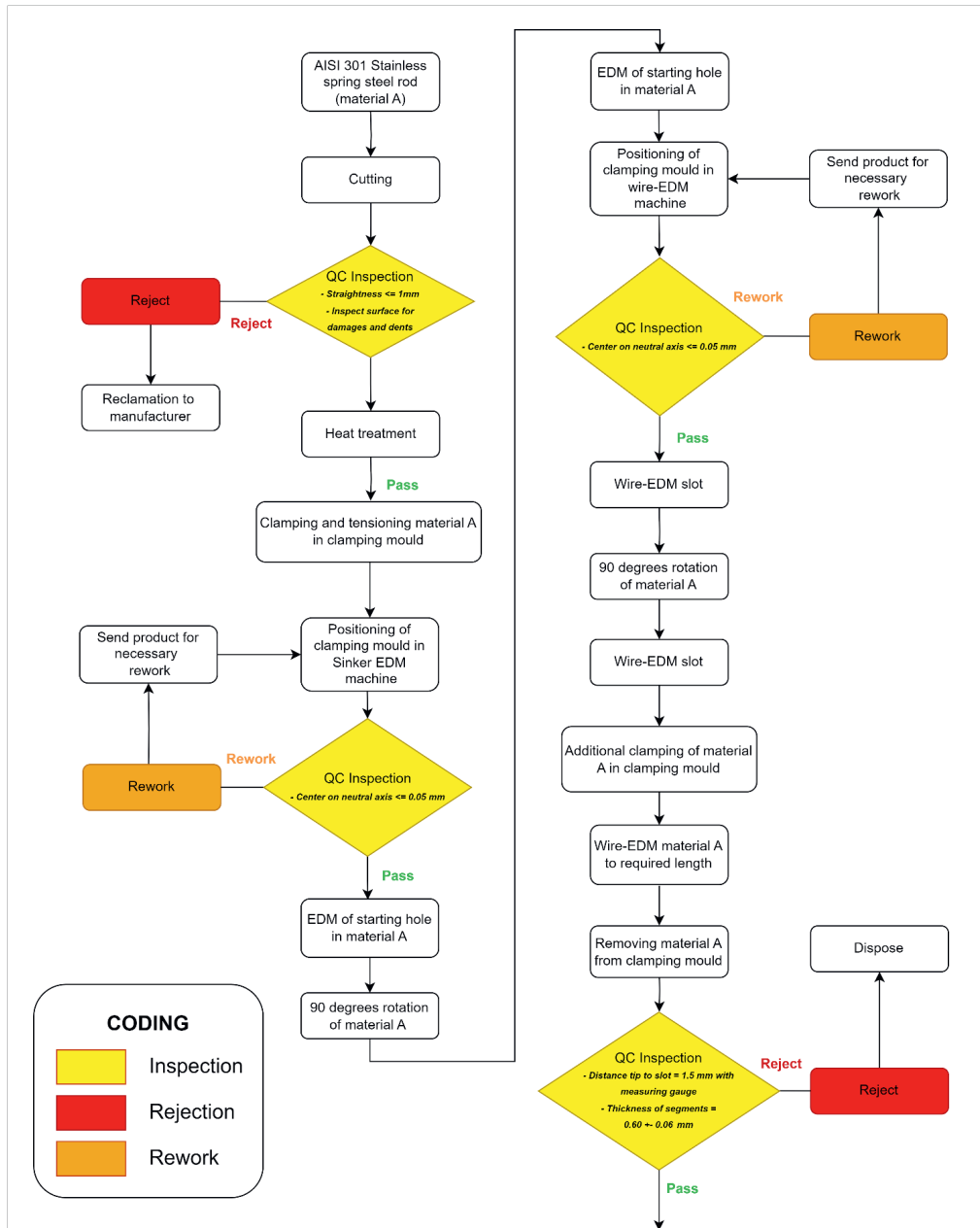
**LOT** P91372\_SO2022

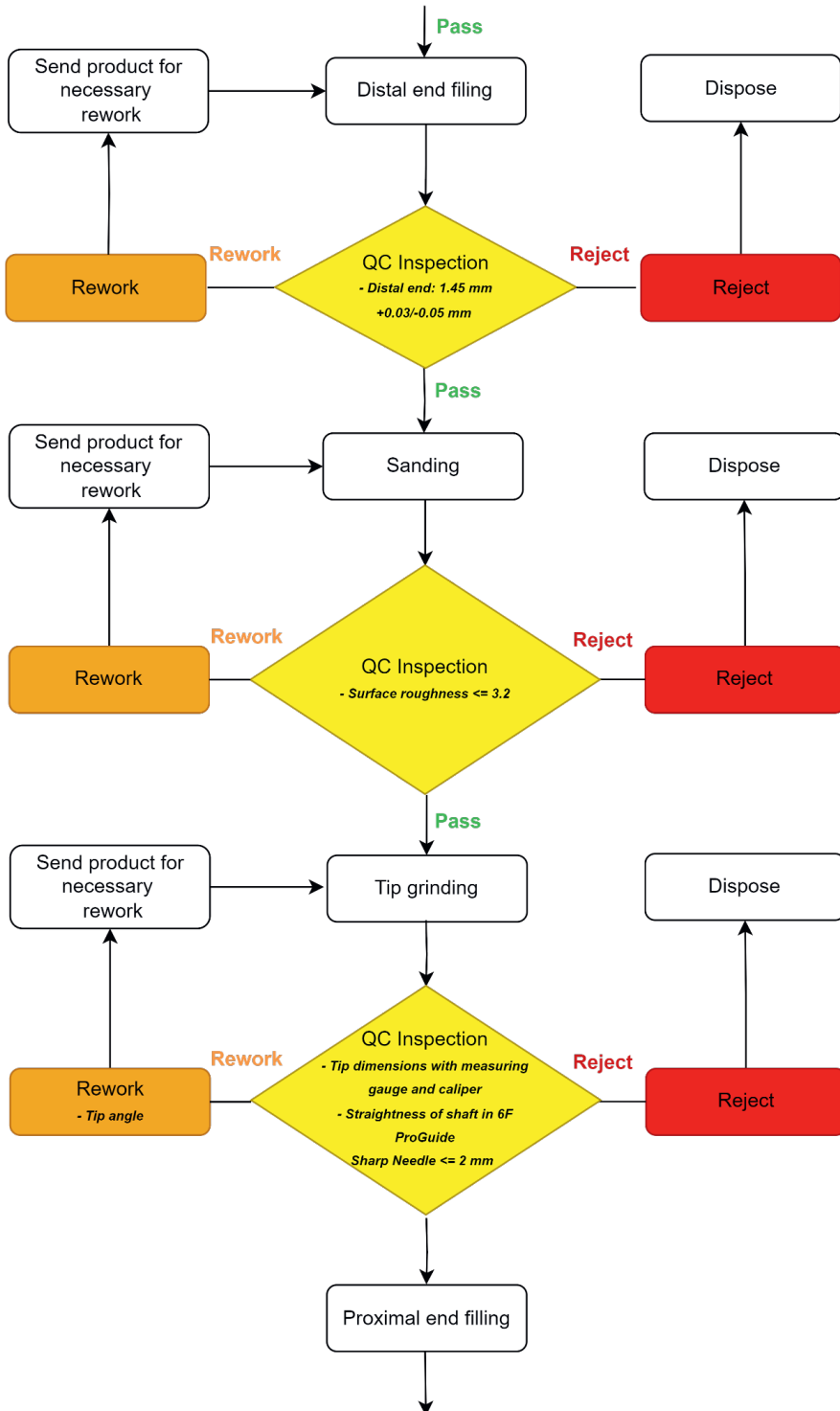
       20xx-xx-xx  20xx-xx-xx

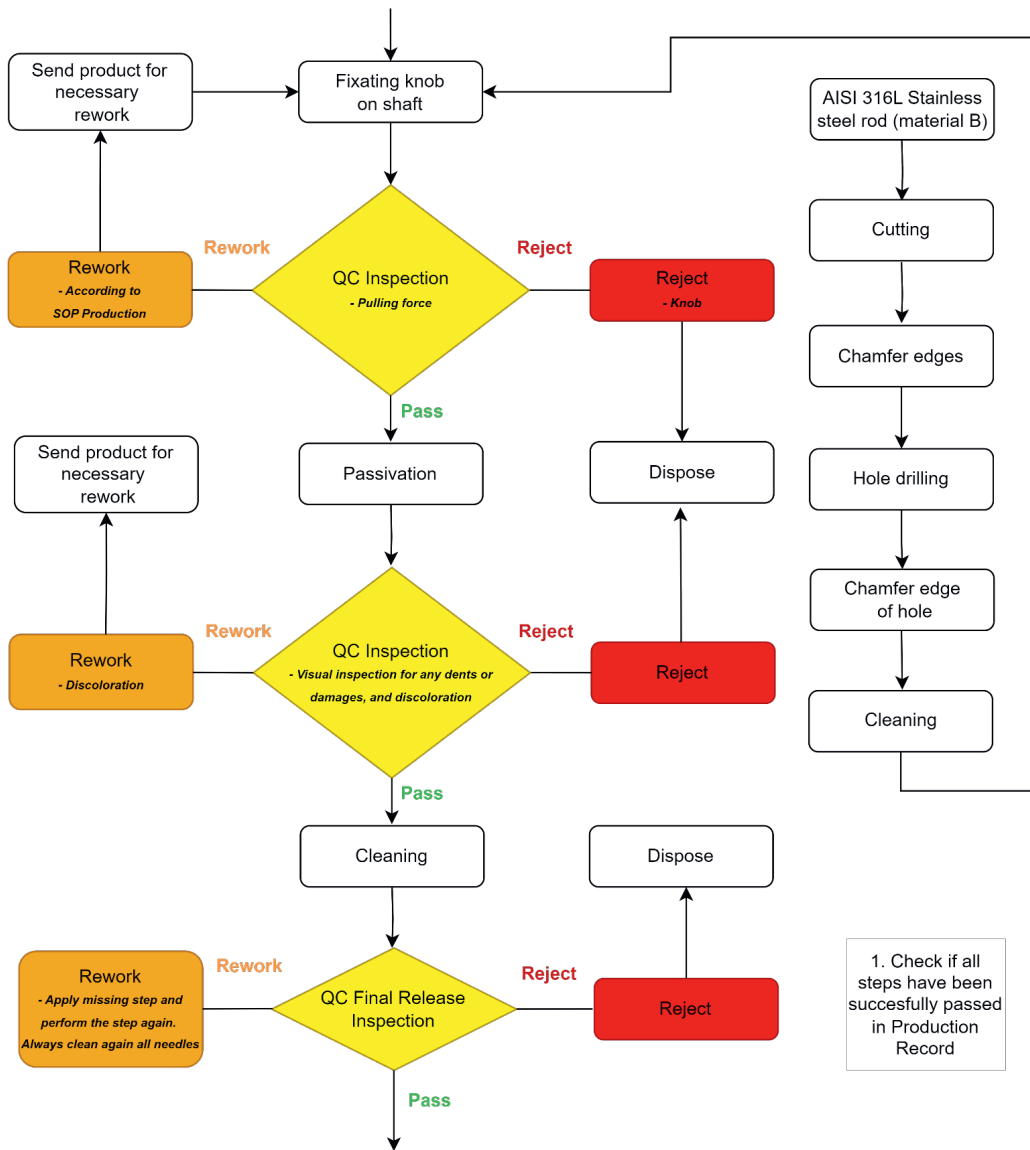
*This label is attached to the batch after manufacturing.  
Note that the label contains the symbol  
"non-sterile". Sterilisation of the medical device is performed at the  
Erasmus MC according to their internal process.  
The label after sterilisation contains the symbol "sterile".*

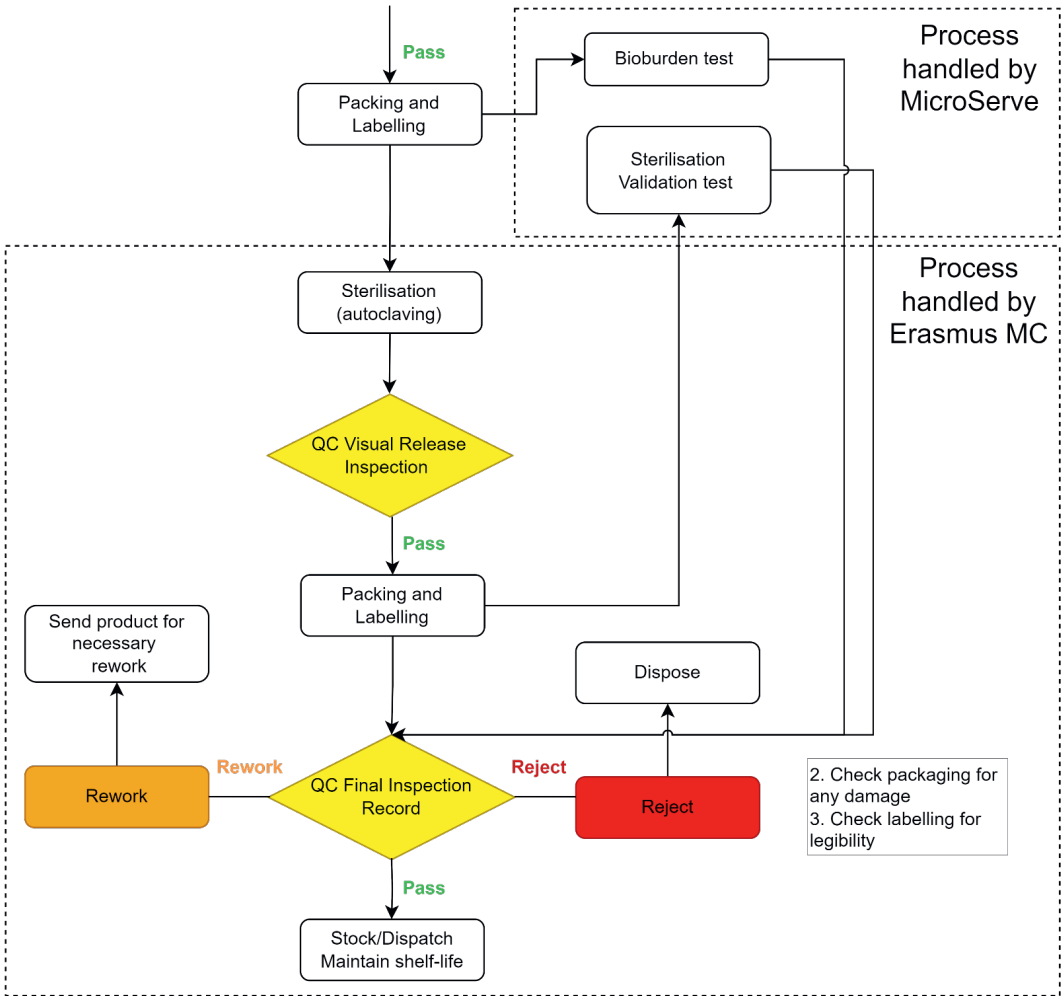
<b>REF</b>	Reference number
<b>LOT</b>	Lot number
	Date of manufacture
	Name and address of manufacturer
	Do not use if package is damaged
	Do not re-use
	Non-sterile
 	Temperature limitation
	Use by date
	MR-unsafe
<b>MD</b>	Medical device

Chapter 3.b – Design and manufacturing process flowchart











## Chapter 6.1.b – Detailed information on the preclinical verification tests performed

Product verification test	Justification / Requirements	Applied Standards	Results	Pass
Material test	Usage of approved stainless steels for manufacturing of Steerable Obturator.	EN 10270-3:2011 EN 10204-3.1:2004 ISO 7153-1:2016	Certificate covers said standards EN 10270-3, EN 10218-2, ISO 693101, EN 10088-3:2014, EN 10088-5:2009, EN 10272:2016. EN 0277-1, EN 10278. Materials conform ISO 7153-1:2016.	Yes
3 Pointbending Test	Evaluation of flexural rigidity for the purpose of the buckling test. Flexural rigidity (E x I): 7000 - 12000 N*mm <sup>2</sup>	ISO 7500-1:2018 ISO 7438:2020	The Steerable Obturator Assembly has a flexural rigidity of 7588 N*mm <sup>2</sup> .	Yes
Buckling Test	Evaluation of potential buckling during skin puncturing.	Not applicable	Buckling will occur during skin puncturing. Pre-puncturing with a Steel Implantation Needle and extra support at the middle of the free length of the Steerable Obturator Assembly are required (indicated in the IFU).	Yes
Uni-axial Tensile Test	- Young's Modulus (E <sub>mod</sub> ) of material: > 180 GPa - Yield Strength (σ <sub>y</sub> ) of material: > 1500 MPa - Ultimate Tensile Strength (UTS) of material: > 1700 MPa	ISO 7500-1 ISO 6892-1:2019 ISO 9513:2012	- E <sub>mod</sub> of material: 196.9 GPa - σ <sub>y</sub> of material: 1582 MPa - UTS of material: 1770 MPa	Yes
Steerability Test	Steering of 15 to 20 mm over 100 mm insertion depth in various tissues.	Not applicable	The Steerable Obturator Assembly allows for lateral steering up 10 and 20 mm over 60 and 100 mm insertion depth, respectively.	Yes
Phantom Evaluation Test	Validation of phantom for the purpose of preclinical user test by medical physicians.	Not applicable	The phantom is suitable for preclinical user test based on comparability to real clinical use by the physicians.	Yes
Preclinical User Test	Evaluation of dosimetric optimisation and preclinical performance with Steerable Obturators in clinical HDR BT setting.	Not applicable	Implantation of the Steerable Obturator Assemblies was possible with excellent agreement between pre,- and post-implantation treatment plan, without major changes in workflow, without changes to the clinical set-up and without significant impact on implantation time.	Yes
Bioburden Test	Evaluation of the amount of micro-organisms on the medical devices during a batch validation.	ISO 11737-1:2018	No micro-organisms found on the medical devices. Batch is approved by MicroServe for clinical test.	Yes
Sterilisation and Validation Test	Evaluation of sterility of the medical devices in final packaging during a batch validation.	ISO 11137-1:2015 ISO 11737-2:2015 ISO 11737-1:2018 ISO 11737-2:2020	No growth of micro-organisms found on the medical devices. Batch is sterile and approved by MicroServe for clinical test.	Yes

### 6.3 CLINICAL RESEARCH PROTOCOL

The clinical research protocol is required for MREC-approval. The summary of our proposed Phase I study with the Steerable Obturators is provided below. Note that the clinical protocol has not yet been submitted to, nor approved by the MREC.

#### *Rationale:*

Sufficient distribution of all HDR BT needles in the prostate is required in high-dose-rate (HDR) prostate brachytherapy (BT) to ensure an effective treatment. Challenges that remain in current clinical practice are patients that experience 1) pubic arch interference (PAI); the pubic arch restricts access to the ventrolateral part of the prostate, 2) too wide prostates; the width of the prostate extends the width of the transperineal template, and 3) lesions ventral to the urethra; the urethra restricts access to the lesion. These challenges can result in inaccessibility of parts in the prostate, thus either underdosage of the target volume or pursuing another therapy. In addition to access restrictions, needle targeting errors induce non-conformity to the pre-treatment plan and potentially less effective therapy outcomes. Physicians are challenged by needle deflections, reported to be up to 3.8 mm from the intended end position. Steerable Obturators are expected to increase the accessibility of the prostate by allowing for curved trajectories during insertion to reach currently inaccessible parts and avoid intermediate structures, while obtaining a high targeting accuracy.

#### *Objective:*

The Steerable Obturator is an investigational device for the purpose of a first in human clinical investigation conform Article 82 of the Medical Device Regulation 2017/745. The primary objective of the proposed phase I study is to show the safety and feasibility of Steerable Obturators in HDR prostate BT. This will be evaluated by the ability to insert the conventional ProGuide outer needles using Steerable Obturators, and control the trajectory of the ProGuide outer needles over a linear trajectory and a curved trajectory.

#### *Study design:*

This phase I study consists of 2 stages, both designed to evaluate safety and feasibility of Steerable Obturators in the clinical HDR prostate BT setting.

- Stage 1) is designed as a non-inferiority phase I study in which 1 patient will be treated using HDR prostate BT monotherapy, using ~50% Steerable Obturators and ~50% ProGuide Obturators [Elekta Instrument AB, Stockholm, Sweden] combined, to evaluate the safety and feasibility of Steerable Obturators in the clinical setting when controlled and inserted over a linear trajectory. The goal is to exactly apply HDR BT as in current clinical practice and to demonstrate the ability to establish equal dosimetric objectives used in current practice when incorporating Steerable Obturators. The rigid ProGuide Obturators have to be inserted straight, parallel to each other with the aid of the transperineal template as in current practice.
- Stage 2) is designed as a phase I study in which 9 patients will be treated using HDR prostate BT monotherapy to evaluate the safety and feasibility of Steerable Obturators in the clinical setting when controlled and inserted over a curved trajectory. The goal is to demonstrate the ability to establish equal dosimetric objectives used in current practice when incorporating 1 Steerable Obturator controlled and inserted over a curved trajectory in combination with ProGuide Obturators for all other insertions. The

ProGuide Obturators have to be inserted straight, parallel to each other with the aid of the transperineal template as in current practice.

*Study population:*

Men with low/intermediate-risk PCa (clinical stage  $\leq$ T2b, prostate-specific antigen (PSA)  $\leq$  15 ng/ml, Gleason score 6 or 7 (3+4)) who are considering HDR prostate BT monotherapy in Erasmus MC are eligible for this study.

*Intervention (if applicable):*

All prostate cancer patients will be treated with HDR prostate BT monotherapy. HDR BT monotherapy is delivered in 2 fractions of either 13.5 Gy as in current practice. The 2 fractions are delivered with at least 6-hour interval. The ProGuide outer needles stay in situ between fractions with the patients in supine position.

*Main study parameters/endpoints:*

The primary endpoint of this study is to determine the safety and feasibility of the Steerable Obturator in HDR prostate BT. This will be evaluated by the ability to insert the ProGuide outer needles using the Steerable Obturator, and control the trajectory of the ProGuide outer needles over a linear and a curved trajectory. Secondary endpoints of this study are to evaluate needle targeting accuracy, conformity to the dose constraints used in current practice, the workflow (procedure time and required modifications compared to current workflow) and the usability.

*Nature and extent of the burden and risks associated with participation, benefit and group relatedness:*

The patient extra burden can be limited to a possible extension of 5 extra minutes under general anaesthesia at the first BT session and possibly the need to replace a ProGuide outer needle placed with a Steerable Obturator with a ProGuide Obturator.

The benefit of participating in this study for all participating men is the satisfaction of participating in a trial in order to determine the safety and feasibility of the Steerable Obturator in HDR prostate BT and with that improve the standard of care for future prostate cancer patients.

## 6.4 CONCLUSION

This chapter outlines the procedure followed for clinical investigation of a developed instrument, ensuring compliance with the requirements specified in Article 82 of the MDR. We manufactured a prototype at an academic institution in accordance with protocols based on ISO 13485 and start the first in human trial with the Steerable Obturators in a hospital upon MREC-approval. This example can be used as guide for future researchers who want to use their technical development for clinical research.

# 7

## MR-guided HDR prostate brachytherapy with teleoperated steerable needles

Martijn de Vries\*, Mart Wijnjtjes\*, Jakub Sikorski, Pedro Moreira, Nick J. van de Berg, John J. van den Dobbelen, Sarthak Misra

*Published in Journal of Robotic Surgery (2023)*

\* Authors contributed equally to the realisation of the paper

## **ABSTRACT**

Conformity of tumour volumes and dose plans in prostate brachytherapy (BT) can be constrained by unwanted needle deflections, needle access restrictions and visualisation limitations. This work validates the feasibility of teleoperated robotic control of an active steerable needle using magnetic resonance (MR) for guidance. With this system, perturbations can be counteracted and critical structures can be circumvented to access currently inaccessible areas. The system comprises of (1) a novel steerable needle, (2) the Minimally Invasive Robotics in an MR environment (MIRIAM) system, and (3) the daVinci Research Kit (dVRK). MR scans provide visual feedback to the operator controlling the dVRK. Needle steering is performed along curved trajectories to avoid the urethra towards targets (representing tumour tissue) in a prostate phantom with a targeting error of  $1.2 \pm 1.0$  mm. This work shows the potential clinical applicability of active needle steering for prostate BT with a teleoperated robotic system in an MR environment.

## 7.1 INTRODUCTION

Prostate cancer is the second most common cause of cancer related deaths among men [1]. High-dose-rate (HDR) brachytherapy (BT) is a form of internal radiotherapy with excellent clinical outcomes for localised prostate cancer [2]. This technique ensures high radiation dose to the target volume while sparing surrounding healthy tissue. For this purpose, radioactive sources are temporarily placed in the target volume using rigid needles and transrectal ultrasound (TRUS) visualisation for guidance [3]. A crucial factor of obtaining conformal dose coverage is high targeting accuracy of the inserted needles [4]; inaccurate needle positioning can lead to misplacement, and consequently, radiation hot- or cold-spots. Unfortunately, TRUS imaging presents limited visual feedback of the internal structures and lesions [5] while needle tip visualisation can be difficult [4,6,7]. To complement TRUS visualisation, magnetic resonance imaging (MR, MRI) has been incorporated in BT protocols for treatment planning. This technique provides anatomical data and functional information of the prostate gland including potential lesions [8]. The disadvantage of MRI-TRUS visualisations is that images are collected at different moments and typically in different rooms, resulting in patient motions and introducing inaccuracies [9,10].

MR-guided prostate BT does not require patient repositioning, and has demonstrated its feasibility in the last decades [11]. This approach posed new challenges such as the use of non-magnetic instrumentation only, and limited workspace within the MR scanner. Accordingly, MR-compatible robotic systems have been developed to perform prostate BT under MR-guidance inside the MR scanner [11–13]. Previously, we have developed the MR-compatible “Minimally Invasive Robotics in an MR environment” (MIRIAM) system [14], with a 5 degree of freedom (DOF) parallel robot and 4 DOF driver for insertion and steering of a bevel-tip biopsy needle under MR-guidance.

Most robotic BT systems are focused on low-dose-rate (LDR) [11,15,16], and some on HDR solutions [17,18]. The systems typically provide needle guide conditions for straight path insertions. To reduce needle misplacements, several developments have aimed to improve the needle placement accuracy, or enhance the accessibility of tumours located ventrally to the urethra or behind the pubic arch, or avoid the penile bulb or neurovascular bundles [10,19–22]. Earlier studies showed that increased accessibility of the prostate could improve dosimetric outcomes [22–25]. To reduce placement errors, Lagerburg et al. developed a robot that performed needle tapping during insertion [26], while other robots performed needle rotation to reduce insertion forces and improve targeting accuracy [27,28]. Steerable needles have been developed to follow curved trajectories and counteract unwanted deflections by actively manipulating the distal tip during the insertion which is manually performed [29–31]. In the work of Kohn et al., a tendon-driven steerable needle system for prostate HDR BT is presented [32]. For needles with compliant parts, local rigidity needs to be carefully attuned, to maintain steerability, mitigate hazards (snapping, buckling), and uphold needle state predictability. It was shown in the study of de Vries et al. that active HDR BT needles can be developed without significantly reducing the axial and flexural rigidity, thus ensuring controllability of the needle trajectory and accurate targeting in various inhomogeneous tissues [29]. Needle steering was possible regardless the initial insertion depth.

The contribution of this work is the validation of feasibility of teleoperated and MR-guided robotic control of an actively steerable HDR BT needle. It therefore combines previously developed components and systems, comprising of the MIRIAM system and the da Vinci Research Kit (dVRK), for MR-guided HDR prostate BT using steerable needles. The system combines high precision of piezoelectric actuation and real-time control of the steerable needle. The multiple DOFs of the system enables control from outside the operating room over the orientation, position, and the degree of steering of the needle. The system architecture and workflow are outlined and teleoperation of the steerable needle is performed in an experiment with a developed prostate phantom in the MR scanner. The purpose of this work is to show the feasibility of the MR-compatible system and the successful workflow by inserting the steerable

needle along a curved trajectory towards an obstructed target in the prostate tissue phantom under MR-guidance. With this, we highlight the ability to perform teleoperated adaptive BT in the MR bore with increased accessibility to the prostate gland.

## 7.2 MATERIALS AND METHODS

### 7.2.1 System components

The teleoperated system integrates three subsystems: 1) the developed MR-compatible steerable needle, based on the design described by de Vries et al. [29], 2) the MIRIAM system designed by Moreira et al. [14] and 3) components from the da Vinci Surgical System which is widespread available in hospitals used for robotic-assisted surgery [33,34].

#### *Steerable needle*

The steerable needle comprises of a flexible outer needle with conical tip of polyoxymethylene (ProGuide sharp 6F needle, Elekta Instrument AB, Stockholm, Sweden) and a superelastic nitinol inner needle of 270 mm. The inner needle is a single-piece rod of  $\varnothing$  1.46 mm machined into four quarters by electric discharge machining along the longitudinal axis of the rod while keeping both ends of the rod connected. Bending the proximal end of the steerable needle results in pulling and pushing forces, which are transferred through the segments of the inner needle. The outer needle prevents sideways movement of the segments which results in distal tip steering in the opposite direction while the needle guide functions as pivot point. After placement, the steerable inner needle can be retracted and re-used, while the outer needle can be connected to the BT afterloader for the introduction of the radioactive source. The inner needle makes no patient contact. The steering principle is depicted in Figure 7.1.

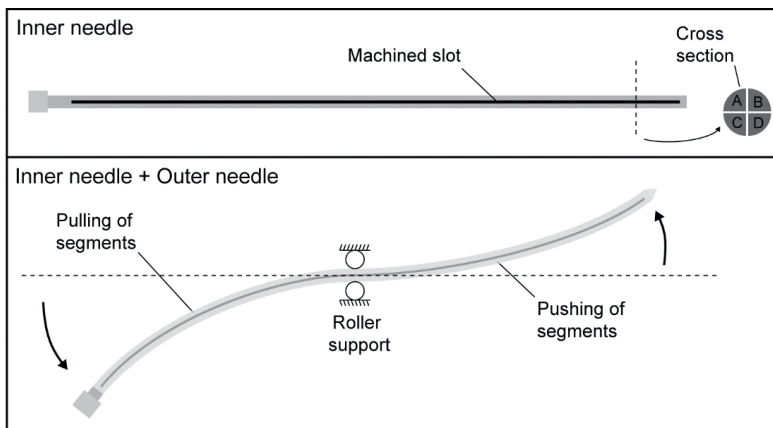


**Figure 7.1 - Needle steering mechanism.** Bending the proximal end of the steerable needle introduces longitudinal movement of the four segments and steering of the distal end in the opposite direction. The needle guide is a roller support allowing for longitudinal movement of the steerable needle while constraining off-axis movement.

#### *MIRIAM system*

The MIRIAM system for prostate biopsies consists of nonmagnetic components, and the low-level controller and motor drivers of the MIRIAM system are located in a controller cabinet outside of the MR

scanner room to minimise electromagnetic interference in the MR scanner and is connected using 10-meter-long shielded cables going through the waveguide [14]. The system is adapted for the purpose of BT omitting the functionality to collect tissue samples for diagnostics via the needle firing system. The adapted MIRIAM system facilitates the attachment and alignment of the steerable needle using a hinge joint and needle guide for guidance as shown in Figure 7.2. The needle attachment point can be moved using a 5-DOF parallel robot actuated by HR2 and HR8 piezo-electric motors (Nanomotion, Yoqneam, Israel). The base structure is made from ceramic rods and the needle attachment point is positioned using five extendable carbon fibre reinforced rods.

### Da Vinci Research Kit

The MIRIAM system is controlled by the dVRK containing components from da Vinci Surgical Systems (Intuitive Foundation, Sunnyvale, CA, USA) and used for minimally invasive surgery [33,34]. The dVRK is a telerobotic surgical research platform that allows 3D visualisation, and position, velocity and current control. The dVRK has a Master Tool Manipulator (MTM) which is controlled by the operator and used as input for the system while a stereo viewer provides visual feedback to the operator.

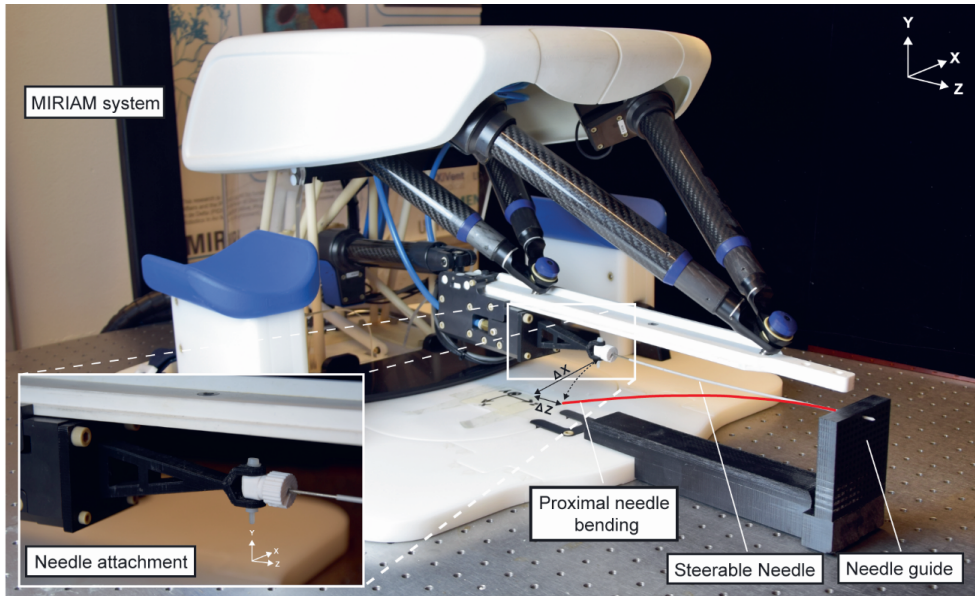


Figure 7.2 – MR-compatible MIRIAM system with the steerable needle attached.

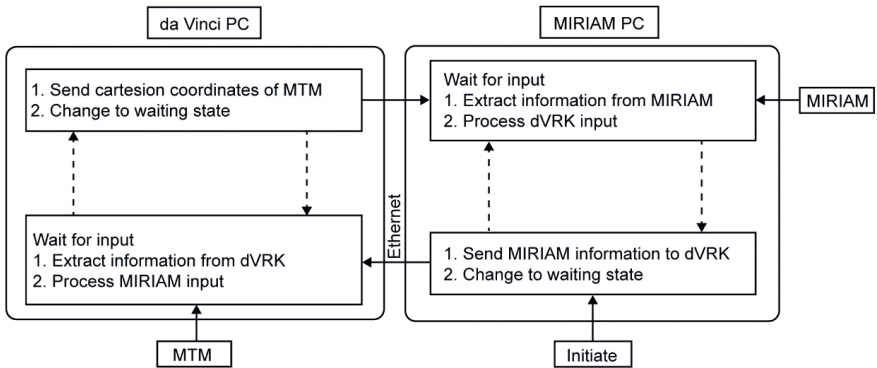
#### 7.2.2 Control and communication

A continuous exchange of information between the MIRIAM system and the dVRK allowed for actuation of the steerable needle in the XZ-plane via velocity control using the equation:

$$v = k \cdot \Delta x, \quad (1)$$



where  $v$  is the velocity (m/s) of the needle attachment point,  $k$  is a scaling constant, and  $\Delta x$  is the change in MTM position (m). The continuous exchange of information through the local area network (LAN) provides plug and play operation of the system, while the user datagram protocol (UDP) ensures fast communication. The dVRK side uses the open source Robotic Operating Software (ROS) package version Noetic Ninjemys and the MIRIAM side uses MATLAB 2016 with a protocol handling the communication between the MIRIAM system and the dVRK (Figure 7.3). Continuous visual feedback collected from the MR scanner is provided to the operator. The actual position and the next position of the MIRIAM system, proposed by the operator using the MTM, are visualised and live updates of the movement are provided to the operator located outside the MR scanner room.



**Algorithm 1** Communication algorithm MIRIAM

```

User initiates communication
New dVRK                                ▷ dVRK Object
New MIRIAM                              ▷ MIRIAM Object
New UDP                                  ▷ UDP Object

function UDP_SEND(sender, variables, receiver)
    Sends variables from sender to receiver on object
    UDP
end function

function SCAN(receiver, Object)
    Scans Object for new messages send to receiver
end function

repeat
    dVRK_pos = dVRK.manipulator_position
    UDP_send(dVRK, dVRK_pos, MIRIAM)

    MIRIAM_input = Scan(MIRIAM, UDP)
    MIRIAM.move(MIRIAM_input)
    MIRIAM_pos = MIRIAM.current_position
    UDP_send(MIRIAM, MIRIAM_pos, dVRK)

    dVRK_in = Scan(dVRK, UDP)
    dVRK.visual(dVRK_in)
until user terminates
    
```

**Figure 7.3 – Communication protocol between the MIRIAM system and the dVRK.** The system is initiated by the operator on the MIRIAM PC, information about MIRIAM is sent to the daVinci PC and the MIRIAM PC returns to a waiting phase. The daVinci PC processes the input, sends information about the MTM of the dVRK to the MIRIAM PC and returns to the waiting phase. The MIRIAM PC processes the information and the loop repeats itself. As both systems wait for an input from the other PC they will remain in synchronisation. Information is exchanged between the two PCs via Ethernet. The dashed arrows relate to the first steps, the other arrows relate to the second steps.

The software of the MIRIAM system is reprogrammed to switch between the steering and the insertion state triggered by the position of the MTM. Reorientation of the tip is performed in the steering state,

while needle insertion is performed in the insertion state following the orientation of the tip. During operation, continuous path length estimations ensure that the carbon fibre reinforced rods of the MIRIAM system have the length required to reach the pre-defined target. This is evaluated for every 50 cycles between the MIRIAM system and the dVRK system to provide fast and accurate communication. In the steering state, the position from the MTM is continuously received and converted to the deviation of the MTM from the starting position where  $\Delta x$  is multiplied by the scaling constant  $k = 0.005$ . The constant is experimentally derived to provide control stability after evaluating the end effector movement with various constants (1, 0.1, 0.01 and 0.005). The output velocity value is coupled to the pre-defined input position for the MIRIAM system and converted into a discrete function via:

$$\frac{\Delta pos}{\Delta t} = \frac{pos_k - pos_{k-1}}{h}, \quad (2)$$

where  $\Delta pos$  is the change in position of the needle attachment point and  $\Delta t$  is the change in time. For every time step ( $h$ ) with a frequency of 100 Hz Equation (3) can be applied by combining Equations (1) and (2):

$$pos_k = pos_{k-1} + 0.01 \cdot k \cdot \Delta x, \quad (3)$$

where  $k$  is a scaling constant and  $\Delta x$  is the change in position of the MTM in the X-direction related to the starting position. Equation (2) is used to change the position for the MIRIAM system based on the input of the MTM after which the X, Y and Z coordinates of the position (see Figure 7.2) are sent to MIRIAM system. MIRIAM X and Z coordinates were coupled so that the needle attachment always moved in an arc-like manner around the needle guide. This prevented needle insertions or retractions (Z coordinate) when steering conditions were changed (X coordinate). For insertion  $\Delta x$  in Equation (3) is replaced by  $\Delta z$ . This method directly translated forward motion of the MTM to the insertion of the steerable needle, while backward motion of the MTM caused needle retraction.

### 7.2.3 Experimental set-up

The MIRIAM system with the steerable needle attached was placed in the MR scanner while the dVRK for the control was at a remote location. The components of the system and a schematic of the targeting experiment in a prostate phantom are shown in Figure 7.4.

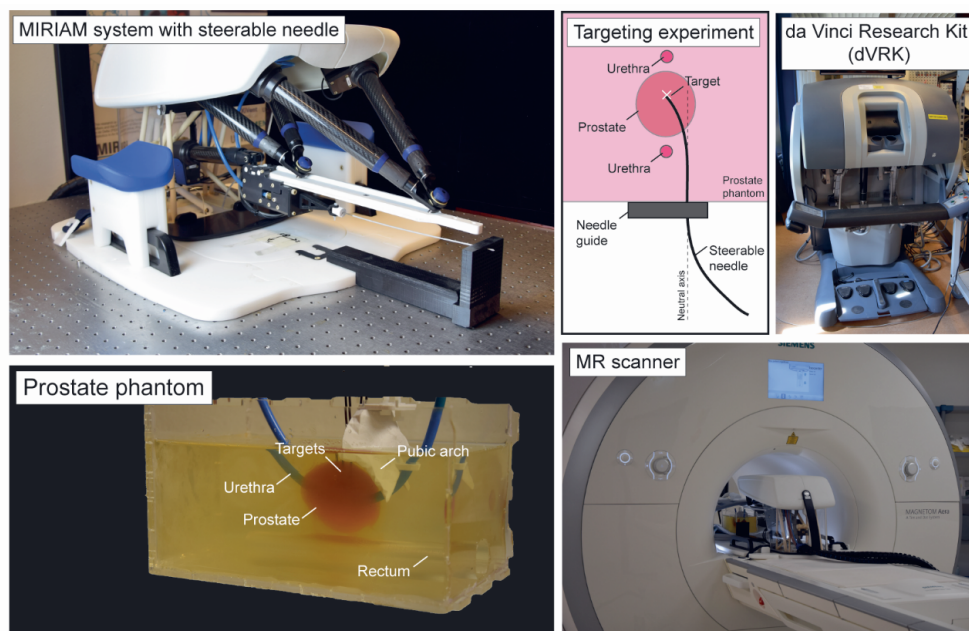


**Figure 7.4 – System components and schematic of the targeting experiment.** The MIRIAM system holds the steerable needle and is placed in the 1.5 T MR scanner. The da Vinci Research Kit (dVRK) is placed outside the MR scanner room and the operator controls the MTM of the dVRK to perform the targeting experiment in which the needle is steered towards a pre-defined target in the prostate phantom. The system is connected via Ethernet using the local area network.

#### 7.2.4 Prostate phantom

The prostate phantom contained targets ventrally located to the urethra at a depth of 80 to 87 mm. The prostate phantom is based on an anonymous patient dataset containing a 65.8 cc prostate and is fabricated of 10 wt.% porcine gelatine (Dr. Oetker, Bielefeld, Germany) approximating the Young's modulus of prostate tissue ( $58.8 \pm 8.2$  kPa) [35]. The MR images are segmented in SolidWorks (Dassault Systèmes SOLIDWORKS Corp.) and a mould is 3D-printed for manufacturing the prostate gland. The phantom contained a prostate gland, adipose tissue, pubic arch of acrylonitrile butadiene styrene, urethra ( $\varnothing$  5 mm silicone rubber rod), rectum and four  $\varnothing$  1 mm targets (carbon fibre reinforced tubes). To distinguish between the prostate and the adipose tissue 5 grams of contrast powder (Sudan orange G, Carl Roth, Karlsruhe, Germany) is added to the prostate.

### 7.2.5 Experimental protocol

The ability to steer the needle along a curved trajectory while avoiding intermediate structures and reach the pre-defined target with the teleoperated system is evaluated for ten insertions in a prostate phantom under MR-guidance (MAGNETOM Aera 1.5T, Siemens Healthineers, Erlangen, Germany). The curvature of the trajectory towards the pre-defined target remained with the operator and adaptations of the input position for the MIRIAM system were allowed during insertion to accurately reach the target. Figure 7.5 shows an example of steering with the steerable needle attached to the MIRIAM system.

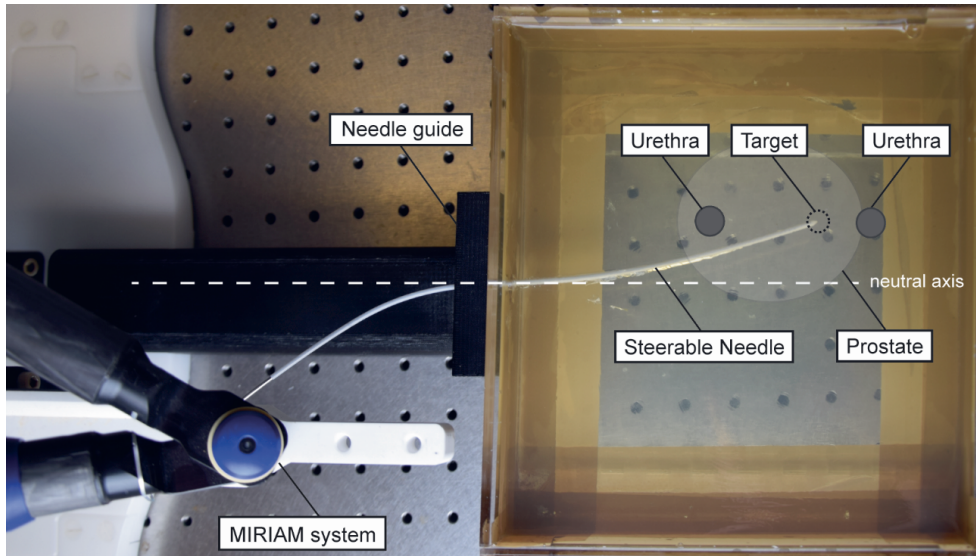


**Figure 7.5 – Steering example with the steerable needle attached to the MIRIAM system.** The steerable needle is inserted in a medium along a curved trajectory to reach a pre-defined target while circumventing the intermediate structure. Steering is applied after penetrating the medium to obtain steering from the neutral axis.

### 7.2.6 Data acquisition and analysis

Real-time T1-Weighted TurboFlash in 2D (T1W-TF2D) scans are acquired. The imaging parameters were: FOV = 191x272 mm; flip angle = 70°; TR/TE = 250.85/1.24 ms; voxel size = 1.31 x 1.31 mm; slice thickness = 8 mm and number of slices = 1. High resolution scans are acquired with imaging parameters: FOV = 150x180 mm; flip angle = 160°; TR/TE = 5590/101 ms; voxel size = 0.56 x 0.56 mm; slice thickness = 3 mm and number of slices = 19. The relatively low resolution of the real-time scans challenged evaluation of the needle tip position. Thus, a second order polynomial fit was made to the simple path curvature to assess the targeting error (see Figure 7.6). The error is assessed in-plane in 2D by the Euclidean distance between the target and the determined end position of the steerable needle tip on the coronal slice.

### 7.3 RESULTS

The communication between the MIRIAM system and the dVRK system, and the control of the steerable needle by the integrated system were successful as teleoperated adaptive steering could be performed with dVRK in the MR environment. Figure 7.6A shows a high resolution MR scan of the phantom in coronal plane and Figure 7.6B shows real-time MR scans with segmented needle trajectories and the resulting 2D-error between the needle tip and target positions.

Trial	Target	Targeting error (mm)
1	Left	0.92
2	Left	1.72
3	Bottom	0.13
4	Bottom	2.33
5	Right	0.41
6	Right	1.32
7	Right	0.56
8	Top	2.72
9	Top	0.81
10	Top	1.12
Mean $\pm \sigma$		1.2 $\pm$ 1.0

**Table 7.1 – Absolute targeting errors in 2D of the steerable needle insertions in the prostate phantom.**  $\sigma$  = standard deviation.

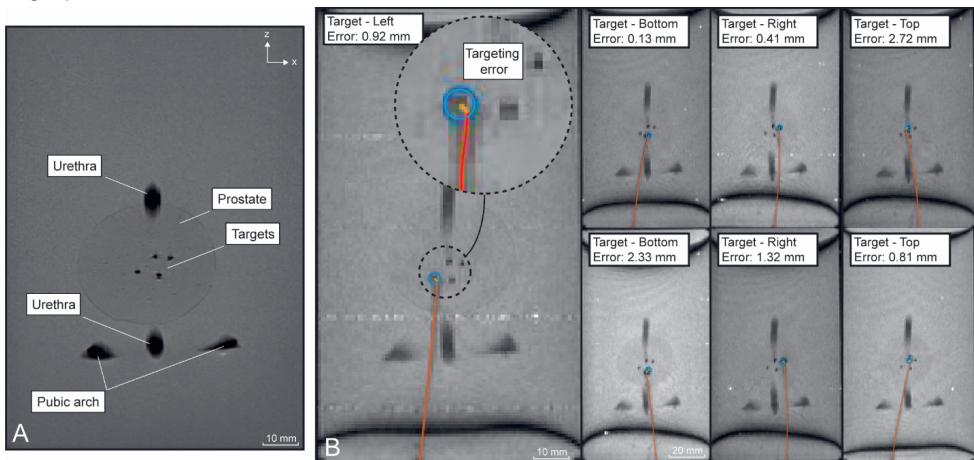


**Figure 7.6 – MR scans in coronal plane of the inserted steerable needle in the prostate phantom.** The opacity of the prostate is changed for visualisation purposes. (A) High resolution MR scan, (B) Real-time MR scans indicating the segmented curved trajectories of the steerable needle (red), the targets (blue) and the targeting errors (orange) for several insertions.

In the steering state, the maximum velocity in X-direction of the needle attachment point was  $\sim 0.001$  m/s, while the maximum insertion velocity was  $\sim 0.02$  m/s. The latency for control between the two systems was on average 8.5 ms (range: 0.43 - 51.7 ms) and MR scans were sent to the operator every 2 seconds. The pre-defined target was reached for all ten insertion after 60 to 180 seconds without any reinsertion required and following different curved trajectories with an average targeting error of  $1.2 \pm 1.0$  mm (Table 7.1).

### 7.4 DISCUSSION

This work presented teleoperated needle steering in an MR environment for the purpose of HDR prostate BT. We showed the feasibility of the teleoperation system and high targeting accuracy of the steerable needle in a prostate phantom. The system integrated three subsystems: 1) the steerable needle, 2) the MIRIAM system and 3) the dVRK, while MR scans provided the ability to continuously

monitor the steerable needle trajectory and adapt the level of steering if required during the procedure. The system is plug and play which allows it to be used in the MR scanner room with minimal adaptations to the set-up. The device places standard ProGuide needles that are directly usable in the subsequent radiotherapeutic workflow. Only positioning of the MIRIAM system in the MR scanner and the HDMI connection for the MR signal are required.

The needle targeting accuracy we obtained in this work is comparable to other studies with MR-compatible BT robots [36]: needle positioning errors of 0.9 to 3.2 mm were reported of which some studies evaluated oblique needle insertions [21]. All errors remained below the limit of 3 to 4 mm used by Borghede et al. [37] when exceeded requiring needle reinsertion. More recently, the CoBra research group developed an MR-compatible robot suitable for LDR prostate BT with active steerable needles to bypass intermediate structures. The system incorporated a module with piezoelectric motors to be mounted on the robot for BT needle steering [38], while our system required attachment of the steerable needle only. As a result of increased accessibility of the target volume and the promising dosimetric outcomes in earlier studies [22–25], one can emphasise that our system ensures a sufficient dose coverage in the prostate.

The integrated system in this work can be classified as a Level II system as “a human specifies general moves or position changes and the machine decides specific movements of its actuators” [21]. To upgrade this human-in-the-loop system to a level IV system in which “the machine will create and complete all its tasks without human interaction”, a predictive model with path planning and closed-loop control should be integrated using visual information of the MR scans. Apart from this, optimisation of the teleoperation system is required. Firstly, the MIRIAM system has limited movement possibilities in the Y-direction while for clinical application steering in X,- and Y-direction is required so that for example pubic arch interference can be overcome. Currently, we are working on scan plane control to automatically reposition the image plane, which will allow for future 3D steering studies. Secondly, the dVRK system allows for 3D visualisation and haptic feedback while not implemented in this work. As the needle has a non-negligible stiffness, the X-Z motion coupling, to move the needle attachment point in an arc-like manner around the entry point in the needle guide, was only sufficient by approximation: slight axial displacements of the needle tip were still observed when the level of steering was adjusted. Thirdly, it was previously shown that in particular open or hollow nitinol structures can cause artefacts in MR images, caused by shielding effects [39,40]. In our case, we did not see such effects, as our most inner component was made from nitinol and we used a polynomial fit on the real-time scans to assist in error determination. Nevertheless, it is recommended to approximate more complex needle trajectories using a higher order polynomial, and to determine the targeting error in 3D. Finally, we recognise that our validations were performed in a static and homogeneous phantom environment. True system validation will require a continuation of this work in a more realistic settings.

The ability to steer the distal tip of the steerable needle allows for counteracting perturbations and follow a pre-defined trajectory. With this, the teleoperation system can be suitable for other treatments such as brachytherapy of the cervix, and biopsies or focal laser ablation of liver and prostate cancers, with only minor changes to workflow and without the need to develop a completely new robotic system.

## 7.5 CONCLUSIONS

This work showed the feasibility of teleoperated MR-guided needle steering for BT interventions in a prostate phantom. The mode of operation of the system was validated and high targeting accuracy was obtained in a prostate phantom. MR scans provided the ability to continuously visualise both the steerable needle and the target position. The teleoperated system allowed for adaptive steering of the needle thus compensating for deviations from the pre-defined trajectory, avoiding intermediate structures and reaching previously inaccessible target locations.



## REFERENCES

- [1] Siegel RL, Miller KD, Fuchs HE, Jemal A. Cancer statistics, 2022. *CA Cancer J Clin* 2022;72:7–33. <https://doi.org/https://doi.org/10.3322/caac.21708>.
- [2] Aluwini S, Busser WMH, Ghidey W, Boormans JL, Kirkels WJ, Jansen PP, et al. Toxicity and quality of life after high-dose-rate brachytherapy as monotherapy for low- and intermediate-risk prostate cancer. *Radiother Oncol* 2015;117:252–7. <https://doi.org/10.1016/j.radonc.2015.09.019>.
- [3] Koukourakis G, Kelekis N, Armonis V, Kouloulis V. Brachytherapy for prostate cancer: A systematic review. *Adv Urol* 2009;2009. <https://doi.org/10.1155/2009/327945>.
- [4] Siebert F-A, Hirt M, Niehoff P, Kovcs G. Imaging of implant needles for real-time HDR-brachytherapy prostate treatment using biplane ultrasound transducers. *Med Phys* 2009;36:3406–12. <https://doi.org/10.1118/1.3157107>.
- [5] Smeenge M, Mischi M, Laguna Pes MP, de la Rosette JJMCH, Wijkstra H. Novel contrast-enhanced ultrasound imaging in prostate cancer. *World J Urol* 2011;29:581–7. <https://doi.org/10.1007/s00345-011-0747-3>.
- [6] Batchelar D, Gaztañaga M, Schmid M, Araujo C, Bachand F, Crook J. Validation study of ultrasound-based high-dose-rate prostate brachytherapy planning compared with CT-based planning. *Brachytherapy* 2014;13:75–9. <https://doi.org/10.1016/j.brachy.2013.08.004>.
- [7] Schmid MG, Crook J, Batchelar D, Halperin R. A phantom study of CT-validation of ultrasound-based planning for HDR prostate brachytherapy. *Brachytherapy* 2011;10:S67–8. <https://doi.org/10.1016/j.brachy.2011.02.003>.
- [8] Tanderup K, Viswanathan AN, Kirisits C, Frank SJ. Magnetic Resonance Image Guided Brachytherapy. *Semin Radiat Oncol* 2014;24:181–91. <https://doi.org/10.1016/j.semradonc.2014.02.007>.
- [9] Whitaker M, Hruby G, Lovett A, Patanjali N. Prostate HDR brachytherapy catheter displacement between planning and treatment delivery. *Radiother Oncol* 2011;101:490–4. <https://doi.org/10.1016/j.radonc.2011.08.004>.
- [10] De Vries M, Wilby SL, Palmer AL, Polak W, Hea IO, Hodgson D, et al. Overcoming pubic arch interference in prostate brachytherapy using steerable needles. *Contemp Brachytherapy* 2022;14. <https://doi.org/https://doi.org/10.5114/jcb.2022.121562>.
- [11] Monfaredi R, Cleary K, Sharma K. MRI Robots for Needle-Based Interventions: Systems and Technology. *Ann Biomed Eng* 2018;46:1479–97. <https://doi.org/10.1007/s10439-018-2075-x>.
- [12] Krieger A, Susil RC, Fichtinger G, Atalar E, Whitcomb LL. Design of a novel MRI compatible manipulator for image guided prostate intervention. *Proc - IEEE Int Conf Robot Autom* 2004;2004:377–82. <https://doi.org/10.1109/robot.2004.1307179>.
- [13] Stoianovic D, Jun C, Lim S, Li P, Petrisor D, Fricke S, et al. Multi-Imager Compatible, MR Safe, Remote Center of Motion Needle-Guide Robot. *IEEE Trans Biomed Eng* 2018;65:165–77. <https://doi.org/10.1109/TBME.2017.2697766>.
- [14] Moreira P, Van De Steeg G, Krabben T, Zandman J, Hekman EEG, Van Der Heijden F, et al. The MIRIAM Robot: A Novel Robotic System for MR-Guided Needle Insertion in the Prostate. *J Med Robot Res* 2017;2:1–13. <https://doi.org/10.1142/S2424905X17500064>.
- [15] Dhaliwal SS, Chettibi T, Wilby S, Polak W, Palmer AL, Reynaert N, et al. Review of Clinical and Technological Consideration for MRI-Guided Robotic Prostate Brachytherapy. *IEEE Trans Med Robot Bionics* 2021;3:583–605. <https://doi.org/10.1109/tmrb.2021.3097127>.
- [16] Muntener M, Patriciu A, Petrisor D, Mazilu D, Bagga H, Kavoussi L, et al. Magnetic resonance imaging compatible robotic system for fully automated brachytherapy seed placement. *Urology* 2006;68:1313–7. <https://doi.org/10.1016/j.urology.2006.08.1089>.
- [17] Garg A, Siauw T, Berenson D, Cunha JAM, Hsu IC, Pouliot J, et al. Robot-Guided Open-Loop Insertion of Skew-Line Needle Arrangements for High Dose Rate Brachytherapy. *IEEE Trans Autom Sci Eng* 2013;10:948–56.
- [18] Strassmann G, Olbert P, Hegele A, Richter D, Fokas E, Timmesfeld N, et al. Advantage of robotic needle placement on a prostate model in HDR brachytherapy. *Strahlenther Onkol* 2011;187:367–72. <https://doi.org/10.1007/s00066-011-2185-y> LB - 21603993.

- [19] Szlag M, Ślosarek K, Rembielak A, Białas B, Fijałkowski M, Bystrzycka J. Real-time brachytherapy for prostate cancer - Implant analysis. *Reports Pract Oncol Radiother* 2008;13:9–14. [https://doi.org/10.1016/S1507-1367\(10\)60076-4](https://doi.org/10.1016/S1507-1367(10)60076-4).
- [20] Smith RL, Hanlon M, Panettieri V, Millar JL, Matheson B, Haworth A, et al. An integrated system for clinical treatment verification of HDR prostate brachytherapy combining source tracking with pretreatment imaging. *Brachytherapy* 2018;17:111–21. <https://doi.org/10.1016/j.brachy.2017.08.004>.
- [21] Podder TK, Beaulieu L, Caldwell B, Cormack RA, Crass JB, Dicker AP, et al. AAPM and GEC-ESTRO guidelines for image-guided robotic brachytherapy: Report of Task Group 192. *Med Phys* 2014;41. <https://doi.org/10.1118/1.4895013>.
- [22] Van den Bosch MR, Lips IM, Lagerburg V, van Vulpen M, Lagendijk JJW, Moerland MA. Feasibility of adequate dose coverage in permanent prostate brachytherapy using divergent needle insertion methods. *Radiother Oncol* 2008;86:120–5. <https://doi.org/10.1016/j.radonc.2007.10.037>.
- [23] Ryu B, Bax J, Edirisinge C, Lewis C, Chen J, D'Souza D, et al. Prostate brachytherapy with oblique needles to treat large glands and overcome pubic arch interference. *Int J Radiat Oncol Biol Phys* 2012;83:1463–72. <https://doi.org/10.1016/j.ijrobp.2011.10.012>.
- [24] Cunha JAM, Hsu I-C, Pouliot J. Dosimetric equivalence of nonstandard HDR brachytherapy catheter patterns. *Med Phys* 2009;36:233–9. <https://doi.org/10.1118/1.3041166>.
- [25] Gibbons EP, Smith RP, Beriwal S, Krishna K, Benoit RM. Overcoming pubic arch interference with free-hand needle placement in men undergoing prostate brachytherapy. *Brachytherapy* 2009;8:74–8. <https://doi.org/10.1016/j.brachy.2008.04.007>.
- [26] Lagerburg V, Moerland MA, Konings MK, Van De Vosse RE, Lagendijk JJW, Battermann JJ. Development of a tapping device: A new angled insertion method for prostate brachytherapy. *Phys Med Biol* 2006;51:891–902. <https://doi.org/10.1088/0031-9155/51/4/009>.
- [27] Podder TK, Clark DP, Fuller D, Sherman J, Ng WS, Liao L, et al. Effects of velocity modulation during surgical needle insertion. *Annu Int Conf IEEE Eng Med Biol - Proc* 2005;7 VOLS:5766–70. <https://doi.org/10.1109/iembs.2005.1615798>.
- [28] Moreira P, Misra S. Biomechanics-Based Curvature Estimation for Ultrasound-guided Flexible Needle Steering in Biological Tissues. *Ann Biomed Eng* 2015;43:1716–26. <https://doi.org/10.1007/s10439-014-1203-5>.
- [29] De Vries M, Sikorski J, Misra S, van den Dobbelaars JJ. Axially rigid steerable needle with compliant active tip control. *PLoS One* 2021;16:e0261089. <https://doi.org/10.1371/journal.pone.0261089>.
- [30] Van de Berg NJ, Van Gerwen DJ, Dankelman J, Van Den Dobbelaars JJ. Design Choices in Needle Steering - A Review. *IEEE/ASME Trans Mechatronics* 2015;20:2172–83. <https://doi.org/10.1109/TMECH.2014.2365999>.
- [31] Yamada A, Naka S, Nitta N, Morikawa S, Tani T. A Loop-Shaped Flexible Mechanism for Robotic Needle Steering. *IEEE Robot Autom Lett* 2018;3:648–55. <https://doi.org/10.1109/LRA.2017.2779273>.
- [32] Konh B, Padasdao B, Batsaikhan Z, Lederer J. Steering a Tendon-Driven Needle in High-Dose-Rate Prostate Brachytherapy for Patients with Pubic Arch Interference. *2021 Int Symp Med Robot ISMR 2021*. <https://doi.org/10.1109/ISMR48346.2021.9661565>.
- [33] Kazanzides P, Chen Z, Deguet A, Fischer GS, Taylor RH, Dimaio SP. An open-source research kit for the da Vinci® Surgical System. *Proc - IEEE Int Conf Robot Autom* 2014:6434–9. <https://doi.org/10.1109/ICRA.2014.6907809>.
- [34] D'Ettoire C, Mariani A, Stilli A, Rodriguez Y Baena F, Valdastris P, Deguet A, et al. Accelerating Surgical Robotics Research: A Review of 10 Years with the da Vinci Research Kit. *IEEE Robot Autom Mag* 2021;28:56–78. <https://doi.org/10.1109/MRA.2021.3101646>.
- [35] Shaaer A, Alrashidi S, Chung H, Loblaw A, Morton G, Paudel M, et al. Multipurpose ultrasound-based prostate phantom for use in interstitial brachytherapy. *Brachytherapy* 2021;20:1139–45. <https://doi.org/10.1016/j.brachy.2021.07.003>.
- [36] Tokuda J, Song S-E, Fischer GS, Seifabadi R, Cho BJ, Tuncali K, et al. Preclinical evaluation of an MRI-compatible pneumatic robot for angulated needle placement in transperineal prostate interventions NIH Public Access. *Int J Comput Assist Radiol Surg* 2012;7:949–57. <https://doi.org/10.1007/s11548-012-0750-1>.
- [37] Borghede G, Hedelin H, Holmäng S, Johansson KA, Sernbo G, Mercke C. Irradiation of localized prostatic



carcinoma with a combination of high dose rate iridium-192 brachytherapy and external beam radiotherapy with three target definitions and dose levels inside the prostate gland. *Radiother Oncol* 1997;44:245–50. [https://doi.org/10.1016/S0167-8140\(97\)00122-9](https://doi.org/10.1016/S0167-8140(97)00122-9).

- [38] Dhaliwal SS, Wilby S, Vries M De, Boni KB, Firouzy S, Navarro SE, et al. CoBra robot for localized cancer treatment and diagnosis under real-time MRI guidance HAL Id : hal-03321170 2021:8–10.
- [39] Wang Y, Truong TN, Yen C, Bilecen D, Watts R, Trost DW, et al. Quantitative evaluation of susceptibility and shielding effects of nitinol, platinum, cobalt-alloy, and stainless steel stents. *Magn Reson Med* 2003;49:972–6. <https://doi.org/10.1002/mrm.10450>.
- [40] Melzer A, Michitsch S, Konak S, Schaefer G, Bertsch T. Nitinol in magnetic resonance imaging. *Minim Invasive Ther Allied Technol* 2004;13:261–71. <https://doi.org/10.1080/13645700410020269>.

# 8

Steering mechanisms for prostate and brain  
brachytherapy

### 8.1 INTRODUCTION

Various steering mechanisms have been investigated in earlier studies [1–6]. In Chapter 4, we proposed a bendable lever for high-dose-rate (HDR) prostate brachytherapy (BT). In this chapter we explore two other steering mechanisms: (1) the pull-push mechanism and (2) the pre-bent tip. The pull-push technique has been developed for the application of low-dose-rate (LDR) prostate BT, using a robotic system for actuation and permanent radioactive seeds for irradiation, in a magnetic resonance (MR)-environment. Pre-bent tip steering has been investigated for the treatment of brain malignancies, in which radioactive microspheres are injected directly into the tumour for local irradiation. This experimental treatment is referred to as micro-brachytherapy (micro-BT) and utilises MR scans for image-guided therapy.

Steering principle (1) enables adaptive steering of the distal needle tip upon actuation of the segments in the axial direction to create a curved trajectory during insertion (Figure 8.1). Retraction of the inner needle from the outer needle creates an open channel towards the target for radioactive seed placement.

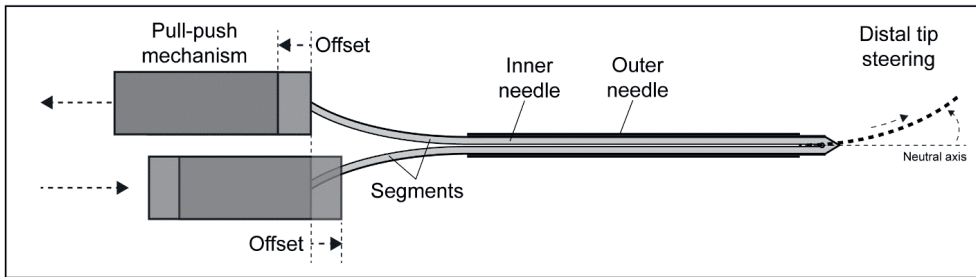


**Figure 8.1 – Steering technique: pull-push.** Axial movement of the segments at the proximal end creates an offset which provides distal tip steering. Drawing is not to scale.

Steering principle (2) ensures a straight channel towards a pre-defined position, after which the pre-bent inner needle is advanced out of the outer needle, allowing for a curved open channel towards the target (Figure 8.2). Axial translation and rotation of the inner needle can be controlled by the operator at the base to reach different targets from the initial straight channel.

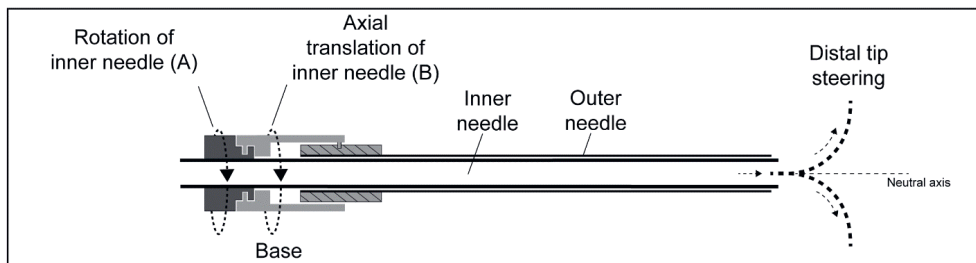


**Figure 8.2 – Steering technique: pre-bent tip.** Rotation of component (A) and (B) at the base enable rotation and axial translation of the inner needle for distal tip steering, respectively. Drawing is not to scale.

## 8.2 PULL-PUSH MECHANISM

In the Interreg 2 Seas CoBra research project a novel robotic device is developed to improve the quality of diagnosis and LDR BT of organ-confined prostate cancers in an MR-environment. At our institution (TU Delft) we developed a LDR BT module including a novel active steerable needle with 2 rotational degrees of freedom at the distal tip to improve access to all parts of the prostate and control unexpected needle deflections during the insertion. This approach potentially improves dose conformity and reduces the number of transperineal insertion points. Focus within this project is on the delivery of permanent seeds for LDR BT as clinical partners had experience in this treatment. MR-guidance is used for high quality images of soft tissues, detection of micro-lesions and adaptive tracking of target motion.

### 8.2.1 Design

The inner needle is manufactured from a  $\varnothing$  1.46 mm superelastic nitinol rod (Confluent Medical Technologies, CA, USA) with a length of 320 mm (Figure 8.1). The inner needle is split into four segments over a distance of 318 mm using the electrical discharge machining process described in Chapter 4. The outer needle comprises of a polyimide tube of 220 mm ( $\varnothing_{\text{inner}}$ : 1.47 mm,  $\varnothing_{\text{outer}}$ : 1.60 mm, Nordson Medical, Westlake, Ohio, USA) and 200 mm superelastic nitinol cannula ( $\varnothing_{\text{inner}}$ : 1.65 mm,  $\varnothing_{\text{outer}}$ : 1.80 mm, Euroflex GmbH, Pforzheim Germany). The degree and direction of needle steering can be controlled upon axial actuation of the piezoelectric motors (MOTOR LT2020C-030D1A00, PiezoMotor Uppsala AB, Sweden) which are connected to the proximal end of the segments (Figure 8.3). To align the segments with the motors a guiding block is 3D-printed using Selective Laser Sintering (SLS). The Acrylonitrile Butadiene Styrene (ABS) block contained four curved channels for guiding the segments. Omnidirectional steering is achieved at the tip by a jointless integrated pull-push mechanism. For example, actuating the two upper and two lower piezoelectric motors to provide a pull and push movement, respectively, causes upward steering of the steerable needle. The most distal 20 mm of the outer needle does not contain nitinol to ensure flexibility of the tip. After needle placement, the inner needle can be retracted to create an open channel for LDR seed delivery via the two-way port. The outer needle remains in the body and can be used to create a new trajectory for subsequent seed delivery.

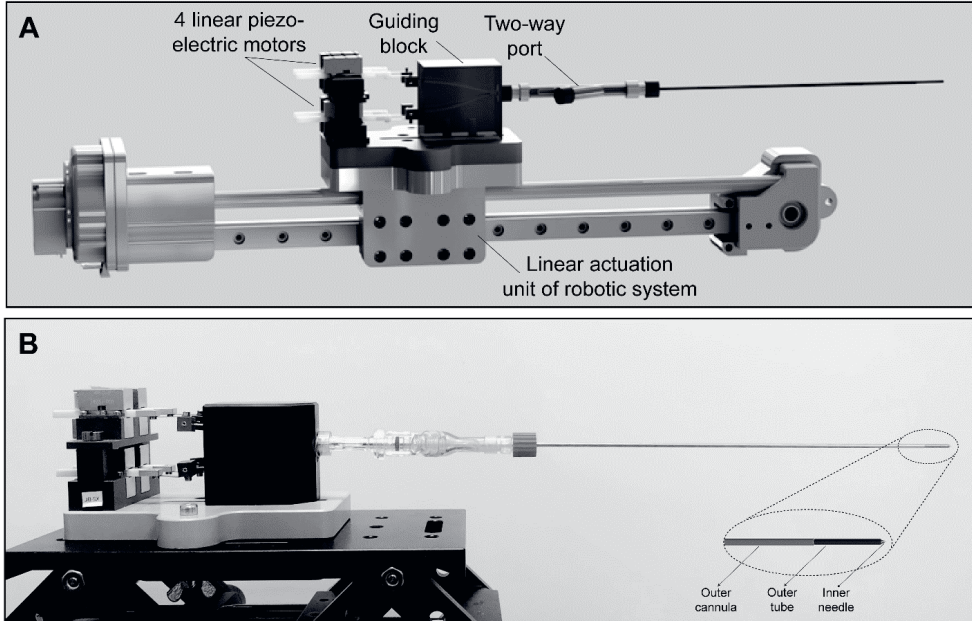


**Figure 8.3 – LDR prostate BT module.** (A) 3D-model of LDR BT module on linear actuation unit of developed robot (see Figure 8.4B) and (B) prototype of LDR BT module. The distal end of the needle is enlarged in the bottom right.

### 8.2.2. Summary of evaluation

The feasibility of needle steering with the LDR BT module is evaluated in experiments with a prostate phantom similar to the phantom described in Chapter 5.2. Active steering in the prostate phantom was possible in all directions and steering up to 15 mm over a 110 mm distance was obtained (Figure 8.4A).

Artefact formation of the needle and piezoelectric motors is evaluated in 3 T magnetic resonance imaging (MRI) (Ingenia system, Philips, Best, the Netherlands) (Figure 8.4B). Figure 8.4C shows that the largest distortion is observed at the distal end of the superelastic nitinol components.

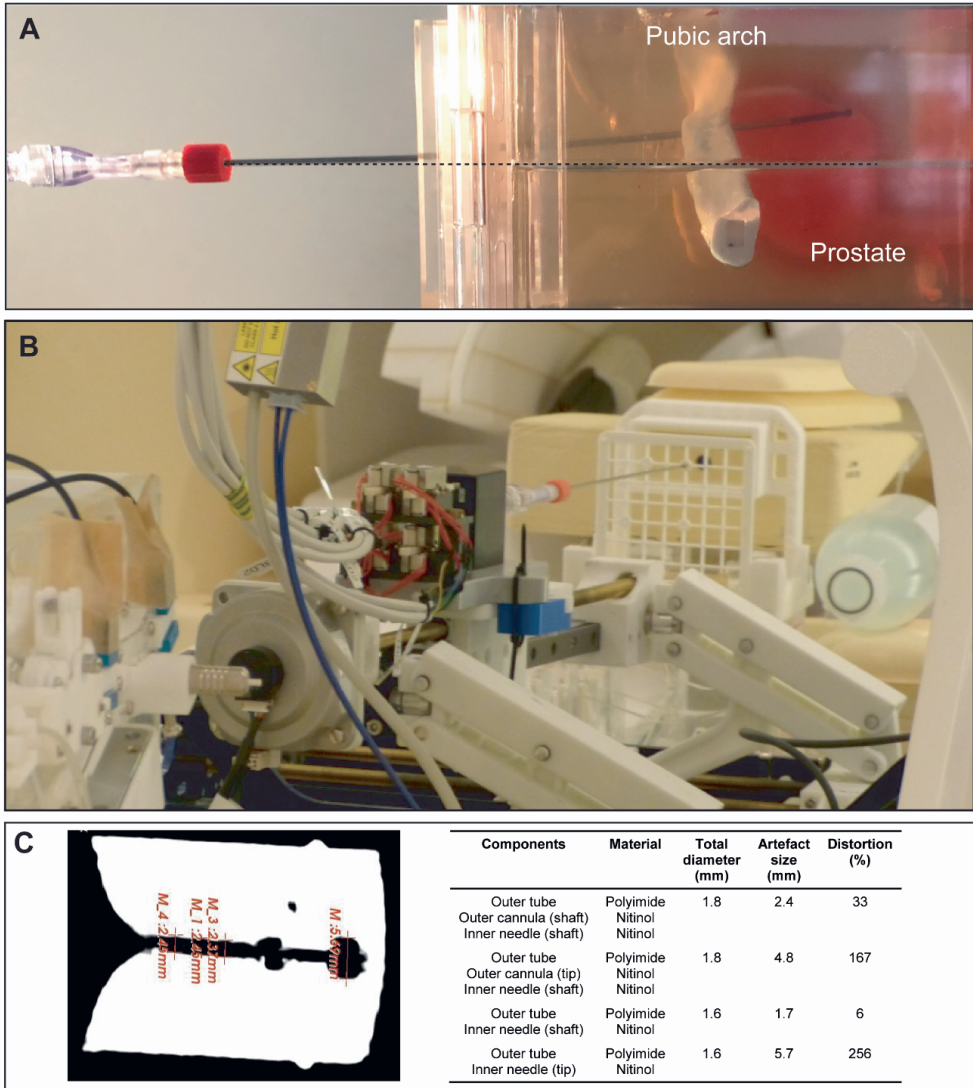


**Figure 8.4 – Evaluation experiments of LDR BT module on developed robotic system in 3T MRI.** (A) upward needle steering to circumvent pubic arch in a prostate phantom, (B) evaluation of LDR BT module on developed robot in 3T MRI on 3D FFE scans for artefact quantification, and (C) artefact measurements on MR scan of distal end of needle as indicated in Figure 8.3B). The imaging parameters were: flip angle = 8°; bandwidth = 271 Hz; slice orientation = coronal, slice thickness = 0.5 mm and number of slices = 101.

### 8.3 PRE-BENT TIP

*Chapter contains the summary of the paper “Dedicated holmium microsphere administration device for MRI-guided interstitial brain microbrachytherapy” published in Medical Engineering & Physics (2021) [7].*

The chapter presents a needle device for the purpose of intratumoural delivery of radioactive holmium-166 microspheres ( $^{166}\text{Ho-MS}$ ) for the treatment of brain malignancies. Direct delivery of radioactive  $^{166}\text{Ho-MS}$  in brain tumours looks promising [8,9], as it minimises toxicity to surrounding healthy tissue while the irradiation dose to the tumour can be high [10,11]. However, currently no dedicated needle systems exist for controlled administration of Ho-MS under MR-guidance. Normal straight syringes lack the ability to distribute the Ho-MS over the whole tumour and multiple punctures through healthy brain parenchyma are not desired as they may increase risk of haemorrhage and dissemination of cancer cells [12,13]. We propose a needle device to bypass the blood-brain barrier and ensure spatial deposition of  $^{166}\text{Ho-MS}$  in the tumour using a pre-bent needle tip. MRI is considered as a promising visualisation method for this application. MRI has high tissue contrast and allows for anatomical tumour reference in combination with quantitative distribution of the injected radioactive ( $^{166}\text{Ho}$ ) and non-radioactive ( $^{165}\text{Ho}$ ) microspheres [11]. This approach may be beneficial in a highly selected group of patients with brain tumours.

#### 8.3.1 Design

The needle device, which is designed to be used under MR-guidance, consists of an outer needle manufactured from the bioceramic material alumina oxide ( $\varnothing_{\text{inner}}$ : 0.8 mm,  $\varnothing_{\text{outer}}$ : 1.6 mm, length: 200 mm, Ortech Ceramics, Sacramento, California, USA) and an inner needle of superelastic nitinol ( $\varnothing_{\text{inner}}$ : 0.42 mm,  $\varnothing_{\text{outer}}$ : 0.71 mm, Euroflex GmbH, Pforzheim Germany) with pre-bent tip (Figure 8.5). Alumina oxide has optimal properties for this application: biocompatibility [14–16], low magnetic susceptibility ( $\chi_{\text{alumina}} = -18.1 \times 10^{-6}$ ) in MR scans [17,18], high material stiffness ( $E_{\text{mod}} = \sim 370 \text{ GPa}$ ) [19] and scratch resistance [14–16]. Superelastic nitinol is reported to be biocompatible, resistant to fatigue and twist, and creates small susceptibility artefacts in MRI. The magnetic susceptibility value of nitinol is  $245 \times 10^{-6}$ , where human soft tissues are estimated to be in a range of  $\sim 20\%$  of  $\chi_{\text{water}} = -9.05 \times 10^{-6}$  [18].

The tip has a curvature with a 15 mm radius over a distance of  $0.5 \pi$  radians. The outer needle can create a linear channel towards the target volume, while the inner needle can be individually controlled by the user for axial translation and rotation using the mechanism at the base. With the pre-bent tip, it becomes possible to target an entire lesion of 30 mm in diameter. The superelastic properties of the material enable the distal tip of the inner needle to have a curvature [20,21]. This curvature adopts a straight orientation when advanced through the outer needle and returns to its pre-bent shape if the tip emerges from the outer needle. To facilitate the injection of Ho-MS, the inner needle can be connected to a syringe containing the Ho-MS suspended in a carrier fluid. This connection is established through a luer-lock mechanism on the proximal end of the instrument.

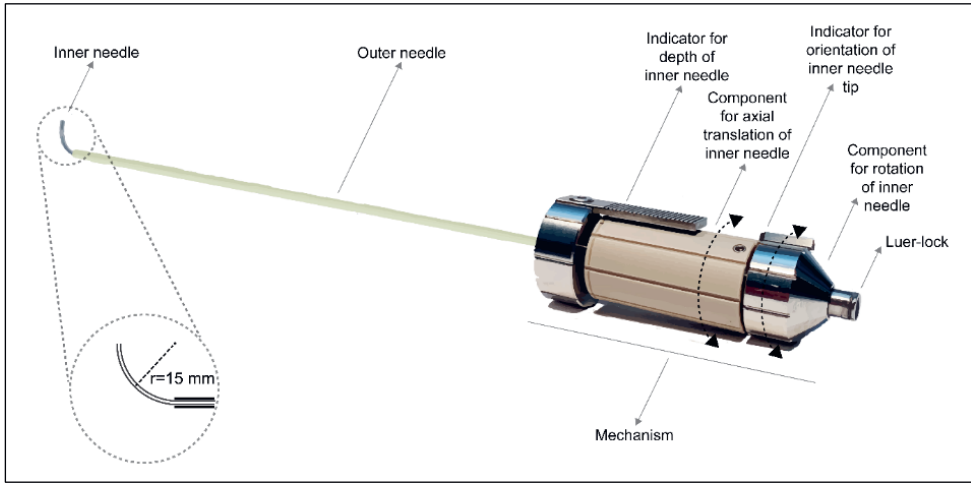


**Figure 8.5 – Needle device with inner needle in its maximum position.** Black arrows indicate intended rotational movement to control the axial translation and rotation of the inner needle. Components are identified by the grey arrows, text and numbers. Cross-section of the inner needle tip is enlarged in the bottom left.

### 8.3.2 Summary of evaluation

The performance of the developed prototype is assessed by measuring targeting accuracy of the inner needle tip after insertions in porcine gelatine phantoms of 13 wt.% (Gelatine, Dr. Oetker, Bielefeld, Germany), approaching the Young's modulus of the stiffest brain tumour tissue found in Abramczyk & Imiela [22] ( $E_{\text{mod}} = 75.7\text{ kPa}$ ). A mean targeting error of  $0.9 \pm 0.6\text{ mm}$  was found in 2D for 168 insertions.

Dose delivery capability with Ho-MS is validated in tissue phantoms mimicking a tumour in brain tissue (Figure 8.6A and 8.6B). This phantom was composed of a baseline composite hydrogel (CH) and incorporated a tumour phantom with a diameter of 50 mm. This diameter allowed for both positioning of the inner needle over a diameter of 30 mm and Ho-MS penetration in the phantom. The baseline CH was obtained by dissolving 1.125 wt% Polyvinyl Alcohol (PVA) and 0.425 wt% Phytigel in deionised water [23]. 0.0012 wt% Manganese chloride ( $\text{MnCl}_2$ ) was added to mimic the T2 MRI contrast of gray matter and tumour tissue [24]. The brain and tumour phantom had the same material composition but had one and two freeze-thaw cycles, respectively. Ho-MS injection was possible in all predefined positions resulting in a sufficient dose distribution of the Ho-MS.

Next to mechanical and dose distribution performance, artefact quantification of the instrument is studied in a 3 Tesla MRI test (Figure 8.6C). The results indicated that the bioceramic material caused smaller distortions compared to the superelastic nitinol which is consistent with the magnetic susceptibility values. Furthermore, a more perpendicular orientation towards the magnetic field resulted in the largest artefacts due to the maximal susceptibility effect and the radio-frequency eddy current.



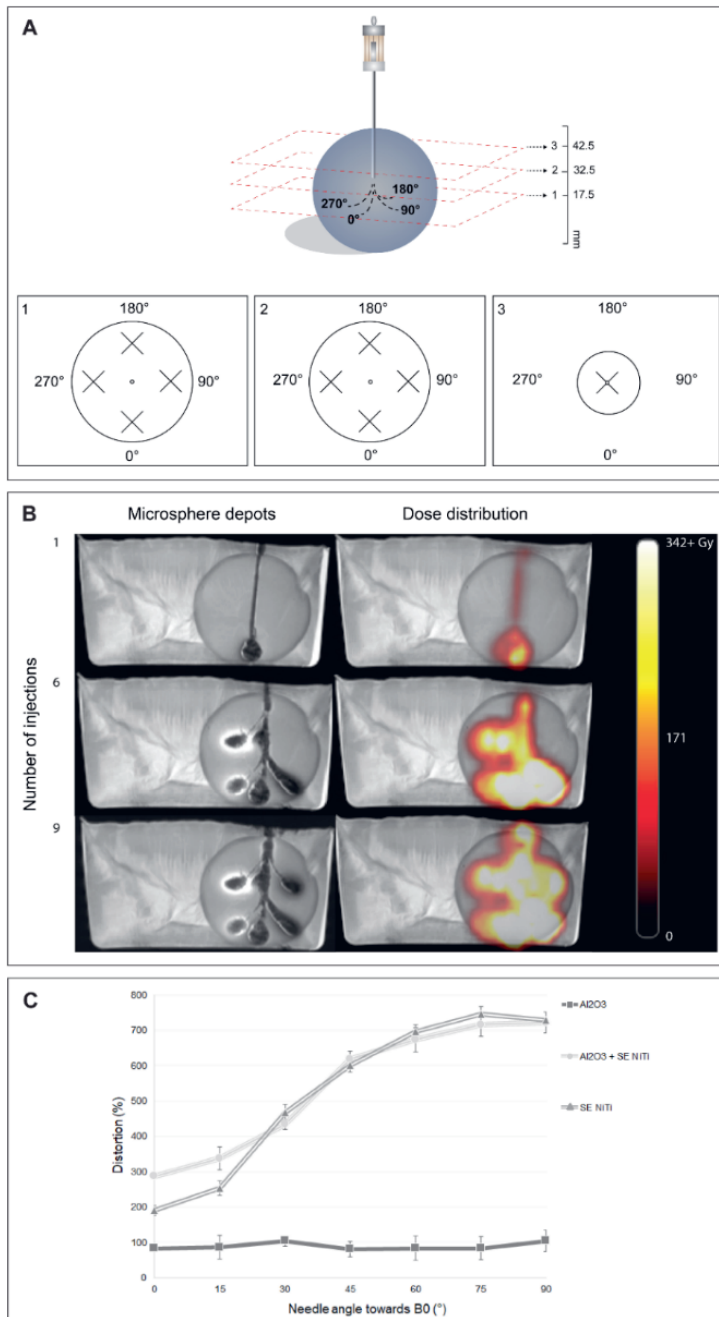


**Figure 8.6 – Evaluation experiments of pre-bent needle.** (A) Injection protocol of the tumour phantom. Three cross-sections in transversal plane at different heights show the Ho-MS injection locations indicated by the cross-marks, (B) Microsphere depots according to Figure 8.6A, and dose distribution in brain tumour phantom. Visualisation is made with a multi-gradient echo MRI scan (left) and using Q-suite (right). Both images are merged with the T2W-TSE scan for visualisation of the instrument and anatomical tumour reference, and (C) artefact measurements on MR scan. Needle angle (°) towards the magnetic field, B<sub>0</sub>, is shown on the X-axis, the amount of distortion in (%) on the Y-axis. Al<sub>2</sub>O<sub>3</sub> = alumina oxide, SE NiTi = superelastic nitinol.

## 8.4 DISCUSSION

The proposed pull-push steering mechanism enables lateral steering up to 15 mm over 110 mm insertion depth in a prostate phantom. The steerable needle can be visualised in 3T MRI; however, distortions occurring at the distal end of the integrated nitinol components can pose challenges in accurately localizing the needle. Retraction of the inner needle creates an open channel towards the target that can be utilised for seed delivery in LDR prostate BT.

The needle device with pre-bent tip can be used to inject Ho-MS directly into a tumour in brain phantom. Visualisation of the needle device and Ho-MS can be performed in 3T MRI. The pre-bent needle steering technique ensures a conformal dose distribution in the tumour requiring only one access channel through healthy brain tissue. The needle device has the potential to be an effective treatment method for brain malignancies and this approach may be beneficial in a highly selected patient group.

The pull-push mechanism and the pre-bent needle approach maintain high axial and flexural rigidity by means of the design and can be used in an MR environment. Both steering techniques are suitable for manual and robotic control, although elaborated in this chapter only for one specific type of control. Differences in the design are a result of the requirements for the associated application: (1) the pull-push mechanism allows active steering of the distal tip, after which the shaft follows the orientation of the tip during the insertion. The smooth curvature of the needle enables seed delivery for LDR prostate BT. Active steering is required for this application as the prostate lies relatively deep in the body and perturbations during an insertion could induce unwanted needle deflection. This steering concept can be used to mitigate deflections and insert the needle according to the treatment plan or to circumvent intermediate structures. Steering principle (2) involves the outer needle creating a straight channel towards the target volume, while the inner needle can be extended from the outer needle to reach multiple targets using its pre-bent tip. This allows for a proper distribution of Ho-MS within the tumour. The brain is a relatively soft organ and it is not likely that needle-tissue interactions will cause needle deflection. Therefore, this steering technique focuses on increasing the accessibility of the tumour while minimising the amount of punctures through healthy tissue, rather than adaptive steering as proposed for HDR and LDR BT.

## REFERENCES

- [1] Van de Berg NJ, Van Gerwen DJ, Dankelman J, Van Den Dobbelsteen JJ. Design Choices in Needle Steering - A Review. *IEEE/ASME Trans Mechatronics* 2015;20:2172–83. <https://doi.org/10.1109/TMECH.2014.2365999>.
- [2] Van de Berg NJ, Meeuwse FC, Doukas M, Kronreif G, Moelker A, van den Dobbelsteen JJ. Steerable needles for radio-frequency ablation in cirrhotic livers. *Sci Rep* 2021;11. <https://doi.org/10.1038/s41598-020-77869-3>.
- [3] Scali M, Pusch TP, Breedveld P, Dodou D. Needle-like instruments for steering through solid organs: A review of the scientific and patent literature. *Proc Inst Mech Eng Part H J Eng Med* 2017;231:250–65. <https://doi.org/10.1177/0954411916672149>.
- [4] Yamada A, Naka S, Nitta N, Morikawa S, Tani T. A Loop-Shaped Flexible Mechanism for Robotic Needle Steering. *IEEE Robot Autom Lett* 2018;3:648–55. <https://doi.org/10.1109/LRA.2017.2779273>.
- [5] Kratchman LB, Rahman MM, Saunders JR, Swaney PJ, Webster III RJ. Toward robotic needle steering in lung biopsy: a tendon-actuated approach. *Med Imaging 2011 Vis Image-Guided Proced Model* 2011;7964:796411. <https://doi.org/10.1117/12.878792>.
- [6] Duong CT, Le CD, Nguyen DN. Effect of Surface Roughness on Friction of CoCrMo-on-UHMWPE Bearing in Total Hip Arthroplasty Under Lubrication of Bovine Serum Albumin. vol. 69. 2020. [https://doi.org/10.1007/978-981-13-5859-3\\_45](https://doi.org/10.1007/978-981-13-5859-3_45).
- [7] De Vries M, Klaassen NJM, Morsink NC, van Nimwegen SA, Nijsen JFW, van den Dobbelsteen JJ. Dedicated holmium microsphere administration device for MRI-guided interstitial brain microbrachytherapy. *Med Eng Phys* 2021;96:13–21. <https://doi.org/10.1016/j.medengphy.2021.07.009>.
- [8] Huh R, Park YS, Lee JD, Chung YS, Park YG, Chung SS, et al. Therapeutic effects of Holmium-166 chitosan complex in rat brain tumor model. *Yonsei Med J* 2005;46:51–60. <https://doi.org/10.3349/ymj.2005.46.1.51>.
- [9] Ha EJ, Gwak HS, Rhee CH, Youn SM, Choi CW, Cheon GJ. Intracavitary radiation therapy for recurrent cystic brain tumors with holmium-166-chico: A pilot study. *J Korean Neurosurg Soc* 2013;54:175–82. <https://doi.org/10.3340/jkns.2013.54.3.175>.
- [10] De Wit TC, Xiao J, Nijsen JFW, Van Het Schip FD, Staelens SG, Van Rijk PP, et al. Hybrid scatter correction applied to quantitative holmium-166 SPECT. *Phys Med Biol* 2006;51:4773–87. <https://doi.org/10.1088/0031-9155/51/19/004>.
- [11] Bult W, Kroeze SGC, Eischot M, Seevinck PR, Beekman FJ, de Jong HWAM, et al. Intratumoral Administration of Holmium-166 Acetylacetonate Microspheres: Antitumor Efficacy and Feasibility of Multimodality Imaging in Renal Cancer. *PLoS One* 2013;8. <https://doi.org/10.1371/journal.pone.0052178>.
- [12] Boctor EM, Stolka P, Kang H, Clarke C, Rucker C, Croom J, et al. Precisely Shaped Acoustic Ablation of Tumors Utilizing Steerable Needle and 3D Ultrasound Image Guidance. *Proceedings of the SPIE*, 2010;7625. <https://doi.org/doi:10.1117/12.846092>.
- [13] Burgner J, Swaney PJ, Bruns TL, Clark MS, Rucker DC, Burdette EC, et al. An Autoclavable Steerable Cannula Manual Deployment Device: Design and Accuracy Analysis. *J Med Devices, Trans ASME* 2012;6:1–7. <https://doi.org/10.1115/1.4007944>.
- [14] Tanzi M, Farè S, Candiani G. *Biomaterials and Applications*. vol. 506. Elsevier Ltd.; 2019. <https://doi.org/10.1016/b978-0-08-101034-1.00004-9>.
- [15] Maccauro G, Rossi P, Raffaelli L, Francesco P. Alumina and Zirconia Ceramic for Orthopaedic and Dental Devices. *Biomater Appl Nanomedicine* 2011. <https://doi.org/10.5772/23917>.
- [16] Daculsi G. *History of development and use of the bioceramics and biocomposites*. Springer International Publishing; 2016. [https://doi.org/10.1007/978-3-319-12460-5\\_2](https://doi.org/10.1007/978-3-319-12460-5_2).
- [17] Matsuura H, Inoue T, Konno H, Sasaki M, Ogasawara K, Ogawa A. Quantification of susceptibility artifacts produced on high-field magnetic resonance images by various biomaterials used for neurosurgical implants technical note. *J Neurosurg* 2002;97:1472–5. <https://doi.org/10.3171/jns.2002.97.6.1472>.
- [18] Schneck J. The role of magnetic susceptibility in magnetic resonance imaging: MRI magnetic compatibility of the first and second kinds. *Med Phys* 1996;23:815–50. <https://doi.org/10.1118/1.597854>.
- [19] Ceramics OA. Alumina Oxide Al<sub>2</sub>O<sub>3</sub> – properties & applications | *Advanced Ceramics* n.d.

<https://www.ortechceramics.com/creamic-materials/alumina-ceramics/> (accessed 14 July 2023).

- [20] Kapoor D. Nitinol for Medical Applications: A Brief Introduction to the Properties and Processing of Nickel Titanium Shape Memory Alloys and their Use in Stents. *Johnson Matthey Technol Rev* 2017;61:66–76. <https://doi.org/10.1595/205651317X694524>.
- [21] Peeters JM, Van Faassen EEH, Bakker CJG. Magnetic resonance imaging of phase transitions in nitinol. *J Biomed Mater Res - Part A* 2007;80:938–45. <https://doi.org/10.1002/jbm.a.30966>.
- [22] Abramczyk H, Imiela A. The biochemical, nanomechanical and chemometric signatures of brain cancer. *Spectrochim Acta - Part A Mol Biomol Spectrosc* 2018;188:8–19. <https://doi.org/10.1016/j.saa.2017.06.037>.
- [23] Forte AE, Galvan S, Manieri F, Rodriguez y Baena F, Dini D. A composite hydrogel for brain tissue phantoms. *Mater Des* 2016;112:227–38. <https://doi.org/10.1016/j.matdes.2016.09.063>.
- [24] Thangavel K, Saritaş EÜ. Aqueous paramagnetic solutions for MRI phantoms at 3 T: A detailed study on relaxivities. *Turkish J Electr Eng Comput Sci* 2017;25:2108–21. <https://doi.org/10.3906/elk-1602-123>.



# 9

Final discussion

### 9.1 SYNOPSIS

The primary aims of this thesis were twofold: first, to demonstrate an innovative design for a steerable needle specifically developed for high-dose-rate (HDR) prostate brachytherapy (BT), and second, to evaluate if this developed steerable needle could make BT accessible for a patient population currently considered non-eligible. These aims were driven by the overarching goal of enhancing needle positioning, thereby improving current BT protocols and expanding the potential group of patients who could benefit from this technique.

In current clinical practice, there is a regular need for improved accessibility of the prostate or adaptability of the needle trajectory once the needle is inserted. Insufficient distribution of needles inside the prostate can adversely affect the treatment plan and may result in the exclusion of patients from this safe and effective therapy. Recognising the challenges associated with needle positioning in prostate BT (Chapter 1), we delved deeper into the subject by conducting an extensive literature review in Chapter 2 and analysing patient datasets in Chapter 3. These endeavours provided valuable insights into the clinical need and the requirements for a steerable needle design which was proposed as a potential solution.

Building upon the identified clinical need, we proposed a novel steering principle and manufactured a prototype, which was evaluated through verification tests in Chapter 4. To assess the dosimetric consequences of using the steerable needle, a preclinical validation study was conducted involving experienced physicians in the field of BT and presented in Chapter 5. The findings from this study provided insights into the potential benefits of utilising the steerable needle in improving dosimetric outcomes. Chapter 6 outlined the path towards conducting the first human trial with the developed medical device. Further explorations have been done in the field of robotic control, magnetic resonance guidance and alternative steering mechanisms in Chapter 7 and 8 to investigate the potential of steering technologies.

This thesis holds significant value for future research in both technical and clinical domains. Engineers can gain insights from the presented steering techniques, defined design requirements, developed tissue phantoms, and the described process towards clinical investigation. From a clinical perspective, patients may benefit from this study in the future. The presented steerable needle has the potential to improve treatment plans and expand the application of BT to patients who are currently excluded due to a large prostate volume and/or excessive pubic arch interference (PAI). By addressing these challenges, the steerable needle technology opens up possibilities for enhanced treatment outcomes and broader eligibility for patients.

*For more specific discussions, please refer to the chapter discussions in this thesis.*

### 9.2 MAIN FINDINGS

In prostate BT, "needle positioning errors" and "PAI" can disrupt the optimal distribution of needles within the target volume, resulting in insufficient dose coverage, *ad hoc* solutions or patient exclusion. The guidelines pertaining to these hazards are documented; however, they suffer from ambiguity. This lack of clarity poses difficulties in differentiating between errors that are considered "acceptable" versus "significant", as well as determining the threshold for classifying PAI as "minor" versus "excessive". We found that positioning errors were considered significant if they were greater than 2-4 mm (off-axis error) and 2-15 mm (longitudinal error). Excessive PAI was determined using various methods, including an overlap distance exceeding 10.0-11.3 mm in the supine position and 4-10 mm in the lithotomy position, an overlap area greater than 25-33.3%, or an angle to the pubic symphysis surpassing 26.3 degrees. However, the response and actions taken when these limits are exceeded vary among institutions and physicians.

The evaluation of prostate volume has traditionally been utilised to assess the risk of prostate inaccessibility during the BT procedure, but no clear relationship was reported between prostate volume and PAI for patients with volumes exceeding 60 cc. Consequently, this method can result in false positives, excluding patients based on assumed PAI without actual evidence, and false negatives, including patients with small prostates but experiencing excessive PAI. Furthermore, prostate volume calculations can be inaccurate, while measurements for PAI and errors are influenced by multiple factors, including imaging technique and specifications, timing and method of assessment, and the assessor. These complexities highlighted the need for a more intraoperative and patient-specific approach that offers greater flexibility in needle positioning.

We developed an active steerable needle to deal with the variability between guidelines and patients and address the aforementioned hazards. The needle was specifically designed to fit the ProGuide 6F outer needle commonly used in current HDR BT procedures. Steering at the distal tip was achieved by bending the proximal end of the needle using an internal compliant mechanism and the transperineal template for pivoting. This design provided sufficient needle rigidity to puncture various heterogeneous tissues while maintaining precise control. These characteristics resulted in similar endpoint accuracy to that of the conventional rigid BT needle when tested in prostate phantoms ( $\leq 2$  mm), while also adding the ability to insert the needle along smooth curved trajectories. It was possible to obtain lateral steering up to 10 mm and 20 mm over insertion depths of 60 mm and 100 mm, respectively, to overcome excessive PAI. Furthermore, we demonstrated that the implementation of this unique steerable needle facilitated the delivery of highly conformal dose distributions in phantoms with larger prostate volumes and excessive PAI, with excellent agreement between pre- and post-implant dosimetry. Incorporating the steerable needle into the BT workflow required only minor adjustments to the existing set-up and did not significantly impact the implantation time.

### 9.3 ACTIVE STEERABLE NEEDLE AS THE SOLUTION!

To enhance prostate BT and enable its application in multiple scenarios, we have explored various strategies. It became apparent that proposed solutions could effectively address specific hazards, but often entail non-desired consequences. For example, hormonal therapy can be used to downsize the prostate and increase the accessibility, but this treatment is associated with a decrease in quality of life and an increase in morbidity and mortality [1–4]. We, therefore, investigated if steerable needles could serve as a solution without resulting in unintended consequences. Active steerable needles would allow for a more intraoperative and patient-specific approach that would go beyond the limitations of existing guidelines, which do not always align with the specific demands of individual patients.

Based on the findings of this thesis, we can confidently conclude that active steerable needles offer a highly promising solution to enhance flexibility in needle positioning and mitigate the hazards associated with restricted access to the prostate and needle targeting errors without introducing additional drawbacks. This solution offers an optimal total needle geometry without introducing major modifications to the clinical set-up and workflow. However, it is important to note that strict conditions for the use of steerable needles in BT relates to the ability to puncture prostate tissue and maintain controllability.

During our investigation into the state-of-the-art of active steerable needles, we discovered that existing designs suffer from limitations such as inadequate degrees of freedom, insufficient needle rigidity for precise trajectory control, reliance on motorised actuation, inability for miniaturisation to fit the conventional HDR BT outer needle, and challenges related to fabrication and cleaning. In contrast, the developed needle exhibits numerous advantages over these existing designs. We ensured sufficient rigidity of the needle through careful consideration of the design, the manufacturing method, and the material used. The incorporation of a compliant mechanism and the utilisation of the transperineal template for pivoting allowed us to eliminate the need for a handle at the base. These design choices



not only maximised the workspace but also minimised the number of parts, facilitating easy assembly and cleaning processes. Preclinical tests in prostate phantoms showed that our steerable needle could be safely used to puncture various tissue types and maintain adequate control within all experiments. In addition, it required only a short training period for the physicians to become proficient in its handling. Considering the steep learning curve, the ease of control by hand and the simplicity of the design, we expect a potentially rapid clinical implementation. This is in contrast to, for example, robotic solutions, which often require a more comprehensive set-up and more extensive technical documentation for their clinical use.

Promising scenarios for the use of the developed steerable needle relate to the accessibility of the prostate involving including patients who are typically excluded based on an unfavourable location of the tumour, their prostate volume and/or the presence of PAI. The incorporation of this group of patients is justified by the favourable outcomes observed in our own research and supported by existing literature, which highlight good dosimetry and biochemical control [5–8]. Our approach eliminates the necessity for prostate volume evaluation to estimate the risk of PAI and makes the assessment of the level of PAI redundant. Other scenarios focus on avoiding the neurovascular bundles or the penile bulb without compromising the dose plan or inserting needles conforming the prostate geometry. Previous studies have discussed that trajectories conforming the prostate geometry can lower the number of needles required by 30% to 80%, potentially reducing edema and urinary incontinence [9,10]. Moreover, steerable needles can be used in patients with a small prostate (< 50 cc) and a narrow pubic arch. The level of PAI is not evaluated in this group of patients, while previous studies reported this hazard in 5 to 25% of patients [11–13]. It is crucial to explore the utilisation of steerable needles in future research for addressing these cases.

Regarding control of the needle trajectory, the steerable needle offers the ability to manipulate the orientation of the tip and make adjustments during the insertion to effectively manage unexpected needle deflections. By combining adaptive control of the needle tip with ultrasound visualisation, it is possible to make real-time modifications to the needle trajectory, ensuring precise alignment with the planned trajectory and maintaining adherence to the intended treatment plan. It is important to note that significant off-axis errors in HDR BT are not very common, but when using fewer needles, such as in the case of focal HDR BT, strict adherence to the treatment plan becomes more crucial. This is because the options for optimising the dose through dwell time and position optimisation are limited.

Overall, we can conclude that the developed active steerable needle holds significant potential benefits in the clinical setting, both for currently included patients, as well as for excluded patients who can benefit from the safe and effective nature of BT [14]. Besides, hospitals can benefit from this approach considering the cost-effectiveness of prostate BT [15,16].

### 9.4 FINDING BALANCE

In our steerable needle design, we aimed for an optimal balance between flexibility, flexural rigidity and axial rigidity. These properties are inextricably linked; changes in flexibility versus rigidity dictate the curvature desired. Initially, we conducted a study to determine the required magnitude of steering based on the level of PAI. Our geometrical study indicated that approximately 10 mm of lateral steering over 60 mm insertion depth could effectively overcome PAI. Next, we incorporated various constraints for the design of the steerable needle. These included requirements regarding the dimensions, the material density for a proper ultrasound visualisation, and the ability to create smooth curved trajectories for afterloading with a radioactive source. To meet the latter requirement, the shaft needed to exhibit sufficient flexibility to align with the orientation of the tip during needle insertion. In addition, the needle required two rotational degrees of freedom to enable tip manipulations in 360 degrees in axial plane. This eliminated the need for rotating the needle around its longitudinal axis to steer in multiple directions reported in earlier studies with steerable needles [17,18]. These constraints touched upon the

complexity of the design, where simplicity was sought to avoid challenges in the manufacturing and cleaning processes. Against the demands of flexibility was the optimisation of rigidity. We maximised the rigidity of the needle by means of the design. A symmetrical pull-push mechanism was integrated in the design, while the number of recesses at the tip was minimised compared to designs reported in literature [9,17,19]. The design consisted of one single structure which was tooled by electrical discharge machining. The two slots created had a width of 0.12 mm, maximising the second moment of inertia ( $I$ ), related to flexural rigidity, and the cross-sectional area ( $A$ ), related to axial rigidity. Furthermore, finite element analysis was conducted to determine the prevailing stresses in the needle during use. It was crucial to ensure that the maximum internal stress remained below the Yield Strength of the material, as exceeding the elastic region would result in plastic deformation or fracture. Lastly, we identified the most suitable and readily available material on the market, and prototypes of the needle design were manufactured. Experiments demonstrated that the local needle rigidity was finely tuned to ensure controllability during needle insertion, while minimising the risk for buckling and maintaining predictable needle behaviour.

## 9.5 LIMITATIONS

Tissue resistance influences the controllability of a needle trajectory during a needle insertion. Our steering mechanism had high local flexural rigidity at the needle tip to overcome the resistance in various heterogeneous tissues and enable tip steering in all our experiments. However, some caution is advised for stiffer tissues as they have not been extensively tested. Especially in these cases, the steerable needle is more prone to unwanted deflection due to the decreased rigidity of the needle if compared to the conventional rigid BT needle. Insufficient control during the insertion could therefore increase the needle positioning error. On the other hand, very soft tissues can pose a challenge after needle implantation. If the needle is inserted along a curved trajectory, the proximal end of the steerable needle needs to be brought to the neutral axis to allow for inner needle retraction. In cases of very low tissue resistance, this can cause movement of the distal tip, leading to a targeting error in softer tissues. While we did not observe significant tip displacement in our phantoms, this aspect should be thoroughly investigated during clinical testing.

In this thesis, we emphasised that utilising steerable needles could enhance current BT cases and enable the inclusion of more complex scenarios. While earlier studies have shown promising results for both standard and complex cases, we expect that the greatest added value will be observed in challenging cases that require improved prostate accessibility and the avoidance of critical structures. The rationale behind this expectation is primarily grounded in the recognition that the more standard cases already show a high level of safety and effectiveness when utilising rigid needles. Nevertheless, further research is necessary to determine whether employing steerable needles to navigate around structures such as the neurovascular bundles or the penile bulb can effectively achieve a sufficient dose plan. It is important to consider the potential for interference of the steerable needles and visual impairments in these situations. Similarly, the use of steerable needles in cases involving small prostates with a narrow pubic arch, where a limited number of needles are required, warrants investigation. By exploring these aspects, the feasibility and efficacy of steerable needles in addressing the unique challenges presented by these cases can be evaluated.

## 9.6 FROM INNOVATION TOWARDS IMPLEMENTATION

The Technology Readiness Level (TRL) is a method for estimating the maturity of technologies and innovations and includes TRL 1 to TRL 9. At academic institutions medical developments generally remain in the concept phase (TRL 1 to TRL 3) which is exempt from the Medical Device Regulation 2017/745 (MDR). The simplicity of our design and the ability to steer and control the needle trajectory in various tissues, convinced us to further develop the instrument's readiness for the first in human trial.

By achieving this milestone, a bridge is built between the technical and clinical domain; a technical solution is developed to address a specific clinical need. We compiled the Investigational Medical Device Dossier (IMDD) according to Article 82 of the MDR, related to TRL 4 to TRL 6. Upon acceptance of the clinical protocol, a phase I study will be performed. This study is related to the safety and feasibility of the medical device. In case of favourable results, a phase II study can be conducted related to the effectivity of the treatment with steerable needles and the patient outcomes. Steering around the urethra or the pubic arch are scenarios that can be addressed to provide an improved total needle geometry, as formerly inaccessible volumes could now be reached and irradiated. Dosimetry and acute toxicity can be compared to historical data of patients when only conventional rigid needles were used. Looking further into the future, the steerable needle could be brought to market and integrated into the existing set of instruments for a HDR prostate BT procedure. Hereto, further investigation should be performed according to Article 62 of the MDR (TRL 7 to TRL 9).

### 9.7 FUTURE PERSPECTIVES AND OTHER APPLICATIONS

Steerable needles hold promising future perspectives as they offer several advantages over traditional rigid needles. They provide physicians with greater accessibility and controllability of the needle trajectory and end position in the patient's body. This potentially leads to improved patient outcomes and reduced risks on negative side effects. Throughout this thesis, we proposed three different steering techniques: the bendable lever, the pull-push mechanism and the pre-bent needle tip. All proposed steering concepts, individually or in combination, can potentially be used for other applications. We believe that the steering principle of the bendable lever holds most potential in the following scenarios, thanks to its unique characteristics and easy implementation: BT in the prostate, cervix or breast; biopsy or ablation of prostate or liver tumours; and treatment of a pancreatic, lung, kidney or spleen tumour [20,21]. Only simple modifications in the design parameters are required for the purpose of the medical application. Easily adaptable parameters are: material, shape (rod or tube), diameter and length of the needle. For example, a material with a higher Young's Modulus or larger diameter provides a higher flexural rigidity and a higher Euler buckling force, while an increased needle length or miniaturisation decreases the resistance against buckling. Furthermore, the steerable HDR BT needle could potentially be used in combination with direct tracking of the needle tip via real-time magnetic resonance imaging, ultrasound or electromagnetic tracking. This ensures automatic reconstruction of curved trajectories and avoids manual verification after placement of the outer needle associated with a high-risk failure mode [22,23]. The physician is no longer bound by the order of implantation, namely from ventral to dorsal to ensure transrectal ultrasound visualisation of the needle, but the physician can control the implant strategy. This allows the physician to use rigid needles for heavy-weighted source implants, while steerable needles are used to tweak the dose distribution and avoid structures such as the penile bulb.

### 9.8 CONCLUSION

Insufficient dose coverage or exclusion of patients from BT protocols can occur due to needle positioning errors and/or PAI. Existing clinical guidelines are ambiguous, and current solution strategies are often suboptimal. We developed a steerable needle that enhances the accessibility to the prostate and offers improved control over the needle trajectory once it has entered the tissue. This unique steerable needle concept facilitates a conformal dose distribution, offering potential improvements in the efficiency and efficacy of HDR prostate BT procedures. This approach makes previously excluded patients with a large prostate volume and/or excessive PAI suitable again for BT protocols. Simple modifications in the design parameters allow the proposed steering principle to be used for other medical applications.

## REFERENCES

- [1] Press RH, Morgan TM, Cutrell PK, Zhang C, Chen Z, Rahnama S, et al. Patient-reported health-related quality of life outcomes after HDR brachytherapy between small (<60 cc) and large (≥60 cc) prostate glands. *Brachytherapy* 2019;18:13–21. <https://doi.org/10.1016/j.brachy.2018.08.009>.
- [2] Kopp RP, Marshall LM, Wang PY, Bauer DC, Barrett-connor E, Parsons JK. The Burden of Urinary Incontinence and Urinary Bother Among Elderly Prostate Cancer Survivors. *Eur Urol* 2013;64:672–9. <https://doi.org/10.1016/j.eururo.2013.03.041>.
- [3] Basaria S, Li JL, Tang AM, Deweese T, Carducci M, Eisenberger M, et al. Long-term effects of androgen deprivation therapy 2002:779–86.
- [4] Saigal CS, Gore JL, Krupski TL, Hanley J, Schonlau M, Litwin MS. Cardiovascular Morbidity in Men With Prostate Cancer. *Am Cancer Soc* 2007. <https://doi.org/10.1002/cncr.22933>.
- [5] Monroe AT, Faricy PO, Jennings SB, Biggers RD, Gibbs GL, Peddada A V. High-dose-rate brachytherapy for large prostate volumes (≥50 cc)-Uncompromised dosimetric coverage and acceptable toxicity. *Brachytherapy* 2008;7:7–11. <https://doi.org/10.1016/j.brachy.2007.10.005>.
- [6] Pham YD, Kittel JA, Reddy CA, Ciezki JP, Klein EA, Stephans KL, et al. Outcomes for prostate glands >60 cc treated with low-dose-rate brachytherapy. *Brachytherapy* 2016;15:163–8. <https://doi.org/10.1016/j.brachy.2015.12.002>.
- [7] Stone NN, Stock RG. Prostate brachytherapy in patients with prostate volumes ≥ 50 cm<sup>3</sup>: Dosimetric analysis of implant quality. *Int J Radiat Oncol Biol Phys* 2000;46:1199–204. [https://doi.org/10.1016/s0360-3016\(99\)00516-7](https://doi.org/10.1016/s0360-3016(99)00516-7).
- [8] Quan AL, Ciezki JP, Reddy CA, Angermeier K, Ulchaker J, Mahadevan A, et al. Improved biochemical relapse-free survival for patients with large/wide glands treated with prostate seed implantation for localized adenocarcinoma of prostate. *Urology* 2006;68:1237–41.
- [9] Rabiei M, Ko SY, Podder TK, Lederer J, Konh B. HDR Brachytherapy Planning using Active Needles-Preliminary Investigation on Dose Planning. *Proc IEEE RAS EMBS Int Conf Biomed Robot Biomechatronics* 2022;2022-Augus:1–20. <https://doi.org/10.1109/BioRob52689.2022.9925426>.
- [10] Podder TK, Dicker AP, Hutapea P, Darvish K, Yu Y. A novel curvilinear approach for prostate seed implantation. *Med Phys* 2012;39:1887–92. <https://doi.org/10.1118/1.3694110>.
- [11] Sejpal S, Sathiseelan V, Helenowski I, Kozlowski J, Carter M, Nadler R, et al. Intra-operative pubic arch interference during prostate seed brachytherapy in patients with CT-based pubic arch interference of ≤1 cm. *Radiother Oncol* 2009;91:249–54. <https://doi.org/10.1016/j.radonc.2009.02.006>.
- [12] Peschel RE, King CR, Roberts K. Pubic arch interference in permanent prostate implant patients. *J Brachytherapy Int* 1998;14:241–8.
- [13] Gibbons EP, Smith RP, Beriwal S, Krishna K, Benoit RM. Overcoming pubic arch interference with free-hand needle placement in men undergoing prostate brachytherapy. *Brachytherapy* 2009;8:74–8. <https://doi.org/10.1016/j.brachy.2008.04.007>.
- [14] Demanes DJ, Rodriguez RR, Altieri GA. High dose rate prostate brachytherapy: the California Endocurietherapy (CET) Method. *Radiother Oncol* 2000;57:289–96.
- [15] Vu CC, Jawad MS, Krauss DJ. The Cost-Effectiveness and Value Proposition of Brachytherapy. *Semin Radiat Oncol* 2020;30:87–93. <https://doi.org/10.1016/j.semradonc.2019.08.007>.
- [16] Shah C, Lanni TB, Ghilezan MI, Gustafson GS, Marvin KS, Ye H, et al. Brachytherapy provides comparable outcomes and improved cost-effectiveness in the treatment of low/intermediate prostate cancer. *Brachytherapy* 2012;11:441–5. <https://doi.org/10.1016/j.brachy.2012.04.002>.
- [17] Van de Berg NJ, Meeuwssen FC, Doukas M, Kronreif G, Moelker A, van den Dobbelsteen JJ. Steerable needles for radio-frequency ablation in cirrhotic livers. *Sci Rep* 2021;11:1–9. <https://doi.org/10.1038/s41598-020-77869-3>.
- [18] Kriegshauser JS, Knuttinen MG, Zhang N, Oklu R. Use of a steerable needle for CT-guided nerve plexus blockade. *Abdom Radiol* 2019;44:327–32. <https://doi.org/10.1007/s00261-018-1721-y>.
- [19] Konh B, Padasdao B, Batsaikhan Z, Lederer J. Steering a Tendon-Driven Needle in High-Dose-Rate Prostate Brachytherapy for Patients with Pubic Arch Interference. *2021 Int Symp Med Robot ISMR 2021*

2021. <https://doi.org/10.1109/ISMR48346.2021.9661565>.
- [20] De Jong TL, van de Berg NJ, Tas L, Moelker A, Dankelman J, van den Dobbelsteen JJ. Needle placement errors: Do we need steerable needles in interventional radiology? *Med Devices Evid Res* 2018;11:259–65. <https://doi.org/10.2147/MDER.S160444>.
- [21] Arcos J De, Wang W, Tokuda J, Vij K, Seethamraju R, Dumoulin C, et al. HHS Public Access. *INT J RADIAT ONCOL BIOL PHYS* 2017;99:618–26. <https://doi.org/10.1016/j.ijrobp.2017.05.054>. Prospective.
- [22] Sauer BC, Dürrbeck C, Bert C. Electromagnetic tracking in interstitial brachytherapy : A systematic review. *Med Phys Imaging* 2022:1–6. <https://doi.org/10.3389/fphy.2022.956983>.
- [23] Wilkinson DA, Kolar MD. Failure modes and effects analysis applied to high-dose-rate brachytherapy treatment planning. *Brachytherapy* 2013;12:382–6. <https://doi.org/10.1016/j.brachy.2013.03.002>.

## DANKWOORD

Daar zit ik dan, op een kruk in de keuken met mijn laptop voor mijn neus terwijl het zonnetje door het raam naar binnen schijnt, de schoolkinderen op het plein achter ons huis rondrennen, Denzel (onze kat) naast mij ligt te slapen, en er, zoals zo vaak, hetzelfde pianospel van de buurman door de muren heen dreunt. Ik probeer het omgevingsgeluid te filteren en ik denk terug aan de afgelopen jaren. In mijn eerste gedachte lijken ze voorbij te zijn gevlogen, maar als ik langer nadenk, blijkt er weldegelijk van alles gebeurd te zijn.

Nadat ik, in 2012, de kamer van de directeur van Sparta Rotterdam binnenstapte en hem vertelde dat ik mijn voetbalcarrière voorgoed vaarwel ging zeggen, kon ik op de valreep nog starten met de bachelor Industrial Design Engineering aan de TU Delft. Nooit had ik (en ik denk velen met mij) verwacht dat ik in 2023 nog steeds in de academische wereld zou rondlopen. Zo gaf ik in eerste instantie, na het afronden van mijn master Biomedical Engineering, ook direct de voorkeur aan een baan in de industrie. Maar, de goede band met mijn scriptiebegeleider John van den Dobbelsteen en het interessante onderwerp van het lonkende promotieonderzoek, op het snijvlak van techniek en gezondheidszorg, hielden mij uiteindelijk op de TU Delft. Nu, blij met de keuzes die ik toentertijd allemaal heb gemaakt en enorm trots op het werk dat er voor u ligt!

Via deze weg wil ik iedereen bedanken die mij in de afgelopen jaren gesteund, gestimuleerd en geholpen hebben. Sommigen waren direct betrokken bij mijn onderzoek en anderen waren juist waardevol op de momenten buiten mijn onderzoek.

In het bijzonder wil ik mijn promotor John van den Dobbelsteen bedanken. Ik heb enorm fijn met jou samen mogen werken. Je stond altijd voor me klaar wanneer ik vragen had, liet me vrij in het maken van keuzes, en gaf advies waar nodig. Daarnaast konden we ook lange tijd over allerlei andere onderwerpen praten. De uren in de auto samen naar Lille, Veenendaal of Nijmegen vlogen zo voorbij. Een perfecte combinatie van gezelligheid en werk. Zonder onze goede relatie was dit proefschrift nooit tot stand gekomen. Dankjewel!

Mijn andere promotor Jenny Dankelman wil ik graag bedanken voor de ondersteuning en positiviteit met betrekking tot mijn werk. Jouw deur stond altijd voor mij open en jouw enthousiasme tijdens onze jaarlijkse meetings stimuleerde mij elke keer weer om door te gaan. Daarnaast waren de BBQ's en de sinterklaasavonden met de afdeling bij jou thuis ook altijd zeer geslaagd!

De leuke collega's uit Kantoor 1 hebben ervoor gezorgd dat het elke keer weer gezellig was op de TU. Ik kijk met veel plezier terug op de lunches, waar het over van alles en nog wat ging, de koffietjes, de borrels, de padelsessies, en andere activiteiten die we samen ondernomen hebben (@mijn paranimf Bart: ik heb volgens mij nog steeds een sjaal thuis liggen...). Het is eigenlijk zonde dat we elkaar tijdens Covid-19 zo'n lang tijd weinig hebben gezien, want het was altijd weer leuk als we met elkaar waren.

Daarnaast wil ik iedereen van de MISIT-groep bedanken. Ik weet dat ik niet bij jullie op de kamer zat (en ja, ik blijf daarom natuurlijk ook een beetje het MISIT-buitenbeetje...), maar ik waardeerde het contact met en de gezelligheid bij jullie altijd weer! Ook wil ik de andere promovendi, de postdocs, het secretariaat en andere collega's enorm bedanken! Of we nu een leuk gesprek op de TU hadden, ergens een koffietje dronken of elkaar tijdens een congres of afdelingsuitje zagen, het contact was altijd heel goed.

Jean-Marc, Lennart, Mario en Jan, enorm bedankt voor de ondersteuning van jullie kant! Ik kijk met een heel goed gevoel terug op onze fijne samenwerkingen. Zonder jullie lagen er nu niet zulke mooie en

doeltreffende medische instrumenten, waren er geen weefsel simulanten geweest om de instrumenten in te testen en had ik waarschijnlijk nog steeds niet geweten wat een SOP en een DoC zijn.

Ook wil ik alle personen bedanken waar ik stuk voor stuk goed mee heb samen gewerkt (o.a. vanuit het Erasmus MC, Radboud UMC, Utrecht University, Portsmouth Hospital University, UT Twente, TU Delft, University of Lille en Elekta). De diversiteit aan mensen en onderzoeken hebben deze jaren voor mij enorm interessant gemaakt en afwisselend gehouden. Inger-Karine, ik wil jou extra bedanken voor de mooie samenwerking die er tot stand is gekomen met het Erasmus MC en voor jouw enthousiasme vanaf het moment dat wij via LinkedIn met elkaar in contact kwamen. Hopelijk is de eerste test met patiënten en de ontwikkelde stuurbare naalden snel een feit!

En natuurlijk mijn familie, met in het bijzonder papa, mama & mijn broer, bedankt voor de fijne momenten als we samen zijn en de steun die jullie me geven! Ik bewonder jullie hulp in mijn leven enorm (zoals bij het kopen en verbouwen van ons huis). Ook al hebben we verschillende interesses als het op werk aankomt, het is mooi om te weten dat jullie trots zijn op wat ik doe en wat mij bezighoudt.

Daarnaast wil ik ook mijn vrienden en schoonfamilie bedanken! Jullie interesse in mijn onderzoek deed me altijd enorm goed, maar ik genoot ook zeker van alle momenten dat het juist over hele andere zaken ging. Thijs enorm bedankt voor het ontwerpen van de geweldige kaft van mijn proefschrift en paranimf Ruben, geweldig dat je mij tijdens mijn verdediging hebt bijgestaan!

Afsluiten doe ik natuurlijk met mijn lieve vriendin Amy. Je zorgt voor gezelligheid en enthousiasme in ons huis en in mijn leven. Je helpt me waar nodig, of het nu gaat om het verbeteren van mijn papers of dat je probeert me te overtuigen even een pauze te nemen. Vooral zorg je ervoor dat we genieten van alle momenten waarin we niet met werk bezig zijn. We weten allebei dat we nogal ambitieus kunnen zijn als het om werk gaat, maar juist daarom zijn die momenten voor mij enorm belangrijk. Dat waardeer ik enorm.

## SCIENTIFIC OUTPUT

**de Vries M**, Bloemberg J, van Riel LAMJG, de Reijke TM, Sakes A, Breedveld P, van den Dobbelssteen JJ. Therapeutic prostate cancer interventions: quantification of pubic arch interference and needle positioning errors. *Under review*.

**de Vries M**, Wilby S, Palmer AL, Polak W, O'Hea I, Hodgson D, van den Dobbelssteen JJ. Overcoming pubic arch interference in prostate brachytherapy using steerable needles. *Journal of Contemporary Brachytherapy*. 2022;14(5):495-500. <https://doi.org/10.5114/jcb.2022.121562>.

**de Vries M**, Sikorski J, Misra S, van den Dobbelssteen JJ. Axially rigid steerable needle with compliant active tip control. *PloS one*. 2021;16(12):e0261089. <https://doi.org/10.1371/journal.pone.0261089>.

**de Vries M**, Christianen MEMC, Luthart L, de Vries KC, Kolkman-Deurloo IKK, van den Dobbelssteen JJ. Dosimetric benefits and preclinical performance of steerable needles in HDR prostate brachytherapy. *Under review*.

**de Vries M**, Wijntjes M, Sikorski J, Moreira P, van de Berg NJ, van den Dobbelssteen JJ, Misra S. MR-guided HDR prostate brachytherapy with teleoperated steerable needles. *Journal of Robotic Surgery*. 2023;17:2461–2469. <https://doi.org/10.1007/s11701-023-01676-x>.

Dhaliwal SS, Wilby SL, Firouzy S, Boni L, **de Vries M**, Navarro SE, Belarouci A, Coelen V, Lakhal O, Pasquier D, Palmer AL, Polak W, Jones D, Labib A, van den Dobbelssteen JJ, Duriez C, Merzouki R. CoBra robot for localized cancer treatment and diagnosis under real-time MRI. *Automation in Medical Engineering*. 2021. <https://doi.org/10.5281/zenodo.4923036>.

**de Vries M**, Klaassen NJM, Morsink NC, van Nimwegen SA, Nijsen JFW, van den Dobbelssteen JJ. Dedicated holmium microsphere administration device for MRI-guided interstitial brain microbrachytherapy. *Medical Engineering & Physics*. 2021;96:13-21. <https://doi.org/10.1016/j.medengphy.2021.07.009>.







# Curriculum Vitae

## MARTIJN DE VRIES

28-03-1992

Born in Rotterdam, the Netherlands

### WORK EXPERIENCE

Jul 2023 – Present

**Innovation Manager Medical Technology** - UMC Utrecht, Utrecht

Apr 2019 – Jun 2023

**PhD Researcher** - BioMechanical Engineering, TU Delft, Delft

Feb 2022 – Apr 2022

**Research and Development Intern** - Elekta Instrument AB, Veenendaal

Jan 2019 – Mar 2019

**Data Analyst** - Rotterdamsche Huizen Maatschappij, Rotterdam

Sep 2017 – Dec 2017

**Healthcare Engineering Intern** - 3D Systems, Leuven, Belgium

Jan 2017 – Feb 2017

**Design Engineer** - Erasmus MC, Rotterdam

Sep 2014 – Apr 2015

**Design Engineer** - ALTHEN Sensors, Rijswijk

Jul 2012 – Sep 2012

**Professional Football Player** - Sparta Rotterdam, Rotterdam

2011 – 2012

**Founder & Co-owner** - BaantjeGezocht.nl, Rotterdam

2009 – 2012

**Professional Football Player** - SBV Excelsior Rotterdam, Rotterdam

### EDUCATION

2015 – 2018

**MSc Biomedical Engineering** – TU Delft, Delft

2012 – 2015

**BSc Industrial Design Engineering** – TU Delft, Delft

2004 – 2010

**Gymnasium** - Erasmiaans Gymnasium, Rotterdam

